Centre Armand-Frappier Santé Biotechnologie

Genetic events responsible for cell shape evolution in multicellular longitudinally dividing (MuLDi) oral cavity *Neisseriaceae*

By

Sammy N. Sichangi

A thesis submitted for the degree of *Doctor of Philosophy* (Ph.D.) in Biology

Evaluation committee members

Jury President and Internal examiner	Prof. Charles Calmettes INRS-Centre Armand-Frappier Santé Biotechnologie Universite du Quebec
External Examiner	Prof. Michael Reed Department of Medicine, Division of Infectious Diseases Department of Microbiology, McGill University
External Examiner	Prof. Rodrigo Reyes Canada Research Chair in Chromosome Biology Department of Biology, McGill University
Supervisor	Prof. Frederic Veyrier INRS-Centre Armand-Frappier Santé Biotechnologie Universite du Quebec

ACKNOWLEDGMENTS

I would like to express my sincere gratitude to my supervisor, Prof. Frederic Veyrier for his continuous guidance and support throughout my Ph.D. research and studies. His patience, encouragement, and exchange of knowledge through creative discussions enabled me to reach this point and above all grow in my professional and scientific skills.

I would also like to thank my thesis committee members: Prof. Charles Calmettes, Prof. Michael Reed and Prof. Rodrigo Reyes for taking their time to review my work and for their encouragement and insightful questions and comments.

My sincere thanks also go to Prof. Silvia Bulgheresi, Philipp Weber, Marie Delaby and Prof. Antony Vincent for their insightful collaboration and help throughout my work.

I would also like to thank my previous and current lab mates, in particular Cecilia Nieves, Martin Chenal, Eve Bernet, Laxmi Sharma,Garima Ayachit, Fransisco Pulido, Alex Rivera and Flourian Coudray for the stimulating discussions and positive criticism that contributed immensely towards the success of my Ph.D. studies. Special thanks also go to Arnaldo Nakamura for the work he put in electron microscopy imaging.

Last but not least, I would like to thank my parents Hellen and Patrick Sichangi, my brothers Michael and Jimmy for their encouragement, mental support and prayers.

ABSTRACT

The bacterial cell shape is an important trait that enhances their survival and colonisation of various ecosystems. Numerous studies over the years have implicated the peptidoglycan together with the cell division and elongation machineries as the main determinants of the bacterial morphology. Indeed, majority of bacterial morphogenesis mechanisms have been described principally in pathogens, particularly using bacilli, cocci and spiral shaped bacterial models. Even more intriguing is the fact that some of these mechanisms are well conserved across species with varying morphologies, while in other species variations in gene conservation and function may exist even in morphologically similar species. These attributes highlight the importance of studying additional bacterial species and varying morphologies to better understand the fundamental biological processes that shape the bacterial cell.

In this thesis, I used the cell shape of 5 multicellular *Neisseriaceae* characterised with incomplete and longitudinal cell division (MuLDi), as models to study cell shape evolution from a bacilli shaped ancestor. The study aimed to use the atypical morphology and cell division of MuLDi bacteria to determine the role of proteins implicated in the morphological transition in addition to describing the cellular and peptidoglycan structure organization during the growth and cell division of these species.

Cells and peptidoglycan extracts were imaged through scanning and transmission electron microscopy techniques to reveal a common outer membrane and lateral peptidoglycan fusion in MuLDi *Neisseriaceae*. Labelling of nascent peptidoglycan using fluorescent D-amino acids revealed longitudinal septation that begins from one end in *Alysiella* species while in *Simonsiella muelleri* and *Conchiformibius* species, septation begins from both ends moving inwards. To determine the genetic factors implicated in the morphological transition, we obtained complete genomes of 5 MuLDi species namely; *S. muelleri, A. filiformis, A. crassa, C. steedae* and *C. kuhniae* plus 16 bacilli *Neisseriaceae* genomes through PacBIO and Nanopore sequencing technologies. A further 20 bacilli *Neisseriaceae* genomes were obtained from the NCBI database. Comparative genomic analyses revealed that the loss of *mraZ*, *rapZ, dgt, gloB*, acquisition of peptidoglycan amidase *amiC2* and amino acid substitutions in divisome and elongasome proteins MreB and FtsA as possible events associated with the evolution of MuLDi morphology. Transcriptomic analysis between bacilli and MuLDi species revealed that the division and cell wall

cluster (*dcw*) genes *ftsI* and *murE* were downregulated in MuLDi species. The deletion of *mraZ* in wildtype *N. elongata* had no morphological changes, significant cell length reduction was however realized upon overexpressing *mraZ*. Transcriptomic analyses revealed the upregulation of the *dcw* cluster genes *mraW, ftsL, ftsI, murE* and *murF* in the *mraZ* overexpressing strain compared to the knock out. The accumulation of 4 gene deletions (*mraZ, rapZ, dgt, gloB*) had no effect on *N. elongata* shape, but insertion of *cdsA-amiC2* and allelic substitution of *N. elongata mreB* with that of *S. mueller* resulted in cells with significantly longer septum and shorter width in both wild-type and four gene mutant *N. elongata*.

Overall, this Ph.D. work highlights *Neisseriaceae* family as an important model to study bacterial morphogenesis, and identifies the loss of *mraZ,* insertion of *amiC2* and amino acid substitutions on MreB as important events associated with the MuLDi to bacilli transition.

RÉSUMÉ

La forme des cellules bactériennes est un trait important qui favorise la survie et la colonisation de divers écosystèmes. Etudes au cours des années ont impliqué le peptidoglycane ainsi que les mécanismes de division et d'élongation cellulaire comme les principaux déterminants de la forme de la cellule bactérienne. En effet, la majorité des mécanismes de morphogenèse bactérienne ont été décrits principalement chez les agents pathogènes, notamment à l'aide de bacilles, de cocci et de modèles bactériens en forme de spirale. Ce qui est encore plus intriguant, c'est que certains de ces mécanismes sont bien conservés entre des espèces de morphologies différentes, alors que chez d'autres espèces, des variations dans la conservation et la fonction des gènes peuvent exister même chez des espèces morphologiquement similaires. Ces caractéristiques soulignent l'importance d'étudier d'autres espèces bactériennes de morphologies différentes afin de mieux comprendre les processus biologiques fondamentaux qui façonnent la cellule bactérienne.

Durant cette thèse, nous avons utilisé la forme cellulaire de cinq *Neisseriaceae* multicellulaires qui résident dans la cavité oropharyngée des mammifères et qui sont caractérisées par une division cellulaire incomplète et longitudinale (MuLDi), comme modèles pour étudier l'évolution de la forme cellulaire à partir d'un ancêtre en forme de bacille. L'étude visait à déterminer le rôle des protéines impliquées dans la transition morphologique ainsi qu'à décrire l'organisation de la structure cellulaire et du peptidoglycane pendant la croissance et la division cellulaire de ces espèces.

Des cellules et des extraits de peptidoglycane ont été imagés par des techniques de microscopie électronique à balayage et à transmission pour révéler la fusion septale. Le marquage du peptidoglycane naissant à l'aide d'acides aminés D fluorescents a révélé une septation longitudinale, avec une division cellulaire unipolaire chez *Alysiella spp*. tandis que *S. muelleri* et *Conchiformibius spp*. ont des modes bipolaires de division cellulaire. Pour déterminer les facteurs génétiques impliqués dans la transition morphologique, nous avons obtenu les génomes complets de 5 espèces de MuLDi, à savoir : *S. muelleri, A. filiformis, A. crassa, C. steedae* et *C. kuhniae*, et 16 génomes de bacilles *Neisseriaceae* grâce aux technologies de séquençage PacBIO et Nanopore. 20 génomes de *Neisseriaceae* bacilles supplémentaires ont été obtenus à partir de la base de données NCBI. Les analyses génomiques comparatives ont impliqué une combinaison de délétions génétiques (*mraZ, rapZ, dgt, gloB*), d'insertions (*amiC2*) et de substitutions d'acides aminés dans MreB et FtsA comme facteurs possibles associés à la morphologie de MuLDi.

La comparaison des données transcriptomiques entre les bacilles et les espèces MuLDi a révélé que les gènes de division et de parois cellulaires (*dcw*) *ftsI* et *murE* étaient moins exprimés chez ces derniers. La délétion du gène *mraZ* chez *N. elongata* sauvage n'a entraîné aucun changement morphologique, alors qu'une réduction significative de la longueur des cellules a cependant été réalisée lors de sa surexpression. Les analyses transcriptomiques ont révélé une augmentation dans l'expression des gènes du cluster *dcw* (*mraW*, *ftsL*, *ftsI, murE* et *murF)* dans la souche surexprimant *mraZ* par rapport à la souche *knock-out.* La délétion de quatre gènes (*mraZ*, *rapZ*, *dgt* et *gloB*) n'a pas eu d'effet sur la forme de *N. elongata*. Cependant, l'insertion de *cdsA-amiC2* et la substitution allélique de *mreB* de *N. elongata* par celui de *S. muelleri* ont mené à la formation de cellules bactériennes avec un septum significativement plus long et une largeur plus courte lorsque ces modifications génétiques étaient effectuées chez *N. elongata* sauvage et chez mutant à quatre gènes.

Dans l'ensemble, ce travail de doctorat met en évidence la famille des *Neisseriaceae* comme un modèle important pour étudier la morphogenèse bactérienne, et identifie la perte de *mraZ*, l'insertion de *amiC2* et les substitutions d'acides aminés sur MreB comme des événements importants associés à la transition de MuLDi à bacilli.

TABLE OF CONTENTS

LIST OF FIGURES

LIST OF TABLES

ABBREVIATIONS

AA	Amino acid
ADP	adenosine diphosphate
ATP	adenosine triphosphate
COG	Clusters of Orthologous Groups
CTL	C-terminal linker
CTT	C-terminal tail
CTV	C-terminal variable region
CW	cell wall
CWD	cell wall deficient
DAPI	4′,6-diamidino-2-phenylindole
DCW	division and cell wall cluster
DD-CPase	D,D carboxypeptidase
DD-Epase	D,D endopeptidase
DNA	Deoxyribonucleic acid
FDAAs	Flourescent D-amino acids
Fts	filamentation temperature sensitive
GI	gastrointestinal
GlcNAc	N-acetylglucosamine
GlmM	phosphoglucosamine mutase
GlmS	glucosamine 6 phosphate synthese
GTases	glycosyltransferases
HPLC	high-pressure liquid chromatography
IMD	Invasive Meningiococcal Disease
LTs	lytic transglycosylases
ML	maximum likelihood
MuLDi	Multicellular longitudinally dividing
MurNAc	N-acetylmuramic acid
NJ	neighbor-joining
NTP	N-terminal peptide
PBPs	penicillin binding-proteins
PG	peptidoglycan
PGAs	PG amidases
RNA	Ribonucleic acid
rRNA	ribosomal RNA
TM	transmembrane
TPases	transpeptidases
UDP-GlcNAc	uridine diphosphate-N-acetylglucosamine
UDP-MurNAc-pp	UDP-*N*-acetylmuramyl-pentapeptide
UPEC	uropathogenic *Escherichia coli*
UppS	Undercaprenyl pyrophosphate synthase

1 INTRODUCTION

The geometry and size of bacterial cells were described for the first time over three centuries ago at the dawn of microscopy innovations. Bacterial cell shapes are diverse and perhaps only a small proportion of all possible morphologies have been described to date (Hug, Baker et al. 2016, Kysela, Randich et al. 2016), this is largely due to difficulties associated with the isolation and culture of species whose growth and nutritive requirements remain a mystery to microbiologists (Lewis, Epstein et al. 2010, Vartoukian, Palmer et al. 2010). However, progress has been made over the years towards understanding bacterial growth requirements leading to the isolation and characterization of a large proportion of bacterial species. Some of the well documented morphotypes include; rods (bacilli) such as *Escherichia coli*; spherical (cocci) like *Staphylococcus aureus*; and curved (helical) shaped species like *Vibrio cholerae*.

Through a combination of different sequencing technologies and bioinformatics tools, comparative genomics and phylogenomic inferences based on partial or whole genome sequences done in multiple studies and at different times, have all shown that the bacilli shape as the ancestral bacterial morphology (Siefert't and Fox 1998, Yulo and Hendrickson 2019, Brandis 2021). Based on 16s rRNA gene-based phylogenies of 180 bacterial species, one of these studies showed that bacilli and filamentous species occupied the deepest branches of the phylogenetic tree, while cocci morphology seemed to have evolved much later (Siefert't and Fox 1998). The acquisition of cocci morphology was considered as the final state of cell shape evolution since upon acquiring this morphology there was no reverting to the "ancestral" form, thereby concluding that the bacilli was the most probable common bacterial cell shape. Similarly, a larger study that used 253 bacterial 16s rRNA sequences in addition to the presence or absence of the bacterial cell elongation gene *mreB* pointed at the bacilli shape as the likely ancestral morphology (Yulo and Hendrickson 2019). To assess the role of *mreB* conservation on cell shape evolution, this study revealed that 63% of all the cocci-shaped species analyzed were emergent upon the loss of *mreB*. A strikingly interesting finding in this study was the reversion of *Deinococcus deserti* from cocci to the ancestral bacilli like morphology, an event that seemed to have occurred after gaining of a single copy of *mreB*.

Other studies have explored further the role of gene content and order on morphological phenotype evolution. Since proteins work as a complex network system, these attributes are

important for example, in the co-transcription of genes in an operon, any particular disorganization of the gene content and order might result in miss-regulation of key cell shape determining proteins or enzymes. The rearrangement of gene order along the chromosome is sometimes lost but fewer genes are retained in close proximity, a feature referred to as the neighbourhood conservation (Dandekar, Snel et al. 1998). Usually, the regulatory features and functional class of the neighbouring genes are retained (Lathe, Snel and Bork, 2000). To demonstrate the relevance of gene order and content, Tamames *et al.*, (2001) showed a strong correlation between the bacterial cell shape with gene content and the order of the division and cell wall cluster (*dcw*) genes.
Studies done using whole-genome sequences have enhanced the opportunity for comprehensive studies on the evolution of genome organization. These works have not only linked the bacilli as the ancestral morphology, but have also shown that multiple evolutionary events associated with gene loss, gain and nucleotide substitutions have culminated in the present day bacterial morphologies. For example, in cocci-shaped *Neisseriaceae* species the loss of *yacF* was the major event that resulted in the transition from bacilli to cocci since it preceded the loss of *mreB* and other associated elongation genes (Veyrier, Biais et al. 2015).

A variety of bacterial morphologies beyond the common bacilli and cocci described in earlier versions of microbiology texts such as Bergey's Manual of Determinative Bacteriology continue to fascinate scientists as shown recently by (Kysela *et al.*, 2016), summarized in Figure 1. Two interesting events were evident in this study, first the repeated appearance of multicellular filaments and helical morphologies in different clusters and secondly the clustering of similar morphologies such as the branching *Actinobacteria* or appendages in *Caulobacteria*. The first case is indicative of independent evolutionary origins while the latter points to common ancestral origins. More intriguing questions arise from these results; for example, during independent evolution origins; are similar molecular mechanisms responsible for a particular cell shape? or do they result from related environmental pressures? Similarly; for common ancestry evolution, at what point is the shape retained even in the presence of continued selective pressure? and finally why do members of the same bacterial genus or families exhibit morphological variations? By and large, the reason why bacteria have myriads of cell shapes and the fact that these morphologies are carefully maintained and passed on from generation to generation highlights the importance of this trait (Young 2006). The relevance and adaptive value of given bacterial morphologies towards colonisation and survival in different environments are affected by a variety of selective pressures including the need for nutrient access, attachment, motility, cell division mode, dispersal or need to escape predation among others. Overall, a multiplicity of factors are involved in determining the bacterial morphology, thus it is not possible to predict the shape based on the environmental conditions or use of the environment to predict the same.

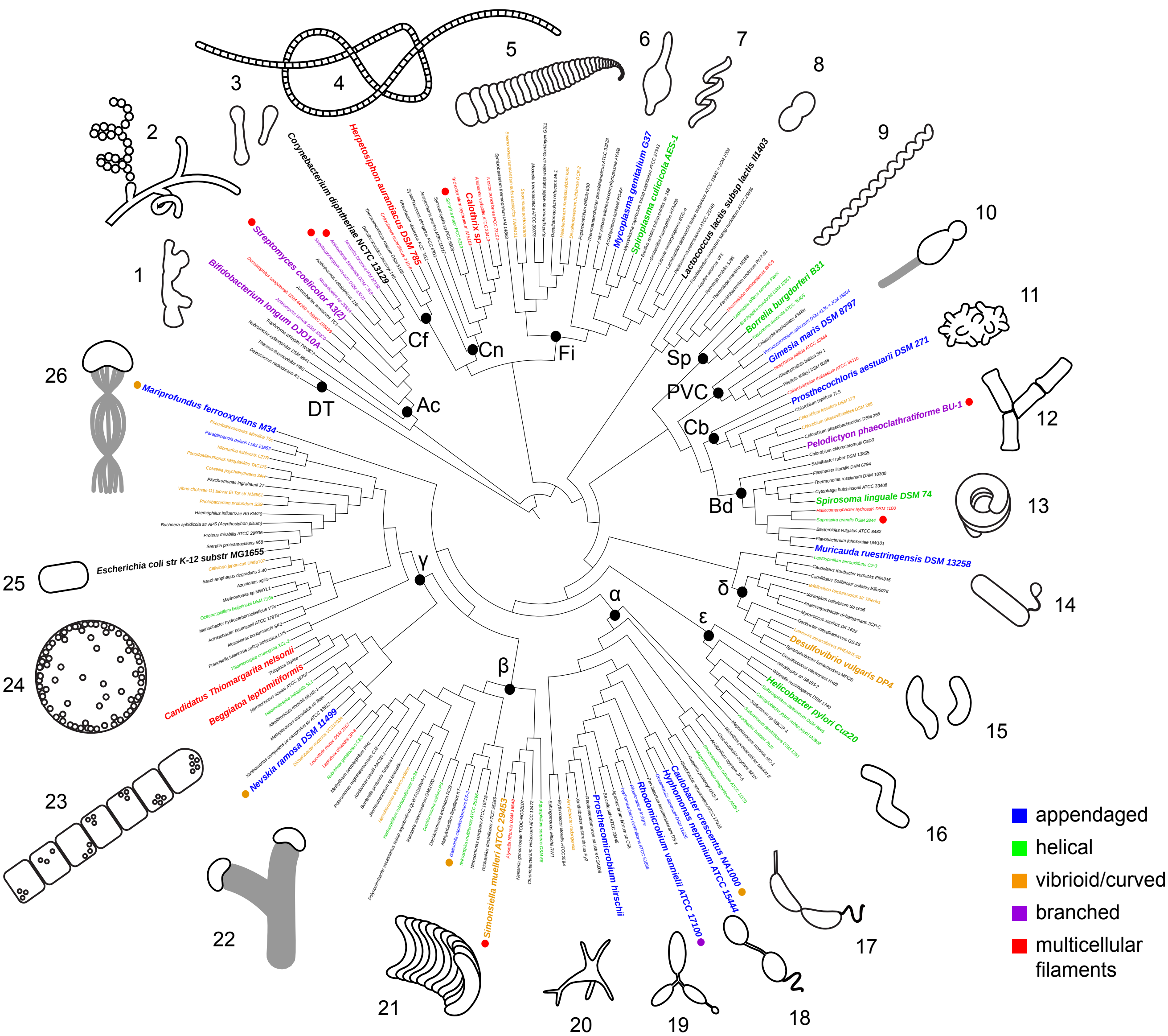

Figure 1.1 : Bacterial morphologies beyond bacilli and cocci in phylogenetically diverse taxa: A maximum likelihood phylogenetic tree showing the clustering of bacterial genomes into 26 morphotypes. Adopted from (Kysela, Randich et al. 2016)

1.1 The importance of the bacterial cell shape

The bacterial morphology is not an accidental attribute, its functional significance is depicted by the fact that a characteristic shape is maintained and accurately passed on from generation to generation (van Teeseling, de Pedro et al. 2017). Sometimes bacteria may temporarily modify their morphologies to adapt, colonize and survive in adverse environmental conditions. However, they can also adopt permanent morphological variations during the course of cell shape evolution as a result of genetic changes affecting key cell shape determining proteins. Species exhibiting certain characteristic morphologies may have the selective advantage to colonize and survive in a given environment over those without as exemplified in numerous mutagenesis studies that altered the bacterial shape. Considering the relevance of shape to motility as an example, when compared to the helical wild-type, straight and curved *Campylobacter jejuni* mutants were associated with decreased motility in soft agar (Frirdich and Gaynor 2013, Frirdich, Vermeulen et al. 2014, Stahl, Frirdich et al. 2016). Similarly, *Helicobacter pylori* mutants with altered helicity showed reduced motility when compared to wild type strains in both soft agar and mucus mimicking gel-like solutions (Sycuro, Pincus et al. 2010, Sycuro, Wyckoff et al. 2012, Martinez, Hardcastle et al. 2016). In the context of pathogenesis, *H. pylori* that is responsible for stomach inflammation leading to peptic ulcers and cancer of the human gastrointestinal (GI) tract, the diarrhoea causing *C. jejuni* and *Vibrio cholerae* use their helical or curved shapes to penetrate the thick mucus layer of the GI tracts to establish an infection (Young, Davis et al. 2007, Bonis, Ecobichon et al. 2010, Sycuro, Pincus et al. 2010, Frirdich, Biboy et al. 2012, Sycuro, Wyckoff et al. 2012, Bartlett, Bratton et al. 2017). The perfect morphotype is determined by selective forces, for example, the need for nutrients, escape predation, attachment and colonisation of surfaces among others.

To enhance the need for efficient nutrient uptake , bacteria may undergo temporary modifications resulting in cell elongation or filamentation in nutrient-deprived conditions; the formation of long stalks (prosthecae) through polar growth by *Caulobacter crescentus* was evidenced when grown in phosphate poor environment (Wagner et al., 2006). The absence of phosphate, glutathione or cysteine results in branched or filamentous rods in *Actinomyces israelli*. *Pseudomonas* species have been shown to elongate resulting in long thin cells while *Salmonella enterica* cells grow wider in rich media. In order to escape phagocytosis, bacteria may increase their size resulting in elongated cells or through the production of secondary structures like prostheceae, while some form aggregates of cells (Young 2006). Reduced cell division coupled with increased longitudinal growth results in cell filamentation, a beneficial attribute in pathogens like *Legionella* species that aids in avoiding the host's immune cells (Li, Zeng et al. 2010). A subset of uropathogenic *Escherichia coli* (UPEC) strains were shown to undergo reduced cell division and responsible for their filamentous morphology that has a selective advantage in evading the host's phagocytic cells (Justice, Hung et al. 2004, Horvath, Li et al. 2011). Other studies have also shown additional uropathogenic isolates from human patients such as *Klebsiella pneumoniae*, *Enterobacter aerogenes* and *Proteus mirabilis* to have a filamentous morphology (Garofalo, Hooton et al. 2007, Rosen, Hooton et al. 2007). Another case of morphological role in evading the immune cells was postulated in cocci-shaped *Neisseria* species whose cell-shape changes associated with peptidoglycan reworking was hypothesized to impact reduced detection by Nod1 and Nod2 immune receptors (Veyrier, Biais et al. 2015).

Filamentous multicellular bacteria are characterized by multiple fused cells, thereby conferring size-related advantages like efficient nutrient uptake, stronger surface attachment and reduced predation among others. Division of labor through cellular differentiation in filamentous bacteria has also been described, for example in cyanobacteria where some cells are responsible for nitrogen fixation while others perform photosynthesis (Flores and Herrero 2010). Phylogenetic evidence in cyanobacteria however suggests that undifferentiated multicellularity emerged before differentiation (Rossetti, Schirrmeister et al. 2010). Species like *Simonsiella muelleri* have evolved mechanisms to enhance the adhesion potential enabling them to colonize the mammalian tongue that is characterized by massive shear movements in form of fluids and other debris. According to Lyons and Kolter (2015), the definition of multicellularity is based on two principles, first there must be cell to cell adhesion to form a single unit and secondly the individual cells must contribute to a coordinated function. Filamentation in this regard refers to the process through which cell separation is inhibited despite continuous cell growth giving rise to elongated and multi-nucleated cells (Jahnke, Terrell et al. 2016). Filamentation can be a temporary or permanent morphological transition state that occurs due to a multiplicity of factors such as; DNA damage, nutritional and oxygen stress and phagocytosis-evasion response among others (Connell, Agace et al. 1996, Steinberger, Allen et al. 2002, Justice, Hunstad et al. 2006, Abboudi, Matallana Surget et al. 2008, Horvath, Li et al. 2011). The length of the filament in cyanobacteria was shown to be dependent on the cell's birth and death rates. Cells with a long generation time (low birth and death rates) were significantly longer than those with a short generation time, and the length of the filament is controlled once it reaches its maximum carrying capacity (Rossetti, Filippini et al. 2011).

Efficient movement is another important survival strategy as bacteria move to access nutrients, colonize surfaces, or even escape predation. The motility efficiency is a factor of the cell shape, as an example, cells that move in groups "swarming cells," tend to be longer bacilli forms because they rely on the larger cell to cell alignment for contact optimisation (Young 2006).

On the other hand, the ability to colonize surfaces under moderate flow conditions is exemplified by the *Caulobacter crescentus* curvature morphology where surface attachment and colonisation of new daughter cells are enhanced through the closer positioning of the piliated poles to the surface shortly before the cell division (Persat et al., 2015). Mutant cells that are unable to produce the filament-like protein Crescentin lack the curvature phenotype important of anchorage and are often washed off. Another example of morphological relevance to attachment is associated with the presence of fimbriae on the entire cell surface of cocci-shaped *Neisseriaceae* was hypothesized to increase the nasopharyngeal attachment efficiency when compared to bacilli species that have polar fimbriae arrangement (Veyrier, Biais et al. 2015).

Feature	Selective force	Rationale
Helical/Spiral	active motility/predation	motility through viscous media, escapes predator through internalisation
Filamentation	nutrient acquisition, movement, predation, corporation	corporation for nutrient intake, movement by gliding, escape predation through size
Rods(bacilli)	motility and attachment	small rods more efficient movement by Brownian motion, large surface for attachment
Cocci (sphere)	motility and predation	small spheres move faster and have a reduced surface for immune recognition
Curved (vibrio)	colonisation	enhanced colonisation of viscous and aquatic environments
Prosthecae and stalks	nutrient access, attachment, escape predation	increased surface enhances nutrient uptake and attachment, large cells escape phagocytes

Table 1.1 : The morphological features associated with bacterial morphology, adapted from (Young, 2006)

1.2 Determinants of the bacterial cell shape

The quest to understand bacterial morphogenesis and establish how and why bacteria exist in different shapes has been on for decades. Work from different groups using various methods including genetic approaches, bioinformatics together with fluorescence and electron microscopy imaging, on different bacterial models have implicated the bacterial peptidoglycan (PG) (Salton and Horne 1951, Weidel, Frank et al. 1960, Holtje 1998, Nanninga 1998) together with other numerous proteins involved in bacterial elongation and cell division processes as the major cell shape architects (Shih and Rothfield 2006, Vats, Yu et al. 2009, Young 2010, Typas, Banzhaf et al. 2011, Dik, Fisher et al. 2018). The detailed review of the bacterial cell shape determinants is discussed in the subsequent sections of this chapter.

1.2.1 The Peptidoglycan

All bacterial cells besides mycoplasmas are surrounded by a giant sac like macromolecular structure (peptidoglycan). This structure has been an interesting research component due to its presence in most bacteria and absence in eukaryotes, thereby making it a powerful antibiotic target, in addition to its immunostimulatory and cytotoxic properties during infection (Nikolaidis, Favini-Stabile et al. 2014, Mayer 2019). The peptidoglycan name is derived from the components of the structure, the disaccharide glycan strands and short peptide chains. Generally the PG forms a rigid mesh-like structure (illustrated in figure 1.2) that surrounds the cytoplasm to define the shape besides protecting the cell from bursting due to excess osmotic pressure (Vollmer, Blanot et al. 2008). Experiments conducted in bacilli-shaped species by use of compounds that disrupt PG synthesis such as penicillin and lysozyme resulted in osmotically sensitive rounded cells (Weibull 1953, Lederberg 1956). Further evidence of PG's role in morphogenesis is shown through electron microscopy imaging of purified PG extracts that accurately retain the shapes of corresponding bacterial cells (Weidel, Frank et al. 1960, Weidel and Pelzer 1964, Mannik, Driessen et al. 2009).

The mode of PG synthesis during growth has also been shown to differ in bacteria with varying morphologies. Thus the consequences of having only septal PG synthesis might imply the presence of fewer morphology determining genes when compared to species with both septal and peripheral complexes. Spherical bacteria for example, lack lateral modes of growth mainly due to the absence of *mreB* gene that encodes for the actin homolog MreB responsible for the lateral growth (elongation) of the bacterial cell. Entirely coccoid/round forms such as *Staphylococcus aureus* rely on PG synthesis at the division septa (septal PG synthesis) during growth, which in fact, results in diplococci appearance. Both septal and peripheral modes of PG synthesis are present in slightly ovoid ovococcoids (elongated ellipsoids) like *Streptococcus pneumoniae.* The *Pneumococcus* lacks MreB but has MreC and MreD proteins responsible for peripheral PG synthesis. Cell division in bacilli shaped species occurs transversally, they, however may present different modes of PG synthesis. For example, Gram-negative *E. coli* and Gram-positive *B. subtilis* have both peripheral and septal PG synthesis while *Mycobacteria* and *Corynebacteria* have a polar PG synthesis (Scheffers and Pinho, 2005). Crescentin (CreS) protein is responsible for curvature (bent shape) in *Caulobacter crescentus*. Localization of CreS in the inner side of the cell wall causes in reduced rate of PG synthesis of the inner murein relative to the outer side resulting in bending attributable to higher mechanical strain on the outer side of the murein (Typas, Banzhaf et al. 2011).

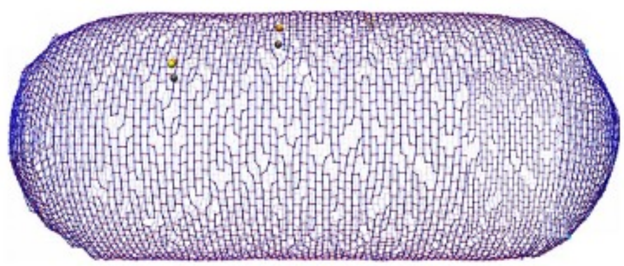

Figure 1.2: An illustration of the circumferential peptidoglycan mesh-like structure of a bacilli shaped bacteria. The rigid mesh-like peptidoglycan (purple) is composed of glycan strands crosslinked by short peptides (Nguyen, Gumbart et al. 2015).

The peptidoglycan is a major constituent of the bacterial cell wall (CW), together with other macromolecules such as polysaccharides, teichoic and lipoteichoic acids. The PG composition is the basis of Gram type classification, where bacteria are divided into Gram-positive and Gram negative groups. The PG architecture varies depending on the Gram-type as illustrated in figure 1.3: note the difference in CW size between Gram-positive (monoderm) and Gram-negative (diderm). The PG layer is thicker with at least 30-300 nm in Gram-positives compared to 4-12nm thick in Gram-negatives (Silhavy, Kahne et al. 2010).

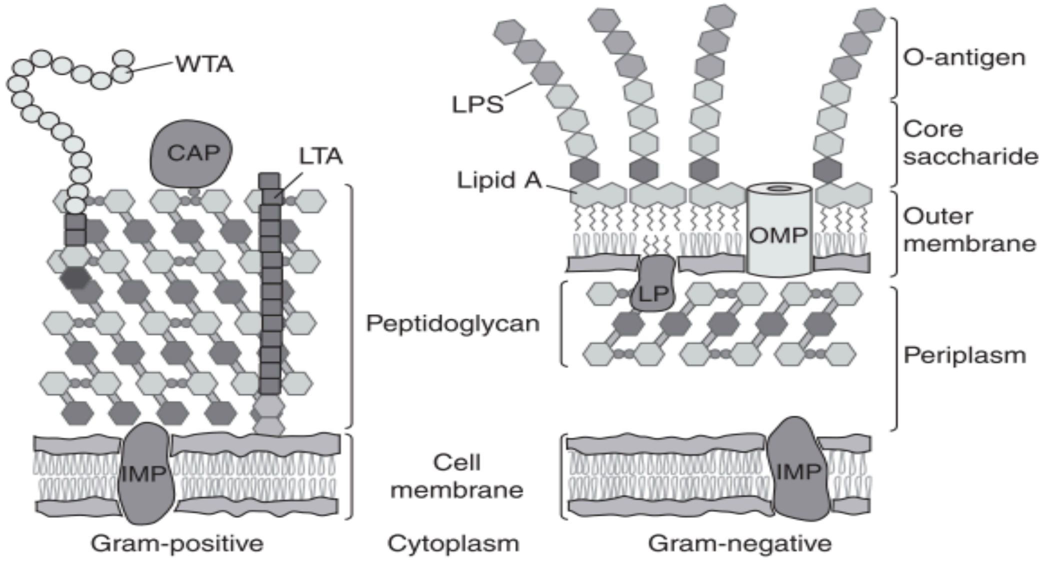

Figure 1.3: Schematic illustration of Gram-positive and Gram-negative cell walls (Silhavy, Kahne et al. 2010). IMP = integral membrane protein, LP = lipoprotein, OMP = outer membrane protein, LTA = lipoteichoic acid, CAP = covalently attached protein, LPS = lipopolysaccharide, WTA = wall teichoic acid

The peptidoglycan, monomeric unit consists of alternating sugar residues *N*-acetylmuramic acid (MurNAc) and *N*-acetylglucosamine (GlcNAc) that are linked by β-1,4 glycosidic bonds with five amino acids peptide chains attached to the lactyl group of MurNAc sugar (Meroueh, Bencze et al. 2006). Alternating GlcNAc and MurNAc sugars are crosslinked by short flexible peptide bridges attached to the D-lactyl group of MurNAc to form the PG polymer (Holtje 1998). Linking of peptide chains occurs through D,D-transpeptidation reactions at the carboxyl group of the fourth D-Ala in one peptide and the amino group of the third diamino acid of the second peptide, either directly or by short peptide bridge (Vollmer, Blanot et al. 2008). Besides 3-4 cross linkage being the predominant kind of cross-linkage, other notable variations such as 2-4 cross linkage present in Corynebacteria (Sauvage, Kerff et al. 2008) and 3-3 cross linkage in β-lactam-resistant *M. smegmatis* strains (Mainardi, Fourgeaud et al. 2005) also exist.

The sugar composition of GlcNAc and MurNAc in most Gram-positives and Gram-negatives are quite conserved although they might also undergo chemical modifications. Similarly the peptide composition may differ. Modifications occurring in the sugars and peptide moieties enable the bacteria to cope with certain environmental constraints such as exposure to antibiotics and host secreted enzymes. Some of the sugar alterations as reviewed (Yadav, Espaillat et al.

2018), include N-deacetylation of MurNAc upon the removal of acetyl group at C-2 position evidenced mostly in Gram-positives like *B. cereus*, *C. difficile, S. suis* and *S. iniae.* Alternatively, N-deacetylation of GlcNAc has been reported in *B. subtilis.* N-glycosylation of MurNAc in Mycobacterium species associated with increased resistance to antibiotics and lysozyme(Raymond, Mahapatra et al. 2005). O-acetylation of MurNAc mainly in pathogenic Gram-positives and Gram-negatives, enabling them to tolerate the hosts muramidase activity (Laaberki, Pfeffer et al. 2011, Bernard, Rolain et al. 2012).

Variations of the peptide stems exist in different species. In most bacterial species, L-Ala is the first amino acid to be added to the peptide strand, however a few exceptions like *Mycobacterium leprae* have Gly or L-Ser instead. Another example is exhibited in *Chlamydia trachomatis* that has either L-Ala, L-Ser or Gly. The third position of the peptide strand varies depending of the bacterial Gram-type, Gram-positives have D-Lys where as in most Gram-negative bacteria and Mycobacteria species have meso-DAP. Thus the peptide composition in Gram-negative and Gram positive bacteria is (GlcNAc-MurNAc-L-Ala-D-Glu-L-DAP-D-Ala-D-Ala) and (GlcNAc-MurNAc-L-Ala-D-Glu-L-Lyse-D-Ala-D-Ala) respectively (Vollmer, Blanot and De Pedro, 2008). Other bacterial species have diamino acids such as; L-ornithine (L-Orn) in *Thermus thermophilus* and L-2,4-diaminobutyric acid in *Corynebacterium* species. In virtually all species D-Ala is the predominant amino acid at position 4, however, D-Lactate (D-Lac) or D-Ser amino acid variants may exist at the fifth position of the peptide therefore decreasing the affinity of vancomycin to the peptidoglycan in vancomycin resistant species such as *Enterococcus gallinarum* and *Lactobacillus casei*.

Ultimately, there is no correlation between glycan strand length and the peptidoglycan thickness as demonstrated across different species, for instance, Gram-positive species like *S. aureus* have short while *B. subtilis* have long glycan strands. Similarly, Gram-negative species like *H. pylori* have short whereas *P. morganii* have long glycan strands (Vollmer, Blanot et al. 2008). In general, 50-250 disaccharide units are present in *B. subtilis*, *Bacillus licheniformis* and *Bacillus cereus* glycan strands while *S. aureus* has an average of about 18 disaccharide units. Gram-negative E. coli has an average of 30 disaccharide units, while *H. pylori* has less than 10 disaccharide units (Chaput, Labigne et al. 2007, Vollmer, Blanot et al. 2008).

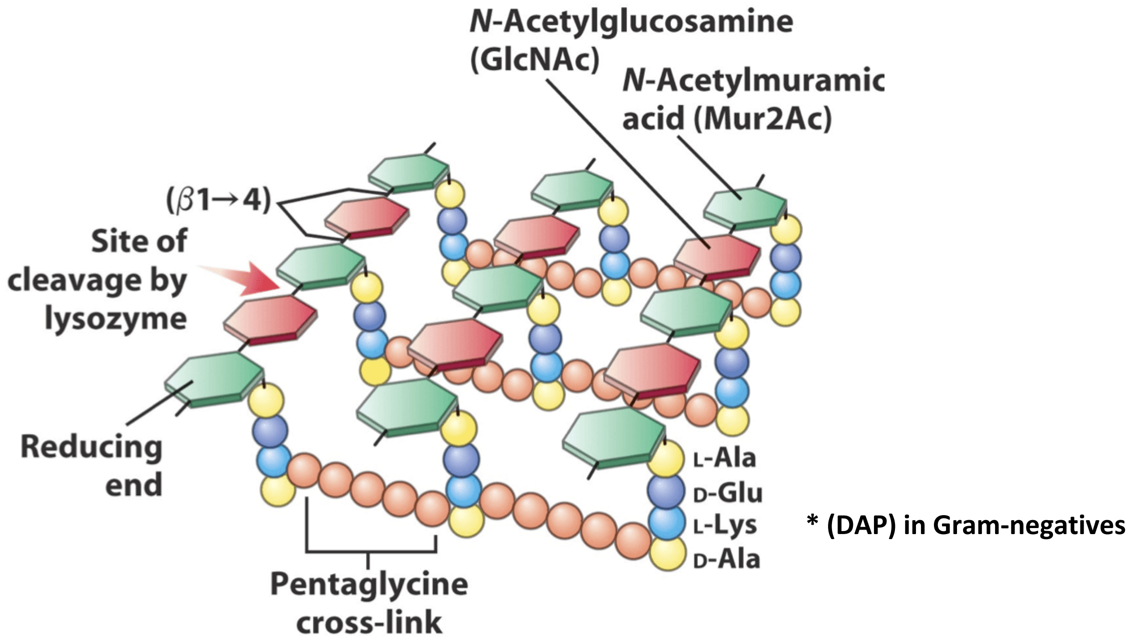

Figure 1.4: Schematic representation of Gram positive peptidoglycan: Note in Gram-negative the third amino acid of the peptide strand is meso diaminopimelic acid shown in brackets (Peptidoglycan Structure Analysis - Creative Proteomics,https://www.creative-proteomics.com/services/peptidoglycan-structure-analysis.htm)

1.2.1.1 Peptidoglycan synthesis

Peptidoglycan synthesis is complex, it involves constant modifications of the PG structure through sequential synthesis of PG muropeptides that are added onto the existing PG and hydrolysis events that modify the PG structure to allow addition of the muropeptides. This process is therefore carefully regulated in order to maintain the stability of the bacterial cell while at the same time preventing cell lysis that may result from excess turgor pressure. Peptidoglycan biosynthesis starts in the cytoplasm with the synthesis of PG precursors before transportation across the cytoplasmic membrane and into the periplasm for incorporation into the existing PG.

During the cytoplasmic phase, fructose-6-phosphate is converted to glucosamine-6-phosphate by the enzyme glucosamine 6 phosphate synthase (GlmS), which is subsequently converted to glucosamine-1-phosphate by phosphoglucosamine mutase (GlmM). Through the action of GlmU, Glucosamine-1-phosphate undergoes acetyltransferase and uridyltransferase reactions resulting in the generation of uridine diphosphate-N-acetylglucosamine (UDP-GlcNAc).

The direct addition of Enolpyruvyl to UDP-GlcNAc results in the formation of UDP-GlcNAc-enolpyruvate that is converted to UDP-*N*-acetylmuramyl (UDP-MurNAc) through the action of MurA and MurB proteins. L-Alanine is added to UDP-MurNAc through the catalytic action of MurC to form UDP-MurNAc-L-Ala. D-glutamic acid is subsequently added to the L-Alanine stem through the action of MurD, later the incorporation of DAP in Gram-negatives occurs through the action of MurE resulting in the formation of UDP-MurNAc-L-Ala-D-Glu-DAP (Barreteau *et al.*, 2008). MurF then catalyses the addition of D-ala-D-ala dipeptide to the stem to form UDP-*N*-acetylmuramyl pentapeptide (UDP-MurNAc-pp). Undecaprenyl pyrophosphate synthase (UppS) catalyses the synthesis of membrane-linked undecaprenyl phosphate that is processed further to yield phosphor -MurNAc-pentapeptide translocase (MraY) substrates UDP-Mpp and C55-P. Membrane PG synthesis is catalysed by MraY where MurNAc-pentapeptide group is transferred from UDP-Mpp to C55-P generating uridine monophosphate (UMP). The transfer of phospho-MurNAc-pentapeptide moiety of UDP-MurNAc-pp to bactoprenol membrane acceptor yields Lipid I (undecaprenyl-pyrophosphoryl-MurNAc-pentapeptide). Next the glycosyltransferase MurG transfers GlcNAc component from UDP-GlcNAc to lipid I yielding undecaprenyl-pyrophosphoryl-MurNAc- GlcNAc (Lipid II). Lipid II is later translocated to the outer membrane by flippases such as FtsW and MurJ (Sham *et al.*, 2014). Bactoprenol is important in transporting hydrophilic components from the aqueous part of the cytoplasm to hydrophobic parts and eventually to the external zone for PG incorporation. Once in the periplasmic side, muropeptide PG precursors are inserted in the existing PG through polymerisation by different classes of penicillin binding proteins (PBPs) glycosyltransferases (GTase) and transpeptidases (TPases) through transglycosylation (linking of sugar chains) and transpeptidation (connecting peptide chains) respectively.

During polymerisation Undecaprenyl diphosphate is liberated and flipped back to the cytoplasm to undergo dephosphorylation and once again reused for the precursor transportation (Manat *et al.*, 2014). Enlargement of the closed PG structure involves the addition of newly synthesized PG to the existing layer, PG amidases (PGAs) hydrolyse the amide bonds of the glycan strands to allow insertion of newly synthesized material into the existing PG. Glycosidases target glycosidic linkages while peptidases act on amino acid amide bonds within the PG (Vermassen *et al.*, 2019).

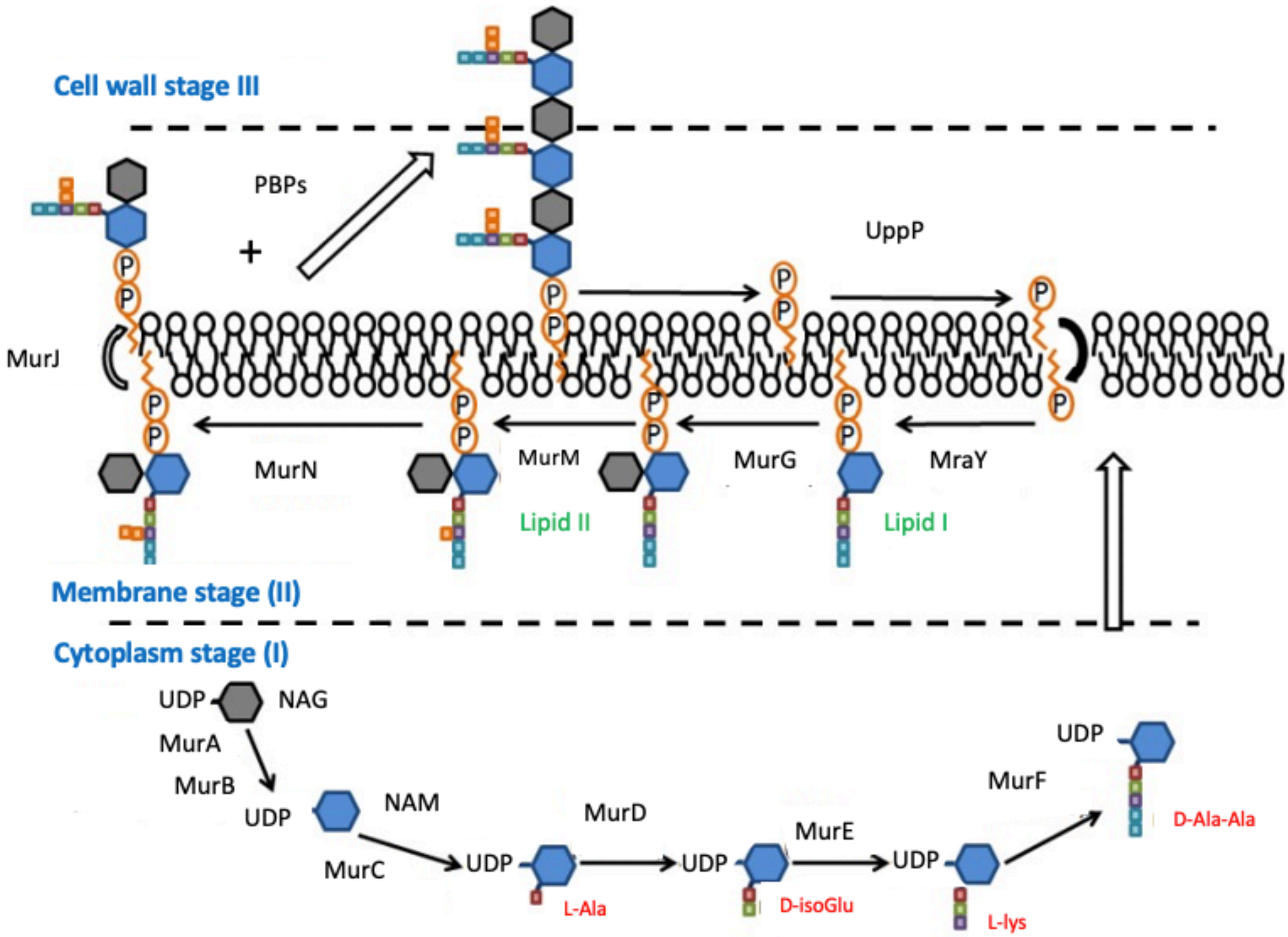

Figure 1.5: An illustration of peptidoglycan synthesis process: adapted from (Hancock, Murray et al. 2014)

Synthases are penicillin binding-proteins (PBPs), they are classified as Class A, Class B and Class C PBPs. Class A and B are high molecular weight (HMW) PBPs, while Class C are low molecular weight (LMW) PBPs (Spratt 1975, Schiffer and Höltje 1999, Sahare and Moon 2014). The classification system is based on the structure, domains sequence similarities and catalytic activity of the N and C-terminal. Class A-PBPs are bifunctional GTase/TPases consisting of the N-terminal GTase domain and C-terminal TPase domain. Class B-PBPs are monofunctional TPases with an active C-terminal domain, the N-terminal domain has no known enzymatic function, but contributes to cell shape through interactions with other proteins involved in the bacterial cell cycle (Scheurwater, Reid et al. 2008). Class-C PBPs have either d,d-carboxypeptidase or d,d-endopeptidase activity that hydrolyze the last D-ala stem peptide or hydrolyze the peptide bond between two glycan strands respectively (Pedro 2019, Shaku, Ealand et al. 2020). Class A , B and C PBPs are sub-divided further into at least 7, 6 and 4 subclasses respectively as shown in table 1.2. The Gram-negative bacteria *E. coli* has three subclasses of Class A-PBPs (PBP1A, PBP1B, PBP1C), while *N. gonorrhoeae* has only one (PBP1). Whereas *E. coli* has two subclasses of Class B-PBPs (PBP2, PBP3), *N. gonorrhoeae* has only one (PBP2). Of note, the divisome protein PBP3 in *E.coli* is referred to as PBP2 in *N. gonorrhoeae,* however, their common name is FtsI. Finally, *E. coli* has all the four subclasses of Class C-PBPs while *N. gonorrhoeae* has only two (PBP3 and PBP4). Moreover, subclass A1 and A2 PBPs are predominantly present in Gram-negative bacteria , while A3, A4 and A5 are found in Gram-positives. Subclass A6 and A7 contains unusual PBPs in *E. coli* and *M. tuberculosis* respectively (Sahare and Moon 2014).

	E. coli	***N. elongata***	***N. gonorrhoeae***	***S. aureus***
Class A - HMW (Transpeptidase and Transglcosylase)	PBP1A PBP1B PBP1C	PBP1	PBP1	PBP2
Class B -HMW (Transpeptidase)	PBP2 PBP3 (FtsI)	FtsI	FtsI	PBP2a PBP1 PBP3
Class C -LMW (Endopeptidase and Carboxypeptidases)	PBP4 PBP5 PBP6 PBP6b PBP7	PBP3 (DacB) PBP4 (DacC)	PBP3 (DacB) PBP4 (DacC)	PBP4

Table 1.2: Classification of penicillin binding proteins. Adapted from (Sahare and Moon 2014, Obergfell, Schaub et al. 2018). High molecular weight PBPs class A have both transpeptidase and transglycosylase activities, while class B are monofunctional transpeptidases. Low molecular weight PBPs have both endopeptidase and carboxypeptidases activities.

1.2.1.2 Peptidoglycan hydrolysis and recycling

During PG synthesis, active incorporation and polymerization of newly synthesized PG into the existing PG layer occurs. On the other hand, during PG hydrolysis up to 50% of the PG is broken down and efficiently recycled. Since the polar regions of the PG are mostly inert during the cell cycle, it is estimated that over 60% of the PG from these regions in recycled (Goodell and Schwarz 1985, Park and Uehara 2008, Uehara and Park 2008). PG recycling is not only beneficial for the conservation and recovery of resources, but it also aids in priming the bacterial cell to detect cell wall targeting antibiotics and through various regulatory pathways the resistance to these antibiotics is enhanced (Johnson, Fisher et al. 2013). Peptidoglycan hydrolysis occurs through the cleavage of peptide chains by peptidases like D,D carboxypeptidase (DD-CPase), D,D endopeptidase (DD-EPase) and the glycan strand cleavage by lytic transglycosylases (LTs). These enzymes are ubiquitous in PG containing bacteria where they are required for the creation of spaces within the existing PG polymer for PG growth, cell division, and accommodation of structures like secretion systems, pili and flagella (Scheurwater, Reid et al. 2008).

Carboxypeptidases act by cleaving the terminal D-Ala of the pentapeptide chain (MurNaC) examples include; PBP5, PBP6a and PBP6b. Studies on *E. coli* have demonstrated the involvement of PBP5 in aiding the orientation of FtsZ septum ring formation, inactivation of PBP5 resulted in irregular Z-ring site formation (Varma and Young 2004). Single deletions of either of these CPase's did not show noticeable phenotypic changes, however double and particularly triple gene deletions were associated with reduced growth rate and morphological changes indicative of redundancy or overlapping functions.

Endopeptidases cleave the interpeptide bonds, examples include PBP4, PBP7 that have been demonstrated to function in concert with elongasome proteins PBP1a and LpoA. The other group of EPase is composed of murein endopeptidases (MepA, MepH, MepM and MepS). Marcyjaniak *et al.*, (2004) showed that MepA acts by cleaving D-alanyl-meso-2,6-diamino-pimelyl amide bond. Despite PG composition alteration, there was no phenotypic effect upon the deletion or overproduction of MepA. MepH, MepM and MepS are not essential for Epase activity but are required for the incorporation of newly synthesized material into the existing PG layer.

The cleavage of the N-acetylmuramoyl-L-alanine amine bond between the L-Ala and MurNaC murein backborne occurs through the action of PG amidases such as AmiA, AmiB and AmiC. These amidases were shown to have functional redundancy in *E.* coli following impaired cell division upon the inactivation of at least two amidases. Alternatively, the overproduction of any one of the three amidases in AmiABC triple mutant suppresses the chaining phenotype (Heidrich, Templin et al. 2001, Lehner, Zhang et al. 2011). AmiB however, seems to have a lesser role in cell septation since its deletion had no phenotype change, and similarly it did not result in noticeable changes when introduced in *amiAC* mutant cells (Heidrich, Templin et al. 2001). The activation of AmiA and AmiB takes place through lysostaphin-type enzymes, D-Ala-D-Ala metallopeptidases (LytM) domain of the EnvC component of the division and cell wall cluster (*dcw)* while the activation of AmiC is activated by NlpD. Activity of at least one of the activators is sufficient for complete cell fission since the inactivation of a single activator did not impede cell fission but cell joining phenotype was obtained upon inactivation of both EnvC and NlpD (Priyadarshini, de Pedro et al. 2007, Uehara, Dinh et al. 2009).

Movement of AmiA and AmiC in the periplasm occurs through the twin-arginine protein transport (Tat) pathway. *E. coli* strains with a defective Tat system also exhibited cell division defects with chaining of cells similar to AmiA-AmiC mutants. Exportation of AmiB on the other hand occurs in a Tat independent manner (Bernhardt and de Boer 2003). The same study showed differential distribution of AmiA and AmiC in the periplasm. Whereas AmiA-GFP remained evenly distributed throughout the periplasm irrespective of the cell cycle stage, AmiC-GFP was significantly concentrated around the septal zone of dividing cells, indicative of AmiC recruitment to the septal ring through the action of FtsN. Peptidoglycan hydrolysis by AmiC and its LytM activator factors EnvC and NlpD have also been described in *Xanthomonas campestris* (Xcc) species (Yang, Gan et al. 2018). Xcc lacks AmiA and AmiB, but instead encodes for two homologues of AmiC (AmiC1 and AmiC2). Cell division was significantly affected resulting in chained cells phenotype upon the inactivation of *amiC1, envC* or *nlpD*, however inactivation of AmiC2 had no effect. Severe septation defects were evident upon the deletion of both *amiC1-amiC2*, while complementation of *amiC1* but not *amiC2* reverted the phenotype. Additionally, Yang, Gan et al. (2018) showed that the virulence of *Xanthomonas campestris* was completely lost upon the inactivation of *amiC1*. This effect was attributable mainly to a defective type 3 secretion system (T3SS) than filamentous cell phenotype.

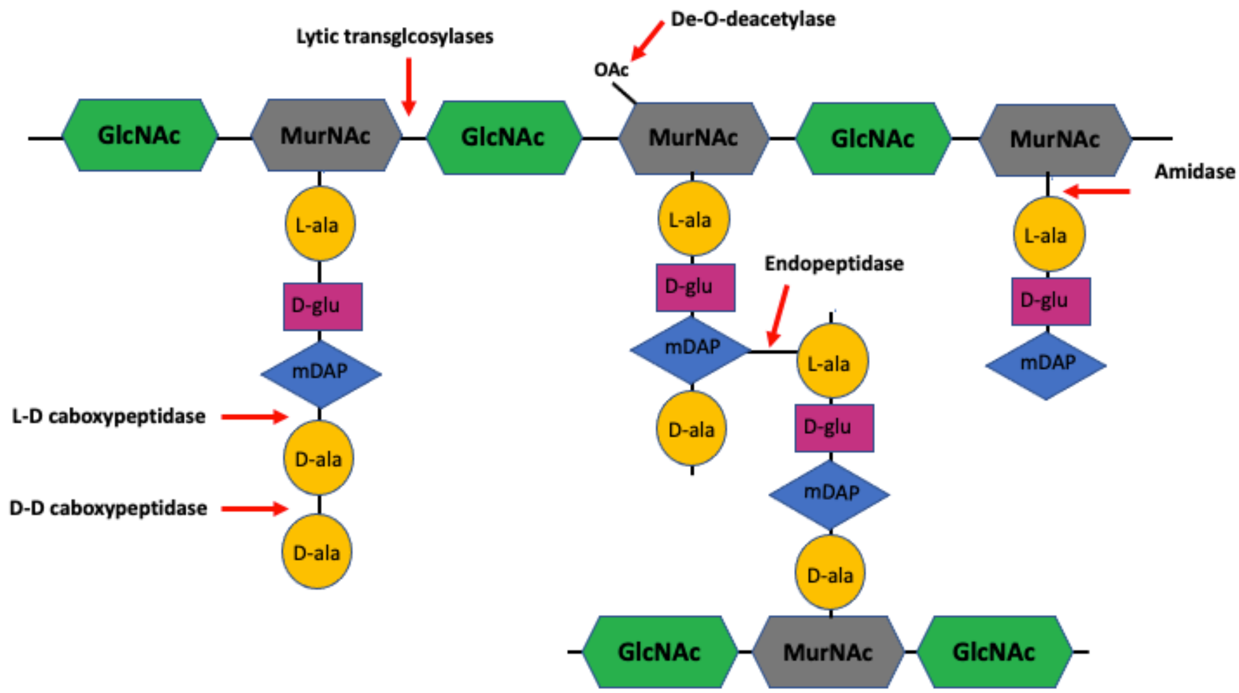

Figure 1.6 : Modes of peptidoglycan hydrolysis during recycling. Cleavage of β-1,-4 link between the *N*-acetylmuramic acid and *N*-acetylglucosamine sugar moieties occurs through the action of lytic transglycosidases, while carboxypeptidases are responsible for shortening of the peptide stem. (Pérez Medina and Dillard, 2018)

Finally lytic transglycosylases (LTs) cleave the glycosidic bond between N-acetylglucosamine and N-acetylmuramic acid disaccharide. Eight LTs have been described in *E. coli,* namely the periplasmic Slt70, outer membrane MltA, MltB, MltC, MltD, MltE and MltF and inner membrane MltG (Dik, Marous et al. 2017). MltG interacts with PBP's of the divisome and its deletion results in the formation of long glycan chains suggestive of PG polymerisation terminating function during cell division. Overexpression of MltA, MltD and MltE resulted in cell shape aberrations. MltA was shown to be active during cell division while MltB and MltC are responsible for the processing of short and long PG strands respectively. The inner membrane permease protein AmpG for example, is involved in the transportation of the glycan and peptide products from the periplasm to the cytoplasm for processing by amidase AmpD before joining the PG synthesis pathway (Johnson, Fisher et al. 2013).

1.2.2 Cell division and elongation

The careful coordination of septal PG synthesis and localization during the bacterial cell growth and division cycle is important in ensuring that the resulting daughter cells are viable. Two modes of peptidoglycan synthesis have been shown to take place during the growth of bacilli. First cell elongation involves lateral PG synthesis resulting in cell length increase, and later cell division or constrictive growth which is characterized by focussed PG synthesis at the mid-cell region while forming the poles for the forming new daughter cells (Szwedziak and Löwe 2013). Inefficient cell division results in the formation of long filaments or chains, whereas the absence of elongation in bacilli results in rounded or ovoid cells. Both cell division and elongation are orchestrated by protein complexes referred to as the “divisome” and “elongasome” respectively (Den Blaauwen, de Pedro et al. 2008). Bacteria employ FtsZ and MreB cytoskeletal elements to position the divisome and elongasome machinery respectively in order to orchestrate cell fission and elongation. This section will review proteins responsible for elongation and division processes and how they impact the bacterial morphology.

1.2.2.1 The elongasome

When not dividing, rod-shaped bacteria have been shown to have peptidoglycan inert hemispherical polar caps, while active peptidoglycan synthesis occurs at the cylindrical side wall resulting in increased cell length (Kawazura, Matsumoto et al. 2017). Growth in bacilli occurs through the gradual increase in length, concomitantly as chromosome replication and segregation takes place before the eventual cell septation that results in new daughter cells. This lateral growth is controlled by an array of proteins referred to as the elongasome. They comprise of the cytoplasmic membrane-associated actin homolog protein MreB, transmembrane proteins PPB2, RodZ and MreC, and integral membrane proteins (IMP) RodA and MreD. MreB is the major protein responsible for elongation and therefore well conserved in bacilli species, while often devoid in most cocci species (Jones *et al.*, 2001). Majority of bacterial species and particularly Gram-negatives have a single copy of *mreB.* However, some rod-shaped Gram-positive species like *B. subtilis* have additional *mreB*-like genes *mbI* and *mreBH* that may have arisen as a result of gene duplication events. The deletion of MreB in *E. coli,* and *B. subtilis* resulted in spherical morphology while crescent-shaped *Caulobacter crescentus* changed to lemon-shaped phenotype with defects in the cell wall integrity resulting in cell lysis (Jones *et al.*, 2001; Figge, Divakaruni and Gober, 2004; Bendezú and De Boer, 2008).

MreB binds to the bacterial cell membrane though the amphipathic N-terminal domain while the C-terminal domain associates with other proteins responsible for the maintenance of cell morphology (Salje, van den Ent et al. 2011). MreB then undergoes polymerization to form short protofilaments that were initially thought to rotate and circumvent the width of rod-shaped cells thereby allowing for lateral PG synthesis (Teeffelen *et al.*, 2011;White and Gober, 2012). On the contrary, recent works have shown that the filaments form short patches that are evenly distributed along the lateral surface of the rods allowing for even PG growth (Errington 2015). MreB protofilaments assemble on the cytoplasmic phase of the cell in an ATP dependent manner, next other elongasome proteins are recruited to direct PG synthesis at the site before hydrolysis of MreB filaments. The movement of these filaments is necessary as it provides the surface required for the insertion of freshly synthesized PG to allow uniform growth during elongation (Garner, Bernard et al. 2011, Strahl, Burmann et al. 2014). Motion of MreB filaments takes place in concert with MreC and MreD proteins, and also RodA-PBP2 complex therefore the loss of any of these proteins may affect the dynamics of MreB (Dominguez-Escobar, Chastanet et al. 2011, Garner, Bernard et al. 2011). Impaired polymerization of MreB monomers into protofilaments can affect the dynamics and eventual localization of the filaments during elongation, as reduced velocity of MreB in S-(3,4-dichlorobenzyl) isothiourea (A22) treated *E. coli* cells was demonstrated (Sun, Weinlandt et al. 2014). Reduced MreB motion in MurA inactivated Fosfomycin treated *E. coli* cells and also in diaminopimelic acid deficient *asd*-1 mutant strain demonstrated that MreB motion is dependent on the availability of PG precursors and new PG synthesis (Teeffelen *et al.*, 2011).

MreB acts as a bridge between the cytoplasmic and periplasmic phases of PG synthesis by orchestrating murein biosynthesis from the cytoplasm through direct or indirect interaction with MreC, MreD, PBP2, RodA and RodZ proteins. Bacterial two-hybrid analysis has shown that MreB interacts with MreC but not MreD, while MreC can interact with both MreB and MreD since it is a linker dimeric transmembrane protein with both cytoplasmic and periplasmic domains. The periplasmic domain is characterized by the presence of β-sandwich core that is flanked by N and C-terminal regions. MreC forms short filaments that associate with MreB in addition to its involvement in the regulation of elongasome activity through the activation of RodA, PBP2 and also interaction with MreD (Rohs *et al.*, 2018; Liu *et al.*, 2020). It has been proposed that RodA-PBP2 complex is a key PG synthase of the cell elongation machinery. Indeed, the interaction of these two proteins activates the respective transglycosylase and transpeptidase activities during elongation.

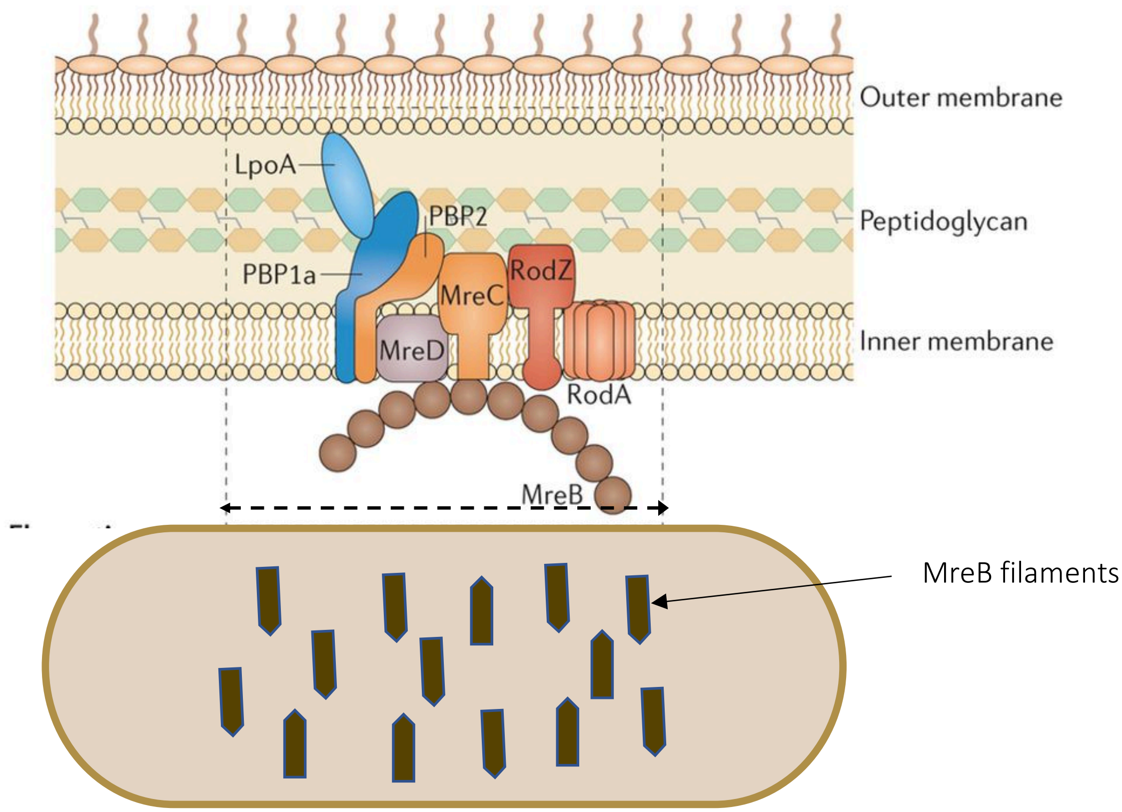

Figure 1.7: Cell elongation components: adapted from (Typas and Sourjik 2015)

In *H. pylori,* PBP2 was shown to poses two structural conformations representing the "active"(on) and "inactive" (off) states in the presence or absence of MreC (Contreras-Martel, Martins et al. 2017). The modulation of PBP2-RodA interaction by MreC and MreD was recently described as a possible mechanism regulating the elongasome system (Rohs, Buss et al. 2018, Liu, Biboy et al. 2020). Through fluorescence resonance energy transfer (FRET) analysis, it was demonstrated that PBP2 interacts with MreC, and similarly PBP2 interacts with MreD. As illustrated in figure 1.8, the enzymatically inactive state of PBP2-RodA complex is activated (on state) upon the interaction of MreC-PBP2 resulting in conformational changes of the PBP2 and ultimately RodA proteins. The activated MreC-PBP2-RodA complex thus promotes MreB filament formation. However an inactive (off state) occurs upon MreD interaction with both MreC and PBP2, thereby supressing the activation of PBP2 by MreC. The inactive "off state" due to MreD interaction with MreC and PBP2 is eventually overcome upon accumulation of cellular MreC that outcompetes MreD thus activating PBP2 and RodA. It is important to also note that RodA has constitutive GTase activity, since it has been shown to have lipid II polymerization activity (Rohs, Buss et al. 2018).

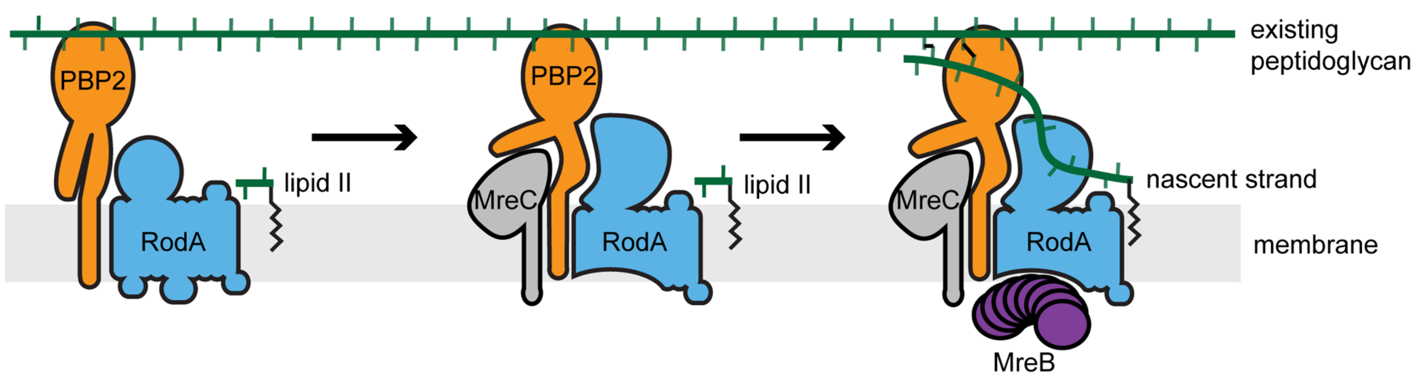

Figure 1.8: Illustration of peptidoglycan regulation during elongation (Rohs, Buss et al. 2018, Liu, Biboy et al. 2020).

Finally, another integral Rod complex transmembrane protein RodZ is important in maintenance of the bacilli morphology since its deletion resulted in rounding of *E.coli* and *B. subtilis* cells. The overproduction resulted in variations of elongated and swollen cells (Shiomi, Sakai et al. 2008, Bendezú, Hale et al. 2009). RodZ also interacts with other elongasome proteins MreB, MreC, MreD, PBP2 and RodA (Ago and Shiomi 2019).

1.2.2.2 The Divisome

Cell division is a complex process that entails the coordination and synchronization of essential functions like PG synthesis, elongation, chromosome replication and segregation. Different studies have used bacterial models like *E. coli, B. subtilis*, *S. aureus, S. pneumoniae* and *C. crescentus* among others to describe at least a dozen essential cell division proteins that are together referred to as the divisome (figure 1.9). The programmed coordination of these proteins ensures that proper PG remodelling, chromosome segregation, complete membrane invagination, and eventual cytokinesis occur without affecting the integrity of the bacterial cell and resulting daughter cells. Genomic analyses of multiple bacterial species have revealed the conservation of most of these proteins, with modest variations in some species. The divisome in *Escherichia coli* is surprisingly similar with most bacterial species, comprising of FtsZ, FtsA, ZipA, FtsI, ZapA, FtsE, FtsX, FtsK, FtsQ, FtsL, FtsB, FtsW, FtsI , FtsN (Du and Lutkenhaus 2017, Choi, Kim et al. 2018). Fts (filamentation temperature sensitive) were initially described in *E. coli* mutants, with FtsZ as the main coordinator for bacterial cell division, cells lacking this protein formed long filaments due to the inability to divide (Hale and de Boer 1997, Sarcina and Mullineaux 2000), while overexpression of FtsZ resulted in *E. coli* mini cells (Ward and Lutkenhaus 1985). A slight variation in some of the divisome proteins in different species is depictive of different protein interactions and by large modes of cell division. For example the divisome of *B. subtilis* comprises of FtsZ, FtsA, FtsL, FtsW, PBP2B (FtsI), ZapA, EzrA, SepF, GpsB, DivIB and DivIVA. In *C. crescentus* the divisome proteins are; FtsZ, ZapA, FtsK, FtsL, FtsW, FtsB, FtsN, FtsQ, FtsI, MipZ, FzlC, FtsE, FzlA, MurG, DipN, FtsA, TolQ, KidO and TipN (Misra, Maurya et al. 2018). It is important to note that other hypothetical proteins that have not been properly characterized also play a role in bacterial cell division. This section reviews some of the common components of the divisome proteins and the overall cell division processes.

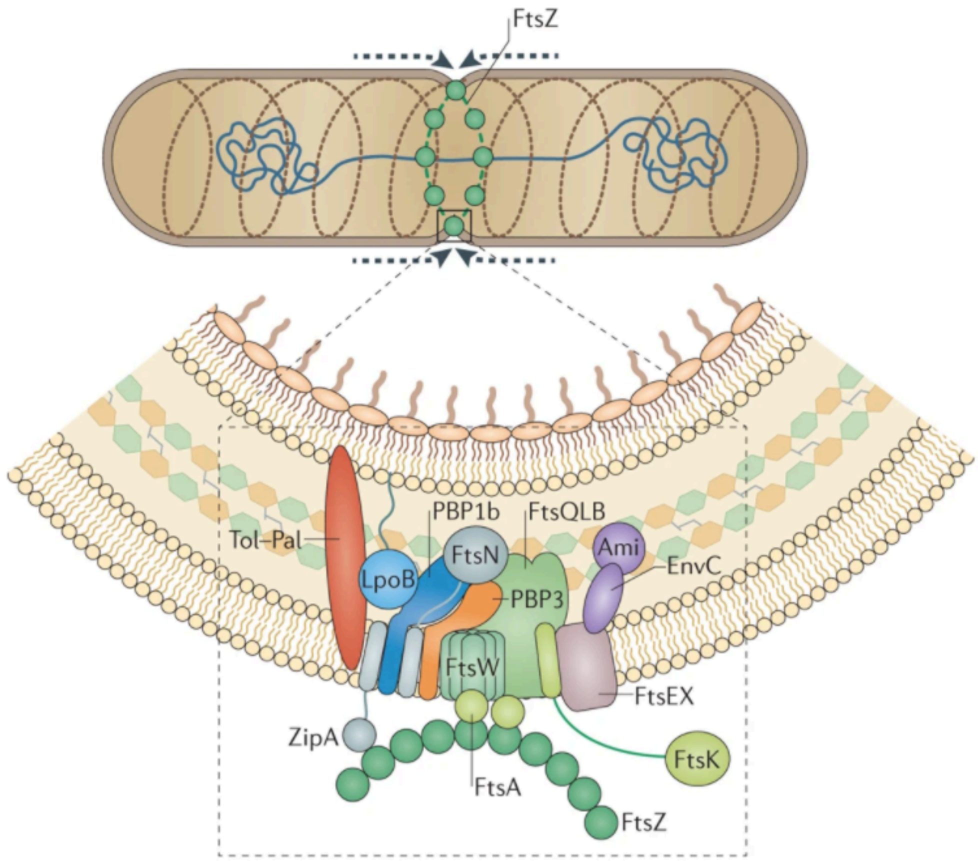

Figure 1.9 : Bacterial cell division machinery (Typas and Sourjik 2015)

In rod-shaped species transverse cell division occurs in three critical steps; (i) chromosome replication, (ii) cell elongation and chromosome segregation (iii) cytokinesis of daughter cells.as illustrated in the *E. coli* in figure 1.10. On the other hand, cocci grow exclusively via division septa whereas ovococci undergo some elongation. Therefore cocci exist as diplococci since they have to divide in order to grow with their division planes alternating in each cell cycle. Ovococci on the other hand have to alternate from peripheral PG synthesis in order to localize new PG at the septum region before division (Zapun, Vernet et al. 2008)

Bacterial cell division begins with the recruitment of tubulin homolog FtsZ to the future site of cell division, here it acts as a hub for sequential recruitment of other divisome proteins. This highly conserved protein is subdivided into 5 domains, the N-terminal peptide (NTP), C-terminal tail (CTT), C-terminal variable region (CTV), C-terminal linker (CTL) and the highly conserved core region that includes N- and C- terminal domains with GTP (Guanosine-5'-triphosphate) -

binding pockets (Vaughan *et al.*, 2003; Buske and Levin, 2012). The C-terminal domain is important for binding and regulating interactions with other divisome proteins. Binding of FtsZ monomers takes place in a GTP-dependent manner resulting in the formation of short FtsZ protofilaments that move across the cell in a treadmilling manner where one end of the polymer grows as the other shrinks to form the Z- ring (García-Soriano *et al.*, 2020). Spatial and temporal regulation mechanisms ensure that the ring forms at the right time in the mid-cell region which is key for the integrity of the dividing cell. Bitopic membrane protein ZipA and actin-like protein FtsA interact with FtsZ through the conserved C-terminal tail to stabilize and anchor FtsZ to the inner membrane.

FtsA protein is responsible for anchoring of the FtsZ ring at the future site of cell division. It also acts by directly interacting and recruiting divisome proteins FtsI and FtsN to the division site. FtsA is also a self-binding protein through its subdomain 2b, the same site that binds FtsZ, hence the cellular concentration of FtsZ to FtsA must be regulated with approximately 5:1 ratio that is established during cell division (Rueda, Vicente et al. 2003). ZipA protein is less conserved than FtsA, however, ZipA performs functions that FtsA cannot, such as the bundling of FtsZ protofilaments, cell membrane invagination and pre-septal PG synthesis (Potluri, Kannan et al. 2012, Cabré, Sánchez-Gorostiaga et al. 2013). Both proteins bind to FtsZ- CTT domain, but ZipA binding deters proteolytic degradation of FtsZ thereby ensuring stability of the forming protofilaments. Both FtsA and ZipA are capable of binding each other and hence can regulate each other. Hydrolytic enzymes like the amidase AmiC and LytM-domain containing EnvC and NlpD are required for PG remodelling and septum fission. In *E. coli* for example, FtsN orchestrates the recruitment of AmiC to the central region of the cell including the septum (Bernhardt and de Boer 2005). Other proteins involved in septal PG synthesis such as PBP3(FtsI) are also recruited at the site of division (Egan, Cleverley et al. 2017). Recruitment of Penicillin-binding proteins PBP1A and PBP1B to the site for pre-septal PG synthesis occurs directly through ZipA or indirectly through FtsA-FtsN protein interactions. It was also demonstrated that Z-ring assembly can occur in the absence of FtsA or ZipA, but consequently the recruitment of divisome proteins FtsE, FtsX and FtsK is not possible unless the two proteins are available (Du, Pichoff et al. 2016).

The assembly of the Z-ring is enhanced through cross-linking of FtsZ polymers by Zap proteins (ZapA, ZapB, ZapC, ZapD and ZapE Deletion of Zap proteins resulted in cell filamentation due to inefficient cell division. ZapA-D are early protofilament proteins that appear at the divisome site before recruitment of ZapE. ZapA facilitates the formation of FtsZ protofilament bundles by reducing GTPase activity of FtsZ. In *E. coli* ZapA was shown to be dispensable during normal growth conditions but essential in stressful conditions (Gueiros-Filho and Losick 2002). Binding of ZapA to FtsZ results in the recruitment of ZapB that enhances chromosome segregation during cell division. Without binding to FtsZ-CTT domain, ZapC uses a different mechanism to regulate Z-ring protofilament stability through its FtsZ-GTPase activity. ZapD (YacF) promotes bundling of FtsZ and its localization to the divisome is FtsZ dependent. It was shown to be the main protein lost during the step-wise cell shape evolution from bacilli to cocci and its deletion in *Neisseria elongata* resulted in cell-shape change (Veyrier *et al.*, 2015). Finally, the exact role of ZapE is still not clear. Early components of the Z-ring are complete upon the incorporation of FtsEX, an ATP-binding cassette transporter-like complex. FtsE forms the nucleotide-binding domain (NBDs) while FtsX is the transmembrane domain (TMD). The FtsEX complex promotes septal PG synthesis and the stability of the divisome by inhibiting FtsA polymerization. Polymerization of FtsA modifies the geometric conformation of the protein hence reducing the tethering efficiency of FtsZ (Hsin, Fu and Huang, 2013). Peptidoglycan hydrolysis during septation is also effected by FtsEX complex as FtsX component associates with LytM domain containing EnvC thereby activating AmiA and AmiB hydrolase activity. FtsEX complex is also necessary for FtsK recruitment to the division site. FtsK localization at the septum occurs through the N-terminal transmembrane domain, while DNA translocation and chromosome segregation occurs through the α and β domains (Du, Pichoff et al. 2016, Du and Lutkenhaus 2017).

In the second phase of cell division, the divisome matures upon the arrival of late divisome proteins, FtsQ, FtsL and FtsB that direct divisome activation by recruiting other divisome proteins and the direct inhibition of PBP1B GTase and PBP3 TPase activities until optimum concentrations of FtsN are obtained at the mid-cell. Localization of FtsQLB complex at the mid-cell occurs through the cytoplasmic N-terminal domains of FtsQ, FtsL and FtsB while the periplasmic C-terminal and transmembrane (TM) domains are important for FtsQLB complex formation. Septum synthesis through transpeptidation and transglycosylation occurs through the ordered recruitment of GTase FtsW, TPase FtsI (PBP3) and the bifunctional PBP1B. FtsW is essential for the localisation of FtsI and PBP1B, FtsW also interacts with other divisome proteins such as FtsL and FtsQ (Boes, Olatunji et al. 2019). Finally, the constriction and cytokinesis of the septum begins upon the accumulation or arrival of FtsN at the division site where it actively recruits PG amidases AmiB and AmiC. Both cytoplasmic and periplasmic cytokinesis occur through FtsN interaction with FtsA and FtsQBL complex respectively (Boes, Olatunji et al. 2019).

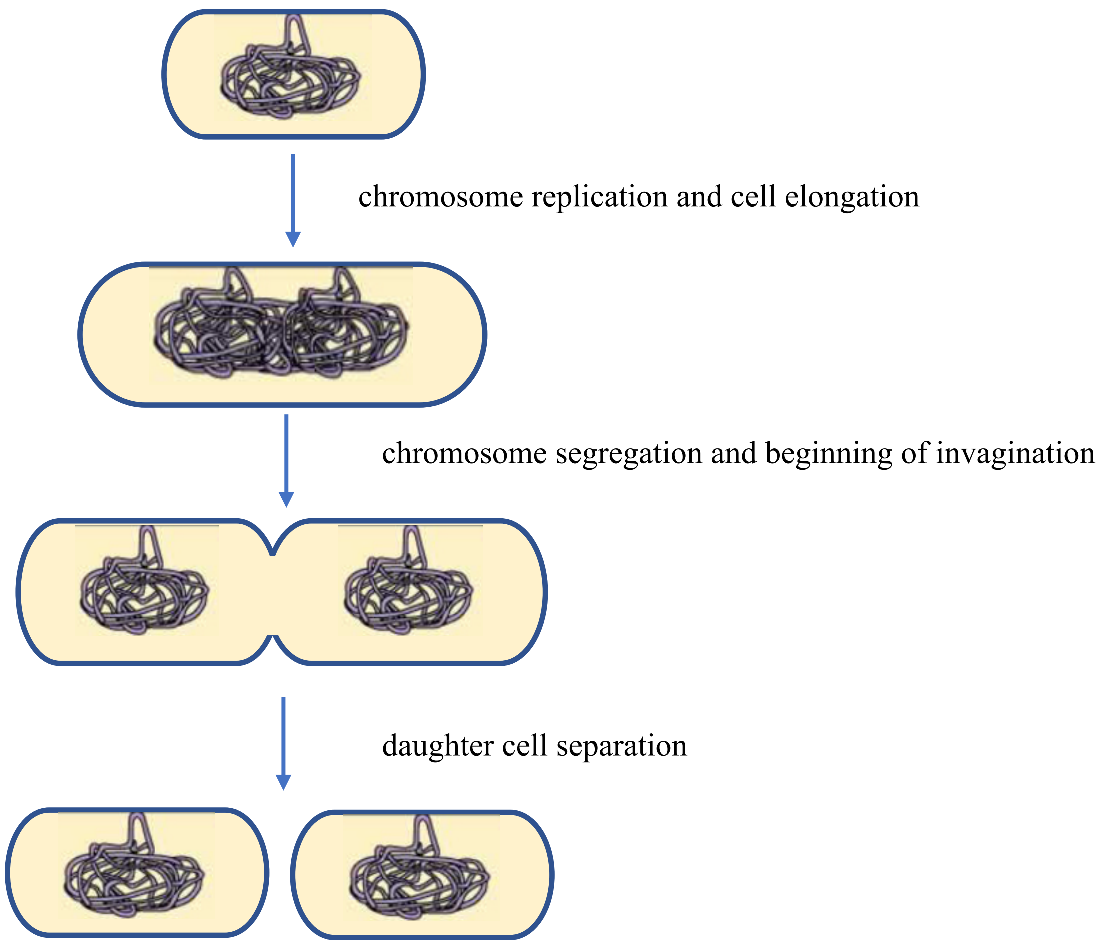

Figure 1.10: Schematic representation of cell division in bacilli shaped *E. coli*. Septation occurs in three steps (i) chromosome replication, (ii) cell elongation and chromosome segregation as cell constriction begins inwards (iii) cytokinesis of daughter cells.

The complexity of bacterial cell division has also been studied in other non-model species, recently Pende *et al.*,(2018) described the molecular mechanisms of divisome and elongasome proteins during the growth and division of a longitudinally dividing rod shaped symbiont of the *Thiosymbion* species. These species colonize the cuticle of marine nematodes, and the longitudinal mode of cell division ensures that both daughter cells remain attached to the nematodes surface upon cell division. By employing fluorescence labelling and high-resolution microscopy, the authors show that the division process starts at the poles, and progress bidirectionally until septation is complete at the mid-region of the cell. The divisome machinery develop from the edges as short arc-shaped complexes which fuse later towards the final stages of septation in a manner similar to Z-ring described in *E. coli.* On the other hand MreB of the elongasome formed medial filaments and that later moved away from the forming septum to localize at the medial regions of the forming daughter cells as illustrated (figure 1.11)

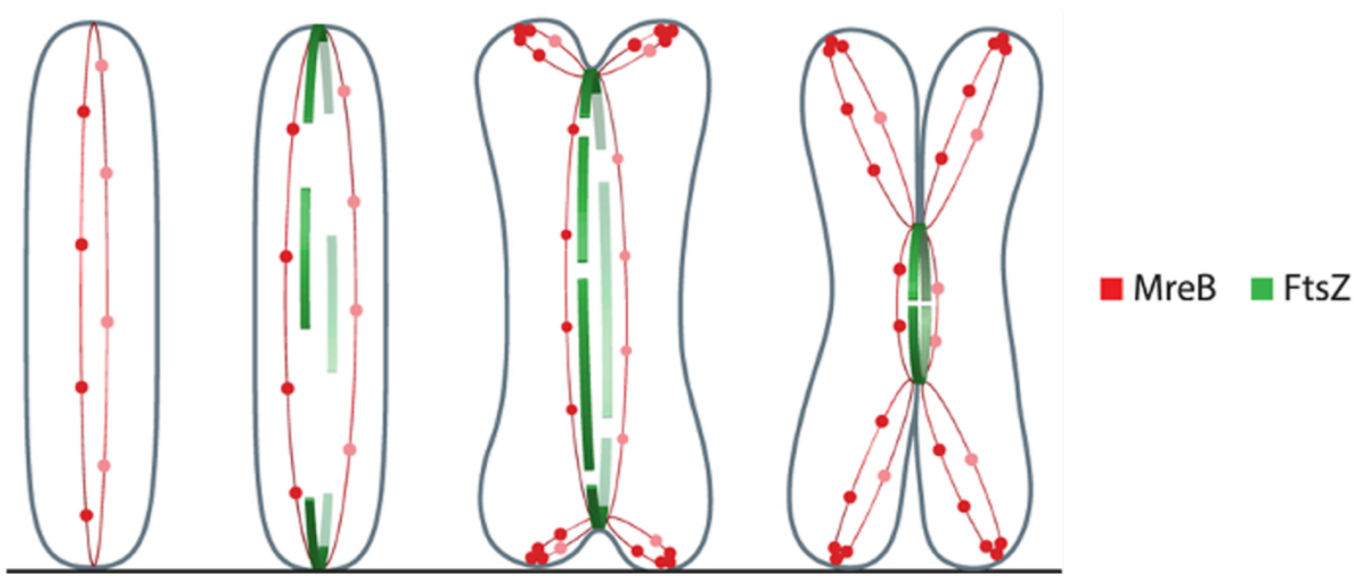

Figure 1.11: The assembly of divisome and elongasome proteins in *Thiosymbion*. The growth pattern of FtsZ and MreB are shown in green and red respectively (den Blaauwen 2018).

1.2.2.3 Positioning of divisome site

The correct positioning of the divisome is paramount for equal partitioning and distribution of chromosomes in newly formed daughter cells. Two negative regulatory mechanisms the Min and Nucleoid occlusion systems ensure the spatiotemporal localization of the Z-ring occurs perfectly by inhibiting its assembly away from the mid-cell region and nucleoid containing regions (Hug, Baker et al. 2016).

1.2.2.4 Min system

Two types of Min systems have been described, , MinCDE is present in Gram-negative bacteria like *E. coli* and DivIVA/MinJ is present in Gram-positives like *B. subtilis*. In *E. coli* the min system defines the mid-cell region for cell division through pole-to-pole oscillation of min proteins, while in a different mechanism that does not involve the oscillation of Min proteins exists in *B. subtilis.* Min systems were described upon the realization that *min* mutants in *E. coli* and *B. subtilis* formed miniature (mini cells) with little or no DNA (Adler *et al.*, 1967). In *E.coli* it is made up of three proteins, MinC, MinD and MinE that are encoded by the *minB* operon. This system prevents Z- ring assembly at and ultimately cell division from taking place at the polar regions of the cell (de Boer, Crossley and Rothfield, 1989). These proteins are partially conserved with few differences in composition across different bacterial lineages, in two bacilli *E. coli* and *B. subtilis*, MinC and MinD are conserved but *B. subtilis* has DivIVA protein in place of MinE. An illustration of the min system is shown in figure 1.12. Transcriptomic analyses studies have shown that MinC and MinD inhibit cell division while MinE acts as a topological specificity factor by confining these proteins at the poles of the cell (de Boer, Crossley et al. 1989). MinC is the effector of the Min system, it is the principal division inhibitor of Z-ring formation. This dimeric protein consists of N- and C-terminal domains on each monomer that are fused by a flexible linker facilitating free movement of the N-terminal domain. The C-terminal domain binds to MinD, and both C and N-terminal domains have FtsZ inhibitory function (Ramm, Heermann et al. 2019). MinC dimers directly bind FtsZ protofilament or indirectly through the action of FtsA or ZipA resulting in protofilament disassembly.

ATP bound MinD interacts with the membrane and subsequently recruits and activates the function of MinC by concentrating it on the membrane. The ATPase-MinD is characterized based on the presence of a conserved N-terminal walker A motif, a central Walker B motif (switch II) and a third motif (switch I), switch I and II mediate the activation and binding of MinC. The C-terminus domain has the membrane-targeting sequence (MTS) for binding the cellular membrane.

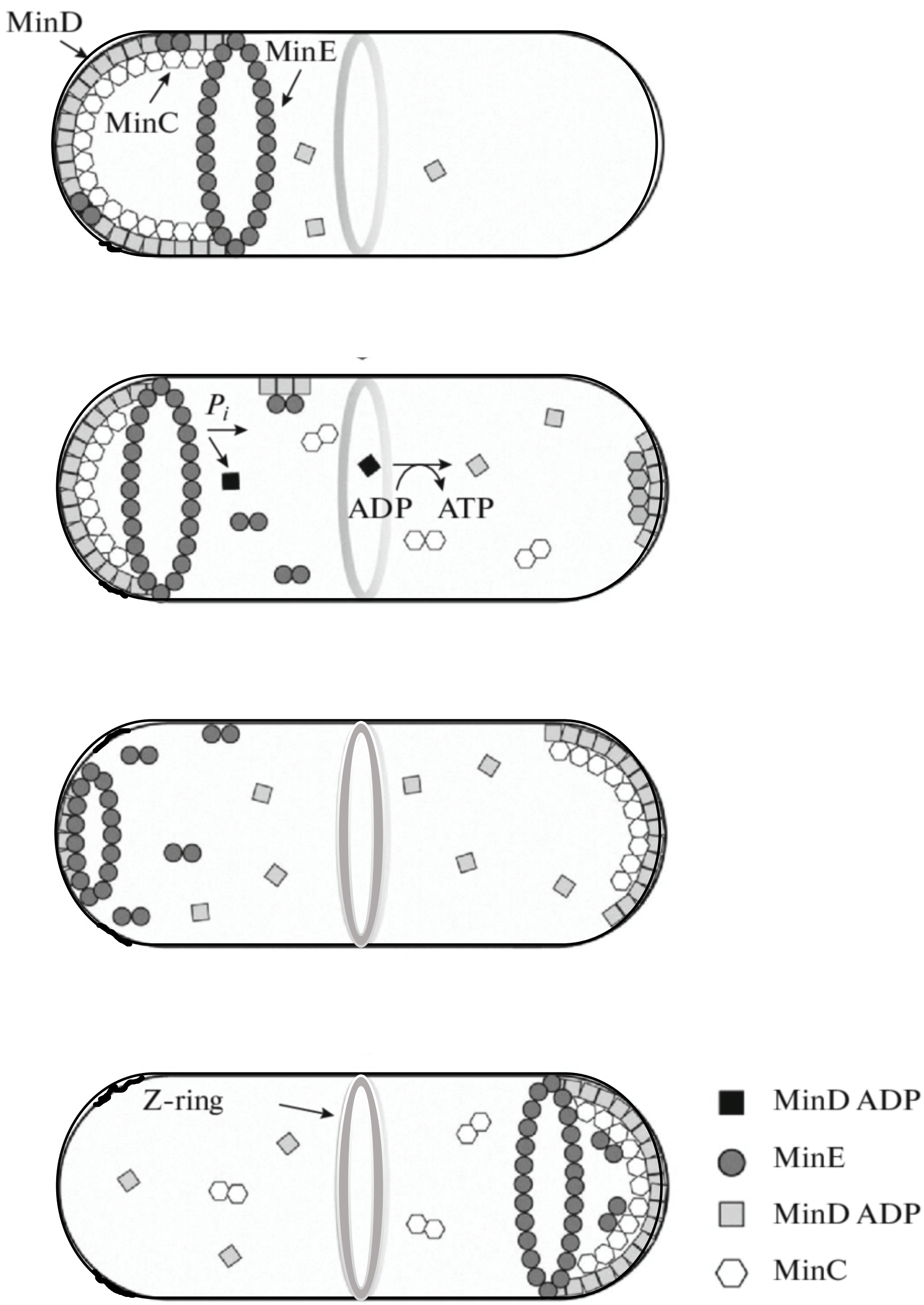

Figure 1.12: Model showing the oscillation of the MinCDE proteins, MinD binds and polymerises on the membrane where it binds MinE and MinC. High concentration of MinC at the poles inhibit the formation of the Z-ring. MinE is responsible for the oscillation of MinCD complex (Dajkovic and Lutkenhaus 2006).

Localization of MinD to the membrane is determined by its nucleotide state, while in its ADP-bound state, MinD is soluble and monomeric, but dimerizes in ATP-bound state facilitating membrane binding. For membrane detatchment to proceed, MinD undergoes ATP hydrolysis reverting to its ADP-bound monomeric state (Ramm, Heermann et al. 2019).

MinE acts as a topology specifying factor for MinCD complex directing the movement form pole to pole in *E. coli* whereas the DivIVA protein in *B. subtilis* is located in the cell poles where it recruits MinCD complex. MinE is a cognate ATPase activator for MinD. This protein has anti-MinCD and topological specificity domains that together restrict the inhibitory role of the min system to the cell poles. The anti-MinCD domain has 2 motifs, the membrane targeting sequence and MinD contact helix. The contact helix is responsible for MinE-MinD interaction that results in ATPase activation of MinD. The anti MinCD domain suppresses the inhibitory activity of MinCD in vivo (Ramm, Heermann et al. 2019).

1.2.2.5 Nucleoid occlusion system

Whereas the Min system ensures that cell division does not occur anywhere but the mid-region of the cell, the Nucleoid occlusion system ensures that the chromosome is not bisected by the newly forming septum during cell division. Aside from protecting DNA, the NO system also helps in the identification of the DNA-free site for divisome assembly (Adams, Wu and Errington, 2014). Two proteins; SlmA in *E. coli* and NoC in *B. subtilis* have been shown to inhibit FtsZ assembly in the chromosome containing regions of the cell. Inactivation of these proteins was associated with cell division occurring over the chromosomes resulting in cell lysis as a consequence of perturbed replication and cell division. These proteins bind to specific DNA binding sequences SBS (SlmA binding sequence) and NBS (NoC binding sequence) present on the entire chromosome. For example the 74 NBS comprising of a 14 bp long inverted repeat sequence in *B. subtilis* (Wu *et al.*, 2009) and 50 SBS comprising of 12 bp palindromic repeats in *E. coli* (Tonthat *et al.*, 2011). The distribution of NBS and SBS is however not uniform with massive under representation in the chromosomal terminal regions present at the mid-cell during later stages of replication indicative of their role in directing of divisome assembly (Wu *et al.*, 2009; Tonthat *et al.*, 2011).

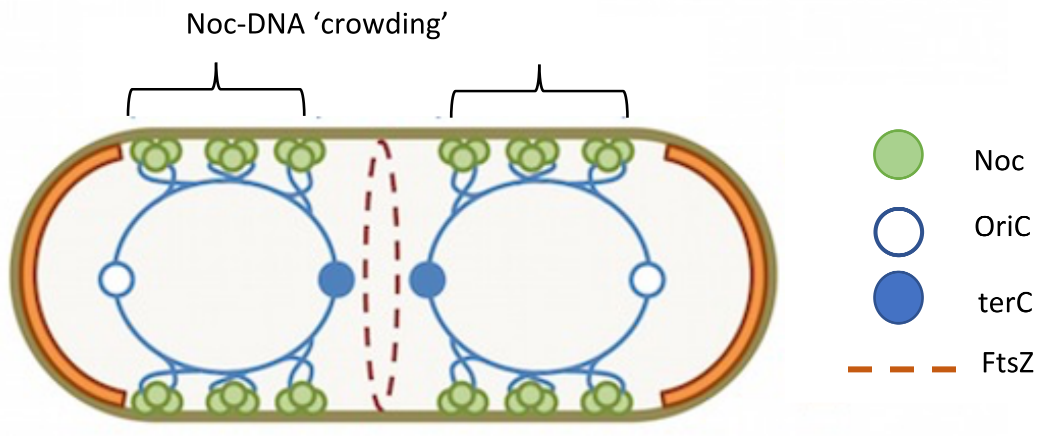

Figure 1.13: The nucleoid occlusion system (Adams, Wu and Errington, 2015)

1.2.2.6 The Division and cell wall cluster

Evolutionary dynamics of bacterial genomes have resulted in few conserved gene clusters, one example is the division and cell wall (*dcw*) cluster that consists of three sets of genes; those involved in the regulation of cluster (*mraZ, mraW*), genes involved in cell division (*ftsL, ftsI, ftsW, ftsQ, ftsA, ftsZ*) and PG synthesis genes (*murE, murF, mraY, murD, murG, murC, ddl)*. Besides majority of the genes in this being oriented in the same direction, conservation in terms of gene content, order and even regulation pattern in evolutionary diverse bacteria and particularly bacilli is remarkable (Martinez-Torro, Torres-Puig et al. 2021). The plausible reason for conservation and ordering patterns across different bacterial lineages, where sets of colocalized genes such as *ddiB -ftsQ-ftsA-ftsZ* exist is the need to have them co-expressed for the coordinated cell cycle process such as cell division (Vincente *et al.*,1998).

The classical example of *dcw* cluster conservation is described in *E. coli* which possesses a large and compact *dcw* cluster consisting of 15 tightly packed genes that span a region of approximately 17.8 kb. Other examples include the 18.9 kb *dcw* cluster in *B. subtilis* that consists of with 17 genes and16 kb long cluster in *H. influenzae* with 17 (Snyder, Saunders et al. 2001). Even though the *dcw* cluster is quite conserved, some variations exist for example; the presence of species-specific genes such as the sporulation essential *spoVD* and *spoVE* in place of *pbpB* and *ftsW* in *B. subtilis.* The cluster in *Neisseria meningitidis* and *Neisseria gonorrhoea* have 15 *dcw* specific genes, with the presence of competency associated *dca* gene between *murE* and *murF*

(Snyder, Saunders et al. 2001). The size of the *dcw* cluster may vary with some species having undergone significant reduction for example cocci shaped *Staphylococcus aureus* has 9 genes while *mycoplasma* species have 3 to 4 genes. Mycoplasma species lost all the peptidoglycan synthesis genes in the cluster but retained the essential genes required for cell division. In some bacterial species, the *dcw* genes are located at different locations in the chromosome while some are characterized with the presence of large intergenic regions. A recent study that looked at *dcw* cluster in 1000 bacterial genomes showed that the cluster was conserved in terms of content and gene order in 57% of the genomes. However 32 % of the genomes had a fragmented cluster while in 10% of the genomes some genes were totally absent or colocalized with other non *dcw* cluster genes elsewhere in the genome (Megrian, Taib et al. 2022).

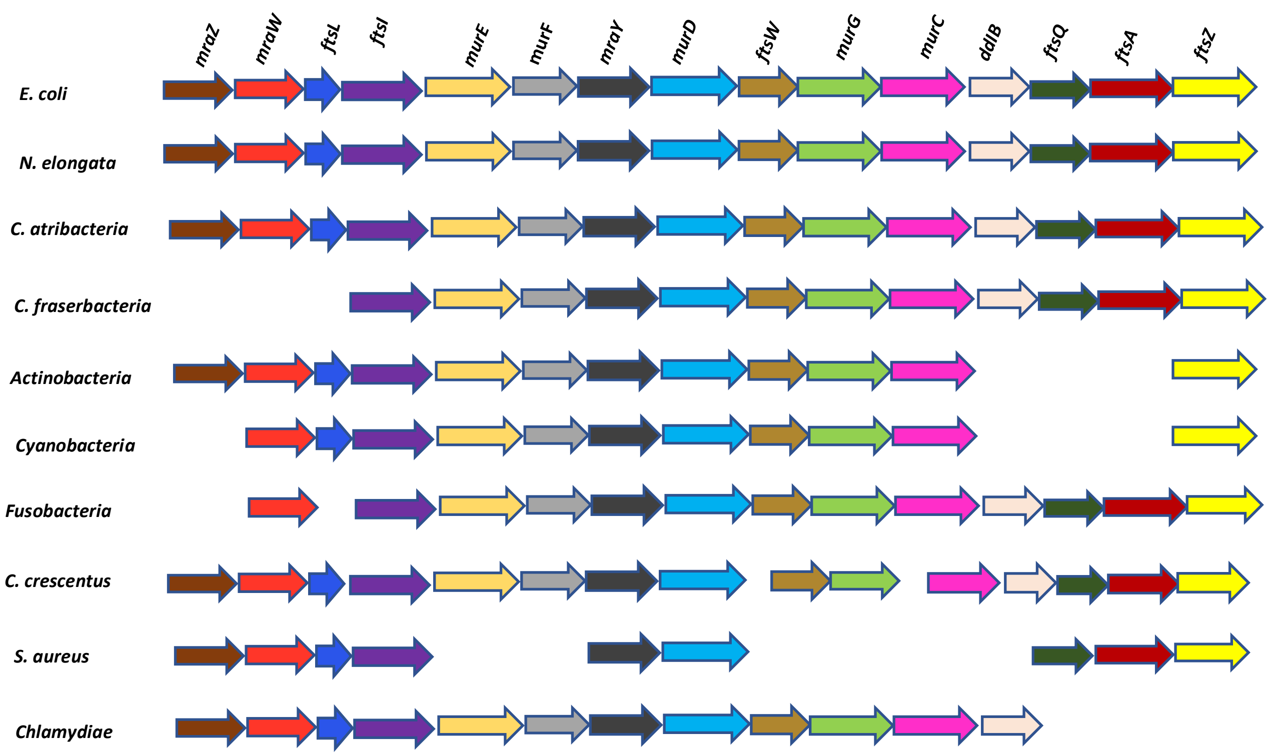

Figure 1.14: Gene content of the division and cell wall cluster across different bacteria. Adapted from (Megrian, Taib et al. 2022)

1.3 Regulation of peptidoglycan synthesis, cell division and elongation genes

Bacteria can sense and respond to various intra and extra-cellular signals through transcriptional regulation of genes required for survival in varying conditions. Transcriptional regulation is the process through which conversion of DNA to RNA and translation of RNA to protein is controlled. A transcriptional unit (TU) comprises of; the promoter, the structural gene and terminator. The TU may consist of only one gene or multiple genes that are transcribed as monocistronic and polycistronic mRNA respectively. Transcription units may overlap when genes are transcribed by multiple promoters. Generally, positive regulators bind upstream the gene promoter to initiate transcription, while negative regulators supress transcription upon binding to the operator sequence. The regulation of peptidoglycan synthesis genes, the elongasome and divisome machinery may have a temporary or even permanent impact on the bacterial morphology. To-date several bacterial proteins have been identified to regulate these processes and in this subsection the roles of MraZ, RapZ and BolA proteins in the regulation of key bacterial cell shape associated factors is reviewed.

1.3.1 Division and cell wall cluster transcriptional regulator protein MraZ

The conservation of *mraZ* gene in terms of sequence and location (the first gene of the *dcw* cluster) in most bacteria highlights its relevance in the regulation of genes in this cluster. Studies in *E. coli* have demonstrated that σ^{70} *mraZ* promoter P_{mra} to inhibit the transcription of upto twelve genes in the *dcw* cluster (Hara, Yasuda et al. 1997, Vicente, Gomez et al. 1998). The possibility of having a single polycistronic mRNA transcript spanning about 17 Kb was recently demonstrated in *B. cenocepacia* J2315(Trespidi, Scoffone et al. 2020). The presence of *mraZ* in cell wall devoid *Mycoplasma* spp. may imply its importance during cell division in these species, besides the possibility of having other unknown regulatory functions (Fisunov, Evsyutina et al. 2016). Eraso, Markillie et al. (2014) demonstrated that MraZ binds to a set of three nucleotide DNA binding repeat sequences "TGGG[A/G]" that are located upstream of *mraZ* gene but downstream of the promoter $P_{mra.}$ The DNA binding repeats are separated by five nucleotide spacer sequences as illustrated in figure 1.15.

Figure 1.15: an illustration of the DNA sequence of the *mraZ* regulatory region; the promoter *Pmra* is highlighted in green, DNA repeat sequences are shown in red and the start of *mraZ* CDS in yellow. Adapted from (Eraso, Markillie et al. 2014).

The authors also show that MraZ to binds to its own promoter, and therefore represses its own expression and a further ten genes of the *dcw* cluster. By overexpressing MraZ, cell division was inhibited resulting in cell filamentation, additionally overexpression was toxic to the cells. The toxicity effect is reversed upon the overexpression of the second *dcw* cluster gene *mraW*. Interestingly in *Mycoplasma* model, three MraZ binding repeat sequences AAAGTG[G/T] were described. Additionally overexpression of MraZ resulted in the upregulation of *dcw* cluster genes and subsequently resulting in moderate filamentation of cells, there were no toxicity effects associated with overexpression of the protein (Fisunov, Evsyutina et al. 2016). Quite recently White, Hough-Neidig et al. (2022) demonstrated the regulatory role of MraZ in *B. subtilis*. They describe GTGG[A/T]G as the MraZ binding repeat in this species. Overexpression of MraZ repressed the expression of MraZ, MraW, FtsL, and PbPB, resulting in filamentation of the cells. Similar to the cytotoxicity effect described in *E. coli,* cell lysis was also observed in MraZ overexpressing in *B. subtilis*. However, overexpressing of MraW did not rescue this toxicity effect as was the case in *E.coli.* Co-overexpression of PbPB and MraZ also resulted in impaired cell division, however proper cell division was restored upon co-overexpression MraZ and FtsL. This finding implicates the repression of FtsL as an important factor associated with impaired cell division in *B. subtilis*. Finally, the authors employed fluorescent D-amino acid labeling to show that PG insertion was dysregulated in the absence of FtsL during cytokinesis.

1.3.2 RNAse adaptor protein RapZ

In Gram-negative bacteria the biosynthesis of peptidoglycan precursors; uridine diphosphate N-acetylglucosamine (UDP-GLcNAc) and glucosamine-6-phosphate (GlcN-6-P) is encoded by the glmUS operon. Glucosamine-6-phosphate synthase (*glmS*) catalyzes the first reaction in the synthesis of D-glucosamine-6 phosphate (GlmS) from D fructose-6 phosphate from glycolysis pathway. Regulation of cellular GlmS concentrations occurs through the activation or inhibition of *glmS* by the adaptor protein RapZ and Hfq-dependent small RNAs; GlmZ and GlmY (Khan *et al.*, 2016, 2020; Gonzalez *et al.*, 2017). Both sRNAs compete for RapZ binding, GlmY outcompetes GlmZ through its translation and functions by acting as a decoy that binds RapZ liberating GlmZ for processing by RNase E.

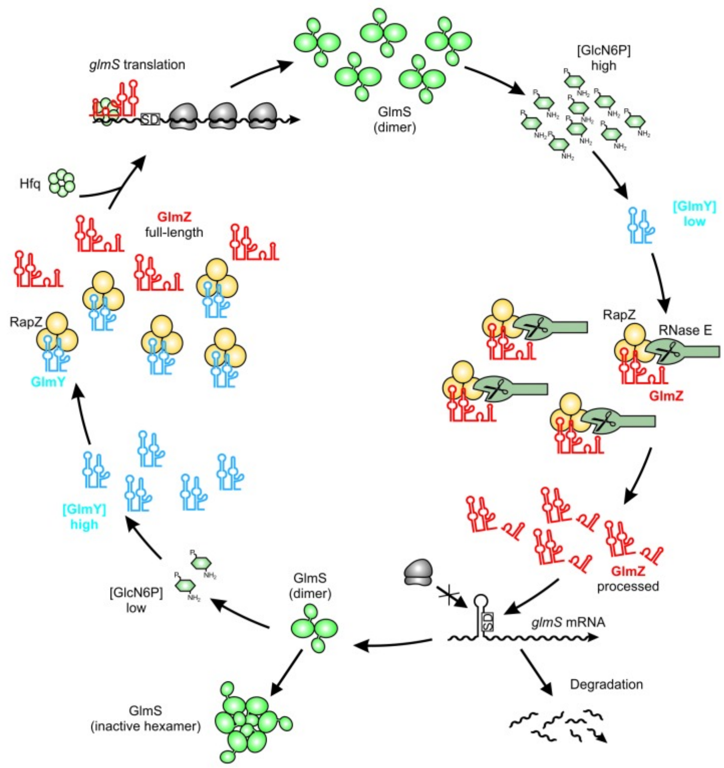

Figure 1.15: Illustration of the regulation of cellular GlcN6P in *E.coli*. Regulation occurs through the action of RapZ and small RNAs GlmY and GlmZ in *E. coli*

As illustrated in figure 1.15, when the intracellular GlcN6P concentrations are high, RapZ binds to GlmZ, RNase E ribonuclease is activated to cleave GlmZ at the *glmS*-binding site resulting in the termination of Glucosamine 6 phospate synthetase (GlmS) synthesis. The depletion of cellular GlcN6P is sensed by RapZ triggering increased transcription of GlmY (Khan and Görke, 2020). GlmY together with processed GlmZ residues that still retain the ability to bind RapZ, sequester the RBP allowing unprocessed GlmZ to bind *glmS* mRNA. This action results in the transcription and translation of GlmS to restore GlcN6P concentrations. GlmY-RapZ binding also diminishes QseE/QseF activation and over time the concentrations of GlmY diminish while GlmZ concentrations increase. The deletion of *rapZ (yhbJ*) in *E. coli* leads to over production of GlmS (Göpel, Khan et al. 2016).

1.3.3 The morpho gene *bolA*

BolA a 13 kilodaltons (KDa) protein is implicated in growth response regulation during the exponential growth phase in the presence of different stress conditions. Two promoters, *bolAp1* and *bolAp2* are responsible for *bolA* regulation. During stressful conditions like heat shock, carbon starvation and osmotic stress. The gearbox promoter *bolAp1* controlled by factor sigma factor σ^S (encoded by *rpoS*) is activated, while the constitutive *bolAp2* controlled by sigma factor σ^{70} is regulates the gene during optimal growth conditions (Aldea *et al.*, 1989; Santos *et al.*, 1999; Freire *et al.*, 2006). BolA protein was demonstrated to impact on bacterial morphogenesis when its overexpression in *E. coli* resulted in a spherical morphology (Aldea *et al.*, 1988). Similarly in filamentous cyanobacterium *Fremyella diplosiphon* , overexpression of BolA resulted in spherical phenotypes (Singh and Montgomery, 2015). Considering that bacilli shaped bacteria become spherical upon the deletion of *mreB* and the fact that overexpressing BolA results in rounding of bacilli, validates the regulatory role of BolA the elongasome machinery. To determine the mechanism through which BolA regulates the elongasome, Freire and colleagues (2009) showed that increased expression of BolA negatively affects the concentration, distribution and dynamics of MreB filament. In this study BolA overexpressing strains were unable to elongate as they showed significant reduction in MreB concentration (3 times reduction compared to the wild type). Further dot-blot analysis showed a reduction in *mreB* transcripts upon overexpression of *bolA*. Indeed increased levels of BolA were shown to downregulate *mreBCD* operon by up to 64%. Extensive research on *bolA* transcription by Freire and other groups have concluded that BolA is a negative regulator of *mreB* and downregulation occurs as a result of direct binding of BolA to the *mreB* promoter. Post-translational modification of BolA through phosphorylation was shown to reduce BolA binding efficacy to *mreB* promoter resulting in increased *mreB* transcription in phosphomutants when compared to BolA overexpressing *E. coli* strain, further corroborating the inhibitory effect of *mreB* by BolA (Galego *et al.*, 2021). Overexpression of both MreB and BolA resulted in mixed cell phenotypes suggesting that overexpression of MreB seemed to reduce BolA rounding effect on cells but is not sufficient to rescue the rounding and shortening of cells. The interaction of BolA with the divisome machinery cell division as active *ftsZ* gene products were required for the realization of spherical morphology in overexpressing *E. coli* strains(Aldea, Hernandez-Chico et al. 1988). Besides being an inhibitor of *mreB* transcription, BolA was shown to upregulate the transcription of D,D carboxypeptidases PBP5 and PBP6 (Aldea *et al.*, 1988; Santos *et al.*, 2002). Overexpression of PBP5 was previously shown to convert *E. coli* cells from bacilli to cocci (Markiewicz *et al.*, 1982). In conclusion overregulation of BolA seems to play a vital role in switching from cell elongation to septation besides being part of a complex network of protein interactions impacting on the bacterial growth, division, peptidoglycan synthesis and overall morphology.

1.3.4 Lipid composition and protein-phospholipid localization

Bacterial membranes are comprised of various phospholipids that interact with several proteins including those of the divisome and elongasome. Initial characterization of bacterial phospholipids was done in *E. coli* and *B. subtilis* revealing a remarkable difference in their percentage composition. In *E. coli* zwitterionic phosphatidylethanolamine forms 70% of the membrane, while anionic phosphatidylglycerol and cardiolipin from 20% and 10% respectively. In *B. subtilis* PE zwitterionic phosphatidylethanolamine composition is 20% while the anionic phosphatidylglycerol and cardiolipin are 40% and 25% respectively while the remaining 15% comprises of zwitterionic lipid lysyl-phosphatidylglycerol (Barák and Muchová 2013). Anionic phospholipids have been shown to be abundant in both *E. coli* and *B. subtilis* polar caps. Additionally they were shown to have preferential interaction with monomeric MreB, compared to MreB polymers, thereby excluding MreB filaments from the poles and hence promoting MreB localization to the cylinder portion of *E. coli* cell to direct elongation (Kawazura, Matsumoto et al. 2017).

The variation in lipid composition may be responsible for differential interactions between membranes and proteins in different species. Presence of Cardiolipin at the bacterial cell poles and also the site of cell septation impacts the localization of several proteins (Barák and Muchová 2013).

Cardiolipin plays a role in *E. coli* division through the direct interaction with the divisome protein MinD to promote localization of MinD to the cell membrane. (Renner and Weibel 2012), Cardiolipin mutant *Rhodobacter sphaeroides* strains had difficulties in dividing resulting in ellipsoid shaped cells (Lin, Santos et al. 2015). Through the membrane targeting sequence (MTS) of MinD the interaction between the protein and membrane lipids is enhanced. MTS in both *E.coli* and *B. subtilis* have been shown to preferentially bind to anionic phospholipids. Another protein FtsA has a positively charged amphipathic helix that is required for membrane binding and hence localization.

Lipid domain/organization	Proteins
Cardiolipin	MreB, MinD
Phosphatidylglycerol	MinD, FtsA, MreB
Negative curvature membranes	DivIVA
Positive curvature membranes	SpoVM
Membrane potential	MinD, FtsA, MreB, Mbl

Table 1.3: Proteins and phospholipids interactions and localization in bacterial cells: Lipid composition of the membrane or membrane domain determines the localization of divisome and elongasome proteins (Barák and Muchová 2013)

1.3.5 Membrane curvature affects divisome localization

The localization of proteins on the cell membrane is also dependent on the curvature of the cell membrane, the negative curvature (concave shape) and positive curvature (convex shape). In *B. subtilis*, DivIVA protein recognizes the negative curvature, therefore localizing at these polar sites and hence recruits the Min system proteins (MinJ, MinD, MinC) that prevent premature septation at these sites (Barak and Wilkinson 2007). DivIVA binding to the cell membrane occurs through its N-terminal domain. The protein distinguishes varying degrees of membrane negative curvature, with preferential localization to the most concave surface. This explains why it localizes at septation sites but not the poles. The effect of positive curvature was also demonstrated during sporulation in *B. subtilis,* where it was linked to asymmetric division through the aid of sporulation protein SpoVM. The cell divides into a larger mother cell and smaller forespore (Ramamurthi, Lecuyer et al. 2009).

2. *NEISSERIACEAE*; A NEW MODEL TO STUDY CELL SHAPE EVOLUTION

Today a better understanding on bacterial cell shape is achievable by taking advantage of technological advances in molecular biology, sequencing and imaging technologies in addition to the increased interest in studying atypical model bacterial species with varying morphologies (van Teeffelen and Renner 2018, Egan, Errington et al. 2020, Hollard 2022). This chapter explores the relevance of using bacteria from the *Neisseriaceae* family as an alternative model to study bacterial morphogenesis. In particular, the oral cavity symbionts *Simonsiella muelleri, Alysiella filiformis, Alysiella crassa, Conchiformibius Kuhniae,* and *Conchiformibius steedeae* that exist as multicellular filaments with longitudinal cells division are presented. Given that bacteria in the *Neisseriaceae* family exist as bacilli, cocci and multicellular filamentous morphologies, it is advantageous to use a common ancestral model "bacilli" shaped *Neisseriaceae* to study cell shape evolution of cocci and multicellular morphologies. Additionally this model can be employed in the study of transverse to longitudinal cell division.

2.1 The oral cavity microbiome in mammals

The collective genome of all microorganisms residing in the oral cavity is referred to as the oral microbiome. In mammals, the abundance and diversity of the oral microbiome is only second to the gut microbiome (Deo and Deshmukh 2019). Bacteria in the oral cavity are adapted to colonize several surfaces including the teeth, tongue, hard palate, soft palate, gingival sacculus and tonsils. The microbiome can be divided into two, the core microbiome that is common in all individuals, while variable microbiome is unique depending on physiological differences, nutrition habits and lifestyle among other factors (Deo and Deshmukh 2019). Additionally, the diversity can also be site specific due to the differences in the biological and physical properties, for example; the tongue area has larger bacterial diversity in comparison to the buccal and palatal mucosa regions (Costello, Lauber et al. 2009, Li, Liu et al. 2022). A symbiotic relationship exists between oral cavity commensals and their hosts. While the bacteria help in maintaining metabolic, immunological and physiological functions such as digestion of food, priming of the host mucosal immune system, and physically by producing antimicrobial compounds that prevent the thriving of pathogenic species, the microbes benefit by utilizing nutrients that the hosts may not need.

Some of the common oral cavity bacterial genera found in healthy humans include; Gram-positive cocci (Streptococcus, *Peptostreptococcu, Stomatococcus, Abiotrophia)* Gram-positive rods (*Lactobacillus, Actinomyces, Corynebacterium, Bifidobacterium, Eubacterium, Pseudoramibacter, Rothia, Propionibacterium*) Gram-negative cocci (*Neisseria, Moraxella, Veillonella)* Grem-negative rods (*Hemophilus,Campylobacter, Desulfobacter, Eikenella, Treponema, Fusobacterium, Leptotrichia, Prevotella, Selemonas, Capnocytophaga, Desulfovibrio, Wolinella)* and Gram-negative multicellular (Simonsiella)(Deo and Deshmukh 2019). The prevalence of *Simonsiella muelleri* isolates in healthy individuals varies from 0.5-32 percent, with highest colonisation occurring on dorsal surface of the tongue and the hard palate containing 95% and 88% of the isolates respectively (Pankhurst, Auger et al. 1988, Dafar, Bankvall et al. 2017). Nyby, Gregory et al. (1977) isolated 66/67 "*Simonsiella*" from cats and dogs, The subsequent sections shall review in details the cellular organization of longitudinally dividing multicellular shaped *Neisseriaceae* genera that reside in the buccal cavity of man and other mammals like cats, dogs and pigs.

2.2 The *Neisseriaceae* family

Members of the *Neisseriaceae* family, order *Neisseriales* are Gram-negative, oxidase-positive, ß-proteobacteria aerobes that mainly colonize the mammalian mucosa. Some avian and insect and environmental *Neisseria* species have also been isolated (England and Gober, 2001). Majority of the members in this family have bacilli and cocci forms, while few exist as unbranched filamentous multicellular forms. According to https://www.mindat.org/taxon-5440.html , the family *Neisseriaceae* consists of 12 genera namely: *Alysiella, Chromobacterium, Conchiformibius, Crenobacter Bergeriella, Eikenella, Kingella, Morococcus, Neisseria, Simonsiella, Snodgrassella, Stenoxybacter, Uruburuella, Vitreoscilla* (Parte 2018, Chen, Rudra et al. 2021). Approximately 26 species in the genus *Neisseria* have been characterized to date, they often colonize the mucosal surfaces without causing disease and are hence referred to as commensal microbiota. Only two species; *Neisseria meningitidis* and *Neisseria gonorrhoeae* are pathogenic to man. *Neisseria meningitidis* (the Meningiococcus) is a leading cause of bacterial meningitis and septicemia. An annual estimate of 500,000-1,200,000 Invasive Meningiococcal Disease (IMD) occur worldwide, with a 10% case fatality rate (Chang, Tzeng and Stephens, 2012; Dwilow and Fanella, 2015). *Neisseria gonorrhoeae* (gonococcus) colonizes the urogenital tract to cause gonorrhoea, a sexually transmitted disease accounting for approximately 87 million cases annually (Yang *et al.*, 2018; Rowley *et al.*, 2019). Cases where gonococcal isolates have also been recovered from rectal, and oropharyngeal surfaces (Kent *et al.*, 2005; Budkaew *et al.*, 2019) is a reason for concern about the evolution of these species majorly through genetic recombination. Infections caused by other *Neisseriaceae* mainly of the *Neisseria* genus have been sporadically documented mostly in immunocompromised individuals or neonates (Whitehouse, Jackson et al. 1987, Garcia, Descole et al. 1996, Safton, Cooper et al. 1999, Han, Hong et al. 2006, Everts, Speers et al. 2010, Humbert and Christodoulides 2019).

2.3 Cell shapes in *Neisseriaceae* family

In terms of morphology, *Neisseriaceae* exist either as bacilli, cocci or filamentous multicellular forms. Each of these morphologies has evolved different mechanisms to potentiate their colonisation and survival in the mammalian mucosa. Considering surface adherence as an example, cocci shaped species have a relatively smaller surface in contact with the host's membrane, whereas the length in bacilli offers a larger surface for adhesion. Examples of filamentous multicellular *Neisseriaceae* include *Simonsiella muelleri*, *Conchiformibius steedae* and *Alysiella filiformis,* all with unique and interesting morphologies. These species are part of the normal flora in the oral cavity of man and other warm-blooded vertebrates including domestic animals like sheep, cats, dogs, rabbits, horses, guinea-pigs, goats, cows and pigs (Nyby, Gregory et al. 1977). Both *Simonsiella* and *Conchiformibius* genera exhibit a dorsal (convex)-ventral (concave) differentiation in relation to the positioning on a solid surface, with the dorsal side orientated away from the contact surface. The ventral surface is associated with the host's squamous epithelial cells where it is important for bacterial attachment through numerous fimbriae consisting of adhesins. These long hair-like proteinaceous structures extend from the outer membrane (in Gram-negatives) and are responsible for stable cell attachment especially under flow conditions. Modes of fimbriae-host cell attachment include hydrophobic interactions between fimbriae and host cell surface and specific binding of fimbriae to glycosylated mammalian cells rich in mannose (Connell, Agace et al. 1996). Besides attachment, fimbriae also facilitate the gliding mode of movement that occurs along the long axis of the filaments (Pangborn, Kuhn et al. 1977, Gregory, Kuhn et al. 1985). McBride (2001) defines gliding motion as "the smooth translocation of cells over a surface by an active process that requires energy expenditure”. During gliding, cell movement follows the long axis and does not require flagella action.

2.3.1 *Simonsiella muelleri*

The typical morphology of *S. muelleri* is composed of an aggregation of approximately 8-12 or even more cells that are fused, forming giant filaments measuring over 50 µm. Each individual cell is relatively flat 0.5-1.3 µm with varying length and width measurements ranging from 0.8-2.6 µm and 0.4-1.0 µm respectively (Kuhn 2006). Cells on the extremes are smaller in size thus resulting in a tapered end appearance and an overall crescent-like shape. The cells have long fimbriae-like structures on both poles that are important for attachment and gliding motion.

2.3.2 *Conchiformibius* species

The *Conchiformibius* genera is composed of two species; *C. steedae and C. kuhniae.* Cells in these species form long ribbon-like filaments (usually longer than *S. muelleri* filament) that are slightly curved with concave and convex sides. A major difference between *Conchiformibius* species and *S. muelleri* is that all cells in the filament are relatively the same size unlike the tapering edges of cells in *S. muelleri* filament. The length of the cells measures approximately 1.8-2.4 µm while the width is 0.4-0.8 µm. *Conchiformibius* species have fimbriae on both poles of the cell, that are important for attachment and movement through gliding.

2.3.3 *Alysiella* species

Alysiella genera is also composed of two species; *A. filiformis* and *A. crassa* that exist as filaments of 4-8 pairs or more cells. Each pair of cells appears to be more tightly fused when compared to the fusion between adjacent pairs. Each individual cell is oblong disk-shaped, lacks the concave or convex sides and also exhibits gliding mode of movement. The cells are relatively uniform in size, each cell measuring approximately 1.6-3.0 µm in length by 0.4-0.8 µm in width (Kuhn 2006). Unlike *S. muelleri* and *Conchiformibius* genera, these species have fimbriae only on the proximal pole.

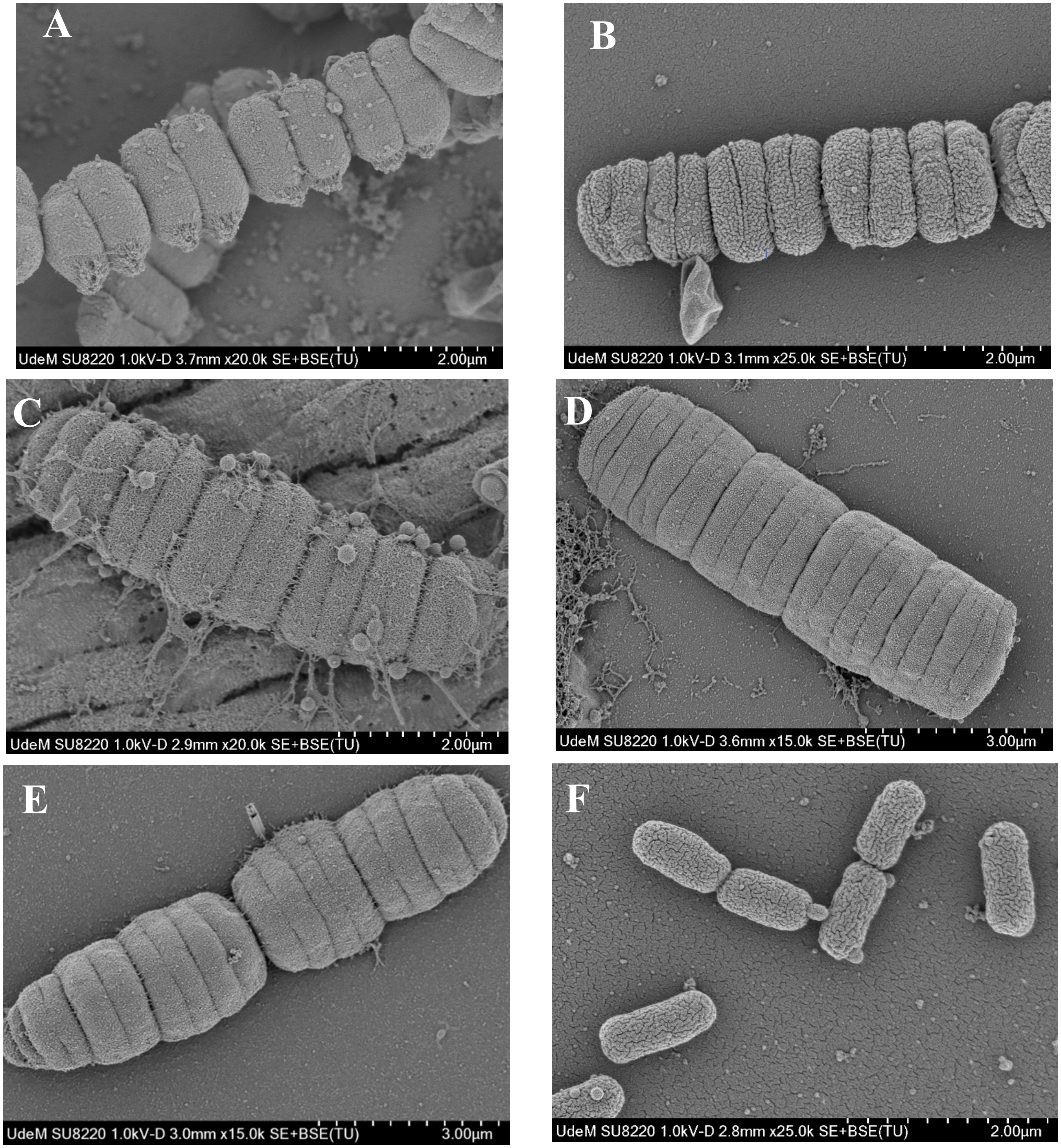

Figure 2.1: Scanning electron microscopy micrographs of *Neisseriaceae* A. *Alysiella filiformis* DSM16848. **B**. *Alysiella crassa* DSM2578, **C**. *Conchiformibius steedae* DSM2580, **D**. *Conchiformibius kuhniae* DSM17694, **E**. *Simonsiella muelleri*, ATCC29453 **F**. *Neisseria elongata subsp. glycolytica* ATCC 29315.

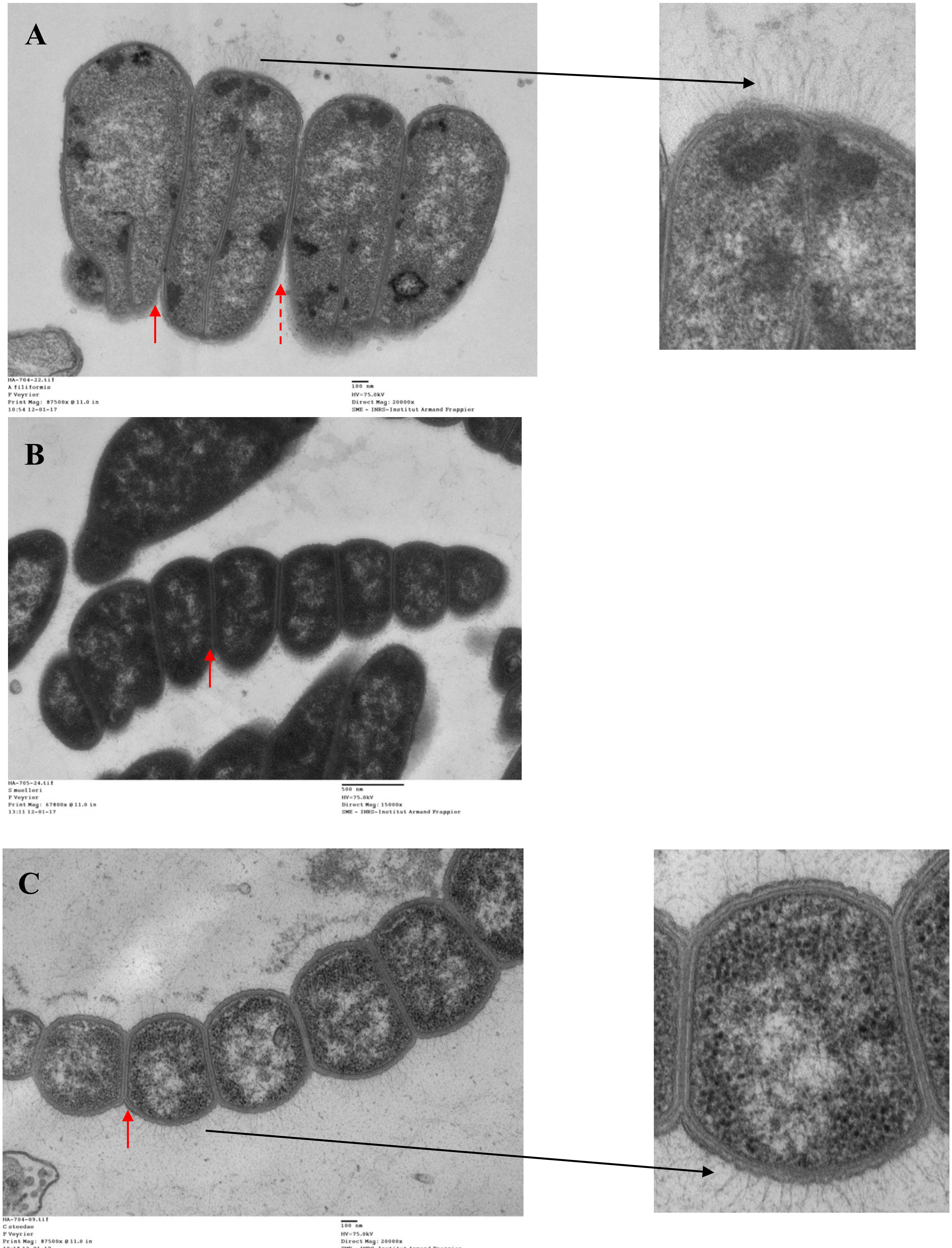
A
HA-704-22.tif
A filiformis
F Veyrier
Print Mag: 87500x @ 11.0 in
10:54 12-01-17
100 nm
HV=75.0kV
Direct Mag: 20000x
SME - INRS-Institut Armand Frappier
B
HA-705-24.tif
S muelleri
F Veyrier
Print Mag: 67800x @ 11.0 in
13:11 12-01-17
500 nm
HV=75.0kV
Direct Mag: 15000x
SME - INRS-Institut Armand Frappier
C
HA-704-09.tif
C steedae
F Veyrier
Print Mag: 87500x @ 11.0 in
10:18 12-01-17
100 nm
HV=75.0kV
Direct Mag: 20000x
SME - INRS-Institut Armand Frappier

Figure 2.2: Whole cell thin section cuts micrographs. A. *Alysiella filiformis* , solid red arrow showing tight and longer cell fusion at the septum, while dotted red arrow shows shorter less tightly fused pair of cells. On the far-right end is a magnified image showing fimbriae-like structures **B**. *Simonsiella muelleri* cells , a solid red arrow showing a fused septum between neighbouring cells. **C.** *Conchiformibius steedeae* cells, red solid arrow showing fused septum while on the right is the magnified image showing fimbriae structures.

2.4 *Neisseriaceae* family phylogeny

Through phylogenomics evolutionary relationships associated with some phenotypes at the organismal level, particularly within a family, genera and species can be determined (Eisen and Fraser 2003, Gomase and Tagore 2009). This field has evolved greatly taking advantage the current sequencing technologies that are faster, cheaper and with great sequence read coverage. Most of the available bacterial phylogenetic studies are based on single gene or a couple of house-keeping genes that were obtained through older sequencing technologies (Hanage, Fraser et al. 2005). However, the main drawback associated with single gene phylogenies is the low level of phylogenetic resolution due to nucleotide or amino acids substitutions. For this reason highly conserved genes such as the 16S rRNA or by using a combination of several house keeping genes have been employed, however these approaches misrepresent the evolutionary history of a species because the genes used have higher sequence conservation than the average genome. Therefore core genome phylogenies that employ the use of hundreds of common genes present in a group of bacteria under study is ideal (Jain, Rodriguez et al. 2018).

Some of the earliest *Neisseiaceae* phylogenetic trees published were based on 16S rRNA sequences. One of these studies showed the clustering of (*N. elongata*, *N. denitrificans, Eikenella* sp. *N. canis*, and *Kingella* species) with human commensals *Simonsiella muelleri* and other non-human commensals *C. kuhniae*, *C. steedae* and *A. crassa* from cat, dog and sheep origin respectively (Hedlund and Staley 2002). The most remarkable finding from this study was that the filamentous multicellular *Neisseriaceae* species (all referred to then as *Simonsiel*la) formed host specific clusters. It was hypothesized that the specific morphological characteristics in these species emerged as a consequence of adaptation to their specific hosts buccal cavity surfaces and dietary related factors. The pathology of oral mucosa squamous epithelial cells vary significantly among these different hosts, therefore the commensal species evolved specific feature to enhance surface attachment and movement in these environments. The role of diet on the composition of the mouth microbiota has been largely documented. It was further established that the prevalence of the human adapted *Simonsiella* species was highly correlated with the dietary composition comprising of proteins and fats but not sugars (Gregory, Kuhn et al. 1985). A study on the fatty acid composition in 48 *Simonsiella* species from man, cat, dog and sheep origins, revealed that strains from the same origin shared common quantitative fatty acid components (Jenkins, Kuhn et al. 1977), similarly other studies showed the dissimilarities in other properties including the guanine and cytosine composition of the DNA, with isolates from dogs and cats having a higher percentage mean GC composition (50-51%) while those from man and sheep had (41-44%) (Kuhn, Gregory et al. 1977).

In yet another study, Xie and Yokota (2005) employed 16S rRNA analyses in combination with fatty acids composition to determine the taxonomic positioning of *Alysiella* and *Conchiformibium* genera from *Simonsiella*. The authors showed that (*Simonsiella*, later subdivided to include *Conchiformibium* genus) was heterogeneous since it formed 3 major clusters that were supported by high bootstrap values between 70-98. The first cluster consisting of *S. muelleri* and *N. denitrificans*, the second cluster was composed of "*S. steedae*" and the "cat" *Simonsiella* species , while the third cluster consisted of *A. filiformis* and strains of "*S. crassa*". Consistent with Hedlund and Staley (2002), Xie and Yokota also showed the clustering of bacilli shaped *Kingella* genus with multicellular *Simonsiella, Alysiella* and *Conchiformibius* genera.

Core genome phylogenies are best suited for resolving evolutionary relationships involving rapid speciation, morphological differences, early divergence and limited sequence variations (Manos, Soltis et al. 2007, Uribe-Convers, Carlsen et al. 2017). In the recent past; through an evolutionary approach, Veyrier, Biais et al. (2015) showed the two major genetic events involved in the morphological transition from bacilli to cocci *Neisseriaceae*. The transition to cocci was initiated upon the loss of cell division gene *yacF* before the loss of other cell elongation machinery comprising of *mreB, mreC, mreD, pbpX, rodA* and *rodZ.* The phylogenetic tree also showed the clustering of multicellular *Neisseriaceae* with bacilli, and particularly with *Kingella* genus indicative of the bacilli as the ancestral form for the multicellular phenotype. A similar conclusion can be inferred from core genome phylogenetic analysis by (Chen, Rudra et al. 2021) and (Veyrier, Biais et al. 2015) shown in figure 2.3.

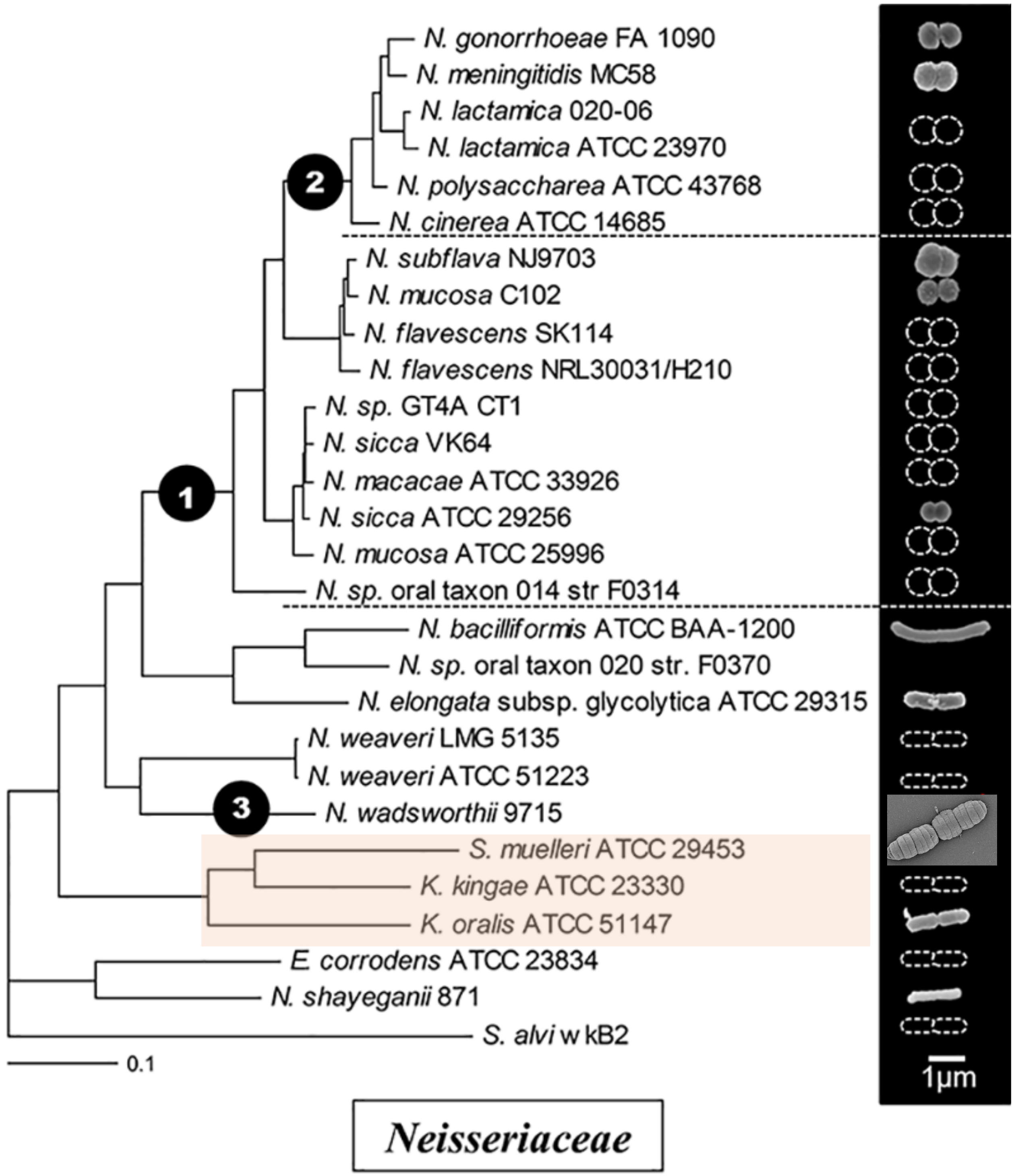

Figure 2.3: Maximum-likelihood phylogenetic tree of *Neisseriaceae* family (Veyrier, Biais et al. 2015). Highlighted in orange *Simonsiella muelleri* clusters with bacilli shaped *Kingella* genus.

2.5 The cell division conundrum in multicellular *Neisseriaceae*

Besides the interesting filamentous multicellular morphology and positioning of the fimbriae in multicellular *Neisseriaceae*, they also have a unique mode of cell division that is incomplete and occurs perpendicular to the short axis as demonstrated with red lines in figure 2.3. The classical cell division involves cell elongation while replicating chromosomes segregate and move to the opposite poles. Cell division occurs at the mid-cell region that is perpendicular to the long axis in bacilli cells like *N. elongata* and at the mid-region of enlarged cocci species. Cocci shaped *N. meningitidis* possesses fimbriae structures around the cell surface, that aid in the attachment to the posterior nasopharynx epithelial cells in man. Bacilli shaped *N. elongata* has fimbriae on the curved polar ends only. Fimbriae in *Alysiella* species are located at the convex proximal pole that interacts with the host membrane, while *Simonsiella* and *Conchiformibius* genera have fimbriae on their concave proximal surface (as demonstrated in figure 2.4).

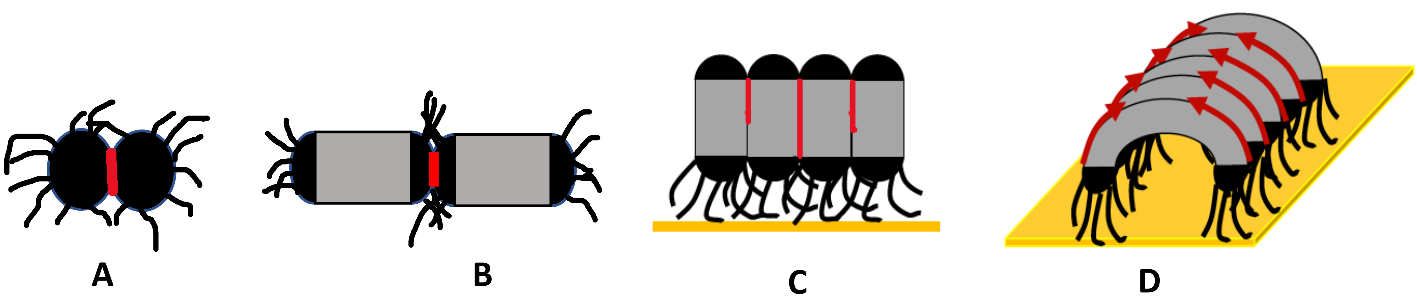

Figure 2.4: Illustration of cell division planes in cocci, bacilli and multicellular *Neisseriaceae*. (red line or arrow) and fimbriae positioning in **A.** cocci, **B**. bacilli, **C.** filamentous *Alysiella* species, **D.** filamentous *Simonsiella* and *Conchiformibius* with bipolar modes of division and fimbriae present on the proximal end. The host mucosa surface is shown in yellow.

Cell division in filamentous multicellular Neisseriaceae occurs perpendicular to the short axis, with cells in the filament remaining fused. It is not clear how and why these species adopted the multicellular morphology with longitudinal cell division, and the presence of fimbriae structures on the proximal surface. The presence of polar fimbriae on the proximal surface of the cell may have influenced the development of longitudinal division because it ensures the continued attachment of dividing cells to the buccal cavity upon cell division. Additionally, we can hypothesize that cells in filamentous species remain fused in order to potentiate surface adherence and movement in the mammalian buccal cavity environment that is characterized with fluid and debri flow.

We can attempt to answer the "How" question first by using various imaging techniques to determine cellular organization. Peptidoglycan and particularly septum growth during cell division can be determined by labeling the PG using fluorescence D-amino acids (FDAA) and visualizing the growth by epifluorescence microscopy. Complete and closed genes using sequencing techniques like Pacific Bioscience long read sequencing, epigenetic factors associated with the phenotype can be determined. Comparative genomics between ancestral and descendant phenotypes enables the determination of genetic modifications (gene deletions, insertions and amino acid substitutions) associated with MuLDi phenotype. The predicted gene deletions, insertions or nucleotide polymorphisms are subsequently introduced in model organisms in order to determine the gene functions and overall impact on the phenotype. Currently *Neisseria elongata* has been used as a bacilli model to study cell shape evolution in *Neisseriaceae* (Veyrier, Biais et al. 2015, Nyongesa, Weber et al. 2022), but there is need to continuously identify other model organisms that might be more closely linked to the phenotype of interest or more suitable for animal model studies.

3 OBJECTIVES

The relevance of the bacterial shape and the mechanisms involved in cell division, cell elongation and peptidoglycan synthesis have been extensively described. However, most of the known mechanisms are based on works obtained from mainly studying model bacilli, cocci and spiral shaped organisms including *E. coli*, *B. subtilis* and *S. aureus*. Cognisant of the large diversity of bacterial shapes, it is important to study other morphologies and additional species in order to better understand this subject. This work attempts to describe the longitudinal and incomplete mode of cell division in multicellular *Neisseriaceae* and also uses an evolutionary approach to determine proteins implicated in the cell shape transition from bacilli to multicellular and longitudinally dividing phenotype.

3.1 Aim of the study

To use the atypical morphology and cell division in Multicellular Longitudinally Dividing (MuLDi) *Neisseriaceae* to study cell shape evolution and ultimately decipher new protein function

3.2 Hypothesis

The multicellular morphology and longitudinal cell division in *Simonsiella, Alysiella* and *Conchiformibius* genera of the *Neisseriaceae* family emerged as result of step-wise genetic changes that occurred in a bacilli shaped ancestor during cell shape evolution.

3.3 Main objectives

1. Develop molecular cloning tools for the genetic manipulation of *Neisseria elongata* in order to study cell shape evolution of MuLDi *Neisseriaceae*
2. Study the cellular organization, cell division and peptidoglycan synthesis patterns in MuLDi *Neisseriaceae*.
3. Use an evolutionary approach to determine genetic events associated transition of bacilli to MuLDi *Neisseriaceae*
4. Determine the implications of identified genetic modifications and reconstruct MuLDi cell evolution events in *Neisseria elongata*

4 ARTICLE 1:

Context of article 1:

Protein function can be determined through mutagenesis studies conducted in model organism. Genome editing of *Neisseriaceae* takes advantage of the ability of species in this family to acquire extracellular DNA and readily recombine through double homologous recombination events (Dillard 2011, Jones, Yee et al. 2022). DNA cassettes comprising of a selectable marker (usually an antibiotic) that is flanked by short DNA sequences of the regions upstream and downstream of the gene of interest are used, and antibiotic resistant mutants selected. Unfortunately the pool of antibiotics used in *Neisseriaceae* studies is limited. Besides, it is important to remove the antibiotic marker to facilitate the recycling of the antibiotic for subsequent gene editing and also eliminate unwanted effects associated with the presence of large DNA cassettes that may impact on gene expression.

To successfully study the implications of identified mutations and also attempt to reconstruct MuLDi phenotype in *Neisseria elongata*, it was paramount to develop a reliable genetic modification tool for use in *Neisseriaceae* species. Bearing in mind that multiple genetic changes had occurred during the course of morphological transition from bacilli to multicellular, the sought after tool was designed to generate unmarked mutants and also genetically modifying multiple loci in a single strain.

This chapter describes the development of 3 gene cassette systems RPLK and RPCC for selection and counter selection of mutants. In this publication Sammy Nyongesa constructed the RPLK cassette, used RPLK to performed marked and unmarked deletion of *mtgA* gene, the sequential deletions of 6 genes (*rapZ, pbp3, gloB, NELON_RS07135_ mtgA* and *mraZ*) in *N. elongata*, sequencing verifications, and writing of the manuscript.

Canadian Journal of
Microbiology

OPEN ACCESS | Methods

Sequential markerless genetic manipulations of species from the *Neisseria* genus

Sammy Nyongesa, Martin Chenal, Ève Bernet, Florian Coudray, and Frédéric J. Veyrier

INRS-Centre Armand-Frappier Santé-Biotechnologie, Bacterial Symbionts Evolution, Laval, Québec, Canada

Corresponding author: **Frédéric J. Veyrier** (email: frederic.veyrier@inrs.ca)

Abstract

The development of simple and highly efficient strategies for genetic modifications is essential for postgenetic studies aimed at characterizing gene functions for various applications. We sought to develop a reliable system for *Neisseria* species that allows for both unmarked and accumulation of multiple genetic modifications in a single strain. In this work, we developed and validated three-gene cassettes named RPLK and RPCC, comprising of an antibiotic resistance marker for positive selection, the phenotypic selection marker *lacZ* or mCherry, and the counterselection gene *rpsL*. These cassettes can be transformed with high efficiency across the *Neisseria* genus while significantly reducing the number of false positives compared with similar approaches. We exemplified the versatility and application of these systems by obtaining unmarked luminescent strains (knock-in) or mutants (knock-out) in different pathogenic and commensal species across the *Neisseria* genus in addition to the cumulative deletion of six loci in a single strain of *Neisseria elongata*.

Key words: *Neisseria*, deletion, gene, insertion, markerless

Résumé

Le développement de stratégies simples et hautement efficaces en matière de modifications génétiques est essentiel pour les études post-génétiques visant à caractériser les fonctions de gènes en vue de diverses applications. Les auteurs ont cherché à développer un système fiable pour les espèces de *Neisseria* qui permet à la fois l'obtention de transformants non marqués et l'accumulation de multiples modifications génétiques dans une seule souche. Dans ce travail, ils ont développé et validé des cassettes à trois gènes identifiées RPLK et RPCC, comprenant un marqueur de résistance aux antibiotiques pour la sélection positive, le marqueur de sélection phénotypique *lacZ* ou mCherry, et le gène de contre-sélection *rpsL*. Ces cassettes peuvent être transformées avec une grande efficacité dans tout le genre *Neisseria* tout en réduisant significativement le nombre de faux positifs par rapport à des approches similaires. Ils illustrent la polyvalence et l'application de ces systèmes en obtenant des souches luminescentes (knock-in) ou des mutants (knock-out) non marqués chez différentes espèces pathogènes et commensales du genre *Neisseria*, en plus de la délétion cumulative de six loci dans une seule souche de *Neisseria elongata*. [Traduit par la Rédaction]

Mots-clés : Neisseria, délétion, gène, insertion, sans marqueur

Introduction

The *Neisseria* genus consists of commensal species that reside in the mammalian mucosa, mainly in the oral cavity, but also two major human pathogens namely *Neisseria meningitidis* and *Neisseria gonorrhoea* (Hitchcock 1989; Perrin et al. 1999; Marri et al. 2010; Brynildsrud et al. 2018). *Neisseria meningitidis* causes invasive meningococcal disease with an annual global incidence of 500 000–120 000 and 10% case fatality rate (Jafri et al. 2013; Deghmane et al. 2022). *Neisseria gonorrhoea* is the causative agent of gonorrhea, a sexually transmitted disease accounting for 87 million new infections in 2016 (Rowley et al. 2019). Both species are highly related (subspecies) as they have emerged from a common commensal symbiont ancestor (Tacconelli et al. 2018). Several groups have already compared *Neisseria* species, focusing mainly on the last step of pathogenic emergence (Bennett et al. 2010; Joseph et al. 2011; Putonti et al. 2013; Maiden and Harrison 2016; Brynildsrud et al. 2018). Others look for stepwise ancestral events at different nodes of evolution that may have drastic consequences on the pathogens as we know them today (Veyrier et al. 2015; Nyongease et al. 2022). This includes the evolutionary events not directly linked to pathogen speciation that could help clarify ecological niche adaptation, enhanced colonization, and (or) virulence of the pathogenic species. These type of studies require multiple successive genetic modifications of both commensal and pathogenic species (gain-of-function or loss-of-function). Although several molecular tools have been developed over the last decades for pathogenic *Neisseria*, only a few attempts have been made to genetically modify commensal species (Higashi et al. 2011; Veyrier et al. 2015; Anonsen et al. 2016; Custodio et al. 2020). Advancements in molecular cloning such as the CRISPR–Cas systems have limitations, such as the associated cytotoxicity due to continuous expression of foreign CRISPR in the bacterial cells (Yan and Fong 2017; Arroyo-Olarte et al. 2021). In the case of the *Neisseria* genus, a functional endogenous CRISPR–Cas9 system has only been identified in a few species and thus requires optimization and implementation efforts to be used in other species (reviewed in Zhang 2017).

Neisseria species are naturally competent, they undergo frequent intra- and interspecies exchange of genetic material through horizontal gene transfers (HGTs). During HGT, exogenous DNA is acquired, translocated across the membranes, and eventually recombined with homologous regions of the chromosome (Frye et al. 2013; Mell and Redfield 2014). Natural competence is enhanced by the presence of factors such as type IV pili and 10–12 bp *Neisseria* specific DNA uptake sequence (DUS) repeats (Goodman and Scocca 1988). Of note, due to strong restriction barriers, the processing of large plasmids into smaller pieces, and the translocation of a single strand of DNA through the inner membrane, replicative plasmids are scarce and of little use for the genetic manipulation of *Neisseria* species (Hamilton and Dillard 2006; Budroni et al. 2011; van Dam and Bos 2012). Integrative DNA constructions are therefore preferred. Natural competence has facilitated genetic manipulation studies to obtain gene deletions, insertions, and point mutations in both pathogenic and commensal *Neisseria* species (Dillard 2011; van Dam and Bos 2012; Veyrier et al. 2015). For example, a marked gene editing strategy, consisting of an antibiotic-resistant marker flanked on both ends by short DNA sequences homologous to the upstream (5′) and downstream (3′) regions of the targeted gene, allows for targeted gene modification through double-crossover homologous recombination. Although seemingly straightforward, this approach is limited by the available antibiotic options for *Neisseria* species (Dillard 2011). The creation of unmarked mutants is advantageous because it allows for antibiotic recycling and further eliminates polar effects associated with the presence of large cassettes that may affect expression of the downstream genes in an operon (Bailey et al. 2019). Unmarked mutants are obtained through a second transformation step that introduces DNA comprising of the flanking 5′ and 3′ regions of the previously edited gene to the marked mutants, thereby removing the resistance marker and associated cassette through double homologous recombination. Screening for the correct unmarked transformants can be laborious without a system that limits the growth of false positive clones. Thus, negative selection markers such as tetracycline sensitivity *tetAR*, sucrose sensitivity *sacB*, and streptomycin sensitivity *rpsL* are employed for counterselection (Reyrat et al. 1998). These systems however have some shortfalls. For example, *tetAR* system is applicable to mostly *Escherichia coli* strains, while *sacB* system is limited by the low selection stringency and need for optimization of strain-specific selection conditions (Reyrat et al. 1998; Li et al. 2013; Li et al. 2014). On the other hand, the *rpsL* system is dependent on the dominance of the wild-type streptomycin sensitive (Sm^S) allele over the streptomycin-resistant (Sm^R) allele, and such a system requires prior genetic modification of the bacteria (Trindade et al. 2009).

There is a never-ending need for the development of new and improved methods that can be easily and cheaply employed for gene editing purposes in bacterial species. In this work, we sought to develop an efficient system for generating unmarked mutants across any *Neisseria* species. Through the use of *lacZ* (blue-white screening) or mCherry (fluorescence) in combination with antibiotic selection markers and the counterselection gene *rpsL*, we created three-gene cassettes named RPLK and RPCC and demonstrated the efficiency and applicability of these systems for genetic editing of different *Neisseria* species.

Materials and methods

Bacterial strains and culture conditions

Bacterial strains and plasmids used in this study are listed in Tables S1 and S2. *Escherichia coli* DH5**α** cells were cultured at 37 °C on lysogeny broth media (Difco) supplemented with either ampicillin (100 μg/mL) for pUC plasmids, kanamycin (50 μg/mL), and X-gal (20 μg/mL) for RPLK-based plasmids, or chloramphenicol (25 μg/mL) for RPCC-based plasmid transformations. *Neisseria* strains were cultured at 37 °C with 5% CO_2 on gonococcal base (GCB) agar (Oxoid) supplemented with Kellogg's supplements as previously described (Kellogg et al. 1963). When required, X-gal (20 μg/mL), kanamycin (100 μg/mL), chloramphenicol (5 μg/mL), and streptomycin (100 μg/mL) were added to the GCB agar.

Generation of streptomycin-resistant *Neisseria* strains

Streptomycin-resistant *Neisseria elongata* strains were obtained by plating wild-type *N. elongata* subsp. *glycolytica* (ATCC 29315) cells on GCB agar containing 20 μg/mL streptomycin for 2 days. DNA was extracted from the resulting clones, and their *rpsL* gene was amplified and sequenced using primers rpsLXbaI_F/rpsLNheI_R to confirm the streptomycin resistance mutation K43R. Subsequently, *N. meningitidis* LNP20553 and *Neisseria musculi* CCUG68283 were transformed with the resulting *rpsL*^{K43R} PCR product as described previously (Dillard 2011; Veyrier et al. 2015). The selection of *rpsL*-mutated clones was done on GCB plates supplemented with streptomycin.

Construction of pRPLK and pRPCC plasmids

Manipulations involving DNA extraction, PCR amplification, restriction enzyme digestion, and ligation were done using standard protocols according to the manufacturers' specifications. Unless otherwise indicated, Phusion polymerase (NEB) was used for the PCR reactions. Restriction enzymes and T4 DNA ligase were purchased from NEB, while the plasmid extraction, PCR, and gel purification kits were from Qiagen. Primers used in the study are listed in Table S3.

The RPLK construct (Fig. 1A) was assembled with the wild-type *N. elongata rpsL*, the constitutive *N. meningitidis* promoter *porB*p controlling the selection markers *lacZ*

Can. J. Microbiol. **00:** 1–10 (2022) | dx.doi.org/10.1139/cjm-2022-0024

Fig. 1. Plasmids for the markerless modification of *Neisseria* species. Circular maps of (A) pRPLK (Addgene 184282) and (B) pRPCC (Addgene 184283) plasmids containing the selection–counterselection cassettes used in this study, as well as (C) p5′3′GOI plasmid for the integration of such cassettes, which is a theoretical construct containing homology regions flanking any gene of interest (GOI). BglII restriction sites are shown, which are used to extract the RPLK or RPCC cassette and subclone it into any *Neisseria* integrative plasmid, herein p5′3′GOI.

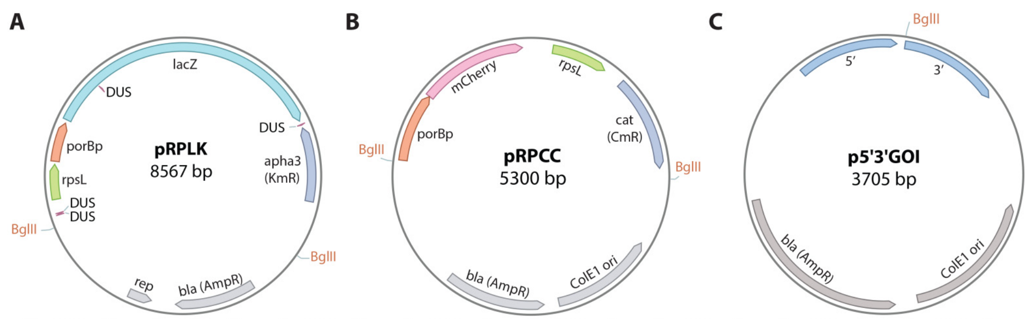

(encoding β-galactosidase) and *apha3* (encoding a kanamycin resistance protein). Promoter *porBp* was amplified from the gDNA of *N. meningitidis* MC58 using primers porBpF/porBpbluntR, *lacZ* was amplified from mini-CTX-lacZ with primers porBplacZF/lacZRKm7up, while the primers Km7up/Km6 were used to amplify *apha3* from pGEM::Km (Becher and Schweizer 2000; Veyrier et al. 2011). Purified PCR products were mixed in equimolar concentrations and fused through a subsequent PCR reaction using primers porBpF and Km6. The resulting 5.5 kb amplicon of porBp-lacZ-Km^R was gel purified, ligated to the pCR4blunt-TOPO vector (Thermo), and subsequently transformed in *E. coli* DH5**α** cells to generate pPCR3 plasmid. Genomic DNA from *N. elongata* was used to amplify *rspL*^{wt} together with a 250 bp intergenic region upstream containing its promoter and a DUS using primer pair rpsLXbaI_F and rpsLNheI_R. Plasmid pPCR3 and the *rspL*^{wt} amplicon were digested using NheI and XbaI–NheI restriction enzymes respectively, before ligation and transformation in *E. coli* DH5**α** cells to obtain pRPLK plasmid. The RPLK cassette was then extracted with BglII digestion for subcloning into *Neisseria* integrative plasmids.

The RPCC cassette was obtained by first synthesizing the *porB*p, mCherry, and *rpsL*^{wt} in the pUC57 vector (Biobasic), resulting in pUC57::RPC. The *cat* gene conferring chloramphenicol resistance was amplified by PCR with primers CmR_SpeI_F and CmR_PpuMI_R, and then inserted into the synthesized plasmid by conventional restriction-ligation with SpeI and PpuMI enzymes, generating pRPCC (Fig. 1B). Of note, in this construct, the native *rpsL* locus from *N. lactamica* was used to show the cross-species applications of our strategy.

Both plasmids have been deposited in Addgene repository (pRPLK, Addgene No. 184282; pRPCC, Addgene No. 184283).

Construction of *Neisseria* integrative plasmids for markerless modifications

Approximately 500 bp regions (5′ and 3′) flanking each gene of interest (GOI) were synthesized in pUC57 by Biobasic with a central BglII site to generate various p5′3′GOI constructs (where 5′3′GOI represent the flanking regions of each GOI) (Fig. 1C). The RPLK or RPCC cassette was then inserted at the BglII site by conventional restriction-ligation, resulting in p5′3′GOI::RPLK or p5″3″GOI::RPCC (Table S2). As a cheaper and sometimes quicker alternative, 5′3′ regions can be generated by overlap extension PCR with overlapping inner primers containing a BglII site, then inserted into pUC57 by blunt ligation into the EcoRV site.

Generation of marked and markerless gene modified *Neisseria* strains

Transformations were done as previously described (Dillard 2011; Veyrier et al. 2015). Briefly p5′3′GOI::RPLK or p5′3′GOI::RPCC constructs were linearized using ScaI. Five to ten microlitres (500 ng) of the linearized plasmid DNA was deposited on a fresh streak of streptomycin-resistant *Neisseria* cells and cultured for 6 h on GCB agar plates containing 10 mmol/L $MgCl_2$. For the RPLK transformations, subculturing was done on GCB plates supplemented with Km and X_gal to obtain blue, Km^R, and Sm^S clones. For the RPCC transformations, subculturing was done on GCB plates supplemented with Cm and fluorescence was verified on a Typhoon FLA9500 imager (GE Healthcare).

To obtain unmarked deletions, p5′3′GOI without RPLK or RPCC were subsequently used to transform the marked *Neisseria* mutants, resulting in the loss of the selection–counterselection cassette (Fig. 2). When removing the RPLK cassette, transformants were selected on GCB agar supplemented with Sm and X_gal to obtain white Sm^R clones. When removing the RPCC cassette, nonfluorescent transformants were selected on GCB agar supplemented with Sm after fluorescence imaging. Unmarked mutants were verified by PCR.

Here, the markerless deletion of MtgA in *N. elongata* was done using the RPLK cassette, and verified with primers RTMtgA-F/MtgAKpnI-R, 5KOmtgA_F/3KOmtgA_R, and Km7up/Km6. Markerless deletion of BolA was also

Fig. 2. Markerless genetic modification workflow. First, the *rpsL* allele in the target *Neisseria* strain is mutated to render it streptomycin resistant (*rpsL*∗ or *rpsL*^{K43R}), which can be done by transformation with annealed oligos containing the K43R mutation. Second, a marked deletion strain is generated using a plasmid containing the RPLK (left panel) or RPCC (right panel) cassette within sequences homologous to the flanking regions surrounding the GOI or area to modify. Third, a plasmid containing the same homology regions with the desired modification in between is used to transform the previous marked strain. In this illustration, a gene deletion workflow is shown. The selection markers to use are indicated. Steps 2 and 3 can be repeated to cumulate a virtually unlimited number of modifications within a single strain. Sm, streptomycin; Cm, chloramphenicol; Km, kanamycin.

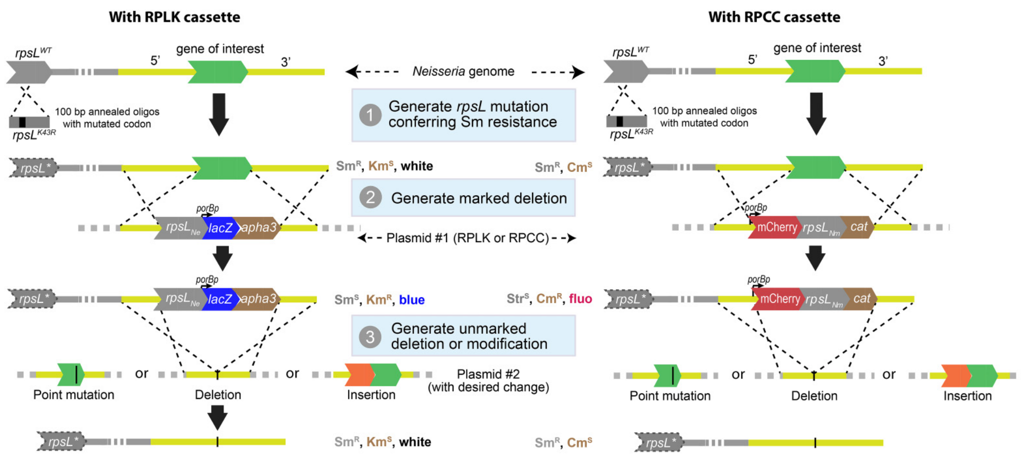

done, this time using the RPCC cassette and verified using primers BolANe_F/BolANe_R, BolA_ExtNe_F/BolA_ExtNe_R, and CmR_SpeI_F/CmR_PpuMI_R. As a species specific control for *N. elongata*, *mraZ* gene was amplified by 5MraZ_F/3MraZ_R primers in both deletions.

Multiple gene deletions were obtained by the sequential transformation of p5′3′GOI::RPLK into the previous unmarked Sm^{R} *Neisseria* mutant, followed by removal of the cassette. Each marked and unmarked mutant was confirmed by PCR using primers RTRapZ_R/RapZKpn1_R, Ne_PbP3_F/Ne_PbP3_R, Ne_gloB_F/Ne_gloB_R, Ne_07135_F/Ne_07135_R, RTMtgA_F/MtgAKpnI_R, RTMraZ_F/MraZKpnI_R, and Km7up/Km6.

Generation of markerless luminescent *Neisseria* strains

The luminescence operon *luxCDABE* was amplified from a luminescent mutant of *N. meningitidis* LNP24198 (Guiddir et al. 2014) using LuxCNcoIF/LuxEPstIR and cloned in p*pilE*pLuc (Veyrier et al. 2015) digested with NcoI and PstI. The *pilE*p promoter that was present in this plasmid was subsequently replaced by *N. meningitidis porB*p amplified with porBp_NheI_F/porBp_NcoI_R using NheI and NcoI to generate pporBLuxCDABE::Km. The luminescence operon along with the promoter was amplified using porBp_EcoRI_F/luxE_EcoRI_R and subcloned in pCR4blunt-TOPO with the Zero Blunt PCR Cloning Kit (Invitrogen) resulting in pCR_porbplux from which the luminescence cassette can be extracted using EcoRI. 1000 bp sequences centered on intergenic regions of *N. meningitidis*, *N. musculi*, and *N. elongata* were synthesized with MfeI and BglII restriction sites in the middle (Biobasic), resulting in pNm, pNmus, and pNelon. The BglII site was used to insert the RPLK cassette, while the MfeI site was used to insert the EcoRI-flanked luminescence cassette, resulting in plasmids pNm::RPLK, pNmus::RPLK, pNelon::RPLK, pNm::lux, pNmus::lux, and pNelon::lux. Each strain was transformed first with the RPLK-containing plasmid, followed by a second transformation with the luminescence-cassette-containing plasmid. Luminescent clones were selected by directly imaging the culture plates with an IVIS Lumina III (PerkinElmer), and their antibiotic susceptibility was assessed to confirm successful removal of RPLK.

Results

Strategy for the markerless deletion and insertion of genes

Our approach is based on three-gene cassette constructs RPLK and RPCC. These cassettes include antibiotic-resistance selection markers (Km or Cm), phenotypic selection markers (lacZ or mCherry) for blue-white screening or fluorescence selection respectively, in addition to the *Neisseria* species wild-type streptomycin sensitive *rpsL*^{wt} gene for streptomycin sensitivity selection of the mutants. The first critical step of this strategy consists of mutating the native *rpsL* locus in the target strain, making it resistant to high levels of streptomycin. This can be achieved by transforming any *Neisseria* species with 100 bp annealed oligonucleotides containing *rpsL* with the K43R mutated codon (Fig. 2), or by culturing the parental strain in gradually increasing concentrations of streptomycin and confirming the proper mutation by sequencing. The second step involves transformation of the RPLK or RPCC cassette into a streptomycin-resistant strain as demonstrated (Fig. 2). Since the selection cassettes are inserted within sequences homologous to the *Neisseria* genomic locus to be modified (5′ and 3′), a double homologous recombination results in the replacement of the gene of interest with the corresponding cassette, thus generating a marked deletion mutant. Transformed clones are easily selected by their ability to grow as blue colonies on media supplemented with kanamycin and X-gal (for RPLK), or fluorescent colonies on media with chloramphenicol (for RPCC). Because of the dominant effect of *rpsL*^{wt} over the native *rpsL*^{K43R} locus, the transformed clones become streptomycin sensitive, which must be verified to minimize false positives in subsequent steps. The third step of this strategy involves removing the selection cassette RPLK or RPCC and replacing it with the desired modification, thus generating markerless mutants. This is achieved by transforming the marked strain from step 2 with a plasmid harboring the same homology regions (p5′3′GOI), with or without the desired DNA sequence inside (Fig. 2). Transformants lose the RPLK cassette and are selected on media supplemented with streptomycin and X-gal as white, Sm^R and Km^S clones. False positives that have not lost the selection cassette will remain blue, avoiding the need for additional screening tests such as verifying for kanamycin sensitivity.

Gene deletion using the RPLK cassette

We used the RPLK cassette to demonstrate the viability of this approach in obtaining marked and unmarked mutants, first through the deletion of *mtgA* in *N. elongata* (Fig. 3A), a gene encoding a peptidoglycan transglycosylase. The RPLK-containing strain (marked deletion) is the only one that grew as blue clones in the presence of kanamycin and X_gal, while only the *rpsL*^{K43R} and the markerless deletion strains could grow in the presence of streptomycin. Two blue colonies were visible on GCB media with streptomycin for the RPLK strain, indicative of natural Sm^R revertants. Correct deletion of *mtgA* was confirmed by PCR using primers amplifying within and around the *mtgA* gene, the kanamycin resistance gene and the control gene *mraZ* (Fig. 3B). Sequencing of the deletion region confirmed that no unwanted modifications were introduced during the cloning steps (Fig. S1).

Gene deletion using the RPCC cassette

To exemplify the versatility of this markerless genetic manipulation method, we designed another cassette named RPCC (*rpsL*$_{wt}$, *porB*$_p$, cat, mCherry). Instead of using *lacZ* for blue-white screening and a kanamycin resistance gene, we used a chloramphenicol resistance gene (cat) coupled to a fluorescence marker. To demonstrate the cross-species potential of our approach, the RPCC cassette contains the *rpsL* gene from *N. lactamica*. In this example, the RPCC cassette was used to delete the *bolA* gene in *N. elongata* (Fig. 4A), which encodes a putative regulator (Santos et al. 2002; Freire et al. 2009). As expected, only the marked mutant is fluorescent and Cm^R, while both the *rpsL*^{K43R} and the unmarked deletion strains are Sm^R. Each strain was verified by PCR using a similar approach as with *mtgA* (Fig. 4B). Sequencing of the deletion region confirmed that no unwanted modifications were introduced during the cloning steps (Fig. S2).

Markerless gene insertions in *Neisseria* species (luminescent strains)

To demonstrate the use of our method for gene insertions, we introduced the 6.3 kb *porB*p-*luxCDABE* luminescence cassette into three *Neisseria* species: *N. meningitidis* LNP20553, *N. elongata* subsp. *glycolytica* ATCC29315, and *N. musculi* CCUG68283 (Fig. 5). The expression of the *lux* operon allows luminescence measurement without the need for exogenous luciferin since it encodes both the luciferase enzyme and the proteins needed to synthesize its substrate. The markerless strains obtained here emitted a persistent luminescent signal. Of note, luminescent strains of *N. meningitidis* have been previously used successfully in murine infection models to measure bacterial burden (Alonso et al. 2003; Zarantonelli et al. 2007; Bernet et al. 2020) and the markerless gene modification option is an added advantage.

Multiple markerless deletions in *N. Elongata*

The most impactful advantage of the strategy described here is the fact that it allows for unlimited genetic modifications in a single strain, since selection markers are used transiently and do not accumulate. To exemplify the endless possibilities offered by such methodology, we used the RPLK cassette to cumulatively delete six genes in *N. elongata* (Fig. 6). Starting with an *rpsL*^{K43R} streptomycin-resistant strain, we replaced one gene at a time with the selection cassette before removing the cassette to make the strain Sm^R once again for the deletion of subsequent genes (Fig. 6A). PCRs were done at each step to confirm the presence of the cassette for marked deletions and its absence for markerless deletions (Fig. 6B).

To determine the frequency of false positives when removing the selection cassette, we quantified both white and blue streptomycin-resistant clones from two independent gene deletions (Table 1). Around one-third of the obtained Sm^R clones were false positives still carrying the RPLK cassette (blue on X-gal), supporting the necessity of adding another selection marker (*lacZ*) to the traditional two-gene cassettes often used for similar purposes.

Discussion

Strategies that allow efficient and accurate genetic modifications such as gene deletions, insertions, and point mutations are crucial for the study of protein functions. This is particularly true in the context of evolutionary studies when multiple genetic events are implicated in the emergence of novel phenotypes (Veyrier et al. 2015). In bacterial mutagenesis studies, mutants are mainly obtained by artificial transformation involving the introduction of DNA containing a

Fig. 3. *mtgA* deletion in *N. elongata* using the RPLK cassette. The methodology described above was used to generate a markerless Δ*mtgA N. elongata* strain. (A) Growth of *N. elongata* at different stages of the deletion strategy: 1, WT strain; 2, *rpsL*∗ strain; 3, RPLK deletion strain; and 4, markerless deletion strain. All plates contain X-gal. (B) PCR confirmation of the genetic manipulations of *N. elongata* throughout the strategy (left), where the colored boxes match the primers imaged on the right. The control gene is *mraZ*. Primers for *mtgA* (green): RTMtgA-F, 3KOMtgA_R. For flanks (orange): 5KOMtgA_F, 3KOMtgA_R. For Km^R (blue): Km7up, Km6. For control (black): 5MraZF, 5MraZR. No amplification is seen with flanking primers for the RPLK strain since the insert is too large for the PCR conditions we used. GCB, GC base agar; Km, kanamycin; Sm, streptomycin.

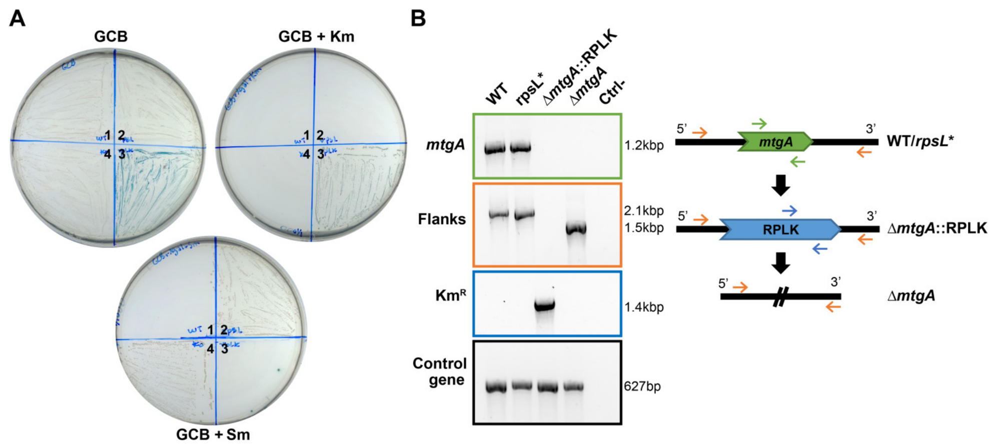

Fig. 4. *bolA* deletion in *N. elongata* using the RPCC cassette. The RPCC cassette was used to generate a markerless Δ*bolA N. elongata* strain. (A) Growth of *N. elongata* at different stages of the deletion strategy: 1, WT strain; 2, *rpsL*∗ strain; 3, RPCC deletion strain; and 4, markerless deletion strain. Plates were photographed (left panel) and imaged for fluorescence with a Typhoon FLA9500 imager (right panel). (B) PCR confirmation of the genetic manipulations of *N. elongata* throughout the strategy (left), where the colored boxes match the primers imaged on the right. The control gene is *mraZ*. GCB, GC base agar; Cm, chloramphenicol; Sm, streptomycin.

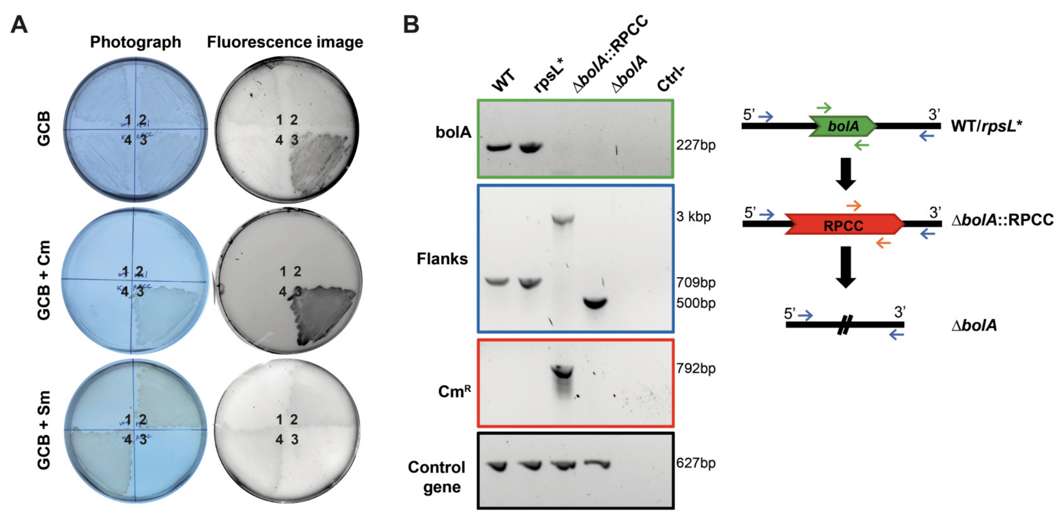

Fig. 5. Generation of markerless luminescent *Neisseria* species. The RPLK cassette was used to introduce the *porBp-luxCDABE* luminescence cassette in *N. meningitidis, N. musculi*, and *N. elongata*. Suspensions from each step of the cloning strategy were plated on X-gal-supplemented GCB, GCB+Km, and GCB+Sm. Luminescence was assayed for the GCB+Sm plates with an IVIS Lumina III (PerkinElmer), for which overlaid images are shown. 1, WT strains; 2, *rpsL** strains; 3, RPLK-insertion strains; 4, markerless luminescent strains. GCB, GC base agar; Km, kanamycin; Sm, streptomycin.

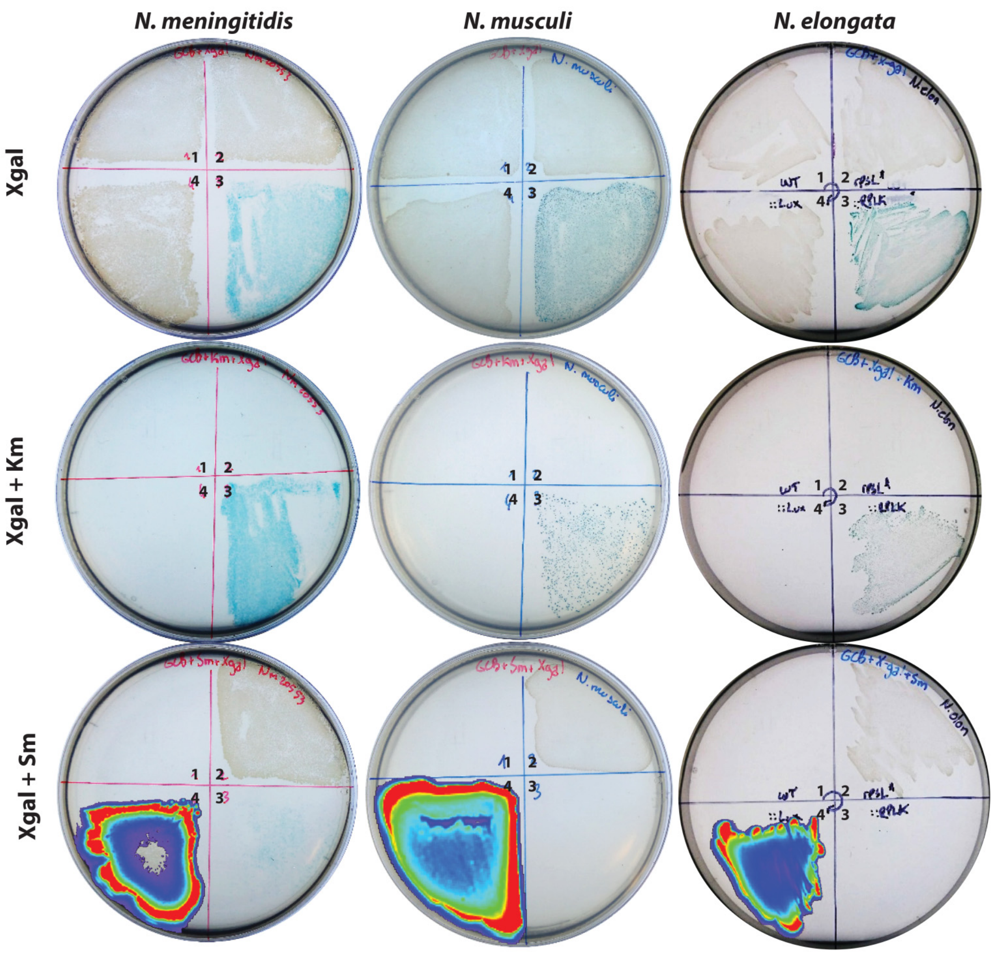

selection marker that facilitates the selection of transformants. Despite the progress made in this field, some of the major challenges include low transformation efficiency that necessitates laborious screening of many clones, the difficulty in creating unmarked mutants, and the inability to reliably modify multiple genes in the same strains (Bosse et al. 2014; Yan and Fong 2017; Arroyo-Olarte et al. 2021). Therefore, the need to develop new methods and continuously improve the existing ones cannot be overemphasized.

Natural competence of *Neisseria* species allows them to be transformed repeatedly with high efficiency, making them a great model for complex or cumulative genetic modifications. Because of an impressive repertoire of restriction-modification systems, replicative plasmids are of limited use (Budroni et al. 2011). Instead, homologous recombination to the genome is favored, requiring sufficient homology with the transforming DNA. Here, we demonstrate an improved three-gene cassette system for markerless and multiple genetic modification of virtually any *Neisseria* species. While most studies focus on only two pathogenic *Neisseria* species in humans, *N. meningitidis* and *N. gonorrhoeae*, we wanted to showcase the versatility of our cloning strategy by using it in multiple species. We performed markerless gene deletions and insertions in several commensal species such as *N. elongata* and *N. musculi* in addition to *N. meningitidis*. Our strategy combined the use of an antibiotic resistance cassette as the

Fig. 6. Multiple markerless deletions in *N. elongata*. Using the RPLK cassette with the methodology described in this work, sequential cumulative gene deletions were performed in *N. elongata*. Six deletions were performed in a single strain. (A) Workflow for multiple deletions. (B) PCR verification of the deleted loci and kanamycin resistance gene (from RPLK) at each step of the process. For simplicity, gene names were replaced with letters (Locus A = *rapZ*, B = *pbp3*, C = *gloB*, D = NELON_RS07135, E = *mtgA* and F = *mraZ*). Km^R, kanamycin resistance gene.

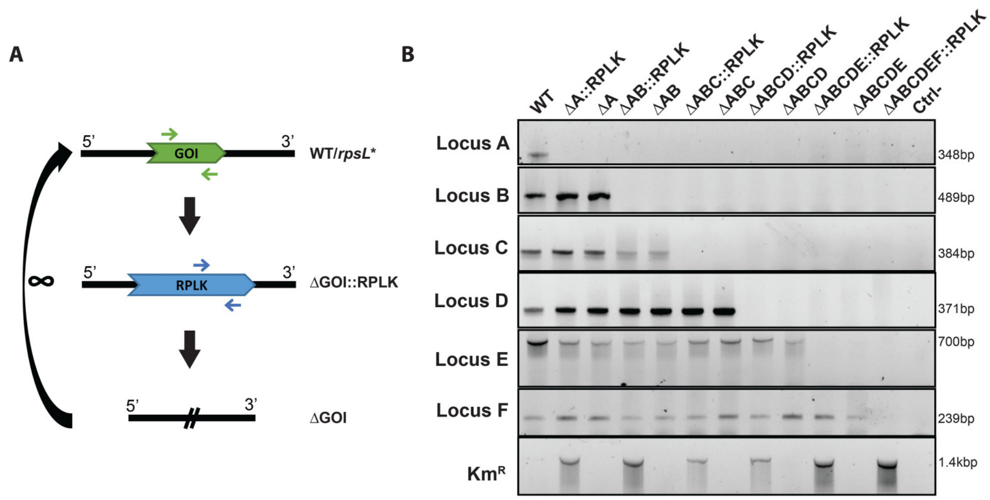

Table 1. False positive rates from two independent gene deletions.

Gene deleted	False positive rate (blue/total CFUs)
Locus C	30% ± 4%
Locus E	33% ± 3%

Notes: The last transformation step was performed in biological triplicates for two independent gene deletions from *N. elongata* made with the RPLK cassette (cf. Fig. 6). Blue and white transformants were counted from GCB plates supplemented with streptomycin and X-gal to determine the rate of Sm^R clones still carrying the RPLK cassette.

positive selection marker, *lacZ* alpha subunit or mCherry as phenotypic selection markers, and streptomycin-sensitive *rpsL*^{wt} allele for the counterselection of transformants. A previous study showed that the *rspL* from *E. coli* is highly inefficient at reversing streptomycin resistance in *N. gonorrhoeae*, raising concerns that a cross-species barrier may exist (Johnston and Cannon 1999). In our gene deletion example with the RPCC cassette, we demonstrated that the *rpsL* allele from *N. meningitidis* or *N. lactamica* could both be used to modify *N. elongata*, suggesting that such a barrier does not exist within the *Neisseria* genus. Finally, as shown in Fig. 2, our approach can be used to generate markerless deletions and insertions (as demonstrated here), but can also be used to generate markerless complementation strains of a previous deletion by inserting the gene in another locus (Nyongesa et al. 2022).

Similar approaches for markerless modifications of bacteria employ the use of two-gene cassettes comprising a resistance gene for selection and *rpsL*^{wt} for counterselection (Johnston and Cannon 1999; Sander et al. 2001; Sung et al. 2001; Bird et al. 2011; Kaczmarczyk et al. 2012). The main drawback of these strategies is the frequent occurrence of Sm^R clones carrying both *rpsL* alleles, leading to a significant proportion of false positives in the last transformation step (Sung et al. 2001; Kohler et al. 2005; Dillard 2011). In our hands, over 30% of transformants were false positives upon removal of the RPLK cassette. Moreover, Sm^R clones were naturally arising even in pure cultures of the RPLK mutants previously screened for Sm sensitivity. It was shown in *N. gonorrhoeae* that this phenomenon is not due to incomplete dominance of the inserted *rpsL*^{wt} allele over the native *rpsL*^{K43R} allele, but rather due to the spontaneous mutation of the inserted allele and recombination events between both alleles (Kohler et al. 2005). The relevance of using additional counterselection markers in reducing the false positivity rate associated with allelic conversion was previously shown (Li et al. 2014). To solve this problem, we added *lacZ* and mCherry under the strong *Neisseria* promoter *porB*p to the RPLK and RPCC selection cassettes, respectively. These elements allow for direct blue-white and fluorescence screening of the Sm^R clones obtained at the last step, therefore increasing the reliability of the strategy besides reducing the need for PCR screening and kanamycin susceptibility testing. Overall, assuming the plasmid constructs are ready, a full markerless gene modification workflow can be accomplished in as little as 5 days, including proper verifications and stock preparation. The efficiency of our cassettes can be improved further by limiting recombination between *rpsL* alleles in the merodiploid strain by using streptomycin-sensitive *rpsL* with low sequence homology to the resistant *Neisseria rspL* gene as demonstrated

Can. J. Microbiol. **00:** 1–10 (2022) | dx.doi.org/10.1139/cjm-2022-0024

previously (Bird et al. 2011). Similarly, the use of other antibiotic resistances and phenotypic selection markers in place of the ones mentioned in the study could improve the versatility of this method.

Although the RPLK and RPCC cassettes are fairly big, 5 and 2.5 kb, respectively, the insert size is not an issue in *Neisseria* species. In fact, using the improved methodology described above, dilution of the transformed cells is often needed to get individual colonies, showcasing the high efficiency of this approach. Insertion of the 6.2 kb *porBp-luxCDABE* luminescence cassette was also not an issue. Generating markerless luminescent or fluorescent strains as exemplified here can be of great use in animal infection model studies, which are severely lacking for commensal *Neisseria* (Weyand et al. 2013; Weyand 2017; Ma et al. 2018). We further demonstrated the strength of our strategy by performing six cumulative gene deletions in *N. elongata*. With the recent leap of genomic and bioinformatics studies, such a tool is invaluable when trying to recreate ancestral evolutionary events leading to speciation, since these events often include several gene insertions, deletions, and point mutations.

To summarize, we improved previous methods of markerless gene modifications by developing three-gene selection–counterselection cassettes that can be transformed with high efficiency into multiple *Neisseria* species. Using this method, we performed large gene insertions and deleted up to six loci in a single strain.

Article information

History dates

Received: 28 January 2022
Revised: 26 March 2022
Accepted: 31 March 2022
Accepted manuscript online: 5 May 2022
Version of record online: 20 July 2022

Copyright

Author information

Author ORCIDs

Martin Chenal https://orcid.org/0000-0003-2298-2845
Ève Bernet https://orcid.org/0000-0001-9566-6320
Frédéric J. Veyrier https://orcid.org/0000-0002-8574-0547

Funding information

This work was supported by the Natural Sciences and Engineering Research Council of Canada (NSERC) discovery grant (RGPIN-2016-04940) (F.J.V.), the Fonds De Recherche du Quebec Nature et technologies (FRQNT) Établissement de la relève professorale (205027) (F.J.V.), and the Canadian Institutes of Health Research (CIHR) (CFJA-184531, F.J.V.). E.B. received a Ph.D. Fellowship from the Fondation Armand-Frappier. F.J.V. received a Junior 1 and Junior 2 research scholar salary award from the Fonds de Recherche du Québec—Santé. The funders had no role in study design, data collection and analysis, decision to publish, or preparation of the manuscript.

Supplementary material

Supplementary data are available with the article at https://doi.org/10.1139/cjm-2022-0024.

References

Alonso, J.M., Guiyoule, A., Zarantonelli, M.L., Ramisse, F., Pires, R., Antignac, A., et al. 2003. A model of meningococcal bacteremia after respiratory superinfection in influenza A virus-infected mice. FEMS Microbiol. Lett. **222**: 99–106. doi:10.1016/S0378-1097(03)00252-0. PMID: 12757952.

Anonsen, J.H., Vik, A., Borud, B., Viburiene, R., Aas, F.E., Kidd, S.W., et al. 2016. Characterization of a unique tetrasaccharide and distinct glycoproteome in the O-linked protein glycosylation system of *Neisseria elongata* subsp. *glycolytica*. J. Bacteriol. **198**: 256–267. doi:10.1128/JB.00620-15. PMID: 26483525.

Arroyo-Olarte, R.D., Bravo Rodriguez, R., and Morales-Rios, E. 2021. Genome editing in bacteria: CRISPR–Cas and beyond. Microorganisms, **9**: 844. doi:10.3390/microorganisms9040844.

Bailey, J., Cass, J., Gasper, J., Ngo, N.D., Wiggins, P., and Manoil, C. 2019. Essential gene deletions producing gigantic bacteria. PLoS Genet. **15**: e1008195. doi:10.1371/journal.pgen.1008195. PMID: 31181062.

Becher, A., and Schweizer, H.P. 2000. Integration-proficient *Pseudomonas aeruginosa* vectors for isolation of single-copy chromosomal *lacZ* and *lux* gene fusions. Biotechniques, **29**: 948–950, 952. doi:10.2144/00295bm04. PMID: 11084852.

Bennett, J.S., Bentley, S.D., Vernikos, G.S., Quail, M.A., Cherevach, I., White, B., et al. 2010. Independent evolution of the core and accessory gene sets in the genus *Neisseria*: insights gained from the genome of *Neisseria lactamica* isolate 020-06. BMC Genomics, **11**: 652. doi:10.1186/1471-2164-11-652. PMID: 21092259.

Bernet, E., Lebughe, M., Vincent, AT., Haghdoost, M.M., Golbaghi, G., Laplante, S., et al. 2020. Sodium tetraphenylborate displays selective bactericidal activity against *N. meningitidis* and *N. gonorrhoeae* and is effective at reducing bacterial infection load. Antimicrob. Agents Chemother. **65**: e00254–e00220.

Bird, A.W., Erler, A., Fu, J., Heriche, J.K., Maresca, M. Zhang, Y., et al. 2011. High-efficiency counterselection recombineering for site-directed mutagenesis in bacterial artificial chromosomes. Nat. Methods, **9**: 103–109. doi:10.1038/nmeth.1803. PMID: 22138824.

Bosse, J.T., Soares-Bazzolli, D.M., Li, Y., Wren, B.W., Tucker, A.W., Maskell, D.J., et al. 2014. The generation of successive unmarked mutations and chromosomal insertion of heterologous genes in *Actinobacillus pleuropneumoniae* using natural transformation. PLoS One, **9**: e111252. doi:10.1371/journal.pone.0111252. PMID: 25409017.

Brynildsrud, O.B., Eldholm, V., Bohlin, J., Uadiale, K., Obaro, S., and Caugant, D.A. 2018. Acquisition of virulence genes by a carrier strain gave rise to the ongoing epidemics of meningococcal disease in West Africa. Proc. Natl. Acad. Sci. USA, **115**: 5510–5515. doi:10.1073/pnas.1802298115. PMID: 29735685.

Budroni, S., Siena, E., Dunning Hotopp, J.C., Seib, K.L., Serruto, D. Nofroni, C., et al. 2011. *Neisseria meningitidis* is structured in clades associated with restriction modification systems that modulate homologous recombination. Proc. Natl. Acad. Sci. USA, **108**: 4494–4499. doi:10.1073/pnas.1019751108. PMID: 21368196.

Custodio, R., Johnson, E., Liu, G., Tang, C.M., and Exley, R.M. 2020. Commensal *Neisseria cinerea* impairs *Neisseria meningitidis* microcolony development and reduces pathogen colonisation of epithelial cells. PLoS Pathog, **16**: e1008372. doi:10.1371/journal.ppat.1008372. PMID: 32208456.

Deghmane, A.E., Taha, S., and Taha, M.K. 2022. Global epidemiology and changing clinical presentations of invasive meningococcal disease: a narrative review. Infect. Dis. (Lond). **54**: 1–7. doi:10.1080/23744235.2021.1971289. PMID: 34459329.

Dillard, J.P. 2011. Genetic manipulation of *Neisseria gonorrhoeae*. Curr. Protoc. Microbiol. **4**: Unit4A.2. PMID: 22045584.

Freire, P., Moreira, R.N., and Arraiano, C.M. 2009. BolA inhibits cell elongation and regulates MreB expression levels. J. Mol. Biol. **385**: 1345–1351. doi:10.1016/j.jmb.2008.12.026. PMID: 19111750.

Frye, S.A., Nilsen, M., Tonjum, T., and Ambur, O.H. 2013. Dialects of the DNA uptake sequence in Neisseriaceae. PLoS Genet. **9**: e1003458. doi:10.1371/journal.pgen.1003458. PMID: 23637627.

Goodman, S.D., and Scocca, J.J. 1988. Identification and arrangement of the DNA sequence recognized in specific transformation of *Neisseria gonorrhoeae*. Proc. Natl. Acad. Sci. USA, **85**: 6982–6986. doi:10.1073/pnas.85.18.6982. PMID: 3137581.

Guiddir, T., Deghmane, A.E., Giorgini, D., and Taha, M.K. 2014. Lipocalin 2 in cerebrospinal fluid as a marker of acute bacterial meningitis. BMC Infect. Dis. **14**: 276. doi:10.1186/1471-2334-14-276. PMID: 24885531.

Hamilton, H.L., and Dillard, J.P. 2006. Natural transformation of *Neisseria gonorrhoeae*: from DNA donation to homologous recombination. Mol. Microbiol. **59**: 376–385. doi:10.1111/j.1365-2958.2005.04964.x. PMID: 16390436.

Higashi, D.L., Biais, N., Weyand, N.J., Agellon, A., Sisko, J.L., Brown, L.M., and So, M. 2011. *N. elongata* produces type IV pili that mediate interspecies gene transfer with *N. gonorrhoeae*. PLoS One, **6**: e21373. doi:10.1371/journal.pone.0021373. PMID: 21731720

Hitchcock, P.J. 1989. Unified nomenclature for pathogenic *Neisseria* species. Clin. Microbiol. Rev. **2 Suppl**: S64–S65. doi:10.1128/CMR.2.Suppl.S64. PMID: 2720633.

Jafri, R.Z., Ali, A., Messonnier, N.E., Tevi-Benissan, C., Durrheim, D. Eskola, J., et al. 2013. Global epidemiology of invasive meningococcal disease. Popul. Health Metr. **11**: 17. doi:10.1186/1478-7954-11-17. PMID: 24016339.

Johnston, D.M., and Cannon, J.G. 1999. Construction of mutant strains of *Neisseria gonorrhoeae* lacking new antibiotic resistance markers using a two gene cassette with positive and negative selection. Gene, **236**: 179–184. doi:10.1016/S0378-1119(99)00238-3. PMID: 10433979.

Joseph, B., Schwarz, R.F., Linke, B., Blom, J., Becker, A. Claus, H., et al. 2011. Virulence evolution of the human pathogen *Neisseria meningitidis* by recombination in the core and accessory genome. PLoS One, **6**: e18441. doi:10.1371/journal.pone.0018441. PMID: 21541312.

Kaczmarczyk, A., Vorholt, J.A., and Francez-Charlot, A. 2012. Markerless gene deletion system for sphingomonads. Appl. Environ. Microbiol. **78**: 3774–3777. doi:10.1128/AEM.07347-11. PMID: 22427496.

Kellogg, D.S., Jr., Peacock, W.L., Jr., Deacon, W.E., Brown, L., and Pirkle, D.I. 1963. *Neisseria gonorrhoeae*. I. Virulence genetically linked to clonal variation. J. Bacteriol. **85**: 1274–1279. doi:10.1128/jb.85.6.1274-1279.1963. PMID: 14047217.

Kohler, P.L., Cloud, K.A., Hackett, K.T., Beck, E.T., and Dillard, J.P. 2005. Characterization of the role of LtgB, a putative lytic transglycosylase in *Neisseria gonorrhoeae*. Microbiology (Reading), **151**: 3081–3088. doi:10.1099/mic.0.28125-0. PMID: 16151218.

Li, X.T., Thomason, L.C., Sawitzke, J.A., Costantino, N., and Court, D.L. 2013. Positive and negative selection using the tetA-sacB cassette: recombineering and P1 transduction in *Escherichia coli*. Nucleic Acids Res. **41**: e204. doi:10.1093/nar/gkt1075. PMID: 24203710.

Li, Y., Thompson, C.M., and Lipsitch, M. 2014. A modified Janus cassette (Sweet Janus) to improve allelic replacement efficiency by high-stringency negative selection in *Streptococcus pneumoniae*. PLoS One, **9**: e100510. doi:10.1371/journal.pone.0100510. PMID: 24959661.

Ma, M., Powell, D.A., Weyand, N.J., Rhodes, K.A., Rendon, M.A., Frelinger, J.A., and So, M. 2018. A natural mouse model for *Neisseria* colonization. Infect. Immun. **86**: e00839–17. doi:10.1128/IAI.00839-17.

Maiden, M.C., and Harrison, O.B. 2016. Population and functional genomics of Neisseria revealed with gene-by-gene approaches. J. Clin. Microbiol. **54**: 1949–1955. doi:10.1128/JCM.00301-16. PMID: 27098959.

Marri, P.R., Paniscus, M., Weyand, N.J., Rendon, M.A., Calton, C.M. Hernandez, D.R., et al. 2010. Genome sequencing reveals widespread virulence gene exchange among human *Neisseria* species. PLoS One, **5**: e11835. doi:10.1371/journal.pone.0011835.

Mell, J.C., and Redfield, R.J. 2014. Natural competence and the evolution of DNA uptake specificity. J. Bacteriol. **196**: 1471–1483. doi:10.1128/JB.01293-13. PMID: 24488316.

Nyongesa, S., Weber, P., Bernet, E., Pullido, F., Nieckarz, M., Delaby, M., et al. 2022. Evolution of multicellular longitudinally dividing oral cavity symbionts (Neisseriaceae). Research Square. doi:10.21203/rs.3.rs-1200288/v1.

Perrin, A., Nassif, X., and Tinsley, C. 1999. Identification of regions of the chromosome of *Neisseria meningitidis* and *Neisseria gonorrhoeae* which are specific to the pathogenic *Neisseria* species. Infect. Immun. **67**: 6119–6129. doi:10.1128/IAI.67.11.6119-6129.1999. PMID: 10531275.

Putonti, C., Nowicki, B., Shaffer, M., Fofanov, Y., and Nowicki, S. 2013. Where does *Neisseria* acquire foreign DNA from: an examination of the source of genomic and pathogenic islands and the evolution of the Neisseria genus. BMC Evol. Biol. **13**: 184. doi:10.1186/1471-2148-13-184. PMID: 24007216.

Reyrat, J.M., Pelicic, V., Gicquel, B., and Rappuoli, R. 1998. Counterselectable markers: untapped tools for bacterial genetics and pathogenesis. Infect. Immun. **66**: 4011–4017. doi:10.1128/IAI.66.9.4011-4017.1998. PMID: 9712740.

Rowley, J., Vander Hoorn, S., Korenromp, E., Low, N., Unemo, M., Abu-Raddad, L.J., et al. 2019. Chlamydia, gonorrhoea, trichomoniasis and syphilis: global prevalence and incidence estimates, 2016. Bull. World Health Organ. **97**: 548–62P. doi:10.2471/BLT.18.228486. PMID: 31384073.

Sander, P., Springer, B., and Bottger, E.C. 2001. Gene replacement in *Mycobacterium tuberculosis* and *Mycobacterium bovis* BCG using *rpsL* as a dominant negative selectable marker. Methods Mol. Med. **54**: 93–104. doi: 10.1385/1-59259-147-7:093. PMID:21341071.

Santos, J.M., Lobo, M., Matos, A.P., De Pedro, M.A., and Arraiano, C.M. 2002. The gene *bolA* regulates dacA (PBP5), dacC (PBP6) and ampC (AmpC), promoting normal morphology in Escherichia coli. Mol. Microbiol. **45**: 1729–1740. doi:10.1046/j.1365-2958.2002.03131.x. PMID: 12354237.

Sung, C.K., Li, H., Claverys, J.P., and Morrison, D.A. 2001. An *rpsL* cassette, Janus, for gene replacement through negative selection in *Streptococcus pneumoniae*. Appl. Environ. Microbiol. **67**: 5190–5196. doi:10.1128/AEM.67.11.5190-5196.2001. PMID: 11679344.

Tacconelli, E., Carrara, E., Savoldi, A., Harbarth, S., Mendelson, M., Monnet, D.L., et al. 2018. Discovery, research, and development of new antibiotics: the WHO priority list of antibiotic-resistant bacteria and tuberculosis. Lancet Infect. Dis. **18**: 318–327. doi:10.1016/S1473-3099(17)30753-3. PMID: 29276051.

Trindade, S., Sousa, A., Xavier, K.B., Dionisio, F., Ferreira, M.G., and Gordo, I. 2009. Positive epistasis drives the acquisition of multidrug resistance. PLoS Genet. **5**: e1000578. doi:10.1371/journal.pgen.1000578. PMID: 19629166.

van Dam, V., and Bos, M.P. 2012. Generating knock-out and complementation strains of *Neisseria meningitidis*. Methods Mol. Biol. **799**: 55–72. doi:10.1007/978-1-61779-346-2_4. PMID: 21993639.

Veyrier, F.J., Boneca, I.G., Cellier, M.F., and Taha, M.K. 2011. A novel metal transporter mediating manganese export (MntX) regulates the Mn to Fe intracellular ratio and *Neisseria meningitidis* virulence. PLoS Pathog. **7**: e1002261. doi:10.1371/journal.ppat.1002261. PMID: 21980287.

Veyrier, F.J., Biais, N., Morales, P., Belkacem, N., Guilhen, C., Ranjeva, S., et al. 2015. Common cell shape evolution of two nasopharyngeal pathogens. PLoS Genet. **11**: e1005338. doi:10.1371/journal.pgen.1005338. PMID: 26162030.

Weyand, N.J. 2017. Neisseria models of infection and persistence in the upper respiratory tract. Pathog. Dis. **75**: ftx031. doi: 10.1093/femspd/ftx031. PMID: 28369241.

Weyand, N.J., Wertheimer, A.M., Hobbs, T.R., Sisko, J.L., Taku, N.A., Gregston, L.D., et al. 2013. Neisseria infection of rhesus macaques as a model to study colonization, transmission, persistence, and horizontal gene transfer. Proc. Natl. Acad. Sci. USA, **110**: 3059–3064. doi:10.1073/pnas.1217420110. PMID: 23382234.

Yan, Q., and Fong, S.S. 2017. Challenges and advances for genetic engineering of non-model bacteria and uses in consolidated bioprocessing. Front. Microbiol. **8**: 2060. doi:10.3389/fmicb.2017.02060. PMID: 29123506.

Zarantonelli, M.L., Szatanik, M., Giorgini, D., Hong, E., Huerre, M., Guillou, F., et al. 2007. Transgenic mice expressing human transferrin as a model for meningococcal infection. Infect. Immun. **75**: 5609–5614. doi:10.1128/IAI.00781-07. PMID: 17893132.

Zhang, Y. 2017. The CRISPR–Cas9 system in *Neisseria* spp. Pathog. Dis. **75**: ftx036. doi:10.1093/femspd/ftx036.

Supplementary material

Table S1: Bacterial strains used in this study

Strain	**Source**
Neisseria elongata subsp. *glycolytica* ATCC 29315	American type culture collection
rpsL^{K43R}	This study
Δ*bolA*::RPCC	This study
Δ*bolA*	This study
Δ*mtgA*::RPLK	This study
Δ*mtgA*	This study
::RPLK	This study
::Lux	This study
ΔA::RPLK	This study
ΔA	This study
ΔB::RPLK	This study
ΔB	This study
ΔC::RPLK	This study
ΔC	This study
ΔD::RPLK	This study
ΔD	This study
ΔE::RPLK	This study
ΔE	This study
ΔF::RPLK	This study
Neisseria meningitidis LNP20553	(Zarantonelli, Lancellotti et al. 2008)
rpsL^{K43R}	This study
::RPLK	This study
::Lux	This study
Neisseria musculi CCUG68283	DSMZ- German collection of Microorganisms and Cell Cultures GmbH
rpsL^{K43R}	This study
::RPLK	This study
::Lux	This study
Neisseria meningitidis LNP24198 lux (Km)	(Guiddir, Deghmane et al. 2014)
Escherichia. coli DH5α	ThermoFisher Scientific

Table S2: Plasmids used in this study

Plasmid	Characteristics	Source
pJet1.2	Cloning vector	Thermo Fisher
pCR4blunt-TOPO	Cloning vector	Invitrogen
pUC57	Cloning vector	Biobasic
pCR3	Contains *porbp-lacZ*-Km^R	This study
pGEM::Km	kanamycin resistance	(Veyrier, Boneca et al. 2011)
mini-CTX-lacZ	lacZ marker	(Hoang, Kutchma et al. 2000)
pRPLK	Contains the *rpsL*-*porbp*-*lacZ*-Km^R cassette	This study
pUC57::RPC	Contains *porb*p-mCherry-*rpsL*	This study
pRPCC	Contains the *porb*p-mCherry-*rpsL*-Cm^R cassette	This study
p5'3'BolANe	Integrative plasmid for the modification of *bolA* in *N. elongata*	This study
p5'3' BolANe::RPCC	RPCC cassette inserted within the *N. elongata* integrative plasmid	This study
ppilEpLuc	Contains the luciferase operon under the *pilE* promoter	(Veyrier, Biais et al. 2015)
pporBLuxCDABE :: Km	Contains the luciferase operon under the *porB* promoter	This study
pCR_porbplux	Contains a *porbp-luxCDABE* cassette flanked by EcoRI sites	This study
pNm	Integrative plasmid that recombines in an intergenic region of *N. meningitidis*	This study
pNm::RPLK	RPLK cassette inserted within the *N. meningitidis* integrative plasmid	This study
pNm::lux	Luminescence cassette inserted within the *Nm* integrative plasmid	This study

pNmus	Integrative plasmid that recombines in an intergenic region of *N. musculi*	This study
pNmus::RPLK	RPLK cassette inserted within the *N. musculi* integrative plasmid	This study
pNmus::lux	Luminescence cassette inserted within the *N. musculi* integrative plasmid	This study
pNelon	Integrative plasmid that recombines in an intergenic region of *N. elongata*	Biobasic
pNelon::RPLK	RPLK cassette inserted within the *N. elongata* integrative plasmid	This study
pNelon::lux	Luminescence cassette inserted within the *N. elongata* integrative plasmid	This study
p5’3’A	Integrative plasmid for the modification of locus A in *N. elongata*	This study
p5’3’A::RPLK	RPLK cassette inserted within the *N. elongata* integrative plasmid	This study
p5’3’B	Integrative plasmid for the modification of locus B in *N. elongata*	This study
p5’3’B:RPLK	RPLK cassette inserted within the *N. elongata* integrative plasmid	This study
p5’3’C	Integrative plasmid for the modification of locus C in *N. elongata*	This study
p5’3’C::RPLK	RPLK cassette inserted within the *N. elongata* integrative plasmid	This study
p5’3’D	Integrative plasmid for the modification of locus D in *N. elongata*	This study
p5’3’D::RPLK	RPLK cassette inserted within the *N. elongata* integrative plasmid	This study
p5’3’E	Integrative plasmid for the modification of locus E in *N. elongata*	This study
p5’3’E::RPLK	RPLK cassette inserted within the *N. elongata* integrative plasmid	This study

p5’3’F	Integrative plasmid for the modification of locus F in *N. elongata*	This study
p5’3’F::RPLK	RPLK cassette inserted within the *N. elongata* integrative plasmid	This study

Note: The p5’3’GOI mentioned in the main article is a theoretical construct containing homology regions flanking any gene of interest. Examples of such constructs are herein named p5’3’A, p5’3’B etc.

Table S3: primers used in this study

Name	**Sequence 5’ – 3’**
porBpF	TTCGCTAGCGTGCTGAAGCACCAAGTG
porBpbluntR	CATGGCTGTATTCCTTTTTTGGTTAAG
porBplacZF	CTTAACCAAAAAAGGAATACAGCCATGACCATGATTACGGATTCACTG
lacZRKm7up	ATTTAGATGTCTAAAAAGCATTCAGACGGCACGCGAAATACGGGCAGACAG
Km7up	GCCGTCTGAATGCTTTTTAGACATCTAAAT
Km6	CCCAGCGAACCATTTGAGG
rpsLXbaI_F	TGA<u>TCTAGA</u>AATTCCTGCAGTATTACGCCG
rpsLNheI_R	TTA<u>GCTAGC</u>CGACGTGCCTATTTAACTCC
CmR_SpeI_F	AAGGCT<u>ACTAGT</u>CCGTGATATAGATTGAAAAGTGGATAG
CmR_PpuMI_R	AAGGCT<u>AGGACCC</u>GAAGTGCGCCCTTTAGTTCC
RTMtgA-F	GGCAGCATACTGACCTACCG
MtgAKpnI-R	GGC<u>GGTACC</u>GCCTTACTATACCCTG
5KOmtgA_F	CGCTCAGGAAGGGGTGGAAATCG
3KOmtgA_R	ACCGTGCCAAATATCGAAAGCCG
BolANe_F	CAGCAAATTCAGACGGCCTT
BolANe_R	CGGATACTGAGGGCATGGAT

BolA_ExtNe_F	TCCAAACCCATTACCCGACA
BolA_ExtNe_R	CCTGCCCTTGTTCCAGTTTC
5MraZF	CGCACCAAATTCGTAAACAATACC
5MraZR	GACCATAATAAATACGCCTAAACTCCG
RTMraZ_F	ATGCCGAAGTTCTGGAAATG
MraZKpnI_R	GACGGTACCATGTTGGAATTCCTGACTGCTC
RTRapZ_F	GAGGCTGGCTGTCGAGATAC
RapZKpn1_R	CGGGTACCATTGGATTGCCATGTTTTTC
Ne_PbP3_F	TGGGGCAAATACGAAAACGG
Ne_PbP3_R	AAAGGCTTGTTTGAACGGGC
Ne_gloB_F	TATCAATCACCGCCATTCCC
Ne_gloB_R	TGTCGCCGCAGAAAACAT
Ne_07135_F	TCCCGTGGTATTGGAAGCAT
Ne_07135_R	TTTTCCGCATCAGTTCGCAG
luxE_EcoRI_R	GCAGAAGAATTCAGTTAATCATGAGCACTGCAG
porBp_EcoRI_F	GCAGAAGAATTCTGCAAATATCGGTCAAAGCTAGC
LuxCNcoIF	GCACCATGGGTCGACATGACTAAAAAAA
LuxEPstIR	AGCCTGCAGTCAACTATCAAACGCTTC
porBp_NheI_F	TTCGCTAGCGTGCTGAAGCACCAAGTG
porBp_NcoI_R	TTTCCATGGCTGTATTCCTTTTTTGGTTAAG

Supplementary figure 1: Sequencing of the markerless *mtgA* deletion strain
Genomic DNA from the markerless *N. elongata* Δ*mtgA* strain was extracted, amplified by PCR using primers 5KOmtgA_F and 3KOmtgA_R and sequenced using the same primers. **A.** Illustration of the wild-type N. elongata genomic DNA (top), aligned with both sequencing products (bottom). Red regions represent unmatched nucleotides showing the deleted gene. **B.** Sequence alignment of A, where the *mtgA* gene is highlighted in yellow and the unmatched nucleotides from the sequencing products are highlighted in red.

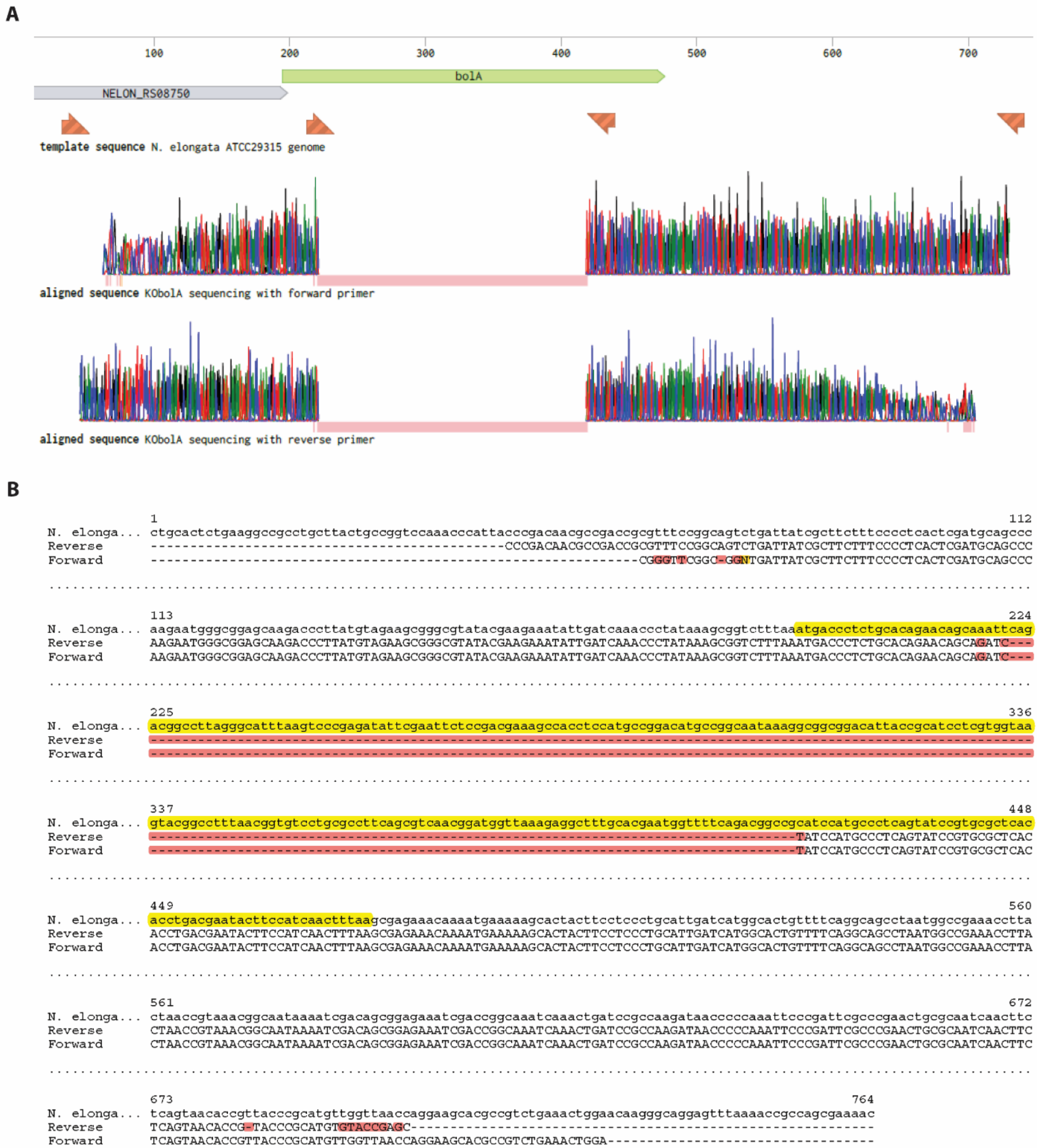

Supplementary figure 2: Sequencing of the markerless *bolA* deletion strain
Genomic DNA from the markerless *N. elongata* Δ*bolA* strain was extracted, amplified by PCR using primers BolA_ExtNe_F and BolA_ExtNe_R and sequenced using the same primers.
A. Illustration of the wild-type *N. elongata* genomic DNA (top), aligned with both sequencing products (bottom). Red regions represent unmatched nucleotides showing the deleted gene.
B. Sequence alignment of A, where the *bolA* gene is highlighted in yellow and the unmatched nucleotides from the sequencing products are highlighted in red. The "AGATC...T" mismatched nucleotides correspond to the BglII site inserted during the markerless cloning procedure.

5 ARTICLE 2:

Context of article 2:

Our current understanding of 5 multicellular longitudinally dividing *Neisseriaceae* residents of the mammalian buccal cavity (*S. muelleri, A. crassa, A. filiformis, C. steedae* and *C. kuhinae*) is based on studies conducted several decades ago. Indeed with the recent advancements in genomics and molecular biology techniques, little interest has been given to these bacteria principally because they are commensals. For this reason we embarked on collecting, imaging and performing whole genome sequencing of these and other commensal *Neisseriaceae* strains in order to establish first, a complete genome database for bioinformatics analysis to better understand the genetic factors responsible for the mode of cell division and multicellular phenotype. Secondly, with the strains collection, we aimed to study cellular organisation and septum PG synthesis during cell division. Finally genetic manipulation studies were conducted to determine the role of specific genetic events that might be associated with the longitudinal cell division and multicellular cell organization.

In general multicellular *Neisseriaceae* have a single 2.1 - 2.82 Mb long circular chromosome , with a GC content ranges between 41.5 and 56.2 %. Even though plasmid DNA is rarely present in *Neisseriaceae,* the *A. crassa* and *C. steedae* strains sequenced here had 1 and 2 plasmids respectively. The chromosome of *Simonsiella muelleri* ATCC 29453 strain, NCBI reference sequence NZ_CP019448.1 is 2.47 Mb long with a GC content of 41.5%. It has 2490 genes encoding for 2346 proteins. 67 pseudogenes are also present. *Alysiella filiformis* DSM16848 genome, NCBI reference sequence: NZ_CP059564.1 has a 2.43 Mb circular chromosome with a GC content of 46.6 %. It has 2364 genes encoding for 2238 proteins. 43 pseudogenes are also present. *Alysiella crassa* DSM 2578 strain has a larger 2.82 Mb circular chromosome with a 45.30 % GC content. A total of 2782 genes encoding for 2649 proteins in addition to 46 pseudogenes are present. A single 40.6 kb plasmid with a GC content of 41.2 % was also identified. *Conchiformibius kuhniae* DSM 17694 has a 2.12 Mb chromosome with relatively high GC content of 56.2 %. It has 2111 genes that encode for 2015 proteins. 28 pseudogenes are present. *Conchiformibius steedae* DSM 2580 strain, NCBI reference sequence NZ_CP059563.1 has a 2.1 Mb chromosome with GC content of 51%. It has 2092 coding genes that encode for 2002 proteins. Only 16 pseudogenes are present. The strain has two plasmids pDSM2580_1 , pDSM2580_2 NCBI reference sequence numbers NZ_CP059561.1 and NZ_CP059562.1 respectively. Plasmid pDSM2580_1 is 30 Kb long with a 40.5 % GC content. It has 16 genes that encode for 15 proteins. The second plasmid pDSM2580_2 is 80 kb long with a GC content of 44.9%. It has 52 genes encoding for 51 protein. Both pDSM2580_1 , pDSM2580_2 plasmids have a single pseudogenes. The Clusters of Orthologous Groups (COG) functions of the annotated plasmid genes displayed in figure 6.2 were predominantly assigned to the intracellular trafficking and cell cycle control categories in pAcrassa. In pDSM2580_1 they were mainly assigned to the replication and repair, secondary structure, and cell cycle control functions, while signal transduction, secondary structure and replication and repair were the predominant functions in pDSM2580_2. A considerable proportion of genes had unknown functions in both pDSM2580_1 and pDSM2580_2.

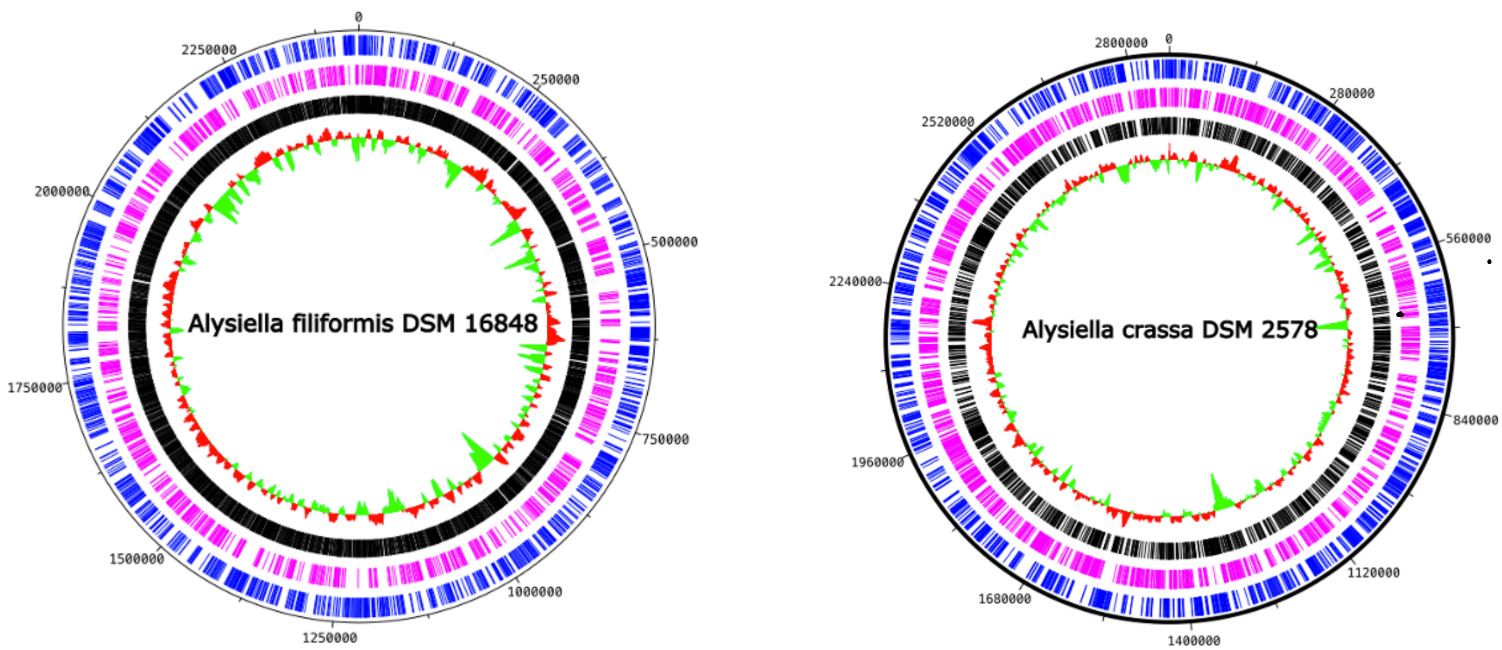

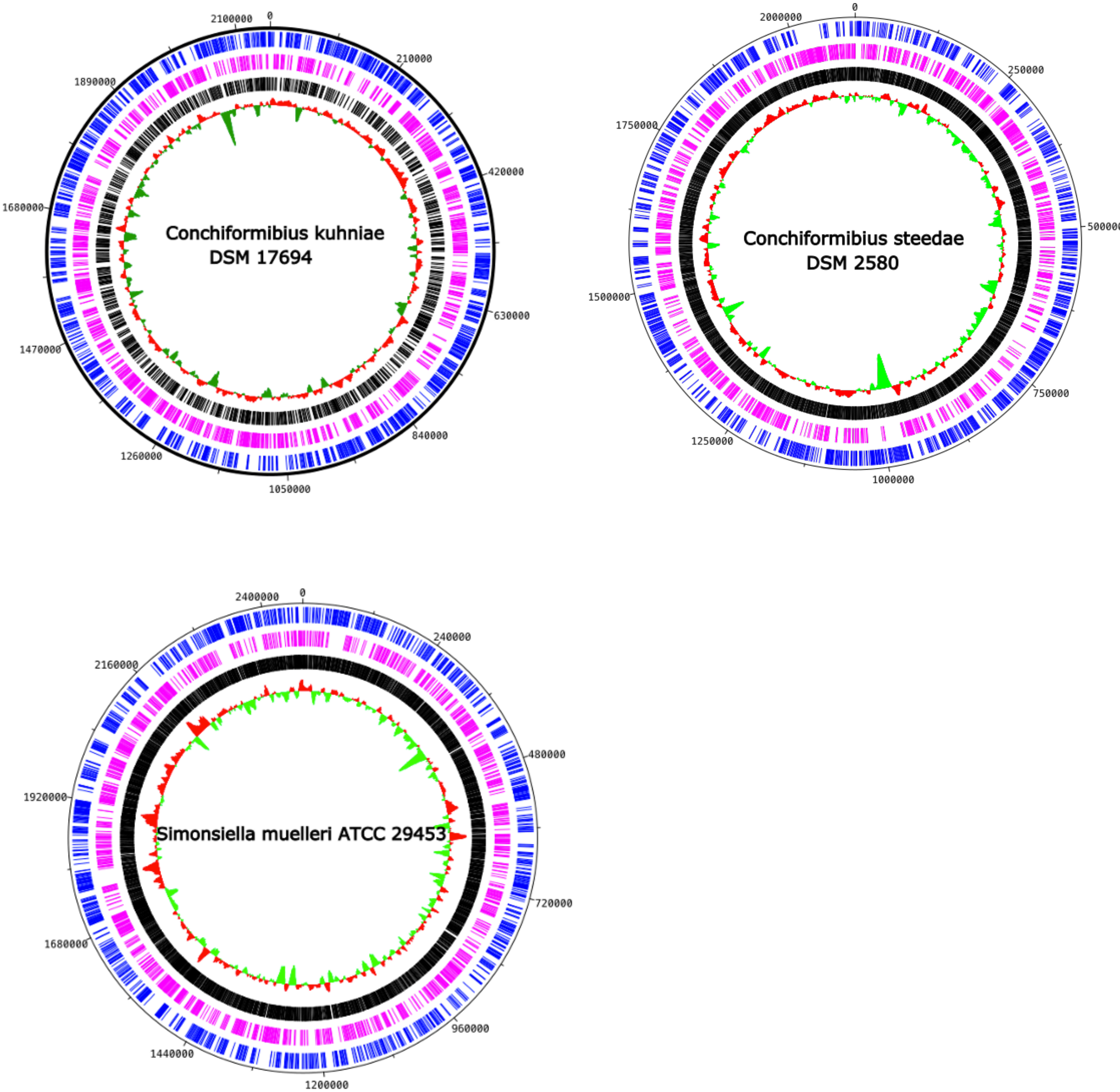

Figure 4.1: Circular representation of multicellular *Neisseriaceae* genomes. *Alysiella filiformis* DSM16848, *Alysiella crassa* DSM 2578, *Conchiformibius steedae* DSM 2580, *Conchiformibius kuhniae* DSM 17694, *Simonsiella muelleri* ATCC 29453 visualized by Artemis DNA plotter. Circles from the center to the outside: GC content (red = above average, green = below average), all genes (black) genes on the reverse strand (pink) genes on the forward strand (blue).

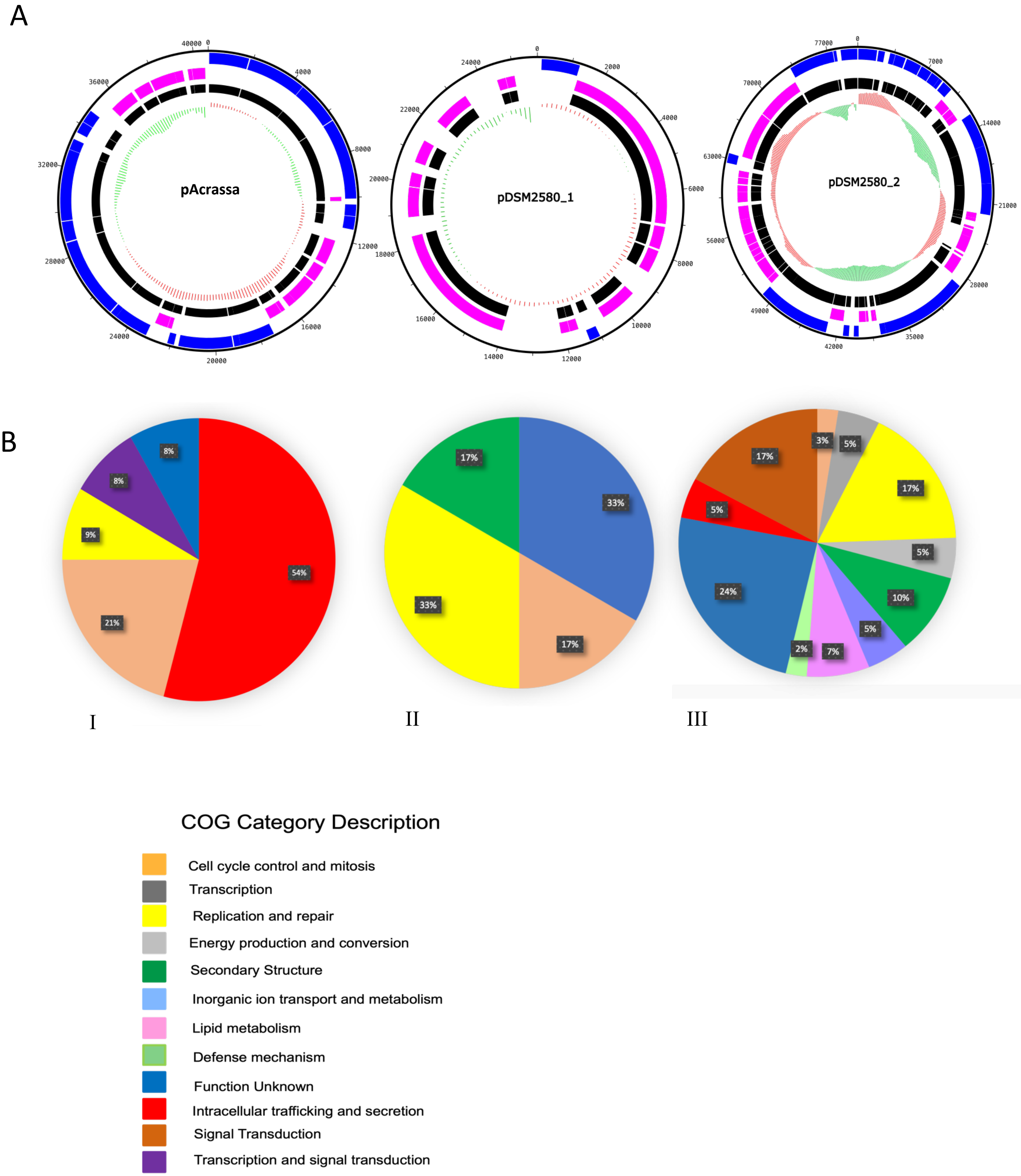
A
pAcrassa
pDSM2580_1
pDSM2580_2
B
I
II
III
COG Category Description
Cell cycle control and mitosis
Transcription
Replication and repair
Energy production and conversion
Secondary Structure
Inorganic ion transport and metabolism
Lipid metabolism
Defense mechanism
Function Unknown
Intracellular trafficking and secretion
Signal Transduction
Transcription and signal transduction

Figure 4.2: A, Circular representation of plasmid DNA visualized by Artemis DNA plotter from multicellular *Neisseriaceae* strains. The first two circles show genes on the forward (blue) and reverse (purple). The black circle represents the total genes while the inner circle shows the GC content where in green are genes with GC below average while in red are genes with GC content above average. B, charts showing the COG proportions of COG categories determined by EggNOG-mapper V. 5.0 (http://eggnog.embl.de). I. pAcrassa, II. pDSM2580_1, III. pDSM2580_2

First co-authors contributions

Through the use of a combination of approaches that included genomics, epiflourescent and electron microscopy imaging, transcriptomic analysis and mutagenesis, we pioneered the quest to understand longitudinal cell division and multicellular appearance in MuLDi *Neisseriaceae*. This work was successfully published our work in Nature communications, additionally this work was featured in multiple press releases and highlighted as one of the best papers recently published in microbiology.

In this publication Sammy Nyongesa did Nucleic acid extractions for genomic sequencing, assisted Prof F. Veyrier with bioinformatics and RNAsequencing analysis, performed peptidoglycan extractions, constructions of all mutants, transmission and scanning electron microscopy whole cell and thin section cuts of MuLDi and other *Neisseriaceae* and manuscripts writing.

Phillip Weber did peptidoglycan labelling assays using FDAA dyes in MuLDi *Neisseriaceae*, determined the pattern of septal peptidoglycan synthesis and cell division through epiflourescent microscopy, visualized the septal PG insertion pattern by confocal microscopy, determined the fimbriae localization pattern through immunolabeling and manuscript writing

nature communications

Article https://doi.org/10.1038/s41467-022-32260-w

Evolution of longitudinal division in multi-cellular bacteria of the *Neisseriaceae* family

Received: 10 January 2022

Accepted: 25 July 2022

Published online: 22 August 2022

Check for updates

Sammy Nyongesa[1,9], Philipp M. Weber[2,3,9], Ève Bernet[1], Francisco Pulido[1], Cecilia Nieves[1], Marta Nieckarz[4], Marie Delaby[5], Tobias Viehboeck[2,3,6], Nicole Krause[2,3], Alex Rivera-Millot[1], Arnaldo Nakamura[1], Norbert O. E. Vischer[7], Michael vanNieuwenhze[8], Yves V. Brun[5], Felipe Cava[4], Silvia Bulgheresi[2,10] & Frédéric J. Veyrier[1,10]

Rod-shaped bacteria typically elongate and divide by transverse fission. However, several bacterial species can form rod-shaped cells that divide longitudinally. Here, we study the evolution of cell shape and division mode within the family *Neisseriaceae*, which includes Gram-negative coccoid and rod-shaped species. In particular, bacteria of the genera *Alysiella*, *Simonsiella* and *Conchiformibius*, which can be found in the oral cavity of mammals, are multicellular and divide longitudinally. We use comparative genomics and ultrastructural microscopy to infer that longitudinal division within *Neisseriaceae* evolved from a rod-shaped ancestor. In multicellular longitudinally-dividing species, neighbouring cells within multicellular filaments are attached by their lateral peptidoglycan. In these bacteria, peptidoglycan insertion does not appear concentric, i.e. from the cell periphery to its centre, but as a medial sheet guillotining each cell. Finally, we identify genes and alleles associated with multicellularity and longitudinal division, including the acquisition of amidase-encoding gene *amiC2*, and amino acid changes in proteins including MreB and FtsA. Introduction of *amiC2* and allelic substitution of *mreB* in a rod-shaped species that divides by transverse fission results in shorter cells with longer septa. Our work sheds light on the evolution of multicellularity and longitudinal division in bacteria, and suggests that members of the *Neisseriaceae* family may be good models to study these processes due to their morphological plasticity and genetic tractability.

[1]INRS-Centre Armand-Frappier Santé Biotechnologie, Bacterial Symbionts Evolution, Laval, QC H7V 1B7, Canada. [2]Department of Functional and Evolutionary Ecology, Environmental Cell Biology Group, University of Vienna, Vienna, Djerassiplatz 1, 1030 Vienna, Austria. [3]University of Vienna, Vienna Doctoral School of Ecology and Evolution, Vienna, Austria. [4]Department of Molecular Biology and Laboratory for Molecular Infection Medicine Sweden (MIMS), Umeå Centre for Microbial Research (UCMR), Umeå University, Umeå SE-90187, Sweden. [5]Département de microbiologie, infectiologie et immunologie, Université de Montréal, Montréal, QC, Canada. [6]Division of Microbial Ecology, Center for Microbiology and Environmental Systems Science, , University of Vienna, Djerassiplatz 1, 1030 Vienna, Austria. [7]Bacterial Cell Biology & Physiology, Swammerdam Institute of Life Sciences, Faculty of Science, University of Amsterdam, Science Park 904, 1098 Amsterdam, the Netherlands. [8]Indiana University, Bloomington, IN 47405, USA. [9]These authors contributed equally: Sammy Nyongesa, Philipp M. Weber. [10]These authors contributed equally: Silvia Bulgheresi, Frédéric J. Veyrier. e-mail: silvia.bulgheresi@univie.ac.at; frederic.veyrier@inrs.ca

Allometry of animal-microbe associations suggests that 10^{25} prokaryotes thrive on animals and 10^{23} on humans[1,2]. Yet, the morphology and growth mode of animal symbionts are underexplored[3]. Although many may form biofilms (see for example refs. 4, 5), intestinal segmented filamentous bacteria (SFB[6–8]) and three genera of *Neisseriaceae* that occur in the oral cavity (e.g., *Alysiell*a, *Simonsiella* and *Conchiformibius*[9–12]), are the only known animal symbionts that may be regarded as multicellular, i.e., they invariably form stable filaments of more than two cells. SFB occur in the small intestine of several animals and play a primal role in pathogen resistance and gut homeostasis[13,14]. In contrast to SFB, multicellular oral cavity *Neisseriaceae* are relatively understudied. They are closely related to the other ≈30 species of *Neisseriaceae* occurring, for the majority, in the buccal cavity of warm-blooded vertebrates. They are cultivable and some are genetically tractable[15,16]. Apart from being multicellular, *Neisseriaceae* may be rod-shaped (e.g., *Neisseria elongata*) or coccoid (e.g., the human pathogens *Neisseria meningitidis* and *Neisseria gonorrhoeae*). *Alysiella filiformis* cells are 2 μm-long and 0.6 μm-wide on average and form upright-standing palisades on the squamous epithelium of the mouth, so that each cell has a proximal pole attached to the host epithelium and a distal, free pole (Figs. 1, 2b, and Supplementary Fig. 2a–d). Furthermore, within each filament, *A. filiformis* cells appear as paired (Fig. 2b, Supplementary Figs. 1c and 2a). Concerning *Simonsiella muelleri* and *Conchiformibius steedae* (previously known as *Simonsiella steedae*[11]) they are thinner, but can be up to 4 and 7 μm-long, respectively. Unlike *A. filiformis*, both poles of *S. muelleri* and *C. steedae* are attached to the mouth[11,17]. This confers *S. muelleri* and *C. steedae* cells a curved (or crescent-shaped) morphology and we will henceforth refer to their host-attached poles as proximal and to their midcell as their most-distal region (Figs. 1, 2c, d; Supplementary Figs. 1d, e and 2d–f).

Besides multicellularity, another peculiarity of *Alysiella*, *Simonsiella* and *Conchiformibius* is that they divide longitudinally ([11,18,19] and this manuscript). This is extraordinary, given that, except for nematode[20,21], insect[22] and dolphin symbionts[23], rod-shaped bacteria typically elongate and divide by transverse fission, two processes coordinated by the elongasome and divisome, respectively. In model bacteria, each of these machineries is constituted by over a dozen proteins, with the actin homolog MreB and the tubulin homolog FtsZ, respectively, orchestrating cell elongation and division[24]: deletion of *ftsZ* results in filamentation[25], whereas inactivation of *mreB* turned rods into cocci[16,26]. Even more striking was the effect of specific amino acid changes: in MreB, they resulted in irregularly sized, bent or branched *Escherichia coli* cells[27,28] and, when affecting FtsZ, they led to misplaced septa in *E. coli*, *Bacillus subtilis* and *Streptomyces* spp.[29–31]. Curiously, single amino acid mutations in the FtsZ-binding protein SsgB resulted in longitudinally dividing *Streptomyces*[32]. Collectively, these findings led to the hypothesis that longitudinal division might have evolved from differential regulation of subtly different MreB and/or FtsZ variants[33,34].

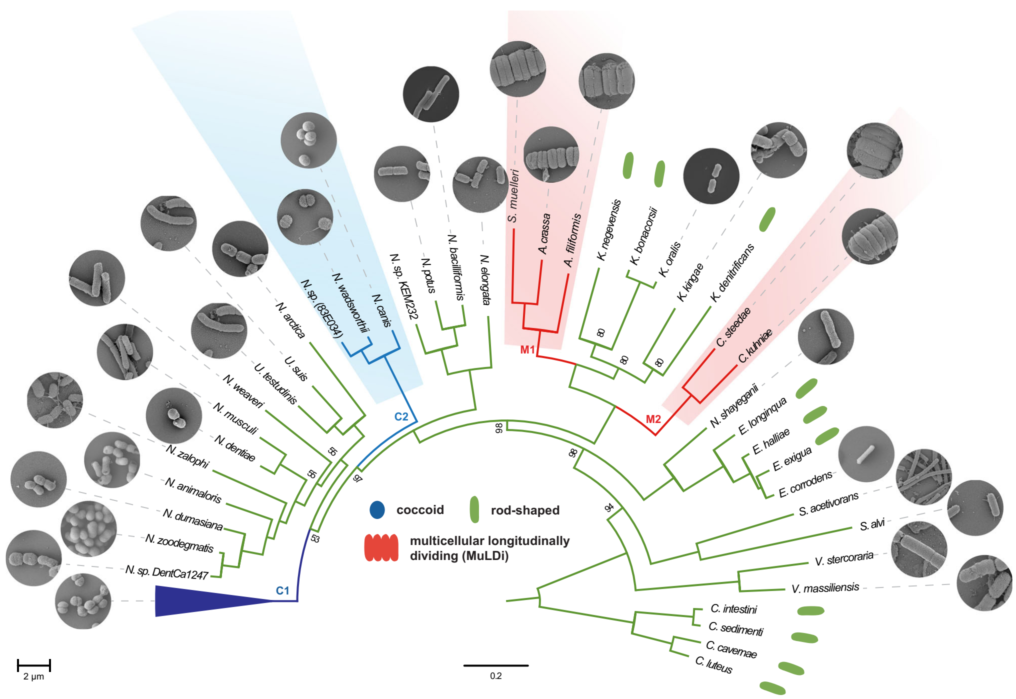

Fig. 1 | Core genome-based phylogeny of rod-shaped, coccoid and MuLDi *Neisseriaceae*. The best evolutionary model for each partition was found by IQ-TREE version 1.6.3[81] and maximum-likelihood phylogenetic analysis was also performed using IQ-TREE[82] using 10,000 ultrafast bootstrap replicates[83]. Above the name of each species, scanning electron microscopy images display their morphology. Dark and light blue: coccoid *Neisseriaceae*; green: rod-shaped *Neisseriaceae*; red: multicellular longitudinally dividing (MuLDi) *Neisseriaceae*. Coccoid lineages 1 and 2 are indicated in blue. MuLDi lineages 1 and 2 are indicated in red. N.: *Neisseria*; U.: *Uruburuella*; S.: *Simonsiella*; A.: *Alysiella*; K.: *Kingella*; C.: *Conchiformibius*; S.: *Snodgrassella*; V.: *Vitreoscilla*; E.: *Eikenella*; C.: *Crenobacter*. *Crenobacter* spp. served as outgroup. In the absence of electron microscopy images, species' morphology was defined as rod-shaped based on the reference strain describe in refs. 94 for *K. negevensis*[95], for *K. bonacorsii*[96], for *K. denitrificans*[97], for *E. longiqua* and *E. haliae*[98], for *Crenobacter luteus*[99], for *C. cavernae*[100], for *C. sedimenti*[101], for *C. intestine*.

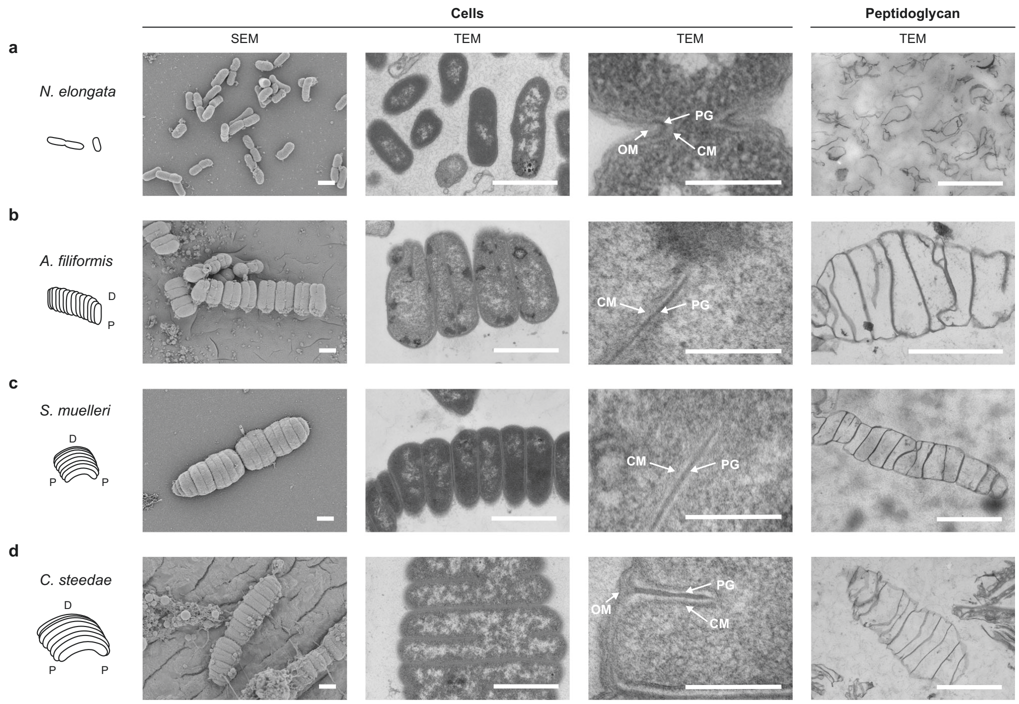

Fig. 2 | Ultrastructural analysis of four oral cavity symbionts belonging to the *Neisseriaceae*. Schematic representations and electron microscope images of **a** *N. elongata*, **b** *A. filiformis*, **c** *S. muelleri* and **d** *C. steedae*. Rightmost panels display extracted sacculi (peptidoglycan) of respective *Neisseriaceae*. P proximal (host-attached) region of the cell, D distal region of the cell, OM outer membrane, PG peptidoglycan, CM cytoplasmic membrane. Scale bars correspond to 1 μm. The results are representative of at least three independent analyses.

In this work, we ask whether a similar path led to the evolution of *Alysiella*, *Simonsiella* and *Conchiformibius* – henceforth, collectively referred to as multicellular longitudinally dividing (MuLDi) *Neisseriaceae*. Phylogenomic analysis coupled with both ultrastructural analysis and peptidoglycan (PG) mass spectrometry indicates that MuLDi *Neisseriaceae* evolved from a rod-shaped ancestor. Moreover, incubation with a palette of fluorescent D-amino acids (FDAAs) shows that nascent septa cross the cells medially as to guillotine them – from the proximal to the distal pole in *A. filiformis*, or from both poles to midcell in *S. muelleri* and *C. steedae*. Finally, comparative genomics-informed recapitulation of MuLDi-specific allelic changes in the rod-shaped *N. elongata* results in longer septa, suggesting that the transition from transverse to longitudinal division required the deletion of *mraZ*, the acquisition of *amiC2* and MreB amino acid permutations.

The capacity of oral cavity *Neisseriaceae* to have evolved – more than once – into coccoid or MuLDi cells from a rod-shaped ancestor, together with their amenability to cultivation and genetic manipulation, makes them ideal models to understand the evolution of bacterial cell division and that of animal-bacterium symbioses.

Results

Core genome-based phylogeny of *Neisseriaceae* suggests that MuLDi *Neisseriaceae* evolved from a rod-shaped ancestor

The *Neisseriales* order comprises the family *Chromobacteriaceae* and the family *Neisseriaceae* and more recently three additional families have been suggested, *Aquaspirillaceae*, *Chitinibacteraceae* and *Leeiaceae*[35]. The family *Neisseriaceae* includes 12 genera (*Alysiella; Bergeriella; Conchiformibius; Eikenella; Kingella; Morococcus; Neisseria; Simonsiella; Snodgrassella; Stenoxybacter; Uruburuella; Vitreoscilla*). We selected species from each of these *Neisseriaceae* genera and used SMRT (PacBio) and Minion (Nanopore) technologies to obtain 21 closed genomes (Supplementary Data 1). Genomes obtained in this study were combined with *Neisseriaceae* draft genomes (a total of 262, only one strain of *N. meningitidis* and one of *N. gonorrhoeae* were included) from the NCBI database to calculate the Average Nucleotide Identity (ANI) (Supplementary Data 2). This enabled us to identify 75 *Neisseriaceae* species with genome ANI > 96%. To assure the quality of the genomic database and to simplify the genomic comparisons, we then selected one genome for each species based on (1) completeness and circularization status, and (2) possibility to morphologically characterize it by either using a strain we have in our collection or by literature search (in the case of morphologically characterized reference strains). These 75 genomes have been used for the construction of a core genome-based phylogeny (Fig. 1, Supplementary Fig. 1, Supplementary Data 3). Of note, although most of the genomes available in the NCBI database are from coccoid *Neisseria* (lineage 1; dark blue in Fig. 1, representing 34 species), the detailed phylogenetic analysis of this lineage, which evolved from an ancestral rod[16] and includes the well-known pathogens *N. meningitidis* and *N. gonorrhoeae*, will be presented elsewhere (Bernet and Veyrier, unpublished data). In this manuscript, we therefore focused on the analysis of the remaining 41 species (Fig. 1, Supplementary Data 1).

Using Scanning-Electron Microscopy (SEM), we imaged all the species available in public collections to classify them as rod, cocci or MuLDi. The cell-shape of 10 species was already known (see references in Fig. 1's legend). Of note, species that could not be unambiguously classified as rods or cocci, were incubated in sublethal concentrations of Penicillin G to test their elongation capacity, as previously described[16]. These morphological analyses revealed that most *Neisseriaceae* are rod-shaped, except for the previously identified coccoid lineage 1[16] and the two closely related species *N. wadsworthii* and *N. canis*. These did not lengthen upon Penicillin G treatment and are henceforth referred to as coccoid lineage C2 (light blue branches in Fig. 1). Remarkably, we found that coccoid species belonging to lineage 2 harbour genes encoding for the elongasome, but lost *yacF/zapD* (Fig. 5). The loss of *yacF/zapD* has already been described as a major genetic event, which also allowed the emergence of coccoid lineage 1[16]. We also observed that MuLDi species are separated into two lineages, henceforth referred to as MuLDi lineage M1 (*Alysiella* spp. and *Simonsiella muelleri)* and M2 (*Conchiformibius* spp.) with the monophyletic *Kingella* genus separating them, in agreement with a recently published study[35]. To extrapolate the shape of the ancestor of all *Neisseriaceae*, we used a Maximum Likelihood method (PastML[36]) which made us infer that the predecessor of all *Neisseriaceae* was a rod (see Supplementary Fig. 1). This conclusion is supported by the fact that species belonging to the closely related family *Chromobacteriaceae* (order *Neisseriales*, as aforementioned) are also described as rod-shaped[37].

Collectively, our phylogenetic analysis indicates that two lineages of cocci (coccoid lineages 1 and 2, referred to as C1 and C2 in Fig. 1) evolved independently from a rod-shaped ancestor, whereas the two lineages of MuLDi *Neisseriaceae* (referred to as M1 and M2 in Fig. 1) evolved from a rod-shaped ancestor. However, PastML-based analysis (Supplementary Fig. 1) was not able to determine the shape of the most recent common ancestor of M1, M2 and *Kingella* spp. This let us envision two evolutionary scenarios: (1) M1 and M2 evolved independently from a rod-shaped bacterium with phenotypic convergence or (2) the common ancestor of M1 (*Simonsiella/Alysiella), Kingella* spp. and M2 (*Conchiformibius*) evolved the MuLDi phenotype once from a rod-shaped bacterium, but *Kingella* spp. reverted to unicellularity and transverse division.

MuLDi *Neisseriaceae* cells are attached to one another by their lateral PG and harbour a characteristic signature in their muropeptide composition

Previous[11,18,19], as well as our, microscopic analyses (see Figs. 1–4, Supplementary Figs. 2c–e, 3–8, and Supplementary Movies 1–4) suggested that *A. filiformis*, *S. muelleri* and *C. steedae* filaments result from incomplete cell separation. Moreover, Nile red staining confirmed the presence of membranes between adjoining cells (Supplementary Fig. 4a, d). To understand whether adjoining MuLDi *Neisseriaceae* share additional cellular structures, that prevent them to separate from one another, we performed transmission electron microscopy (TEM) of sacculi extracted from *A. filiformis*, *S. muelleri* and *C. steedae*, as well as from the transversally dividing rod-shaped *N. elongata*, for comparison (rightmost panels in Fig. 2b–d). We observed that the sacculi of the three MuLDi symbionts remained attached laterally, even after the harsh extraction procedure (rightmost panels in Fig. 2b–d). Moreover, higher magnification of TEM images revealed that cells belonging to the same filament shared their outer membrane (OM; arrows in Fig. 2b–d). We concluded that in the *Neisseriaceae A. filiformis*, *S. muelleri* and *C. steedae* multicellularity results from adjoining cells, retaining their cytoplasmic membranes (CM), but being attached to one another by their lateral PG and surrounded by a common OM (and periplasm) (see Supplementary Fig. 3).

We previously showed that a modification in the PG composition of the *Neisseriaceae* (i.e., increased proportion of pentapeptides) accompanied their rod-to-coccus transition[16]. To find out whether the rod-to-MuLDi transition would also correlate with a change in total muropeptide composition, we applied mass spectrometry to analyze the PG of three MuLDi: *A. filiformis*, *S. muelleri* and C. *steedae*, as well as that of 14 rod-shaped *Neisseriaceae* (Supplementary Fig. 5, Supplementary Data 4). The abundance of dimers (Di), trimers (Tri) and tetramers (Tetra) relative to the abundance of monomers and the estimated total crosslinked were generally higher in MuLDi (Supplementary Fig. 5c, d). We concluded that, compared to rod-shaped *Neisseriaceae*, MuLDi *Neisseriaceae* PG was more cross-linked (Supplementary Fig. 5).

Alysiella filiformis nascent septa guillotine the cells from their distal to their proximal poles

Fimbriae-like structures were detected by TEM on the regions of *A. filiformis* attached to oral epithelial cells[17–19]. To confirm the presence of fimbriae at the proximal pole, we immunostained them with an anti-fimbriae antibody and found its signal to be localized at the proximal pole, consistent with the seminal ultrastructural data. Moreover, we noticed that, when observed at the epifluorescence microscope, the proximal, fimbriae-rich side of each filament was invariably the convex one (Supplementary Fig. 4a–c, f), which allowed us to determine *A. filiformis* polarity in the absence of fimbriae localization in all the subsequent microscopic analyses.

After confirming *A. filiformis* polarity, we proceeded to determine its growth mode by tracking PG synthesis by consecutively applying the three fluorescent D-amino acids (FDAAs) HADA (blue), BADA (green) and TADA (red), which are labeled D-Ala residues incorporated into the peptide side chains of new PG. When observed by fluorescence microscopy, *A. filiformis* cells sequentially labeled with HADA 30 min, BADA 15 min and TADA 15 min showed strongest fluorescent signal at their septation planes. The virtual time-lapse obtained by the triple FDAAs labeling revealed that *A. filiformis* starts to septate at the distal pole and that PG synthesis proceeded unidirectionally toward the proximal cell pole (blue, green and red signal in representative septa in Fig. 3a). Of note, within each filament, newly completed septa (asterisks) alternate with nascent septa (arrowheads in Fig. 3a right panel). This indicates that septation starts as soon as cells are born (or even before). Plotting the total fluorescence of HADA, BADA and TADA against the cell long axis in a representative nascent septum (septum 1; Fig. 3b, left plot), in an almost completed septum (septum 2; Fig. 3b right plot), as well as in ten *A. filiformis* cells undergoing ten subsequent septation stages (Supplementary Fig. 6a–c) confirmed the distal-to-proximal PG incorporation pattern (Fig. 3c) and was consistent with that observed by thin-section TEM (Fig. 2b).

To view the PG insertion pattern in 3D, we performed confocal microscopy (Fig. 3d, Supplementary Fig. 6d and Supplementary Movie 5). Surprisingly, the septal signal appeared as a sheet when viewed from the side in completed and nascent septa (asterisks and arrowheads, respectively, in Fig. 3d left panel; Supplementary Fig. 6d) and, contrarily to what observed by 3D-Structured Illumination Microscopy in other longitudinally[38] or transversally dividing bacteria[39,40], we did not observe PG disks, rings or arcs at any septation stage.

In conclusion, we showed that *A. filiformis* septation is unidirectional (i.e., it proceeds from the distal to the proximal pole) and that the PG is not inserted concentrically, from the periphery to the center of the cell, but as a sheet that guillotined each cell from its distal to its proximal pole.

Simonsiella muelleri and *Conchiformibius steedae* septation starts at both poles synchronously and proceeds from the poles to midcell

Based on previous ultrastructural studies, *S. muelleri* fimbriae are situated on the cell side facing the epithelial cells[17,19], here referred to as the proximal side. To test whether this was also the case for *C. steedae*, we immunostained it with an anti-fimbriae antibody and confirmed that fimbrial appendages covered the proximal (concave) side of each filament (Supplementary Fig. 4e, f).

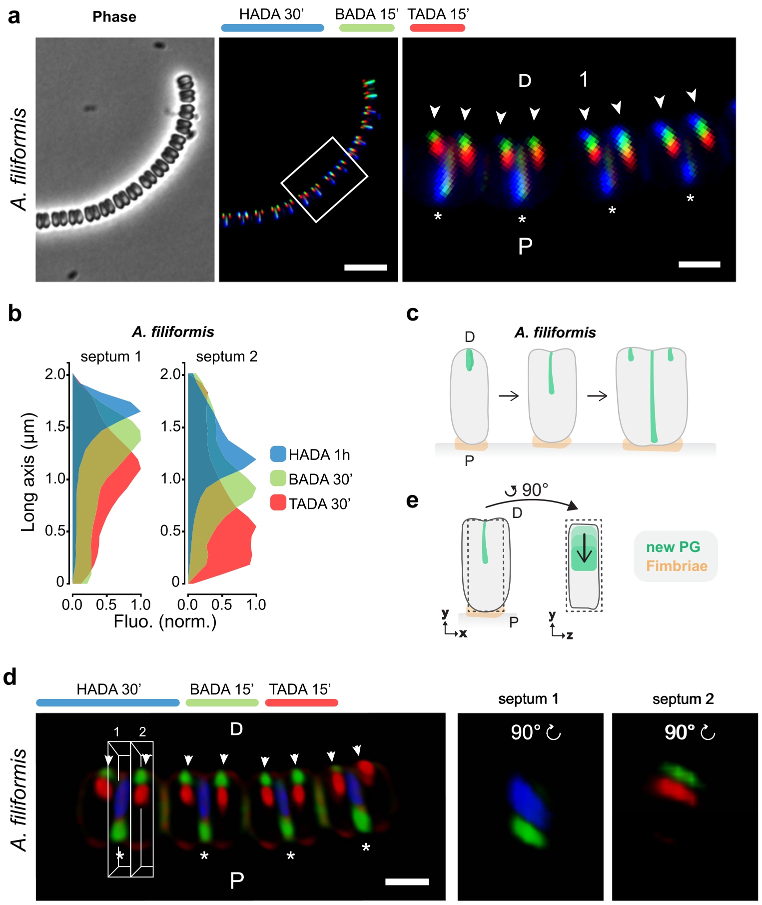

Fig. 3 | Epifluorescence and confocal microscope-based PG insertion pattern in *A. filiformis*. **a** Phase contrast image (left panel), corresponding epifluorescence image (middle panel) and enlarged selected regions (white frames in right panel) of *A. filiformis* consecutively labeled with HADA, BADA and TADA for 30 min, 15 min and 15 min, respectively. Asterisks point at newly completed septa and arrowheads point to nascent septa. Scale bars are 5 µm (middle panels) and 1 µm (right panels). **b** Septal fluorescence of HADA, BADA and TADA was plotted onto the long axis for two representative *A. filiformis* cells. Source data are provided as a Source Data file. **c** Schematic representation of *A. filiformis* growth mode. **d** Confocal images of *A. filiformis* consecutively labeled with HADA, BADA and TADA for 30 min, 15 min and 15 min, respectively. Asterisks point at newly completed septa and arrowheads point at nascent septa in a filament (left panel). Fluorescence emitted by a newly completed septum (septum 1 in white box in left panel) and by an incoming septum (septum 2 in white box in left panel) were rotated by 90° and are displayed in the middle and the right panels, respectively. Scale bar is 1 µm. **e** Schematic representation of *A. filiformis* growth mode. D distal, P proximal. The results are representative of at least three independent analyses.

To find out how *S. muelleri* and *C. steedae* grow, we then tracked the synthesis of PG by successively labeling them in three differently colored FDAAs, namely with HADA for 30 min, BADA 15 min and TADA 15 min, and with HADA for 1 h, BADA 45 min and TADA 45 min, respectively (Fig. 4a–d and Supplementary Fig. 7a–c). When imaged by epifluorescence microscopy, both species showed strongest fluorescent signal at the septation plane. However, the virtual time-lapse obtained by the triple FDAAs labeling differed from that obtained for *A. filiformis*. Namely, *S. muelleri* and *C. steedae*, appeared to start septation at both poles synchronously and PG insertion continued until midcell was reached (Fig. 4a–d and Supplementary Fig. 7a–c).

To view the PG insertion pattern in 3D, we performed confocal microscopy on FDAA- labeled *C. steedae* (Fig. 4e, f and Supplementary Fig. 8a, b; Supplementary Movie 6). When pulsing filaments with HADA, TADA and BADA, septation appeared to begin at the poles and proceeded towards midcell (blue, green and red signal in completed and nascent septa, indicated by asterisks or arrowheads, respectively, in Fig. 4e). When visualizing single cells turned of 90 degrees (Fig. 4e bottom images and Supplementary Fig. 8b), FDAA signal appeared as two juxtaposed triangular sheets, each emerging from one cell pole (green and red signal in septa 1 and 2 Fig. 4e). With septation progression, the two leading edges merged at midcell (red oval signal in Fig. 4e, septum 2) and finally appeared as a circular disk at the very last septation stage (red signal in Fig. 4e, septum 3 and one septum in Supplementary Fig. 6b).

Summarizing, we propose that the two curved oral symbionts *S. muelleri* and *C. steedae* start septation at each pole independently,

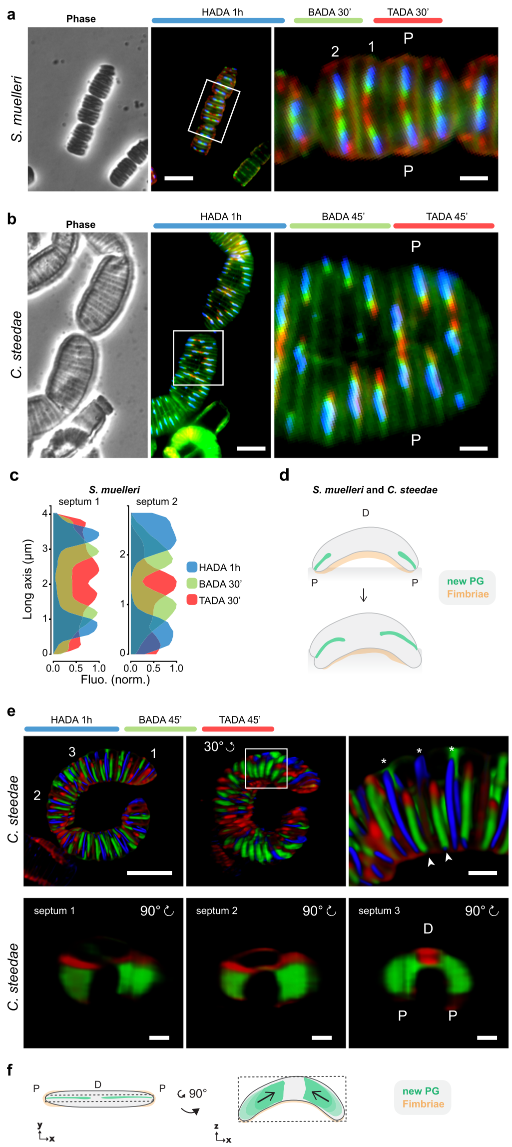

Fig. 4 | Epifluorescence and confocal microscopy-based PG insertion pattern in *S. muelleri* and *C. steedae*. Phase contrast images (left panels), corresponding epifluorescence images (middle panels) and enlarged selected regions (right panels; the white frames indicate the selected regions) of *S. muelleri* (**a**) labeled with HADA, BADA and TADA for 1 h, 30 min and 30 min, respectively and of *C. steedae* (**b**) labeled with HADA, BADA and TADA for 1 h, 45 min and 45 min, respectively. Scale bars are 5 µm (middle panels) and 1 µm (right panels). **c** For two representative *S. muelleri* septa (septum 1 and septum 2, left and right panel), fluorescence of HADA, BADA and TADA was plotted onto the long axis. Scale bars are 5 µm (left and middle panel) and 1 µm (right panel). Source data are provided as a Source Data file. **d** Schematic representation of *S. muelleri* and *C. steedae* growth mode. **e** Confocal images of one *C. steedae* filament labeled with HADA, BADA and TADA for 1 h, 45 min and 45 min, respectively (top panels). Top left panel displays the filament from which the three septa shown in the bottom panels belong to. Middle panel shows the same filament rotated by 30° of which an enlarged region of interest (white frame) is shown in the top right panel; arrowheads point to nascent septa, asterisks to newly completed ones. Bottom panels: three septa at consecutive septation stages (septa 1–3 in top left panel) were rotated by 90° and ordered from the youngest to the oldest (left, middle and right panel, respectively). D distal, P proximal. Scale bars are 5 µm (left upper corner) and 1 µm. **f** Schematic representations of *C. steedae* septation mode (top view in left panel, side view in right panel). The results are representative of at least three independent analyses.

but synchronously, and septation ends when the two pole-originated PG sheets meet and merge at midcell (Fig. 4f).

Multiple genetic events associated with the cell shape transition from rod-shaped to MuLDi *Neisseriaceae*

By applying exhaustive comparative genomics, we previously discovered that mutations at specific genetic loci mediated the rod-to-coccus transition of the ancestor of pathogenic *Neisseria*[16]. We therefore hypothesized that mutations at specific genetic loci had mediated their evolution from an ancestral, transversally dividing rod-shaped *Neisseriaceae* (Fig. 1). To identify these genetic loci, we applied previously described pipelines[16,41,42] to determine the presence/absence of proteins in 37 species of *Neisseriaceae* (all displayed in Fig. 1), 32 rod-shaped and 5 MuLDi *Neisseriaceae* (the *Simonsiella/Alysiella* lineage M1 and the *Conchiformibius* lineage M2). Of note, we excluded both lineages of coccoid *Neisseriaceae* from our analysis, as they underwent a different evolutionary path[16].

By using MycoHIT (based on tblastn) and by taking either the genome of the MuLDi *S. muelleri* or that of the rod-shaped *N. elongata* as a reference, we searched for genes specifically present in MuLDi or specifically present in rod-shaped *Neisseriaceae*, respectively. Firstly, using *S. muelleri* as a reference and 55% of similarity as a cut-off for assessing orthologs, we identified seven genes that were exclusively present in MuLDi, but absent in rod-shaped *Neisseriaceae* (Fig. 5a). These included a gene encoding for an AmiC-like amidase, henceforth referred to as AmiC2. Interestingly, the *amiC2* gene chromosomally co-locates with *cdsA*, a gene encoding for the phosphatidate cytidylyltransferase CdsA in all MuLDi species (Supplementary Fig. 9). As *amiC2* and *cdsA* are either flanked by a transposase (in the MuLDi lineage 1) or by a restriction/modification system (in the MuLDi lineage 2), we hypothesize that *amiC2* was acquired by horizontal gene transfer, possibly from a *Fusobacterium*-related bacterium (see AmiC1 and AmiC2 phylogeny in Supplementary Fig. 10). Intriguingly, Fusobacteria, as the *Neisseriaceae*, are common members of the oral, gastrointestinal and genital flora[43]. As for the remaining six MuLDi-specific genes, four are predicted to encode for hypothetical proteins and two for the hemolysin transporter ShlB[44].

Secondly, using *N. elongata* as a reference, we found that only four genes were exclusively absent in MuLDi *Neisseriaceae* when compared to rod-shaped ones (Fig. 5a), two of which, *mraZ* and *rapZ*, have been implicated in PG synthesis and cell division. *mraZ* is the first gene of the *dcw* cluster (Supplementary Fig. 9) in most bacteria, where it encodes for the poorly characterized, but highly conserved transcriptional regulator MraZ[45–47]. *rapZ* encodes for the small RNA adaptor protein RapZ, implicated in cell envelope precursor sensing and signaling[48]. As for the other two, *dgt* and *globB*, the former encodes for a dGTPase[49] and the latter for a hydroxyacylglutathione hydrolase that hydrolyzes S-D-lactoyl-glutathione into glutathione and D-lactic acid[50]. Of note, as the loss or gain of genes in the most recent common ancestor of the M1, M2 and *Kingella* spp. could have laid the foundation for further evolution, we also detected the presence of 14 genes and the absence of four genes in MuLDi as compared to other rod-shaped *Neisseriaceae* excluding the *Kingella* spp. (Supplementary Data 5).

Third and finally, we used the CapriB software[41] to search for amino acid changes in the 438 proteins strictly conserved among the

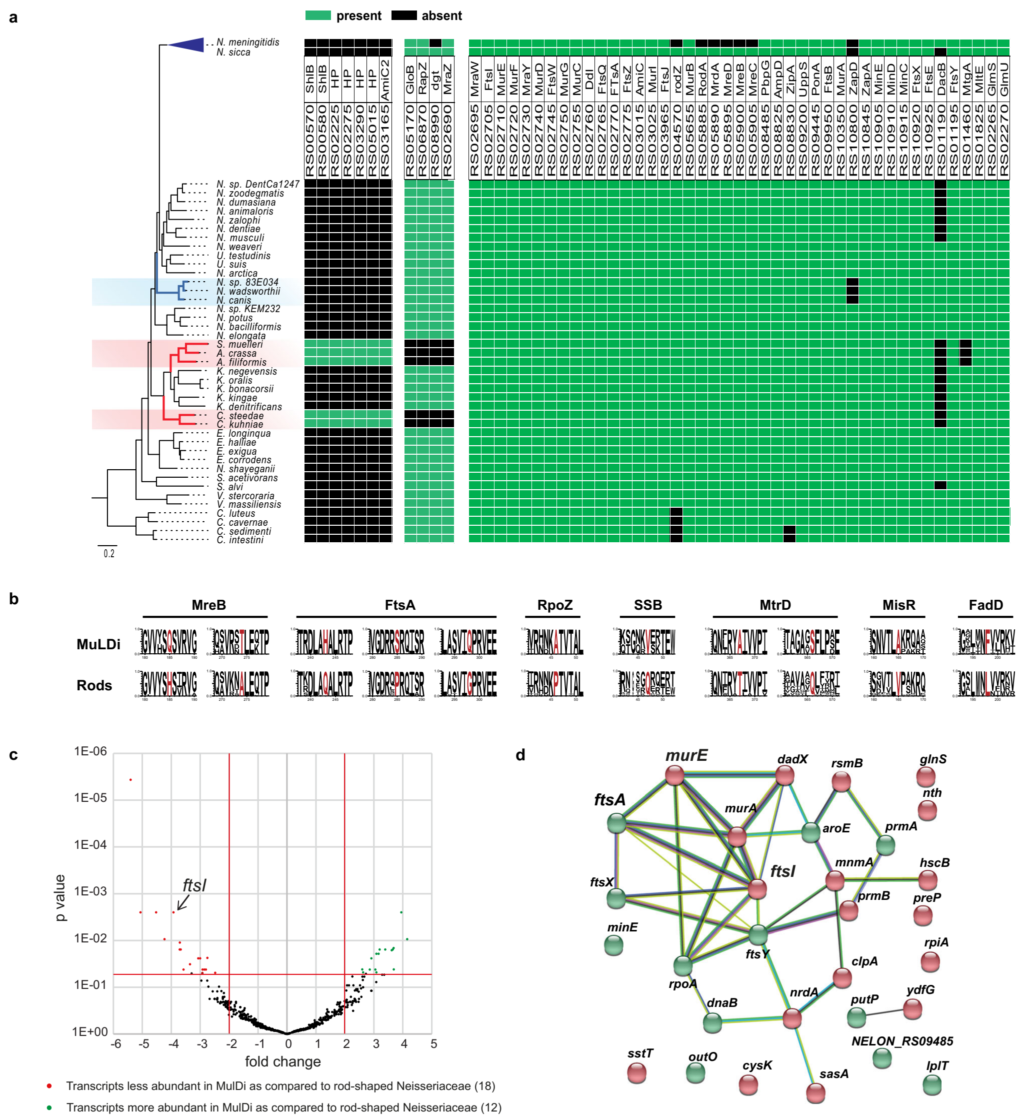

Fig. 5 | **Comparative genomics and transcriptomic of rod-shaped and MuLDi *Neisseriaceae*.** **a** Phylogenetic tree of *Neisseriaceae* species (left) and table displaying the distribution, within the family, of putatively inserted (left) or deleted (middle) genes. In addition, selected genes known to be involved in cell growth and/or division are shown (right). Individual genes were considered to be present when they had a sequence similarity ≥60% relative to *N. elongata* [an e-value cut-off of $1e^{-10}$ has also been applied in TBLASTN version 2.7.1 (Altschul et al.[102]). Present genes are indicated with *S. muelleri* locus_tag (such as RS00570 for BWP33_RS00570). All other genes are indicated with *N. elongata* locus_tag (such as RS02740 for NELON_RS02740). The putative encoded protein associated with each gene are also specified. The green and black squares indicate genes that are present or absent, respectively. HP hypothetical protein. **b** Weblogo of the amino acid sequences, of the 7 proteins displaying amino acid permutations rod-shaped or for MuLDi, detected with amino acid permutations between rod-shaped and MuLDi *Neisseriaceae*. **c** Volcano-plot: *p* value is plotted against fold change calculated using DeSeq2. Red and green points correspond to transcripts that are less or more abundant in MuLDi as compared to rod-shaped *Neisseriaceae*, respectively. Source data and statistics are provided as a Source Data file. **d** STRING association analysis. *ftsA*, *ftsI* and *murE* from the *dcw* cluster are highlighted. In red are transcripts that are less abundant in MuLDi *Neisseriaceae* and in green are transcripts that are more abundant in MuLDi as compared to rod-shaped *Neisseriaceae*.

37 *Neisseriaceae* species (core proteome) (Fig. 5b). Strikingly, we detected amino acid permutations in only seven out of the 438 proteins (1.6%). Namely, three and two permutations were found in FtsA and MreB, respectively, two proteins which are both involved in bacterial morphogenesis[51]. Consistently, the phylogeny based on FtsA or MreB protein sequences (Supplementary Fig. 10) revealed that all the MuLDi sequences clustered together, suggesting convergent evolution of these proteins or horizontal gene transfer between MuLDi species. In addition to FtsA and MreB, we also found two permutations in the efflux pump membrane transporter MtrD, and one permutation in the DNA-directed RNA polymerase subunit RpoZ, the single stranded DNA-binding protein Ssb, the two-component regulator MisR and the long-chain-fatty-acid-CoA ligase FadD.

Altogether, comparative genomics of rod-shaped versus MuLDi *Neisseriaceae* identified 18 genetic loci whose presence, absence or mutation strictly correlate with the rod-to-MuLDi transition. Notably, these genetic loci include *amiC2*, encoding for a cell wall amidase, the *dcw* cluster regulator-encoding gene *mraZ* and the actin homolog-encoding gene *mreB*.

Downregulation of *dcw* cluster genes in MuLDi *Neisseriaceae*

As several genes encoding for regulators were mutated in MuLDi *Neisseriaceae*, we employed RNAseq to determine differential gene expression patterns between MuLDi ($n = 5$) and rod-shaped ($n = 5$) *Neisseriaceae* cultured in the same conditions (GCB agar Media, 6 h, 37 °C 5% CO_2). To compare gene expression between species, we standardized the annotation of the five rod-shaped and the five MuLDi *Neisseriaceae* genomes by inferring gene orthology using BlastP (55% of similarity as a cut-off). Using the NetworkX python programming package[52], we reannotated clusters of homologous genes in each genome (for example, the *ftsZ* gene will be called NEISS_1241 in all genomes). By doing so, we could count the reads that mapped to each gene in each species and perform DESeq2 statistical analyses using the core transcriptome. Strikingly, our analysis (Fig. 5c, d) showed that the majority of the significantly differentially regulated genes are involved in cell envelope synthesis (as demonstrated by their clustering in the String analysis shown in Fig. 5d). Namely, 12 genes appeared upregulated in MuLDi species, including *minE, ftsA, ftsX and ftsY* involved in cell division. More importantly, the 19 downregulated genes in MuLDi species included *murE* and *ftsI*, which are part of the *dcw* cluster.

To conclude, based on comparative interspecies RNA-seq, the absence of *mraZ* correlates with a downregulation of the *dcw* cluster (including *ftsI*) in MuLDi *Neisseriaceae*.

Downregulation of *dcw* cluster genes in *N. elongata mraZ* deletion mutants

To test whether deletion of *mraZ* in the rod-shaped *Neisseriaceae N. elongata* could cause downregulation of *dcw* cluster genes (consistent with the apparent downregulation of the *dcw* cluster in MuLDi *Neisseriaceae* that naturally lost *mraZ*, see previous section), we compared the transcriptomes of wild-type *N. elongata* and a *mraZ* deletion mutant thereof. This revealed that five genes located downstream of *mraZ* (*mraW, ftsL, ftsI, murE* and *murF*) were downregulated (Fig. 6a, b). These results were confirmed by quantitative real-time PCR (Fig. 6c). Moreover, overexpressing *mraZ* (by inserting it, ectopically, downstream of the *nrq* locus in the *N. elongata* Δ*mraZ* mutant) led to overexpression of the first seven genes of the *dcw* cluster (Fig. 6a–c). Although the *N. elongata* Δ*mraZ* mutant did not display significant morphological defects (Fig. 6d), *N. elongata* overexpressing *mraZ* under the *porB* promoter (Δ*mraZ porBp-mraZ*) were smaller (Fig. 6d, e).

Collectively, we showed that *mraZ* is regulating transcription of the first five genes of the *N. elongata dcw* cluster and that expression of these genes impacts *N. elongata* cell length.

Recapitulation of MuLDi-specific genetic changes in the rod-shaped *Neisseriaceae, N. elongata*, resulted in longer septa

After deleting *mraZ*, we tested whether individual changes at other MuLDi-specific loci could turn the rod-shaped *Neisseriaceae N. elongata* in a MuLDi bacterium. Deletion of *dgt, gloB*, or *rapZ* did not change *N. elongata* morphology (Supplementary Fig. 11a). All the same, introduction of *amiC2* (along with its neighboring gene *cdsA*) in *N. elongata* did not result in significant shape or growth anomalies (Fig. 7a). However, the allelic exchange of *N. elongata mreB* with *S. muelleri mreB* resulted in significantly longer cells (Fig. 7a and Supplementary Fig. 11b, c).

In a final attempt to turn the rod-shaped *N. elongata* into a MuLDi *Neisseriaceae*, we used an unmarked deletion-based technique developed by us[15] to concomitantly delete *dgt*, *gloB*, *mraZ* and *rapZ*, substitute *N. elongata mreB* with *S. muelleri mreB* and introduce *amiC2*/*cdsA*. As shown in Fig. 7a and Supplementary Fig. 11b, c, N. *elongata* Δ*dgt*, Δ*gloB*, Δ*mraZ*, Δ*rapZ* with $mreB_{sm}$ were longer and branched. More importantly, the substitution of $mreB_{ne}$ with $mreB_{sm}$ together with the introduction of *amiC2/cdsA* resulted in cells with a longer septum and shorter axis perpendicular to the septum (Fig. 7b–d). Namely, the ratio between the two cell axes changed from 0.61 ± 0.25 ($n = 186$), in the wild-type, to 0.95 ± 0.29 ($n = 174$) in the mutant *N. elongata*.

All in all, even if our attempt to genetically manipulate the rod-shaped *N. elongata* into a MuLDi bacterium did not result into a complete transverse-to-longitudinal division switch (ratio between the two cell axes >1), the observed increase in septum length suggests that the genetic events identified by comparative genomics have participated in the rod-to-MuLDi *Neisseriaceae* transition.

Discussion

There is a huge discrepancy between the number of known prokaryotic species and the number that have been characterized morphologically. This makes it hard to predict how the shape and the growth mode of bacteria evolved. In an attempt to fill this knowledge gap, we focused on MuLDi *Neisseriaceae* occurring in the oral cavity of warm-blooded vertebrates, including humans. Whole genome-based phylogenetic analysis, coupled with ultrastructural analysis, indicated that MuLDi bacteria evolved from a rod-shaped ancestor. Although rod-shaped *Neisseriaceae* septate transversally, our incubations with a set of fluorescently labeled PG precursors showed that MuLDi *Neisseriaceae* septate longitudinally – in *A. filiformis* in a distal-to-proximal fashion, in *S. muelleri* and *C. steedae* synchronously, from both poles to midcell (notably, the other two known species of the *Alysiella* and *Conchiformibius* genera, *A. crassa* and *C. kuhniae*, also septate longitudinally, the former unidirectionally and the latter bidirectionally; Supplementary Figs. 6e and 8c, respectively). Furthermore, we observed that in these bacteria, new PG was not inserted concentrically, but as a medial sheet guillotining each cell. Finally, full-scale comparative genomics revealed MuLDi-specific differences that set them apart from rod-shaped members of the *Neisseriaceae* (e.g., *amiC2* acquisition, *mraZ* loss and amino acid changes in the cytoskeletal proteins MreB and FtsA). Supporting the role of specific genetic changes in the rod-to-MuLDi transition, introduction of *amiC2* and allelic substitution of *mreB* in the rod-shaped *Neisseriaceae N. elongata* resulted in cells with longer septa. Taken together, we presented two novel modes of septal growth and we identified genetic events that likely contributed to the evolution of bacterial multicellularity, longitudinal division and, possibly, polarization in a group of mammalian symbionts.

Multiple phylogenetic studies have suggested that the wide palette of bacterial morphotypes we observe today evolved from rod-shaped bacteria, which makes us consider their shape as the ancestral one[53,54]. Our genome-based phylogenetic reconstruction revealed that also MuLDi *Neisseriaceae* evolved from an ancestral rod-shaped

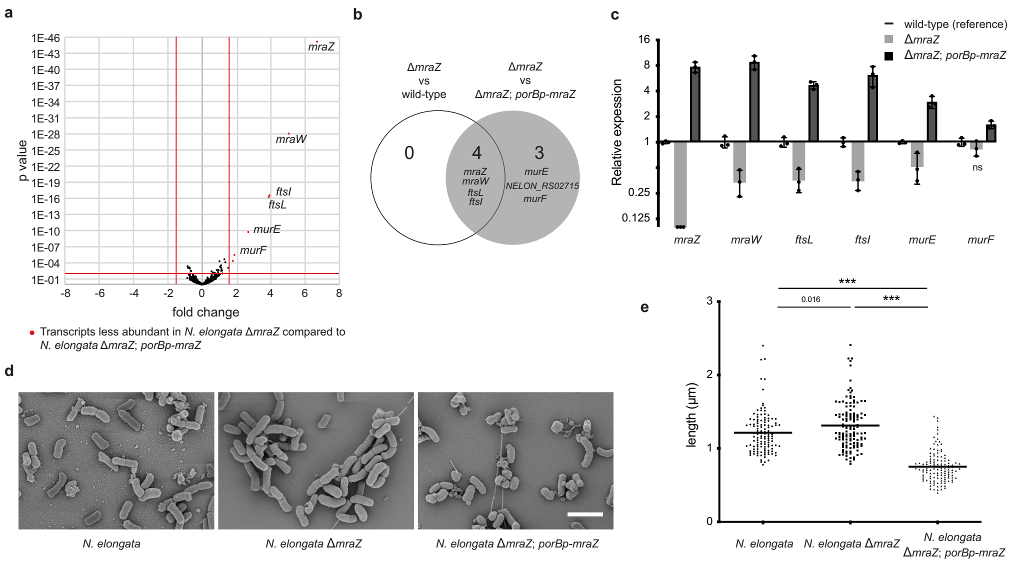

Fig. 6 | Downregulation of the *dcw* cluster in *N. elongata* ΔmraZ. **a** Volcano plot of RNAseq analysis of an *N. elongata* Δ*mraZ* and complemented. *p* value is plotted against fold change and were calculated using DeSeq2. Red points represent genes upregulated in MraZ-overexpressing *N. elongata* (Δ*mraZ*; *porBp-mraZ* – i.e., *mraZ* under the control of the strong and constitutive *porB* promoter), as compared to *N. elongata* Δ*mraZ*. **b** Venn diagram showing genes (*mraZ, mraW, ftsL and ftsI)* upregulated in *N. elongata* wild-type as compared to *N. elongata* Δ*mraZ*. **c** Transcript abundance of *dcw* cluster genes measured by qRT-PCR in *N. elongata* expressing or not expressing MraZ. Data represent mean ($n = 3$ biologically independent samples ± SD) and are representative of three independent experiments. Statistical test used was Unpaired *t* test with Welch's correction by comparing ΔmraZ to the parental wild-type and the Δ*mraZ; porBp-mraZ* to the parental Δ*mraZ* (ns not significant). **d** Scanning electron microscopy of *N. elongata* expressing or not expressing MraZ. Scale bar is 2 μm. **e** Median cell length measurements of *N. elongata* expressing or not expressing MraZ ($n = 120$ biologically independent cells). Data are presented with the median and are representative of at least two independent experiments. Statistical test used was One-way ANOVA, with Bonferroni's multiple comparisons test (***$p < 0.001$). Source data and statistics are provided as a Source Data file (for **a**, **c** and **e**).

bacterium. It remains uncertain whether these two MuLDi lineages evolved independently but convergently or whether species belonging to the genus *Kingella* also evolved the MuLDi phenotype, but subsequently reverted to transverse division. This could be resolved in the future by isolation of more species closely related to MuLDi or *Kingella* spp. As for what makes *Conchiformibius* and *Simonsiella* divide from both poles and *Alysiella* from one pole only, comparison of their genomes and transcriptomes is needed to decipher the underlying mechanisms. Irrespective of differences in the directionality of cell wall construction, we speculate that the MuLDi phenotype may have favored colonization of (or nutrient uptake from) the buccal cavity, which is characterized by rapidly epithelial cells shedding and salivary flow[55]. Indeed, multicellularity makes cooperation between cells possible, for example in the form of division of labor, and may therefore help bacteria to survive nutritional stress (see for example ref. 56). Although previous morphological studies suggested that the terminal cells of *S. muelleri*[10,17] and *C. steedae*[11] might phenotypically differ from the central ones and although we observed cells with thicker PG every 14 cells in *C. steedae* (Supplementary Figs. 2e, 8a and Supplementary Movie 7), future studies are needed to clarify whether different cell types exist within each filament.

Multicellularity may arise via three distinct processes: (1) aggregation of individual cells resembling the initial stages of biofilm formation[57]; (2) the formation of syncytial filaments via crosswalls segmenting the mother cell, but not separating it into daughter cells (streptomycetes[58]); and (3) incomplete cell fission after cell division to produce chains of cells (referred to as clustered growth, e.g., filamentous cyanobacteria[59]). TEM analysis of MuLDi symbionts revealed that these *Neisseriaceae* share their lateral PG and are surrounded by a common outer membrane which makes them resemble to cyanobacteria. If MuLDi cells belonging to the same filament appear to be synchronized (Figs. 3 and 4; Supplementary Figs. 6 and 7), additional studies are needed to find out whether division of labor occurs among cells belonging to the same filament and whether their cytoplasms are connected by septal junctions and/or hemidesmosomes[59]. As for the mechanism underlying MuLDi cell septation, ultrastructural analysis suggests that, after a first round in which PG is synthesized and the CM invaginates, a second round occurs where the PG layer is split into two, concomitantly with the invagination of the outer membrane until midcell (Supplementary Fig. 3).

Although longitudinal septation is clearly not a prerequisite of bacterial multicellularity (here defined as clusters of at least three cells), these two phenotypic traits appeared to have evolved jointly in the *Neisseriaceae*. Longitudinal septation has also been shown in the nematode symbionts *Candidatus Thiosymbion oneisti* and *T. hypermnestrae*[20,21], as well as in the fruit fly endosymbiont *Spiroplasma poulsonii*[22]. In these three unicellular symbionts, the tubulin homolog FtsZ is localized at the septal plane and is therefore thought to mediate septal PG insertion. As for the actin homolog MreB, it was shown to form a medial ring-like structure in *Ca*. Thiosymbion throughout the cell cycle and to be required for septal FtsZ localization and PG insertion[38]. Indeed, its pharmacological inactivation impaired both *Ca*. Thiosymbion growth and division[38]. Although the localization pattern of MreB in MuLDi *Neisseriaceae* is currently unknown, (1) its presence in their genomes, (2) its transcriptional expression, (3) the identification of two MuLDi-specific amino acid permutations (H185Q and

https://doi.org/10.1038/s41467-022-32260-w

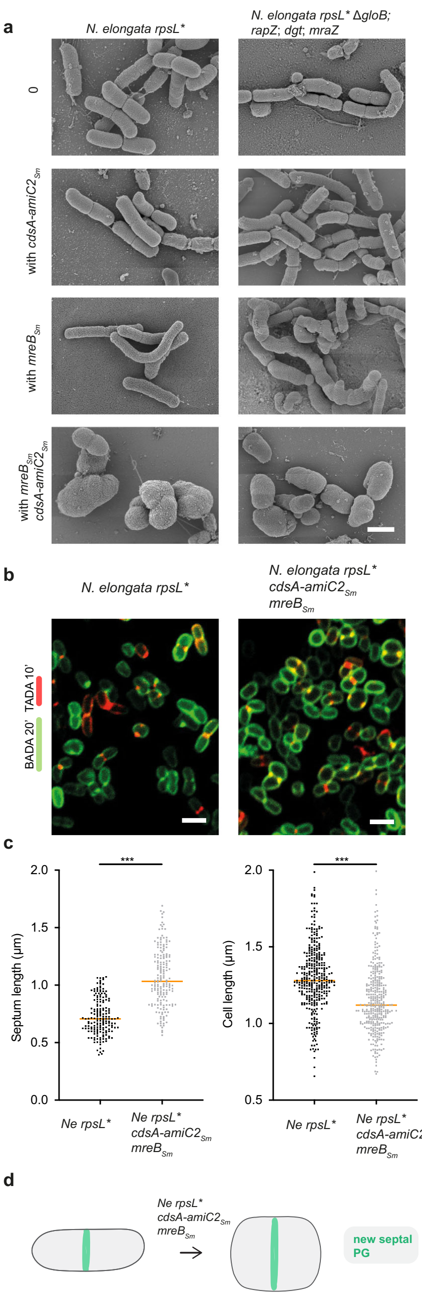

Fig. 7 | Recapitulation of MuLDi-specific genetic changes in the rod-shaped *Neisseriaceae N. elongata*. **a** Scanning Electron Microscopy of *N. elongata* (*rpsL**) wild-type (left panels) or harboring multiple deletions (Δ*dgt*, Δ*gloB*, Δ*mraZ*, Δ*rapZ*, right panels), with or without the *mreB$_{Ne}$*/*merB$_{Sm}$* allelic exchange, with or without the addition of *cdsA-amiC2*. The results are representative of at least three independent analyses. **b** *N. elongata* (*rpsL**) wild-type (left) or harboring the *mreB$_{Ne}$*/*merB$_{Sm}$* allelic exchange and *cdsA-amiC2* (right) and **c** median length of the septum (n = 170 biologically independent cells) and of the cell axis perpendicular to the septum (n = 340 biologically independent cells) in *N. elongata* (*rpsL**), wild-type (left) or harboring the *mreB$_{Ne}$*/*merB$_{Sm}$* allelic exchange and *cdsA-amiC2* (right). Data are presented with the median and are representative of at least two independent experiments. Statistical test used was Unpaired Two-Tailed T test (***$p < 0.001$). Source data and statistics are provided as a Source Data file. **d** Schematic representation of a septating wild-type (*rpsL**) *N. elongata* (left) and of *N. elongata* harboring the *mreB$_{Ne}$*/*merB$_{Sm}$* allelic exchange and *cdsA-amiC2* (right). Scale bar is 1 µm.

T247A), and (4) the fact that introducing a MuLDi MreB in the rod-shaped *N. elongata* (with the concomitant insertion of *amiC2* or deletion of *dgt*, *gloB*, *mraZ*, *rapZ*) led to shape aberrations suggest that MreB is involved in PG insertion in MuLDi *Neisseriaceae*. Intriguingly, amino acid 185, located after the GVVYS motif, is substituted in MuLDi MreBs when compared to rod-shaped *Neisseriaceae* (H185Q), but also in longitudinally dividing *Ca*. Thiosymbion when compared to *E. coli* (S185N)[33]. It should also be noted that the effect of the allelic substitution of MreB on the morphology of *N. elongata* depended on the genetic background (i.e., presence of MuLDi-specific genes and/or absence of rod shape-specific genes). This, in addition to the pleiotropic effect of MreB reported in other studies[28], can make this protein accountable for accommodating multiple cell shape adaptations (e.g., rod-to-coccus, rod-to-MuLDi). If we still do not know whether MreB and/or FtsZ place the insertion of the PG synthesis machinery at the septum, based on our confocal-based 3D reconstructions, new septal PG is not inserted in successive, concentric rings or ellipses, as shown for model rods[39,40,60] and nematode symbionts[38], respectively.

In addition to MreB amino acid changes, MuLDi-specific loss of *mraZ* led to the misregulation of the *dcw* cluster. MraZ has been described as a highly conserved transcriptional regulator of the *dcw* cluster, of which *mraZ* is the first gene[45,46]. The *dcw* cluster is a group of genes involved in the synthesis of PG precursors and cell division[61] that is conserved in most bacterial genomes[62–64]. Throughout the *Neisseriaceae*, the *dcw* cluster consists of 14–16 tightly packed genes in the same orientation and mostly in the same order, with *midA* located before the cluster in reverse orientation (Supplementary Fig. 9). The fact that, in the *Neisseriaceae*, the gene content and orientation of the *dcw* cluster mostly mirrored the phylogenetic placement of each species, suggests that the *dcw* cluster evolved vertically. Moreover, having a fragmented *dcw* cluster (as in the case of MuLDi *Neisseriaceae* and some *Kingella* species) does not seem to impact cell morphology, given that both rod-shaped and MuLDi species may bear or not bear split *dcw* clusters. Of note, in spite of fragmentation, bacteria can retain some gene sub-clusters (e.g., "*mraW-ftsL, ftsI, murE* and *murF*", "*ftsW, murG*" and "*murC, ddl, ftsQ, ftsA, ftsZ*"), probably because the genes grouped in a given sub-cluster need to be co-transcribed (Mingorance et al.[65]). If several studies agree on the regulatory role of MraZ on the *dcw* cluster expression[45,46,66,67], a lot remains to be done to understand the details of this regulation (e.g., what triggers MraZ activity). In this study, *dcw* cluster upregulation in MraZ-overexpressing *N. elongata* led to shorter cells. This agrees with observing the opposite phenotype (filamentation) in *E. coli* when the *dcw* cluster was downregulated[45]. Altogether, these studies suggest that MraZ controls cell division rate by regulating the *dcw* cluster and we speculate that, in *mraZ*-less MuLDi *Neisseriaceae*, its absence may have altered the balance between the divisome and the elongasome machineries (i.e, the elongasome might contribute to PG synthesis at the septum).

Finally, comparative genomics highlighted the importance of the acquisition of the *cdsA/amiC2* locus in MuLDi *Neisseriaceae*. Although its sole addition in *N. elongata* does not result in morphological changes, when we combined it with the allelic substitution of *mreB$_{sm}$*, we observed cells with longer septa. This suggests that the AmiC2 amidase may regulate MuLDi septation. Intriguingly, HPLC analyses of PG extracted from 17 rod-shaped bacteria and from three MuLDi

Neisseriaceae (*A. filiformis*, *S. muelleri* and *C. steedae*) showed that MuLDi PG is richer in M44 (Supplementary Fig. 5e), suggesting higher amidase activity in these *Neisseriaceae*. Concerning the *amiC2*-associated genetic locus *cdsA*, it encodes for a phosphatidate cytidylyltransferase putatively implicated in phospholipid biosynthesis. Given that the presence of anionic phospholipids (cardiolipin and phosphatidylglycerol) has been shown to repel MreB[68], we can hypothesize that CdsA affects the composition of the membrane and, therefore, the localization of MreB.

Despite all our efforts, we could not turn the rod-shaped *N. elongata* into a complete MuLDi *Neisseriaceae* even upon, concomitantly, replacing MreB, inserting *amiC2/cdsA* and deleting *dgt*, *gloB*, *mraZ* and *rapZ*. This could be because we could not recreate all genetic events (such as replacing $ftsA_{ne}$ with $ftsA_{sm}$ due to its proximity to *ftsZ*), or it could be due to the existence of other undetected events (such as species-specific events that resulted in a convergent phenotype), or finally, to prior events such as those that are also present in rod-shaped *Kingella* spp. (see Supplementary Data 5) but that do not cause the MuLDi phenotype.

How could rod-shaped, transversally dividing bacteria evolve into longitudinally dividing ones? Permanent cell shape transitions may have resulted from modifications (e.g., gene deletions, insertions and nucleotide polymorphisms) of genetic loci involved in morphogenesis (e.g., *mreB*, *amiC2*) and, additionally, in those involved in their transcriptional regulation (e.g., *mraZ*). Two evolutionary scenarios were proposed[33,34,38]: (1) an ancestral rod was compressed by its poles so that it got shorter and fatter, or (2) an ancestral rod rotated its septation axis by 90 degrees. Our results suggest that, in the course of evolution, the cell width of an ancestral rod increased (and its length decreased), perhaps following a misbalance between elongation and division. However, genetic tools are needed to gain insights on MuLDi *Neisseriaceae* evolution by, for example, visualizing the localization pattern of FtsZ and MreB or by attempting reversion into unicellular, and possibly, into transversally dividing bacteria such as *N. elongata*.

To date, most protein function studies have been conducted in either pathogenic or bacterial species that are easy to culture and manipulate in the laboratory such as *E. coli* and *B. subtilis*. In addition to these models, efforts to study other morphologies including commensal species are necessary to understand bacterial cell evolution, but also to increase the pool of protein targets (e.g., antibiotic targets) for industrial and biopharmaceutical applications. Throughout their evolution, *Neisseriaceae* succeeded in repeatedly, and seemingly effortlessly, evolve different cell shapes (e.g., coccoid, MuLDi). Moreover, they are the only known multicellular longitudinally dividing bacteria that may thrive in humans, but which are also cultivable and, likely, genetically tractable. We hence propose the use of *Neisseriaceae* as models to study how longitudinal division and multicellularity evolved, as well as the molecular and cell biological mechanisms underlying the establishment of bacterium-animal symbioses.

Methods

Bacterial strains and culture conditions

The bacterial strains *Neisseria elongata* subsp. *elongata* (DSM 17712), *Alysiella filiformis* (DSM 16848), *Simonsiella muelleri* (DSM 2579), and *Conchiformibius steedae* (DSM 2580) were obtained from the German Collection of Microorganisms and Cell Cultures GmbH (DSMZ). *Neisseria elongata* subsp. *glycolytica* (ATCC 29315) and *Simonsiella muelleri* (ATCC 29453) were obtained from the American Type Culture Collection (ATCC). *N.* sp. DentCa1/247 was a gift from Dr. Nathan Weyand (U. of Ohio). For FDAA incubations, western blots, immunostaining and membrane staining, we used BSTSY (*N. elongata*, *C. steedae*), PY (*A. filiformis*), or meat extract (*S. muelleri*) agar plates that were incubated overnight at 37 °C. For BSTSY, PY and meat extract media composition please refer to Supplementary Table 1. For all other experiments, bacteria were streaked from −70 °C freezer stocks onto Gonococcal culture media supplemented with Kelloggs supplement (GCB) and grown overnight at 37 °C in 5% CO_2 incubator. Single colonies were subcultured into the respective liquid media with agitation at 120 rpm and grown to exponential phase (OD_{600} 0.1–0.6). For cloning experiments *E. coli* DH5α cells were cultured onto Lysogeny broth (LB) media at 37 °C. When required, antibiotics were used as follows: kanamycin (50 µg/ml for *E. coli*; 100 µg/ml for *N. elongata*), erythromycin (300 µg/ml for *E. coli*; 3 µg/ml for *N. elongata*), chloramphenicol (25 µg/ml for *E. coli*; 5 µg/ml for *N. elongata*), and streptomycin (100 µg/ml for *N. elongata*). Transformation of *N. elongata* was done using linearized plasmid or PCR product by dropping ~500 ng of DNA on fresh cultures on GCB media supplemented with 10 mM $MgCl_2$ and incubated for 6–12 h before subculturing on GCB media containing the appropriate antibiotics and Xgal if needed as described previously[16].

Time-lapse imaging of *N. elongata*

Strains were streaked from −70 °C freezer stocks onto BSTSY agar plates and grown overnight at 37 °C with 5% CO_2. Single colonies were transferred to liquid culture and grown to exponential phase (OD_{600} 0.2). Cells were spotted onto pads made of 0.8% SeaKem LE Agarose (Lonza, Cat. No. 50000) in BSTSY and topped with a glass coverslip. Cells were transferred to an Okolab stage top chamber to control temperature (37 °C) and gas (CO_2 5% and O_2 18%). Images were recorded with inverted Nikon Ti-2 microscopes using a Plan Apo 100 × 1.40 NA oil Ph3 DM objective using Hamamatsu Orca FLASH 4 camera. Images were processed with NIS Elements 5.02.01 software (Nikon). In all experiments, multiple x/y positions were imaged. Representative images were processed using the Fiji 2.1.0/1.53c software package.

Time-lapse imaging of *A. filiformis*, *S. muelleri* and *C. steedae*

Strains were streaked from −70 °C freezer stocks onto PY (*A. filiformis*), meat extract (*S. muelleri*) or BSTSY (*C. steedae*) agar plates grown overnight at 37 °C with 5% CO_2. Single colonies were transferred to liquid culture and grown to exponential phase (OD_{600} 0.2–0.5) at 37 °C shaking at 180 rpm agitation. For all strains, 250 µL of diluted exponential phase cultures (OD 0.025) were loaded into the cell loading well of a prepared (shipping solution removed and washed three times with sterile appropriate media) B04A-03 microfluidic plate (Merck-Millipore). Time-lapse imaging was performed using CellASIC® ONIX Microfuidic System. The ONIX manifold was sealed to the B04A-03 plate. CellASIC® ONIX2 System was used as the microfluidics control software. First, a flow program was set up to prime flow channel and culture chamber by flowing medium from inlet wells 1–5 at 34.5 kPa for 2 min. Second, cells were loaded onto the plate at 13.8 kPa for 15 s. Priming run was performed for 5 min with pressure set to 34.5 kPa. The medium flow was set at 12 kPa throughout the experiment for 12 h with sterile appropriate media. Images were recorded with an inverted Nikon Ti-E microscope using a Plan Apo 60XA oil Ph3 DM objective using Hamamatsu Orca FLASH 4 camera. Images were processed with NIS Elements 5.02.01 software (Nikon). In all experiments, multiple x/y positions were imaged. Representative images were processed using the Fiji 2.1.0/1.53c software package.

Electron microscopy

For transmission electron microscopy, half a loopful of 6–8 h old bacterial cultures were fixed by direct resuspension in 500 µl of 2.5% glutaraldehyde in 0.1 M cacodylate buffer and incubated for at least 1 h at 4 °C. Cells were then pelleted through centrifugation at 3075 × *g* for 3 min and washed 3 times in 500 µl 0.2 M cacodylate wash buffer solution (pH 7.2). 30–50 µl of wash solution containing bacterial cells was pipetted onto Formvar Carbon 200 mesh copper grids (Sigma-Aldrich) and negative staining done using 1% phosphotungstic acid (PTA) for 2 s before imaging at the INRS-CAFSB platform using a Hitachi H-7100 electron microscope with AMT Image Capture Engine (version 600.147).

For scanning electron microscopy, fresh bacterial cells were cultured for 6 h in liquid media containing poly-L-Lysine (Sigma) coated glass slides. Cells were fixed using 2.5% glutaraldehyde in 0.1 M cacodylate buffer for 1 h at 4 °C then rinsed 3 times in 0.2 M cacodylate wash buffer solution (pH 7.2). Post fixation was subsequently done using 1% osmium tetroxide (in 0.2 M cacodylate) before gradual dehydration through increasing ethanol concentrations (25%, 50%,75%, 95% and 100%). Carbon dioxide critical point drying (CPD) and gold sputtering were done on Leica EM CPD300 and Leica EM ACE600 instruments respectively. The imaging was done at the electron Imaging Facility (Faculty of dental medicine, Université de Montréal, Québec, Canada) using a Hitachi Regulas 8220 electron microscope with the SEM operation software Regulus 8200 series.

Peptidoglycan extraction and analysis

Peptidoglycan (PG) extraction was performed as previously described[16]. Bacterial cultures were harvested from solid agar plates using inoculation loops and emulsified in 10 ml of distilled water, the suspension mix was added drop by drop into 10 ml of 8% boiling sodium dodecyl sulfate (SDS) and boiled for and extra hour. After overnight storage at room temperature, the cells were washed six times using distilled water (pH 6.0) through ultracentrifugation at 39,000 × *g* for 30 min. The final pellet was lyophilized and resuspended in distilled water (concentration 6 mg/ml or more) and stored at −20 °C until further use. Analysis of the muropeptide composition was performed essentially as described previously[69]. Samples were treated with Proteinase K (20 µg/mL, 1 h, 37 °C). The reaction was heat-inactivated and sacculi were further washed by ultracentrifugation. Finally, samples were digested overnight with muramidase (100 µg/mL) at 37 °C. Muramidase digestion was stopped by boiling and coagulated proteins were removed by centrifugation (3075 × *g*, 15 min). For sample reduction, the pH of the supernatants was adjusted to pH 8.5–9.0 with sodium borate buffer and sodium borohydride was added to a final concentration of 10 mg/mL. After incubating for 30 min at room temperature, pH was adjusted to 3.5 with orthophosphoric acid. The soluble muropeptides were analyzed by high-performance liquid chromatography (HPLC; Waters Corporation, USA) on a Kinetex C18 column (150 × 4.6 mm; 2.6 µm particle size, 100 Å) (Phenomenex, USA) and detected at 204 nm with UV detector (2489 UV/Visible, Waters Corporation, USA). Muropeptides were separated with organic buffers at 45 °C using a linear gradient from buffer A (formic acid 0.1% (v/v) in water) to buffer B (formic acid 0.1% (v/v) in 40% acetonitrile) in an 18-min-long run with a 1 ml/min flow. Quantification of muropeptides was based on their relative abundances (relative area of the corresponding peak) normalized to their molar ratio. The molar percentage was calculated for each muropeptide. This relative molarity was also used to calculate the molar percentage of crosslinked muropeptides. The Waters Empower 3, build 3471 software (Waters Corporation, USA) was used for acquiring and managing the chromatographic information. Muropeptide identity was confirmed by MS analysis, using a UPLC–MS (UPLC system interfaced with a Xevo G2/XS Q-TOF mass spectrometer from Waters Corporation, USA). Data acquisition and processing was performed using UNIFI software platform (Waters Corporation, USA).

FDAA incubations

To sequentially label cells with HADA (7-hydroxycoumarin-3-carboxylic acid-D-alanine, blue), BADA (BODIPY FL-D-alanine; green) and TADA (TAMRA-D-alanine; red), all three provided by Michael van-Nieuwenhze, exponential phase cells were pelleted, resuspended in medium containing the first label and then grown at 37 °C. Media composition is described in Supplementary Table 1, and incubation times and order for each *Neisseriaceae* species are listed in Supplementary Table 2, respectively. After the first interval cells were washed twice with fresh medium (37 °C) and centrifuged between washes (7000 × *g* for 2 min at RT). After this, the cell pellets were resuspended in pre-warmed medium containing label two. For triple labeling, cells were washed twice and resuspended in medium containing the third label. Cells were then immediately treated with 70% ice-cold ethanol and incubated on ice for 1 h. Ethanol-fixed cells were collected via centrifugation (7000 × *g* for 2 min at RT), washed twice with 4 °C 1 × Phosphate Buffered Saline (PBS, pH 7.4), resuspended in PBS, and stored on ice before imaging.

EDA-DA incubation and click-chemistry

To track symbiont cell wall growth followed by immunolabeling *A. filiformis* cells were grown over night on PY plates. Single colonies were incubated in 10 mM ethynyl-D-alanyl-D-alanine (EDA-DA, a D-amino acid carrying a clickable ethynyl group) for 30 min, resuspended in pre-warmed PY medium, washed twice (7000 × *g* for 2 min at RT) and treated with 70% ethanol like described before. After that, cells were rehydrated and washed in PBS containing 0.1% Tween 20 (PBT). Blocking was carried out for 30 min in PBS containing 0.1% Tween 20 (PBT) and 2% (wt/vol) bovine serum albumin (blocking solution) at room temperature. An Alexa488 fluorophore was covalently bound to EDA-DA via copper catalyzed click-chemistry by following the user manual protocol for the Click-iT reaction cocktail (Click-iT EdU Imaging Kit, Invitrogen). The cells were incubated with the Click-iT reaction cocktail for 30 min at RT in the dark. Unbound dye was removed by a 10-min wash in PBT and one wash in PBS. For immunostaining of clicked bacterial cells, cells were washed for 10 min in PBT and subsequently incubated with blocking solution for 30 min at room temperature in the dark. From here on, immunostaining was performed as described below.

Western blots

Proteins from bacteria cells were separated by reduced sodium dodecyl sulfate (SDS)-polyacrylamide gel electrophoresis (PAGE) on NuPAGE 4%–12% Bis-Tris pre-cast MOPS gel (Invitrogen), respectively, and each blotted onto Hybond ECL nitrocellulose membranes (Amersham Biosciences). Membranes were blocked for 45 min in PBS containing 5% (wt/vol) nonfat milk (PBSM) at room temperature and incubated overnight at 4 °C with a 1:1,000 dilution of sheep polyclonal anti-*E. coli* K88 fimbrial protein AB/FaeG antibody (ab35292, Abcam) in PBSM. For the negative control, the primary antibody was omitted. After five 6 min-long washes in PBSM and one final wash in PBS containing 0.1% Tween20, the blot was incubated for 1 h at room temperature with a horseradish peroxidase-conjugated anti-sheep secondary antibody (1:10,000; Amersham Biosciences) in PBSM. Protein-antibody complexes were visualized using ECL Plus detection reagents (Amersham Biosciences).

Immunostaining

Exponential phase cells were fixed overnight in 3% formaldehyde at 4 °C. Cells were collected via centrifugation (7000 × *g* for 2 min at RT), washed twice with PBS and resuspended in PBS containing 0.1% Tween 20 (PBT). Blocking was carried out for 1 h in PBT containing 2% (wt/vol) bovine serum albumin (blocking solution) at room temperature. After that, cells were incubated with a 1:500 dilution of sheep polyclonal anti-*E. coli* K88 fimbrial protein AB/FaeG antibody (ab35292, Abcam) overnight at 4 °C in blocking solution. Upon incubation with primary antibody (or without in the case of the negative control) samples were washed three times in PBT and incubated with an Alexa555 conjugated anti-sheep antibody (Thermo Fisher Scientific) at 1:500 dilution in blocking solution for 1 h at room temperature. Unbound secondary antibody was removed by two washing steps one in PBT and one in PBS. Cell pellets were resuspended in PBS containing 5 µg/mL Hoechst for 20 min and subsequently washed and resuspended with PBS. 1 µL of the bacterial solution was mixed with 0.5 μL of Vectashield mounting medium (Vector Labs) and mounted on an agarose slide.

Nile red membrane staining

Exponential phase cells were fixed overnight in 2% formaldehyde at 4 °C. Cells were collected via centrifugation (7000 × *g* for 2 min at RT), washed twice with PBS and resuspended in PBS containing 10 μg/mL Nile Red (Stock is prepared with DMSO; ThermoFisher N1142) and 5 μg/mL Hoechst for 15 min in the dark at room temperature. Cells were washed and resuspended in PBS and subsequently 1 μL of the bacterial solution was mixed with 0.5 μL of Vectashield mounting medium (Vector Labs) and mounted on an agarose slide.

Fluorescence microscopy

For Figs. 3a, b, 4a–c, Supplementary Figs. 4, 6a–c, and 7a–c immunostained or FDAA-labeled bacteria were imaged using a Nikon Eclipse NI-U microscope equipped with a MFCool camera (Jenoptik) and images were acquired using the ProgRes Capture Pro 2.8.8 software (Jenoptik). For Figs. 3d, 4e, Supplementary Figs. 6d, e, and 8a–c, FDAA-labeled bacteria were visualized with a Leica TCS SP8 X confocal laser scanning microscope. Images were taken with a 63X Plan-Apochromat glycerin objective with a NA of 1.30 and a refraction index of 1.46 (glass slide, glycerin and antifade mounting medium). The Leica software LASX (3.7.2.22383) including the Lightning deconvolution software package (Leica) was used for image acquisition and post-processing if necessary.

For Fig. 7b and Supplementary Fig. 11b, FDAA-labeled *N. elongata* wild type (*rpsL**) and mutant (*rpsL**; *cdsA-amiC*$_{SM}$; *mreB*$_{SM}$) were imaged at the INRS-CAFSB platform with a Zeiss LSM 780 AxioObserver confocal microscope equipped with a Zeiss Plan-Apochromat 100x/1.4 Oil M27. The Zeiss software Zen 2011 was used for image acquisition.

FDAA fluorescence quantification and statistical analysis

Microscopic images were processed using the public domain software ImageJ 1.53k[70] in combination with plugin Fil-Tracer (this study). Cell outlines were traced and morphometric measurements recorded. Fluorescent intensities were measured along the septal plane and plotted as fraction of the normalized cell length. Automatic cell recognition was double-checked manually. For representative images, the background subtraction function of ImageJ 1.53k was used and brightness and contrast were adjusted for better visibility. Data analysis was performed using Excel 2021 (Microsoft Corporation, USA), plots were created with ggplot2 in R (http://www.R-project.org/). Septa length (Fig. 7 and Supplementary Fig. 11) of BADA and TADA labeled cells were analyzed using the public domain software Fiji[71]. Cell and septa lengths were measured manually. Notably, only cells that showed a BADA and TADA signal were considered for the septa length measurements. Two-tailed unpaired T tests were performed using GraphPad Prism version 9.3.0 for Mac (La Jolla California USA, www.graphpad.com). Figures were compiled using Adobe Photoshop 2021 and Adobe Illustrator 2021 (Adobe Systems, USA).

Genome sequencing and assembly

Genomic DNA for WGS of *Neisseriaceae* species and PCR amplification of DNA used for cloning purposes or sequence verifications were extracted using Genomic Tip 20/G or 100/G kits (Qiagen) according to the manufacturer's instructions. The genome sequencing results are presented in Supplementary Data 1. Genomes were sequenced either using a Pacific Biosciences RS II system at the Génome Québec Innovation Centre (McGill University, Montréal, Canada) or using Oxford Nanopore technologies at the Bacterial Symbiont Evolution Lab (INRS, Laval, Canada). For PacBio, the reads were assembled de novo using HGAP v.4[72] available on SMRT Link v.7 (default parameters, except, min. subread length: 500; estimated genome size: 2.7 Mb). For nanopore sequencing, DNA libraries were prepared following the Native barcoding genomic DNA procedure (with EXP-NBD104, EXP-NBD114, and SQK-LSK109) with MinIon MK1C device using the MinKNOW 21.05.10 software. The base call was carried out using guppy_basecaller (version 5.0.11 + 2b6dbff) in sup mode. Reads were filtered by quality Q > 8 and separated by barcodes using guppy_barcoder (version 5.0.11 + 2b6dbff). The genome assembly was made by 3 programs: Canu (https://github.com/marbl/canu), Flye (https://github.com/fenderglass/Flye)[73] and Miniasm (https://github.com/lh3/miniasm)[74]. Then each ensemble was corrected in bases using Pilon (https://github.com/broadinstitute/pilon)[75]. Racon (https://github.com/isovic/racon)[76] Medaka (https://github.com/nanoporetech/medaka). All assemblies and assembly corrections were analyzed with Quast (https://github.com/ablab/quast)[77] and BUSCO (https://gitlab.com/ezlab/busco)[78]. The assembly with the least number of contigs and the greatest completeness was chosen.

Core genome-based phylogeny of *Neisseriaceae*

All the *Neisseriaceae* genomes present on NCBI database at the time of the analyses were downloaded and the Average Nucleotide Identity (ANI) values were determined using GET_HOMOLOGUES version 20092018. Genome were grouped by their ANI > 96%. To simplify the analyses and to assure their quality (such as avoiding multiple contigs) a reference genome was selected in each group. A complete circular genome from a reference strain was preferred when possible (see Supplementary Data 1). All genomes were annotated with Prokka v1.14.5[79] providing the annotation files for further analysis. A nucleotide-level multifasta alignment of those genes included in the core-genome of *Neisseriaceae* family was performed with MAFFT by using the *-e–mafft* options within Roary v3.11.2[80]. A minimum percentage of 50% identity, and occurrence in 80% of the isolates was also considered by entering the *-i 50 -cd 80* options, respectively, to the Roary command line. Under these parameters, a total of 401 genes were finally included in the core-genome (see Supplementary Data 3). The resulting alignment was used for the subsequent phylogenetic analysis. Best evolutionary model was determined by ModelFinder within IQ-TREE version 1.6.3[81]. The best-fit model according to the Bayesian Information Criterion (BIC) was GTR + F + R10. Maximum-likelihood phylogenetic analysis was also performed with IQ-TREE[82] using 10,000 ultrafast bootstrap replicates[83]. The final phylogenetic tree was drawn with FigTree v1.4.4 (http://tree.bio.ed.ac.uk/software/figtree/) and rooted in *Crenobacter*. The results of this analyses are provided in Supplementary Data 6. The phylogenetic tree displayed in Fig. 1, and csv file associating genome name with morphology were used in PastML with default parameters to assess ancestral morphology. The prediction method was maximum-likelihood-MPPA (marginal posterior probabilities approximation), F81 model.

Phylogenies of individual proteins

Individual phylogenies were performed for six proteins: N-acetylmuramoyl-alanine AmiC1 from *S. muelleri* ATCC 29453 (accession number AUX62143.1), and AmiC2 from *C. kuhniae* (accession number WP_027009548.1); division/cell wall cluster transcriptional repressor MraZ from *N. elongata* (accession number WP_204812527.1); RNase adapter RapZ from *N. elongata* (accession number WP_074896150.1); cell division protein FtsA from *Neisseria spp*. (accession number WP_003779891.1); and rod shape-determining protein MreB from *Neisseria spp*. (accession number WP_003747269.1). Protein sequences were searched against all the *Neisseriaceae* genomes included in the core-genome-based phylogeny, as well as in the complete bacterial repertoire found at NCBI. For this purpose, two separate databases were created: *Neisseriaceae*, including the genomes above mentioned; and *Bacterial*, which includes all the representative genomic sequences from the RefSeq database. The protein sequences of all the genomes in each of the two datasets were concatenated and the protein databases created with the *makeblastdb* tool from BLAST version 2.6.0+. The resulting databases were used to investigate the presence of aforementioned proteins by BLASTP. Sequences with an e-value and similarity percentage greater than or equal to $1e^{-10}$ and 50%, respectively, were retained for downstream analysis. Truncated proteins (i.e., split into contiguous coding sequences) were not considered to avoid artefacts in the clustering. Amino acid sequences of the hits obtained by BLASTP were retrieved from the entire set of genomes using faSomeRecords (https://github.com/santiagosnchez/faSomeRecords/blob/master/faSomeRecords.pl). The resulting multifasta were aligned with MAFFT v7[84], and maximum-likelihood phylogenetic analysis was performed using IQ-TREE using 1000 ultrafast bootstrap replicates. Evolutionary models were estimated with ModelFinder in IQ-TREE, and best-fits according to BIC were as follows: AmiC1 LG + F + I + G4; AmiC2 LG + R10; FtsA JTT + R4; MraZ LG + I + G4; MreB JTTDCMut+R3; RapZ LG + R4. Final trees were drawn with FigTree v1.4.4 and rooted in *Crenobacter*. The results of this analyses are provided in Supplementary Data 6.

Genomic comparisons

For gene insertion and deletion, we have used the previously described MycoHIT pipeline[42,85]. We used complete genomes of all the rod-shaped and MuLDi *Neisseriaceae* species presented in Fig. 1. We excluded the second coccus lineage (*Neisseria wadsworthii*, *Neisseria canis* and *N*. sp. 83E034). We performed an alignment search with the standalone TBLASTN program[86] using the 2105 predicted proteins from *N. elongata* ATCC29315 or the 2349 predicted proteins from *S. muelleri* as the query sequences to search for matches in the genomic DNA of other organisms. We obtained two matrices of around 80,000 scores (2063 or 2105 protein sequences blasted against 37 genomes) providing two types of output: categorical (hit versus no hit) and quantitative (degree of similarity). To categorically assign that there was no hit, we employed the default E-value of e^{-10}. Thus, if the statistical significance ascribed to a comparison was greater than this E-value, we assigned a percentage of similarity of 0% to that comparison. To analyze quantitative results, we used MycoHIT[42] to assign absence of gene in all MuLDi *Neisseriaceae* and presence of the gene in all rod-shaped *Neisseriaceae* or vice versa. "Absence" was defined as lower values than 50% and "presence" as higher values than 55%.

Possible correlation between amino acid changes and cell shape was sought using CapriB[41]. Briefly, two databases were generated taking MuLDi *Simonsiella muelleri* ATCC 29453 (accession number GCA_002951835.1) and rod-shaped *Neisseria elongata* subsp. *glycolytica* ATCC 29315 (accession number GCA_000818035.1]) as references. The proteins encoded by each genome under study here were further compared against these two references by TBLASTN. Once the blast results were obtained, and the groups to be compared were defined, i.e., MuLDi versus rod-shaped, amino acid changes in proteins shared by both groups (identity threshold 60%) were investigated focusing on those amino acids conserved in the members of both groups but different between the two groups (I vs D option).

RNA sequencing and analysis

Total RNA was extracted from 6 h cultures grown on GCB agar plates. The cells were harvested in RNA protect reagent (Qiagen). RNeasy Mini Kit (Qiagen) with RNase Free DNAse set (Qiagen) was used for RNA extraction according to the manufacturer's instructions.

The removal of ribosomal RNA for cDNA synthesis was done with NEBNext rRNA Depletion kit with 1 µg of total RNA in the purification using 1.8X Cytiva Sera-mag. For results presented in Fig. 6, the rRNA depleted mRNA were processed using the Illumina® Stranded mRNA Prep protocol without modification by Génome Québec Innovation Centre (McGill University, Montréal, Canada). 100 bp Pair-End Sequencing was performed with the NovaSeq 6000 system. FastQ Reads have deposited on SRA database (PRJNA859935). Sequence reads were processed with FastQC (Version 0.73) to determine the quality before grooming by FastQ Groomer (Version 1.1.5). Paired FastQ reads were then aligned against *Neisseria elongata* subsp. glycolytica ATCC 29315 (accession number NZ_CP007726.1) genome using Bowtie2 (Version 2.4.2) and read counts were determined using htseq_count (Version 0.9.1) tool. Subsequently the gene expression of the transcripts was determined using DESeq2 (Version 2.22.40.6). Visualization of differentially expressed genes was done with Venn diagrams, drawn by a Web-based platform Venny 2.1 (https://bioinfogp.cnb.csic.es/tools/venny/).

For intra-genus transcriptomic comparison presented in Fig. 5, rRNA depleted mRNA were treated using the RevertAid RT Reverse Transcription Kit (K1691; Thermo Scientific™) with some adjustments. For first strand cDNA synthesis, 1 µl of random primer (3 µg/µL; 48190011; Invitrogen™) was added and the solution was incubated at 65 °C. For the second strand cDNA synthesis, procedure was followed without RNA removal step and by purifying the double-stranded cDNA with 1.8X Cytiva Sera-mag. The cDNA was eluted in 24 µL of nuclease-free water. Libraries were prepared by PCR BARCODING (96) AMPLICONS (SQK-LSK109) and PCR BARCODING (SQK-PBK004) (Oxford Nanopore technologies), as described by the manufacturer. FastQ Reads have deposited on SRA database (PRJNA859916).The base call was carried out using guppy_basecaller (version 5.0.11 + 2b6dbff) in sup mode, adapters were removed and filtered by quality Q > 8, they were separated by barcodes using guppy_barcoder (version 5.0.11 + 2b6dbff). In parallel, the ten indicated genomes were annotated with Prokka v1.14.5[79]. Using each of the protein sequences (.faa) files, a standalone BLASTP[87] was performed for each dyad possibility. Network connection was thereafter established with the python programming package NetworkX version 2.6.2[52] with a cut-off of 60% of similarity. Basically, all proteins showing more than 60% similarities with one of the members (putative homologs) were clustered together. Each cluster of proteins was named (example NEISS_1) and this name was used to replace the original locus-tags in the .GFF file (previously generated by Prokka). This was done using an homemade python script and has generated a new file that we called .GTF. This file was used to map the reads to the corresponding genomes using minimap2[88]. The .GTF and .sam files were used to perform the reads counts using featureCounts v2.0.1 of Subread package[89]. The count files for each sample were joined into a table using a homemade script and these results were analyzed using DESeq2 version 3.14[90]. Parameter used were Reads >1 in the 10 genomes (core-transcriptome: genes that were showing at least one read mapped in all genomes). We investigated the biological functions of the gene differentially expressed and the putative pathways that could link them through a STRING analysis[91].

Quantitative real-time PCR

RNA samples were standardized to a final concentration of 1 µg with addition of DNaseI Amplification grade (Invitrogen) for genomic DNA removal. Random primers (Invitrogen), and RevertAid H-Minus reverse transcriptase (Thermo Scientific) were used for complementary DNA synthesis (cDNA) according to the manufacturer's instructions. Absence of contaminating gDNA was verified by conventional PCR of RNA samples in the absence of reverse transcriptase. Gene expression of *dcw* cluster was verified by quantitative real-time PCR (qRT-PCR) using Power SYBR Green PCR master mix (Applied Biosystems) using primers listed in Supplementary Table 3. Differential gene expression was calculated using ΔΔCT method using the mean CT value of each target obtained with the StepOneTM Software v2.3, normalization was done relative to *gyrA* gene. Standard T-test using (GraphPad Prism v9.0; GraphPad Software, CA) was used to ascertain statistical significance of gene expression between the strains, where $P < 0.05$ was considered significant.

Genomic organization of the *dcw* cluster and *cdsA* loci in the *Neisseriaceae*

Coordinates of the *dcw* cluster and of the *cdsA* loci were obtained by tblastn for each *Neisseriaceae* genome. Once the genomic location of each sequence was determined, the sequences were extracted using tools available in the EMBOSS package[92]. The resulting sequences were annotated with Prokka, and the output gbk files were used to construct the synteny by employing Easy Fig 2.2.2[93].

Construction of mutant strains

Neisseria elongata mutant strains were done in *N. elongata* subsp. *glycolytica* (ATCC 29315) for single gene mutation and its streptomycin-resistant variant with a point mutations K88R *rpsL** for unmarked and multiple gene editing. *mraZ* was deleted by replacing *mraZ* with an mCherry-encoding gene. The construct for *mraZ* deletion was obtained by fusing multiple PCR fragments using Phusion DNA polymerase according to the protocol (New England Biolabs) as follows: firstly, *N. elongata* gDNA was used to amplify ~500 bp of regions up and down stream of *mraZ* using, respectively, primer pairs 5′KoMraZF-R and 3′KoMraZF-R. The promoter "pdcwSm", located upstream the *S. muelleri dcw* cluster, was amplified from *S. muelleri* gDNA using primer pairs pdcwsmF/pdcwsmR. Primer pairs 5MraZKmF and KmpSimR were used to amplify the kanamycin resistance cassette from pGEM::Km plasmid DNA[16], while the Mcherry cassette was obtained by PCR amplification of pMcherry10 (Addgene) using primer pairs pdcwsmMcherry F and McherryNsilR. Subsequently, the 5′MraZ and Km cassette were fused using primer pairs 5KoMraZF and KmpSimR, while Mcherry and 3′MraZ were fused using primer pairs pdcwMcherryF and 3′KoMraZ R. Finally, 5′MraZ-KM, pdcwSm and Mcherry-3′MraZ fragments were fused using primer pairs 5KoMraZ F and 3KoMraZ R and the resulting DNA was used for transformation in *N. elongata*.

To overexpress *mraZ*, *Neisseria meningitidis* promoter, *porB* was amplified from *N. meningitis* gDNA using primer pairs (porBpF-porBpbluntR) while the *mraZ* gene was amplified from *N. elongata* gDNA using primer pairs (MraZSphIF-3MraZR). The *porB* promoter from *N. meningitidis* and the *mraZ* gene from *N. elongata* were subsequently fused by PCR. This resulted in an ~1.6 kb-long porBp*mraZ* cassette that was digested using the restriction enzymes NheI and KpnI and then ligated with NheI-KpnI digested plasmid p5nrq3::Cm[16]. The ligation mix was transformed in *E. coli* DH5α cells to obtain the porBMraZ::p5nrq3::Cm plasmid. The plasmid was subsequently linearized before transformation into the *Neisseria elongata ΔmraZ* strain.

For the single knockout of *ΔmraZ*, *ΔrapZ*, *ΔgloB* or *Δdgt*, we used a cassette developed in our laboratory named RPLK[15] that contains the wild-type *N. elongata rpsL* gene, *N. meningitidis* promoter *porBp*, the blue-white screening selection marker *lacZ* and the kanamycin resistance marker that facilitated the generation of unmarked deletion in addition to multiple gene editing. We used synthesized DNAs (Bio-Basic) that contain ~500 bp each 5′ and 3′ regions surrounding the respective genes with a central BglII restriction site and cloned into pUC57 plasmid. The plasmids were linearized using BglII and ligated with RPLK cassette[15]. Mutants were obtained by transforming either *N. elongata* wild-type (single knockout) or an *N. elongata* streptomycin-resistant strain (indicated *rpsL**) (multiple knockout) with the linearized plasmid of the targeted gene that resulted in blue, kanamycin-resistant, streptomycin sensitive clones. Markerless deletion was achieved by introducing DNA of the 5′–3′ homologous regions of the target gene thereby excising the RPLK cassette resulting in white, kanamycin sensitive and streptomycin resistant clones. Subsequent genes of interest were edited by repeating this procedure and verifications of the correct excision was done by PCR.

For allelic switching of *N. elongata mreB* with that from *S. muelleri*, plasmid pMreBSimon-3′RD3Ne was obtained by amplifying *S. muelleri mreB* using primer pairs MreBsimonF – MreBsimonR, while the subsequent region of the locus (3′RD3Ne that comprise a piece of *mreCD*) was amplified from *N. elongata* using primer pairs 3′RD3NeF-3′RD3NeR. The two products were fused using primer pairs MreBsimonF – 3′RD3NeR. This generated a cassette of $mreB_{sm}$ fused with $mreCD_{ne}$ that was then digested by restriction enzymes BamHI and SpeI before ligation with plasmid p5KORD1Ne::cm[16] digested with the same enzymes to obtain plasmid pMreBsimon3′RD3Ne::cm. The plasmid was linearized with ScaI before transformation in *N. elongata* strains. $mreB_{\mathrm{sm}}$ positive and $mreB_{\mathrm{ne}}$ negative clones were confirmed by PCR.

For the *cdsA-amiC2* knock-in constructs, we used the plasmid pUCNe::ampR that contains 5′ and 3′ *Neisseria elongata* homologous regions to the intergenic locus between two genes coding for hypothetical proteins at position 888015 (insertion site). We first constructed the pUCNe::RPLK plasmid by ligating the RPLK cassette using BglII. Secondly, *cdsA-AmiC2* PCR product was obtained using primer pairs cdsAmiC2F-amiC2R, was digested using BglII and ligated to pUCNe::ampR to produce the pUCcdsamiC2::ampR plasmid. The mutants were obtained with a two-step method[15]. First, we transformed the plasmid pUCNe::RPLK into *N. elongata rpsL** to obtain *N. elongata* RPLK (RPLK inserted at position 888015). In the second step, we have replaced the RPLK cassette with *cdsA-amiC2* genes, by transforming the pUCcdsamiC2::ampR plasmid linearized using ScaI into *N. elongata* RPLK. *cdsamic2* positive transformants were confirmed by PCR.

Reporting summary

Further information on research design is available in the Nature Research Reporting Summary linked to this article.

Data availability

The genome datasets generated during and/or analyzed during the current study (see Supplementary Data 1) are available in the NCBI genome repository (https://www.ncbi.nlm.nih.gov/genome/browse#!/overview/) under the accession codes: GCA_022870985.1, GCA_014055025.1, GCA_000818035.1, GCA_022870825.1, GCA_022870885.1, GCA_900637855.1, GCA_008807015.1, GCA_014055005.1, GCA_014297595.1, GCA_001308015.1, GCA_014054885.1, GCA_900636765.1, GCA_900638685.1, GCA_022870865.1, GCA_022870845.1, GCA_022870905.1, GCA_002951835.1, GCA_014054525.1, GCA_022871045.1, GCA_900177895.1, GCA_022871005.1, GCA_014054985.1, GCA_016623605.1, GCA_016127355.1, GCA_014054725.1, GCA_022871025.1, GCA_000745895.1, GCA_022870965.1, GCA_022870945.1, GCA_022870925.1, GCA_001648355.1, GCA_001648475.1, GCA_008805035.1, GCA_900187105.1, GCA_014054965.1, Raw reads data are available on SRA database under the accession codes: PRJNA788950, PRJNA859696, PRJNA859916, PRJNA859935. Source data and the corresponding statistics are provided as a Source Data file and at the Cell Image Library repository [https://doi.org/10.7295/W9NC5ZC0]. Source data are provided with this paper.

Code availability

The codes used in this study have been reported previously and are available as described in the corresponding M&M section. The documentation for the ImageJ plugin Fil-Tracer can be accessed here: https://sils.fnwi.uva.nl/bcb/objectj/examples/Fil-Tracer/MD/Fil-Tracer.html. The other custom codes generated during the current study are available from the corresponding authors on reasonable request.

References

1. Kieft, T. L. & Simmons, K. A. Allometry of animal-microbe interactions and global census of animal-associated microbes. *Proc. R. Soc. B Biol. Sci.* **282**, 20150702 (2015).
2. Whitman, W. B., Coleman, D. C. & Wiebe, W. J. Prokaryotes: the unseen majority. *Proc. Natl Acad. Sci. USA* **95**, 6578–6583 (1998).

3. Bulgheresi, S. Bacterial cell biology outside the streetlight. *Environ. Microbiol*. **18**, 2305–2318 (2016).
4. Buskermolen, J. K. et al. Development of a full-thickness human gingiva equivalent constructed from immortalized keratinocytes and fibroblasts. *Tissue Eng. - Part C. Methods* **22**, 781–791 (2016).
5. Kosten, I. J., Buskermolen, J. K., Spiekstra, S. W., De Gruijl, T. D. & Gibbs, S. Gingiva equivalents secrete negligible amounts of key chemokines involved in langerhans cell migration compared to skin equivalents. *J. Immunol. Res*. **2015**, 627125 (2015).
6. Hampton, J. C. & Rosario, B. The attachment of microorganisms to epithelial cells in the distal ileum of the mouse. *Lab. Investig.* **14**, 1464–1481 (1965).
7. Jonsson, H., Hugerth, L. W., Sundh, J., Lundin, E. & Andersson, A. F. Genome sequence of segmented filamentous bacteria present in the human intestine. *Commun. Biol.* **3**, 1–9 (2020).
8. Schnupf, P. et al. Growth and host interaction of mouse segmented filamentous bacteria in vitro. *Nature* **520**, 99–103 (2015).
9. Hedlund, B. P. & Kuhn, D. A. The Genera Simonsiella and Alysiella. *Prokaryotes* **5**, 828–839 (2006).
10. Hedlund, B. P. & Tønjum, T. Simonsiella. *Bergey's Man. Syst. Archaea Bact*. 1–12. https://doi.org/10.1002/9781118960608.GBM00983 (2015).
11. Kuhn, D. A., Gregory, D. A., Buchanan, G. E., Nyby, M. D. & Daly, K. R. Isolation, characterization, and numerical taxonomy of Simonsiella strains from the oral cavities of cats, dogs, sheep, and humans. *Arch. Microbiol.* **118**, 235–241 (1978).
12. Xie, C. H. & Yokota, A. Phylogenetic analysis of Alysiella and related genera of Neisseriaceae: proposal of Alysiella crassa comb. nov., Conchiformibium steedae gen. nov., comb. nov., Conchiformibium kuhniae sp. nov. and Bergeriella denitrificans gen. nov., comb. nov. *J. Gen. Appl. Microbiol.* **51**, 1–10 (2005).
13. Ericsson, A. C., Hagan, C. E., Davis, D. J. & Franklin, C. L. Segmented filamentous bacteria: commensal microbes with potential effects on research. *Comp. Med.* **64**, 90–98 (2014).
14. Schnupf, P., Gaboriau-Routhiau, V., Sansonetti, P. J. & Cerf-Bensussan, N. Segmented filamentous bacteria, Th17 inducers and helpers in a hostile world. *Curr. Opin. Microbiol.* **35**, 100–109 (2017).
15. Nyongesa, S., Chenal, M., Bernet, È., Coudray, F. & Veyrier, F. J. Sequential markerless genetic manipulations of species from the Neisseria genus. *Can. J. Microbiol*. https://doi.org/10.1139/cjm-2022-0024 (2022).
16. Veyrier, F. J. et al. Common cell shape evolution of two nasopharyngeal pathogens. *PLoS Genet.* **11**, 1–23 (2015).
17. Pangborn, J., Kuhn, D. A. & Woods, J. R. Dorsal-ventral differentiation in Simonsiella and other aspects of its morphology and ultrastructure. *Arch. Microbiol.* **113**, 197–204 (1977).
18. Kaiser, G. E. & Starzyk, M. J. Ultrastructure and cell division of an oral bacterium resembling Alysiella filiformis. *Can. J. Microbiol*. **19**, 325–327 (1973).
19. Murray, R. G., Steed, P. & Elson, H. E. The location of the mucopeptide in sections of the cell wall of Escherichia Coli and other gram-negative bacteria. *Can. J. Microbiol.* **11**, 547–560 (1965).
20. Leisch, N. et al. Growth in width and FtsZ ring longitudinal positioning in a gammaproteobacterial symbiont. *Curr. Biol.* **22**, R831–R832 (2012).
21. Leisch, N. et al. Asynchronous division by non-ring FtsZ in the gammaproteobacterial symbiont of *Robbea hypermnestra*. *Nat. Microbiol.* **2**, 16182 (2016).
22. Ramond, E., Maclachlan, C., Clerc-Rosset, S., Knott, G. W. & Lemaitre, B. Cell division by longitudinal scission in the insect endosymbiont Spiroplasma poulsonii. *MBio* **7**, 1–5 (2016).
23. Dudek, N. K. et al. Previously uncharacterized rectangular bacteria in the dolphin mouth. *bioRxiv* https://doi.org/10.1101/2021.10.23.465578 (2021).
24. Szwedziak, P. & Löwe, J. Do the divisome and elongasome share a common evolutionary past? *Curr. Opin. Microbiol.* **16**, 745–751 (2013).
25. Bi, E. & Lutkenhaus, J. FtsZ ring structure associated with division in Escherichia coli. *Nature* **354**, 161–164 (1991).
26. Höltje, J.-V. Growth of the stress-bearing and shape-maintaining murein sacculus of Escherichia coli. *Microbiol. Mol. Biol. Rev*. **62**, 181–203 (1998).
27. Shi, H. et al. Deep phenotypic mapping of bacterial cytoskeletal mutants reveals physiological robustness to cell size. *Curr. Biol*. **27**, 3419–3429.e4 (2017).
28. Shi, H., Bratton, B. P., Gitai, Z. & Huang, K. C. How to build a bacterial cell: MreB as the foreman of E. coli construction. *Cell* **172**, 1294–1305 (2018).
29. Addinall, S. G. & Lutkenhaus, J. FtsZ-spirals and -arcs determine the shape of the invaginating septa in some mutants of Escherichia coli. *Mol. Microbiol*. **22**, 231–237 (1996).
30. Monahan, L. G., Robinson, A. & Harry, E. J. Lateral FtsZ association and the assembly of the cytokinetic Z ring in bacteria. *Mol. Microbiol.* **74**, 1004–1017 (2009).
31. Sen, B. C. et al. Specific amino acid substitutions in β strand S2 of FtsZ cause spiraling septation and impair assembly cooperativity in Streptomyces spp. *Mol. Microbiol.* **112**, 184–198 (2019).
32. Xiao, X. et al. Ectopic positioning of the cell division plane is associated with single amino acid substitutions in the FtsZ-recruiting SsgB in Streptomyces. *Open Biol*. **11**, 200409 (2021).
33. den Blaauwen, T. Is longitudinal division in rod-shaped bacteria a matter of swapping axis? *Front. Microbiol*. **9**, 822 (2018).
34. Thanbichler, M. Cell division: symbiotic bacteria turn it upside down. *Curr. Biol.* **28**, R306–R308 (2018).
35. Chen, S., Rudra, B. & Gupta, R. S. Phylogenomics and molecular signatures support division of the order Neisseriales into emended families Neisseriaceae and Chromobacteriaceae and three new families Aquaspirillaceae fam. nov., Chitinibacteraceae fam. nov., and Leeiaceae fam. nov. *Syst. Appl. Microbiol.* **44**, 126251 (2021).
36. Ishikawa, S. A., Zhukova, A., Iwasaki, W., Gascuel, O. & Pupko, T. A fast likelihood method to reconstruct and visualize ancestral scenarios. *Mol. Biol. Evol*. **36**, 2069–2085 (2019).
37. Adeolu, M. & Gupta, R. S. Phylogenomics and molecular signatures for the order Neisseriales: proposal for division of the order Neisseriales into the emended family Neisseriaceae and Chromobacteriaceae fam. nov. *Antonie van. Leeuwenhoek. Int. J. Gen. Mol. Microbiol.* **104**, 1–24 (2013).
38. Pende, N. et al. Host-polarized cell growth in animal symbionts. *Curr. Biol.* **28**, 1039–1051.e5 (2018).
39. Bisson-Filho, A. W. et al. Treadmilling by FtsZ filaments drives peptidoglycan synthesis and bacterial cell division. *Science.* **355**, 739 LP–739743 (2017).
40. Yang, X. et al. GTPase activity-coupled treadmilling of the bacterial tubulin FtsZ organizes septal cell wall synthesis. *Science* **355**, 744–747 (2017).
41. Guerra Maldonado, J. F., Vincent, A. T., Chenal, M. & Veyrier, F. J. CAPRIB: a user-friendly tool to study amino acid changes and selection for the exploration of intra-genus evolution. *BMC Genomics* **21**, 1–14 (2020).
42. Veyrier, F., Pletzer, D., Turenne, C. & Behr, M. A. Phylogenetic detection of horizontal gene transfer during the step-wise genesis of Mycobacterium tuberculosis. *BMC Evol. Biol.* **9**, 1–14 (2009).
43. Brennan, C. A. & Garrett, W. S. Fusobacterium nucleatum — symbiont, opportunist and oncobacterium. *Nat. Rev. Microbiol. 2018 173* **17**, 156–166 (2018).
44. Poole, K., Schiebel, E. & Braun, V. Molecular characterization of the hemolysin determinant of Serratia marcescens. *J. Bacteriol.* **170**, 3177–3188 (1988).

45. Eraso, J. M. et al. The highly conserved MraZ protein is a transcriptional regulator in Escherichia coli. *J. Bacteriol.* **196**, 2053–2066 (2014).
46. Fisunov, G. Y. et al. Binding site of MraZ transcription factor in Mollicutes. *Biochimie* **125**, 59–65 (2016).
47. Mengin-Lecreulx, D. et al. Contribution of the P(mra) promoter to expression of genes in the Escherichia coli mra cluster of cell envelope biosynthesis and cell division genes. *J. Bacteriol.* **180**, 4406–4412 (1998).
48. Khan, M. A., Durica-Mitic, S., Göpel, Y., Heermann, R. & Görke, B. Small RNA-binding protein RapZ mediates cell envelope precursor sensing and signaling in Escherichia coli. *EMBO J.* **39**, e103848 (2020).
49. Beauchamp, B. B. & Richardson, C. C. A unique deoxyguanosine triphosphatase is responsible for the optA1 phenotype of Escherichia coli. *Proc. Natl Acad. Sci. USA* **85**, 2563–2567 (1988).
50. Sukdeo, N. & Honek, J. F. Microbial glyoxalase enzymes: metalloenzymes controlling cellular levels of methylglyoxal. *Drug Metabol. Drug Interact.* **23**, 29–50 (2008).
51. Busiek, K. K. & Margolin, W. Bacterial actin and tubulin homologs in cell growth and division. *Curr. Biol.* **25**, R243–R254 (2015).
52. Hagberg, A. A., Schult, D. A. & Swart, P. J. Exploring network structure, dynamics, and function using NetworkX. 7th Python in Science Conference (SciPy 2008) (2008).
53. Siefert, J. L. & Fox, G. E. Phylogenetic mapping of bacterial morphology. *Microbiology* **144**, 2803–2808 (1998).
54. Young, K. D. The selective value of bacterial shape. *Microbiol. Mol. Biol. Rev.* **70**, 660–703 (2006).
55. Mark Welch, J. L., Ramírez-Puebla, S. T. & Borisy, G. G. Oral microbiome geography: micron-scale habitat and niche. *Cell Host Microbe* **28**, 160–168 (2020).
56. Claessen, D., Rozen, D. E., Kuipers, O. P., Søgaard-Andersen, L. & Van Wezel, G. P. Bacterial solutions to multicellularity: a tale of biofilms, filaments and fruiting bodies. *Nat. Rev. Microbiol.* **12**, 115–124 (2014).
57. Monds, R. D. & O'Toole, G. A. The developmental model of microbial biofilms: ten years of a paradigm up for review. *Trends Microbiol.* **17**, 73–87 (2009).
58. Zhang, L., Willemse, J., Claessen, D. & Van Wezel, G. P. SepG coordinates sporulation-specific cell division and nucleoid organization in Streptomyces coelicolor. *Open Biol.* **6**, 150164 (2016).
59. Flores, E., Nieves-Morión, M. & Mullineaux, C. W. Cyanobacterial septal junctions: properties and regulation. *Life* **9**, 1 (2019).
60. Du, S. & Lutkenhaus, J. At the heart of bacterial cytokinesis: the Z ring. *Trends Microbiol.* **27**, 781–791 (2019).
61. Ayala, J. A., Garrido, T., De Pedro, M. A. & Vicente, M. Chapter 5 molecular biology of bacterial septation. *N. Compr. Biochem.* **27**, 73–101 (1994).
62. Nikolaichik, Y. A. & Donachie, W. D. Conservation of gene order amongst cell wall and cell division genes in Eubacteria, and ribosomal genes in Eubacteria and Eukaryotic organelles. *Genetica* **108**, 1–7 (2000).
63. Tamames, J., González-Moreno, M., Mingorance, J., Valencia, A. & Vicente, M. Bringing gene order into bacterial shape. *Trends Genet.* **17**, 124–126 (2001).
64. Vicente, M., Gomez, M. J. & Ayala, J. A. Regulation of transcription of cell division genes in the Eschericia coli dcw cluster. *Cell. Mol. Life Sci.* **54**, 317–324 (1998).
65. Mingorance, J., Tamames, J. & Vicente, M. Genomic channeling in bacterial cell division. *J. Mol. Recognit.* **17**, 481–487 (2004).
66. Martínez-Torró, C. et al. Functional characterization of the cell division gene cluster of the wall-less bacterium Mycoplasma genitalium. *Front. Microbiol.* **12**, 695572 (2021).
67. Wang, B. et al. Functional insights of mraZ on the pathogenicity of Staphylococcus aureus. *Infect. Drug Resist.* **14**, 4539–4551 (2021).
68. Kawazura, T. et al. Exclusion of assembled MreB by anionic phospholipids at cell poles confers cell polarity for bidirectional growth. *Mol. Microbiol.* **104**, 472–486 (2017).
69. Alvarez, L., Cordier, B., van Teeffelen, S. & Cava, F. Analysis of gram-negative bacteria peptidoglycan by ultra-performance liquid chromatography. *Bio. Protocol* **10**, e3780 (2020).
70. Schneider, C. A., Rasband, W. S. & Eliceiri, K. W. NIH Image to ImageJ: 25 years of image analysis. *Nat. Methods* **9**, 671–675 (2012).
71. Schindelin, J. et al. Fiji: an open-source platform for biological-image analysis. *Nat. Methods* **9**, 676–682 (2012).
72. Chin, C. S. et al. Nonhybrid, finished microbial genome assemblies from long-read SMRT sequencing data. *Nat. Methods* **10**, 563–569 (2013).
73. Koren, S. et al. Canu: scalable and accurate long-read assembly via adaptive κ-mer weighting and repeat separation. *Genome Res.* **27**, 722–736 (2017).
74. Li, H. Minimap and miniasm: fast mapping and de novo assembly for noisy long sequences. *Bioinformatics* **32**, 2103–2110 (2016).
75. Walker, B. J. et al. Pilon: an integrated tool for comprehensive microbial variant detection and genome assembly improvement. *PLoS One* **9**, e112963 (2014).
76. Vaser, R., Sović, I., Nagarajan, N. & Šikić, M. Fast and accurate de novo genome assembly from long uncorrected reads. *Genome Res.* **27**, 737–746 (2017).
77. Gurevich, A., Saveliev, V., Vyahhi, N. & Tesler, G. QUAST: quality assessment tool for genome assemblies. *Bioinformatics* **29**, 1072–1075 (2013).
78. Manni, M., Berkeley, M. R., Seppey, M., Simão, F. A. & Zdobnov, E. M. BUSCO update: novel and streamlined workflows along with broader and deeper phylogenetic coverage for scoring of eukaryotic, prokaryotic, and viral genomes. *Mol. Biol. Evol.* **38**, 4647–4654 (2021).
79. Seemann, T. Prokka: rapid prokaryotic genome annotation. *Bioinformatics* **30**, 2068-2069 (2014).
80. Page, A. J. et al. Roary: Rapid large-scale prokaryote pan genome analysis. *Bioinformatics* **31**, 3691–3693 (2015).
81. Kalyaanamoorthy, S., Minh, B. Q., Wong, T. K. F., Von Haeseler, A. & Jermiin, L. S. ModelFinder: fast model selection for accurate phylogenetic estimates. *Nat. Methods* **14**, 587–589 (2017).
82. Nguyen, L. T., Schmidt, H. A., Von Haeseler, A. & Minh, B. Q. IQ-TREE: a fast and effective stochastic algorithm for estimating maximum-likelihood phylogenies. *Mol. Biol. Evol.* **32**, 268–274 (2015).
83. Hoang, D. T., Chernomor, O., Von Haeseler, A., Minh, B. Q. & Vinh, L. S. UFBoot2: improving the ultrafast bootstrap approximation. *Mol. Biol. Evol.* **35**, 518–522 (2018).
84. Katoh, K., Misawa, K., Kuma, K. I. & Miyata, T. MAFFT: a novel method for rapid multiple sequence alignment based on fast Fourier transform. *Nucleic Acids Res.* **30**, 3059–3066 (2002).
85. Veyrier, F. J., Dufort, A. & Behr, M. A. The rise and fall of the Mycobacterium tuberculosis genome. *Trends Microbiol.* **19**, 156–161 (2011).
86. Gerts, E. M., Yu, Y. K., Agarwala, R., Schäffer, A. A. & Altschul, S. F. Composition-based statistics and translated nucleotide searches: Improving the TBLASTN module of BLAST. *BMC Biol.* **4**, 1–14 (2006).
87. Camacho, C. et al. BLAST+: architecture and applications. *BMC Bioinforma.* **10**, 1–9 (2009).
88. Li, H. Minimap2: pairwise alignment for nucleotide sequences. *Bioinformatics* **34**, 3094–3100 (2018).
89. Liao, Y., Smyth, G. K. & Shi, W. FeatureCounts: an efficient general purpose program for assigning sequence reads to genomic features. *Bioinformatics* **30**, 923–930 (2014).

90. Love, M. I., Huber, W. & Anders, S. Moderated estimation of fold change and dispersion for RNA-seq data with DESeq2. *Genome Biol.* **15**, 1–21 (2014).
91. Szklarczyk, D. et al. The STRING database in 2021: customizable protein-protein networks, and functional characterization of user-uploaded gene/measurement sets. *Nucleic Acids Res.* **49**, D605–D612 (2021).
92. Rice, P., Longden, L. & Bleasby, A. EMBOSS: the European molecular biology open software suite. *Trends Genet.* **16**, 276–277 (2000).
93. Sullivan, M. J., Petty, N. K. & Beatson, S. A. Easyfig: a genome comparison visualizer. *Bioinformatics* **27**, 1009–1010 (2011).
94. El Houmami, N. et al. Isolation and characterization of Kingella negevensis sp. Nov., a novel kingella species detected in a healthy paediatric population. *Int. J. Syst. Evol. Microbiol.* **67**, 2370–2376 (2017).
95. Antezack, A., Boxberger, M., Rolland, C., Monnet-Corti, V. & Scola, B. LA. Isolation and characterization of Kingella bonacorsii sp. nov., a novel Kingella species detected in a stable periodontitis subject. https://doi.org/10.3390/pathogens (2021).
96. Snell, J. J. S. & Lapage, S. P. Transfer of some saccharolytic Moraxella species to Kingella Henriksen and Bovre 1976, with descriptions of Kingella indologenes sp. nov. and Kingella denitrificans sp. nov. *Int. J. Syst. Bacteriol.* **26**, 451–458 (1976).
97. Bernard, K. A., Burdz, T., Wiebe, D. & Bernier, A. M. Description of Eikenella halliae sp. nov. and Eikenella longinqua sp. nov., derived from human clinical materials, emendation of Eikenella exigua Stormo et al. 2019 and emendation of the genus Eikenella to include species which are strict anaerobes. *Int. J. Syst. Evol. Microbiol.* **70**, 3167–3178 (2020).
98. Dong, L. et al. Crenobacter luteus gen. nov., sp. nov., isolated from a hot spring. *Int. J. Syst. Evol. Microbiol.* **65**, 214–219 (2015).
99. Zhu, H. Z., Jiang, C. Y. & Liu, S. J. Crenobacter cavernae sp. nov., isolated from a karst cave, and emended description of the genus Crenobacter. *Int. J. Syst. Evol. Microbiol.* **69**, 476–480 (2019).
100. Yang, Z. et al. Crenobacter caeni sp. nov. isolated from sludge. *Curr. Microbiol.* **77**, 4180–4185 (2020).
101. Shi, S. B. et al. Crenobacter intestini sp. nov., isolated from the intestinal tract of Konosirus punctatus. *Curr. Microbiol.* **78**, 1686–1691 (2021).
102. Altschul, S. F. et al. Gapped BLAST and PSI-BLAST: A new generation of protein database search programs. *Nucleic Acids Res.* **25**, 3389–3402 (1997).

Acknowledgements

The authors are extremely grateful to: Markus Christian Schmid and the Department of Microbial and Ecosystem Science of the University of Vienna for providing the Leica SP8 confocal laser scanning microscope and superb technical support; Belma Bejtovic and Mary Ward for performing preliminary experiments; Nathan Weyand for providing us with *Neisseria* sp. DentCa1/247; Tanneke den Blaauwen (University of Amsterdam) for inspiring and constructive discussions; Antony Vincent (University Laval) for his help in genome assemblies; Dennis Claessen for valuable comments on the manuscript. This work was supported by the Natural Sciences and Engineering Research Council of Canada (NSERC) discovery grant (RGPIN-2016-04940) (F.V.), the Fonds De Recherche du Quebec Nature et technologies (FRQNT) Établissement de la relève professorale (205027) (F.V.) and the Austrian Science Fund (FWF) project P28593-B22 (S.B., P.M.W., T.V., N.K.). P.M.W. also received DOC-fellowship 25240 from the Austrian Academy of Science and a PhD completion grant from the University of Vienna. E.B. received a Ph.D. Fellowship from the Fondation Armand-Frappier. M.D. was partially supported by a postdoctoral fellowship from the Swiss National Science Foundation (project #P2GEP3_191489). C.N. Received a Ph.D. studentship Calmette & Yersin from the Institut Pasteur International Network. Research in the Cava lab was supported by The Swedish Research Council (VR), The Knut and Alice Wallenberg Foundation (KAW), The Laboratory of Molecular Infection Medicine Sweden (MIMS), and The Kempe Foundation. M.N. was funded by a postdoctoral fellowship from the Swedish Society for Medical Research (SSMF). Y.V.B. is also supported by a Canada 150 Research Chair in Bacterial Cell Biology. F.J.V. received a Junior 1 and Junior 2 research scholar salary award from the Fonds de Recherche du Québec - Santé. The funders had no role in study design, data collection and analysis, decision to publish, or preparation of the manuscript.

Author contributions

S.N. and P.M.W did most experiments, visualization and formal analysis, wrote and revised the manuscript. E.B.; F.P; M.N.; M.D; C.N.; T.V.; N.K.; A.R.M. and A.N. did some experiments and formal analysis and critically revised the manuscript. N.O.E.V. contributed ImageJ analysis tools (ObjectJ, Fil-Tracer). M.V. contributed materials. Y.B. acquired funding and analysis tools. F.C. acquired funding, did formal analysis and revised manuscript. S.B. conceptualized and supervised the work, acquired funding, provided resources, wrote and revised the manuscript. F.J.V. did experiments, formal analysis, conceptualized and supervised the work, acquired funding, provided resources, wrote and revised the manuscript. Equally contributing authors were listed in alphabetical order.

Competing interests

The authors declare no competing interests.

Additional information

Supplementary information The online version contains

supplementary material available at https://doi.org/10.1038/s41467-022-32260-w.

Correspondence and requests for materials should be addressed to Silvia Bulgheresi or Frédéric J. Veyrier.

Peer review information *Nature Communications* thanks Pierre Garcia, Brian Hedlund and the other, anonymous, reviewers for their contribution to the peer review of this work. Peer reviewer reports are available.

Reprints and permission information is available at http://www.nature.com/reprints

Publisher's note Springer Nature remains neutral with regard to jurisdictional claims in published maps and institutional affiliations.

Supplementary material

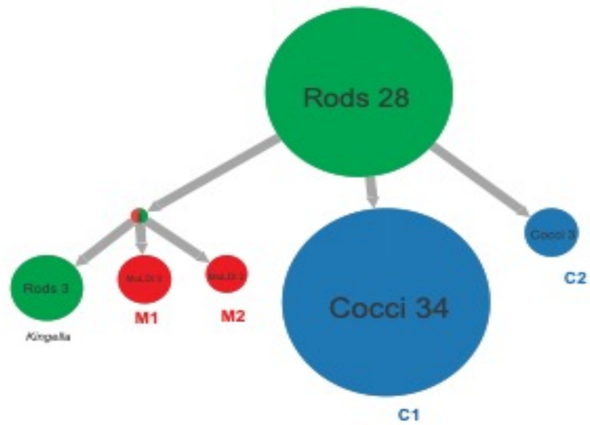

Supplementary Figure 1. The ancestor of the *Neisseriaceae* was rod-shaped. (a) Maximum Likelihood method (PastML; Ishikawa, S. A., Zhukova, A., Iwasaki, W., Gascuel, O. & Pupko, T. (2019). A Fast Likelihood Method to Reconstruct and Visualize Ancestral Scenarios. Molecular Biology and Evolution, 36(9), 2069–2085. https://doi.org/10.1093/molbev/msz131) indicating that the ancestor of all *Neisseriaceae* was rod-shaped.

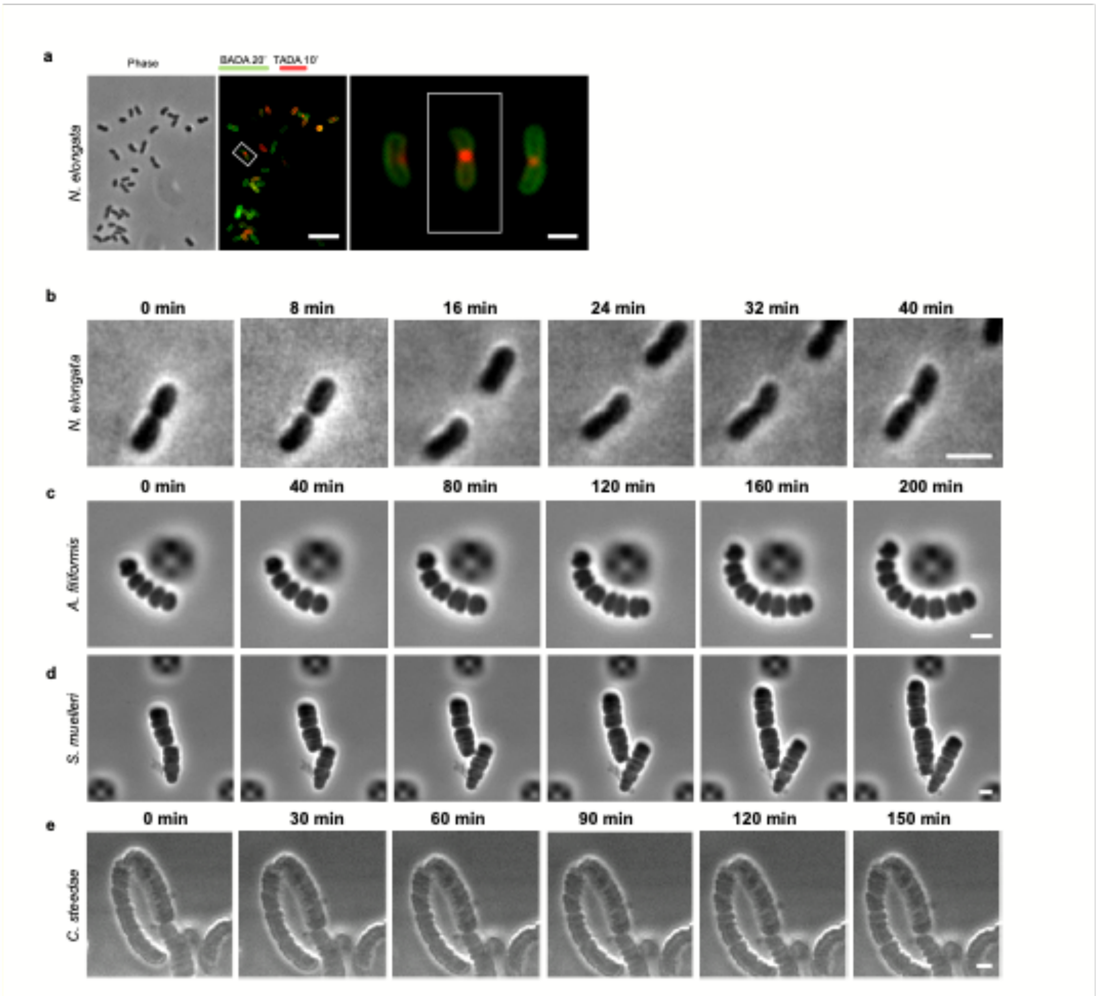

Supplementary Figure 2. Different growth modes of four oral cavity symbionts. (a) *N. elongata* was incubated for 20 min with BADA (green) and, subsequently, for 10 min in TADA (red). Scale bars are 5 µm (middle panel) and 1 µm (right panel). (b-e) Time-lapse microscopy montage showing dividing *N. elongata* (b), *A. filiformis* (c), *S. muelleri* (d) and *C. steedae* (e). Frames show images taken every 8 min for *N. elongata*, every 40 min for *A. filiformis* and *S. muelleri*, and every 30 min for *C. steedae*. The results are representative of at least three independent analyses. See also Supplementary Movies S1, S2, S3 and S4.

a

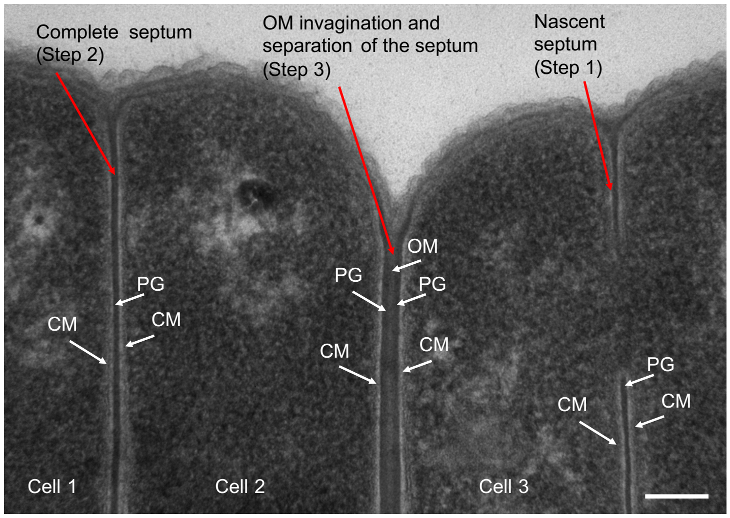

b

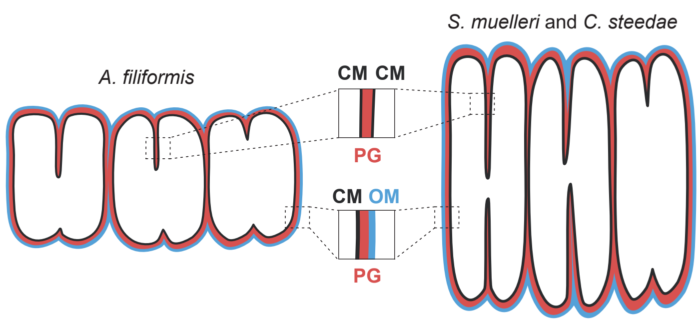

Supplementary Figure 3. Cytoplasmic membrane invagination appears to precede outer membrane invagination in MuLDi *Neisseriaceae*. (a) High magnification transmission electron microscopy image of *S. muelleri*. The results are representative of at least three independent analyses. Scale bar is 100 nm. (b) Schematic representation of the MuLDi envelope.

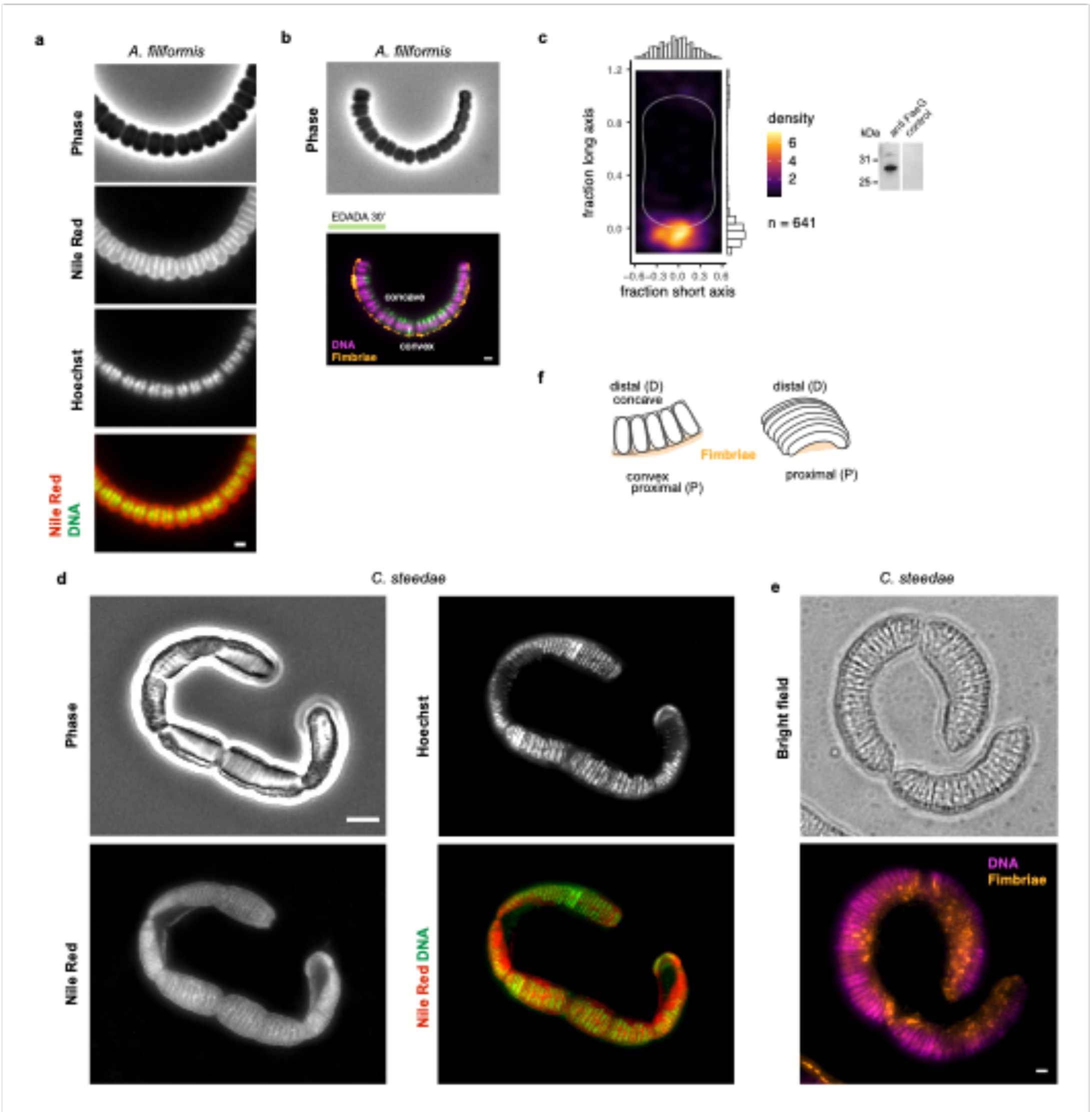

Supplementary Figure 4. Membrane staining and cell polarization of *A. filiformis* and *C. steedae*. (a) Phase contrast image of an *A. filiformis* filament and corresponding membrane staining (Nile red), DNA (Hoechst) staining and overlay are displayed from top to bottom. (b) Phase contrast image (top) and corresponding epifluorescence image (bottom) of *A. filiformis* filament labelled for 30 min with EDA-DA, immunolabelled with an anti-fimbriae antibody and stained with Hoechst. Scale bars are 1 µm. (c) Quantitative analysis of the position of anti-fimbriae antibody fluorescence maxima within 641 individual cells and Western blot of *A. filiformis* protein extracts probed with an anti-fimbriae antibody. (d) Phase contrast image of a *C. steedae* filament (top left) and corresponding membrane (Nile red) staining (bottom left), DNA (Hoechst) staining (top right) and overlay (bottom right). Scale bars are 2 µm (a-d), 1 µm (e) and 5 µm (f). (e) Bright field image (left) and corresponding epifluorescence image (right) of a *C. steedae* filament stained with Hoechst and immunolabelled with an anti-fimbriae antibody. (f) Schematic representations of an *A. filiformis* filament (left) and of a *C. steedae* filament (right). The results are representative of at least three independent analyses. Scale bars are 2 µm (d) and 1 µm (e).

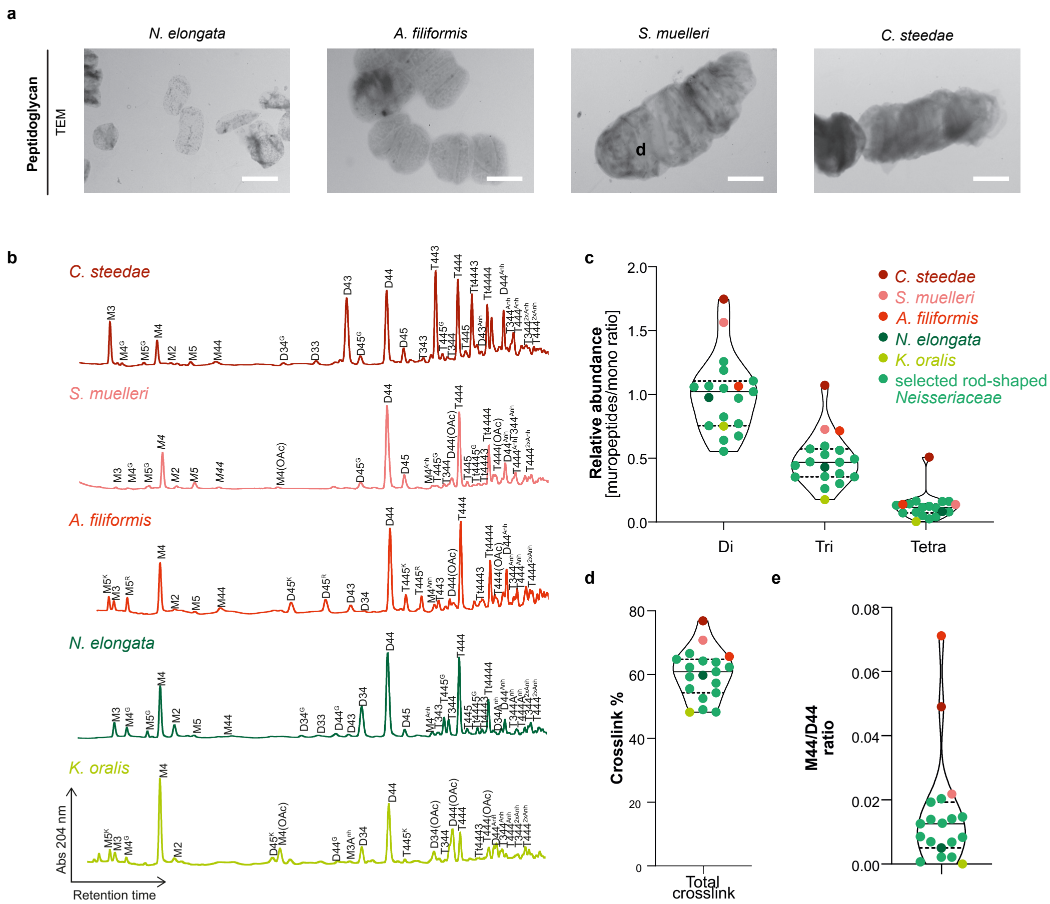

Supplementary Figure 5. TEM of extracted PG of *N. elongata, A. filiformis, S. muelleri* and *C. steedae* and muropeptide analysis of members of the family *Neisseriaceae*. (a) Representative TEM images of sacculi of *N. elongata*, *A. filiformis*, *S. muelleri* and *C. steedae* (from left to right). (b-e) Muropeptide analysis of members of the family *Neisseriaceae*. (b) HPLC chromatograms of muropeptides from *C. steedae* DSM 2580, *S. muelleri* ATCC 29453, *A. filiformis* DSM 16848, *N. elongata* subspglycolytica ATCC 29315, *K. oralis* DSM 18271. Muropeptides characterized by MS are labelled. (c) Distribution of the abundance of dimers (Di), trimers (Tri) and tetramers (Tetra) relative to the abundance of monomers. (d) Overall cross-linking. (e) Relative abundance of the amidase-derived muropeptide product disaccharide octapeptide (M44) relative to its D44 dimer substrate. *C. steedae* DSM 2580, *S. muelleri* ATCC 29453, *A. filiformis* DSM 16848, *N. elongata* subspglycolytica ATCC 29315, *K. oralis* DSM 18271 are labelled in dark red, salmon, red, dark green and yellow green, respectively. Other rod-shaped *Neisseriaceae* (*Neisseria bacilliformis* ATCC BAA-1200, *Neisseria potus* NCTC 13336, *Neisseria musculi*, *Neisseria dentiae* DSMZ 19151, *Neisseria dumasiana* DSMZ 10467, *Neisseria zoodegmatis* DSMZ 21643, *Neisseria species* Dent CA1/247, *Neisseria animaloris* DSMZ 21642, *Neisseria zalophi* DSMZ 102031, *Neisseria weaveri* DSMZ 17688, *Neisseria arctica* DSMZ 103136, *Uruburuella suis* DMSZ 17474, *Uruburuella testudinis* DSMZ 26510, *Neisseria shayeganii* DSMZ 22244 are pale green. The results are representative of at least three independent analyses. Source data are provided as a Source Data file.

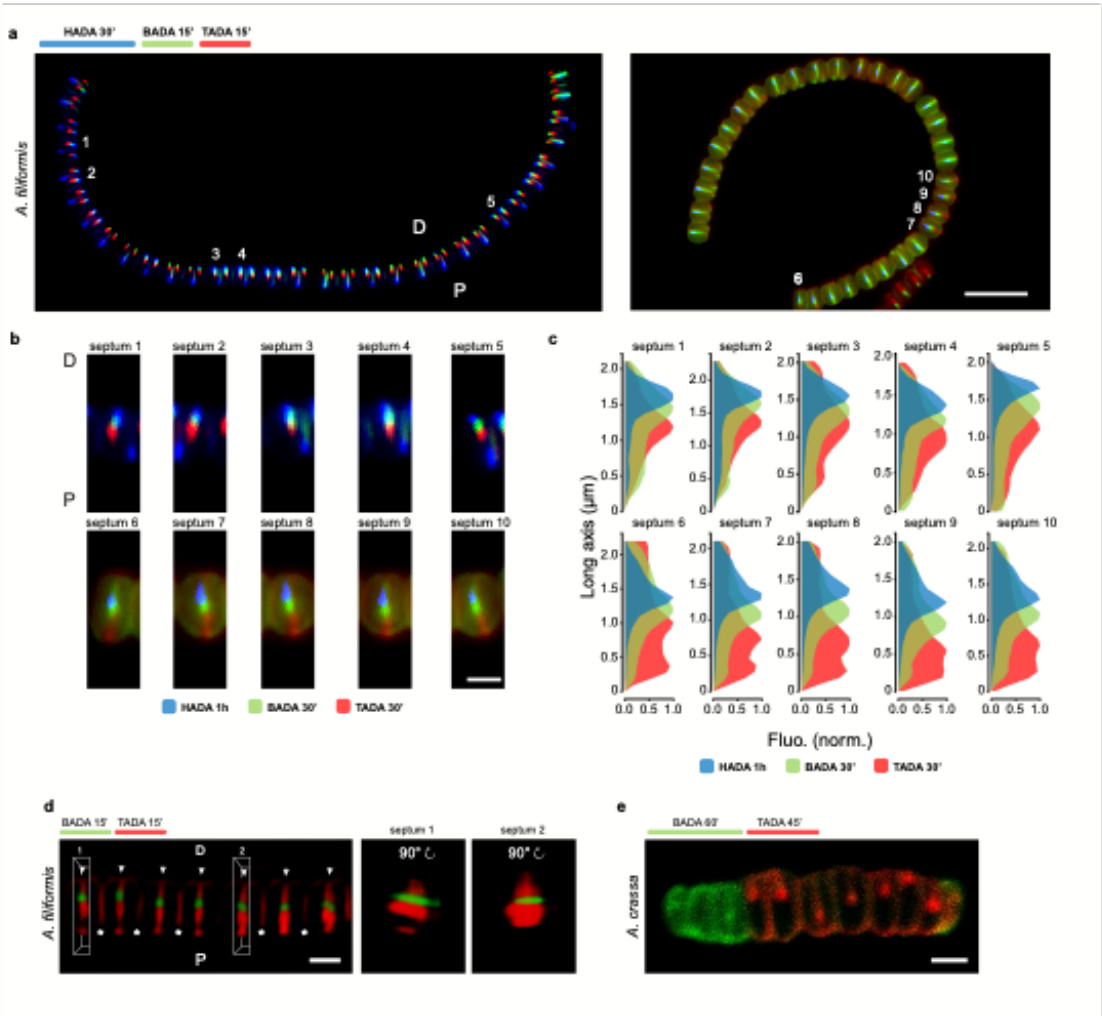

Supplementary Figure 6. Localization of newly synthesized PG in ten *A. filiformis* and in *A. crassa*. (a-c) Epifluorescence microscope-based images of *A. filiformis* consecutively labelled with HADA, BADA and TADA for 30 min, 15 min and 15 min, respectively. (a) Two representative filaments of *A. filiformis*, (b) ten representative *A. filiformis* cells and (c) corresponding septal fluorescence profiles of HADA, BADA and TADA plotted along the long axis. (d) Confocal microscope-based images of *A. filiformis* consecutively labelled with BADA and TADA for 15 min each. Arrowheads point to almost or just completed septa. Asterisks indicate previously competed septa. Fluorescence emitted by an almost completed septum (septum 1; in white box in left panel) and by a just completed septum (septum 2; in white box in left panel) were rotated by 90° and are displayed in the middle and the right panels, respectively. (e) Confocal microscope image of a representative filament of *A. crassa* consecutively labelled with BADA and TADA for 60 min and 45 min, respectively. The results are representative of at least three independent analyses. Source data are provided as a Source Data file. Scale bars correspond to 5 µm (a) or 1 µm (b, d and e).

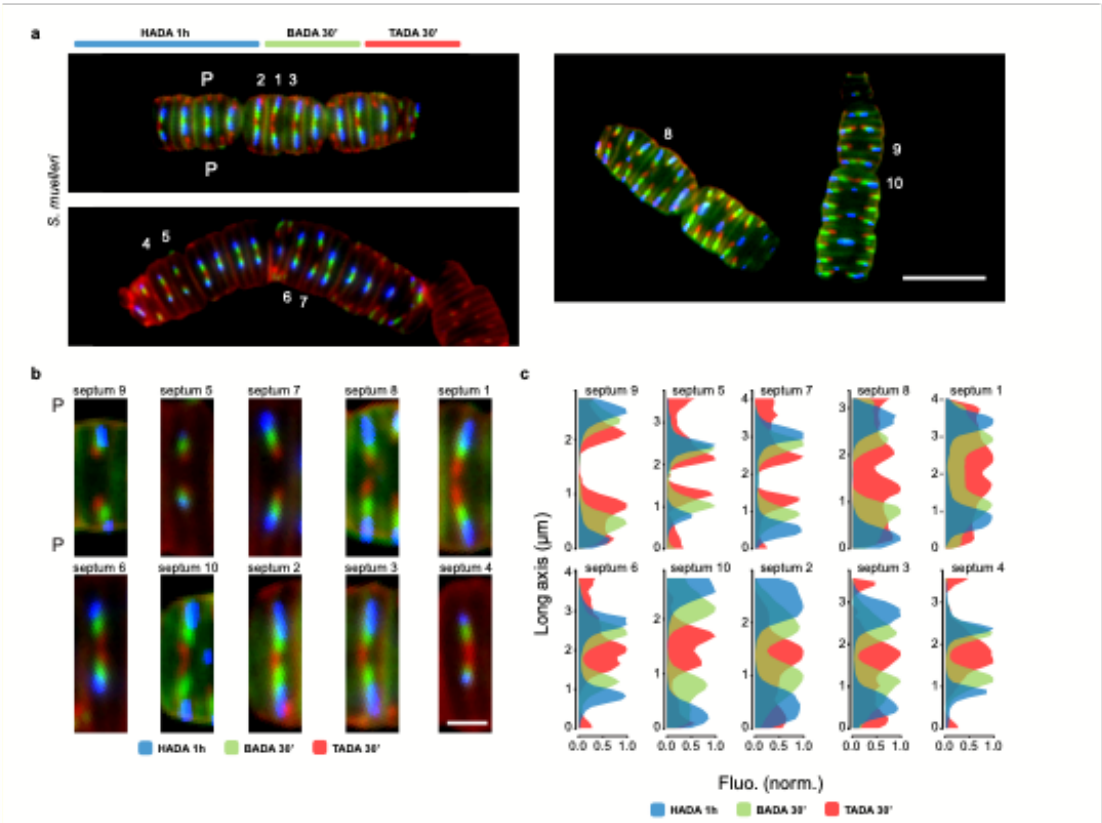

Supplementary Figure 7. Epifluorescence microscope-based localization of newly synthesized PG in ten *S. muelleri*. (a-c) *S. muelleri* was labelled with HADA, BADA and TADA for 1 h, 30 min and 30 min, respectively. (a) Four representative filaments of *S. muelleri*, (b) ten representative cells and (f) corresponding septal fluorescence profiles of HADA, BADA and TADA plotted along the long axis of the 10 cells displayed in (e). The results are representative of at least three independent analyses. Source data are provided as a Source Data file. Scale bars are 5 µm (a) and 1 µm (b).

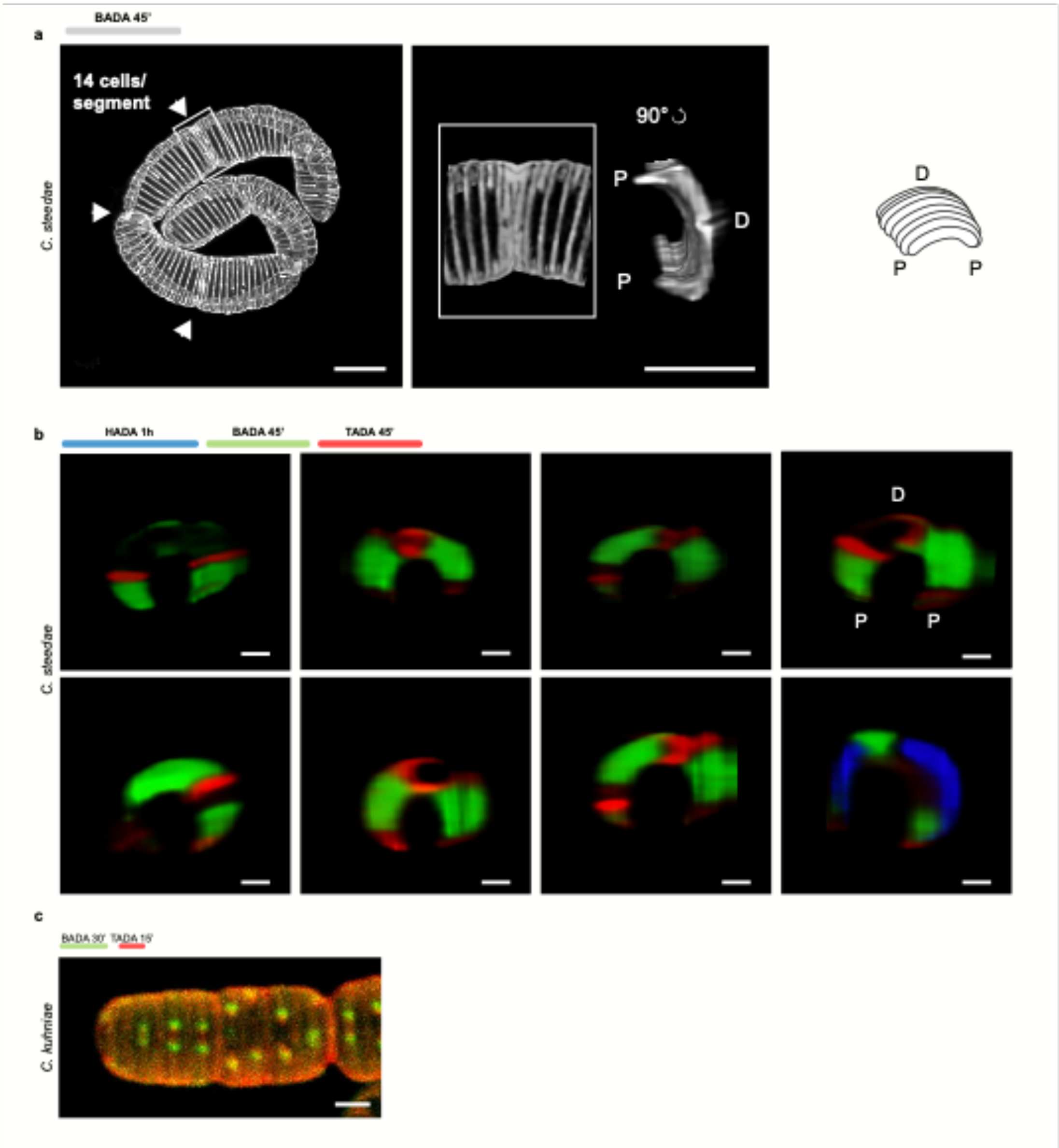

Supplementary Figure 8. Confocal microscopy-based localization of newly synthesized PG in *C. kuhniae* and *C. steedae*. (a) Left panel shows a Z projection of a representative *C. steedae* filament incubated for 45 min with BADA. White arrowheads point at three walls, which appear thicker than the others and which separate two clusters of 14 cells each. Middle and right panels display a lateral view and a 90° rotated view, respectively, of one of the seemingly thicker walls displayed in the left panel (white frame). Scale bar is 5 µm. (b) *C. steedae* septa were cut out of the 3D reconstruction of a filament incubated with HADA for 1h, followed by two pulses with BADA and TADA for 45 minutes. Scale bars represent 1 µm. (c) *C. kuhniae* was labelled consecutively with BADA and TADA for 30 min and 15 min, respectively, and one representative filament was shown. The results are representative of at least three independent analyses. Scale bars correspond to 1 µm.

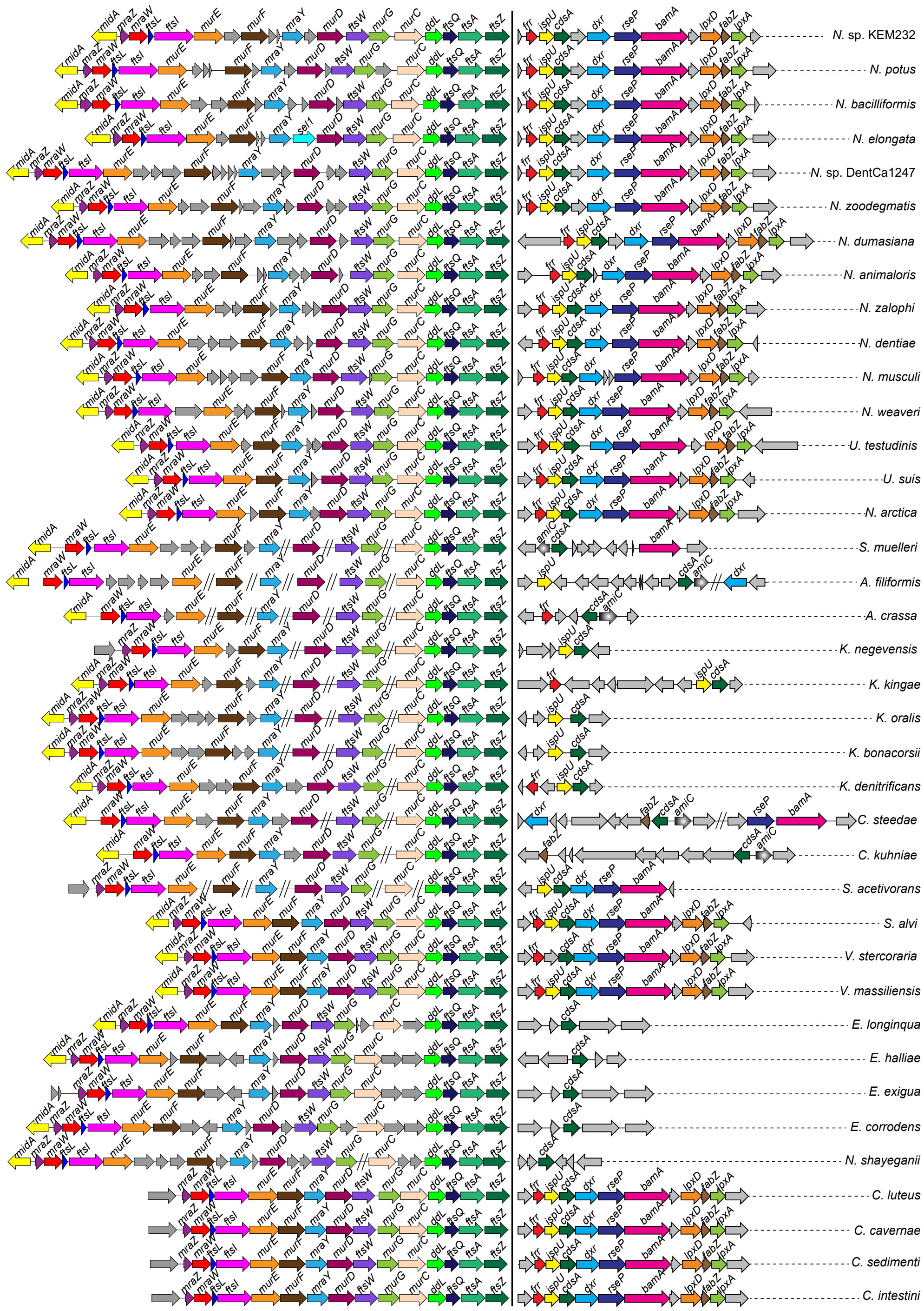

Supplementary Figure 9. The genomic organization of the *dcw* cluster and *cdsA-amiC* loci in the family *Neisseriaceae*.

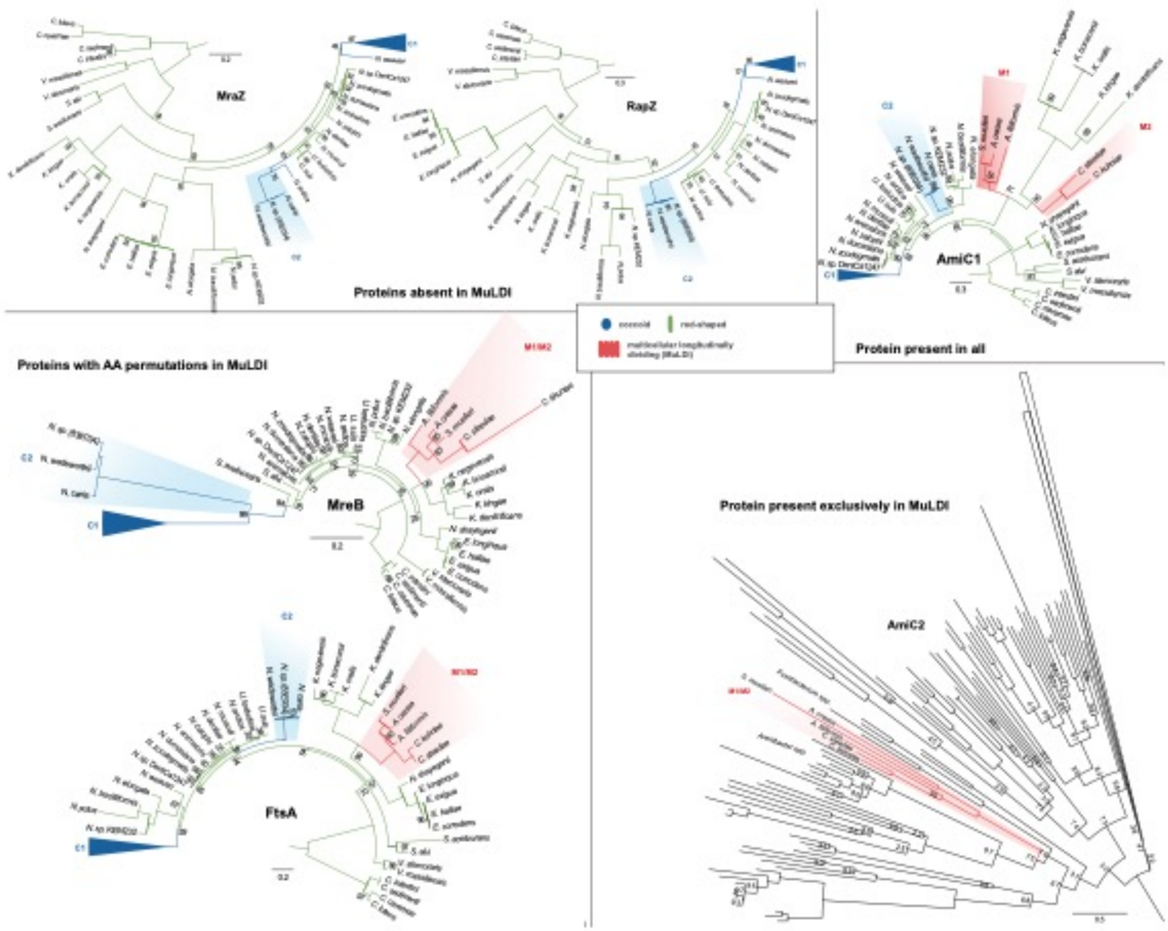

Supplementary Figure 10. RapZ, MraZ, MreB, FtsA, AmiC1 and AmiC2 phylogenies.

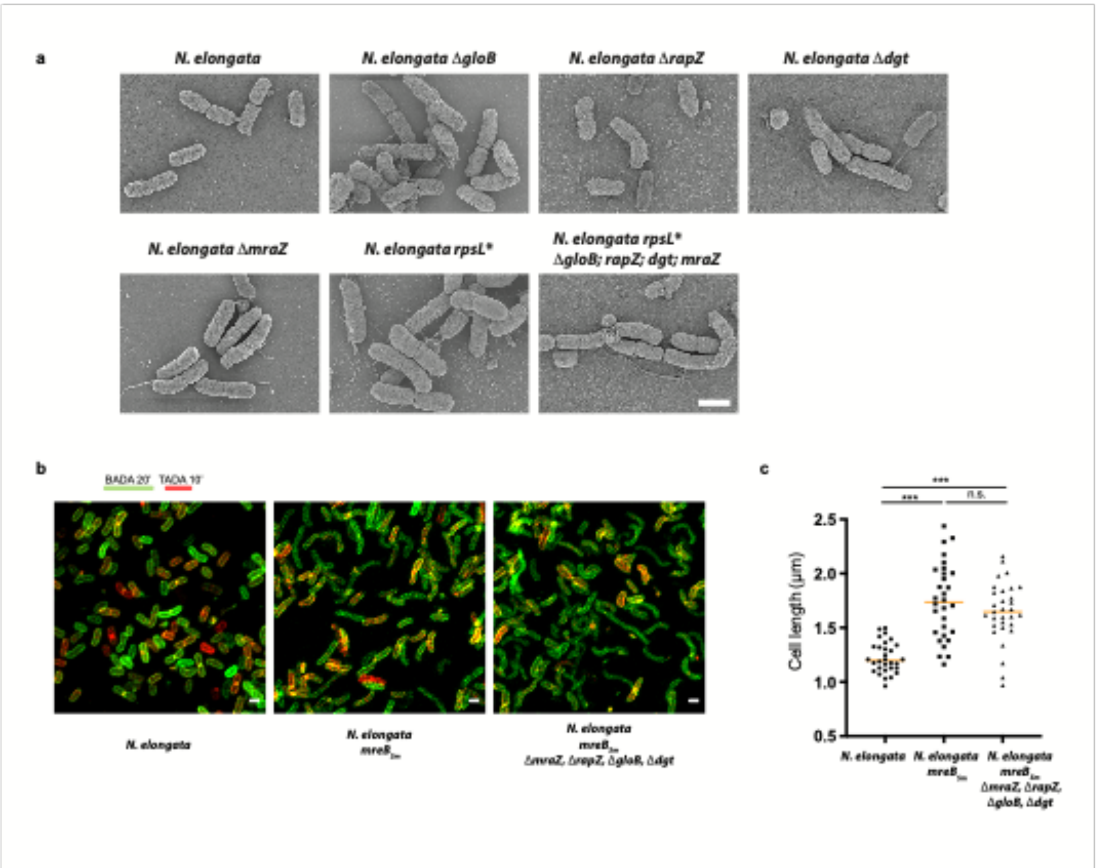

Supplementary Figure 11. Effect of single mutations and of *mreB*$_{Ne}$/*mreB*$_{Sm}$ allelic exchange in wild-type *N. elongata*. (a) Scanning Electron micrographs of *N. elongata* wild-type or harbouring a single deletion in addition to *N. elongata* (*rpsL**) or multiple deletions (Δ*mraZ*, Δ*rapZ*, Δ*gloB*, Δ*dgt*). (b) FDAA labelling of wild-type (*rpsL**) *N. elongata* or harboring the *mreB*$_{Ne}$/*mreB*$_{Sm}$ allelic exchange without (*N. elongata mreB*$_{Sm}$) or with Δ*mraZ*, Δ*rapZ*, Δ*gloB* or Δ*dgt* (*N. elongata* Δ*mraZ*, Δ*rapZ*, Δ*gloB* or Δ*dgt*; *mreB*$_{Sm}$) and (c) cell length measurements (n=30 biologically independent cells. Data are presented with the median). Statistical test used was One-way ANOVA, with Bonferroni's multiple comparisons test (*** $p<0.001$). The results are representative of at least three independent analyses. Source data and statistics are provided as a Source Data file.

Peptone-Yeast Medium	Peptone from meat	7.5 g
	Yeast extract	1.5 g
	NaCl	2.5 g
	K_2HPO_4	0.5 g
	for prerparing plates add Agar-Agar	6 g
	Distilled water	500 ml
BSTSY Medium (Kuhn et al., 1978)	Tryptone Soja Buillon w/o Dextrose	13.75g
	Yeast extract	2 g
	for prerparing plates add Agar-Agar	7.5 g
	Distilled water	450 ml
	Add 50 mL FBS (Bio-Sell FBS.GP.0100) after autoclaving	
Meat extract Medium	Meat extract (Roth X975.1)	8.5 g
	Yeast extract (Oxoid, Fish.Sc. 10108202)	3.5 g
	NaCl	2.5 g
	K_2HPO_4	1.25 g
	for prerparing plates add Agar-Agar	7.5 g
	Destilled water	500 ml

Supplementary Table 1. Composition of PY, meat extract and BSTSY media

	Label 1	Label 2	Label 3
N. elongata	BADA, 20 min, 1 mM	TADA, 10 min, 1 mM	-
A. filiformis	HADA, 30 min, 2 mM	BADA, 15 min, 1 mM	TADA, 15 min, 1 mM
S. muelleri	HADA, 60 min, 2 mM	BADA, 30 min, 1mM	TADA, 30 min, 1 mM
C. steedae	HADA, 60 min, 2 mM	BADA, 45 min, 1mM	TADA, 45 min, 1 mM
C. kuhniae	BADA, 60 min, 1 mM	TADA, 45 min, 1 mM	-
A. crassa	BADA, 30 min, 1 mM	TADA, 15 min 1 mM	-

Supplementary Table 2. FDAA incubation interval, color and order.

Purpose	Name	Sequence: 5’ – 3’
Generation of mutant strains	porBp F	TTCGCTAGCGTGCTGAAGCACCAAGTG
	proBp blunt R	CATGGCTGTATTCCTTTTTTGGTTAAG
	proBp lacZF	CTTAACCAAAAAAGGAATACAGCCATGACCATGATTACGGATTCACTG
	LacZRKm7up	ATTTAGATGTCTAAAAAGCATTCAGACGGCACGCGAAATACGGGCAGACAG
	Km7-Up	GCCGTCTGAATGCTTTTTAGACATCTAAAT
	Km6	CCCAGCGAACCATTTGAGG
	5 MraZF	CGCACCAAATTCGTAAACAATACC
	5 MraZR	GACCATAATAAATACGCCTAAACTCCG
	3 MraZF	AAGTTTCAGCTATGAGCAGTCAGGAATTC
	3 MraZR	CTTCAAGCTCACGGTTGATGAAAATC
	5 MraZKmF	CGGAGTTTAGGCGTATTTATTGCCGTCTGAATGCTTTTTAGACATCTAAATCTAGG
	KmpsimR	CTAATCTAAAATTATCTATATACTTCCCAGCGAACCATTTGAGG
	PdcwSm F	GGGAAGTATGTAGATAATTTTAGATTAG
	PdcwSm R	AGACCATAATATTCAATTGGTTTGGCTGAAAGG
	pdcwMcherryF	CCTTTCAGCCAAACCAATTGAATATTATGGTCTCGAAGGGCGAGGAGG
	Mcherry Pcil F	GATACATGTTCTCGAAGGGCGAGGAG
	Mcherry NsiI R	GATATGCATTCACTTGTACAGCTCGTC
	CdsAAmiC2F	CTAAGATCTTTATTTATTTTTTAATCTTCC
	AmiC2F	ATGAGATCTGGTAATAATATTAATGCTGTCAAAATC
	AmiC2R	TGGAGATCTTTTTTGAACGAGCTGATTG
	MreBSimonF	ATGATGGATCCTTAAAAATTTAGTTTAGTAAAATCTG
	MreBSimonR	CATGGTTTGCAATGGTGGTGGAAATTATGGATTATTGATAAAAATTGAGTTGA
N. elongata dcw qPCR	RT-*mraZ* F	ATGCCGAAGTTCTGGAAATG
	RT-*mraZ* R	CAATTCGGATGCCAATTCTT
	RT-*mraW* F	GGTGAAGAGCGGTTTAGTCG
	RT-*mraW* R	GAAAATCCGAATGGCTTGAA
	RT-*ftsL* F	CCGTGGTTACCCAGCAAA
	RT-*ftsL* R	GCTCGGCTGTACCAATTTTC
	RT-*ftsI* F	AAGCCGTCTGAACTGGAAAA
	RT-*ftsI* R	GGGTTTCATCTGCCGTTTTA
	RT-*ftsQ* F	AAATCCGATTGAGTGAGCGC
	RT-*ftsQ* R	TGTCCTTTGAATTGCGGCAA
	RT-*ftsA* F	GGCCGAATTGATGGCTGATT
	RT-*ftsA* R	CGATATCCGCCTGACTGACT
	RT-*ftsZ* F	CGCTGGTGTGATTACGTCTG
	RT-*ftsZ* R	AATGCTTCCTCTTTGACGGC
	RT-*gyrA* Nelong F	GCAACCATCTACGGCTTGAG
	RT-*gyrA* Nelong R	ATGATGATGGCTTCGCGTTC

Supplementary Table 3. Primer sequences used for generating the mutant strains and for *N. elongata dcw* quantitative real-time PCR

6 GENERAL DISCUSSION

It is remarkable how vast the bacterial shapes are, even more intriguing is how each species maintains this trait with great precision over generations. In order to gain survival advantages and adapt to different environments, bacteria may undergo multiple genetic changes that include gene deletions, insertions, and nucleotide polymorphisms. These changes have been shown to impact on different proteins and pathways involved in peptidoglycan synthesis as well as bacterial cell division and elongation, the key factors known to determine the bacterial shape. Genomic analyses involving the study of co-evolved and co-transcribed genes, gene synteny and the use of phylogenomics has emerged as a powerful approach in establishing evolutionary and genetic links to infer evolution of a given phenotype (cell shape in this case). Eearlier phylogenomic studies were limited by the lack of complete and closed genome sequences (most were based on contig assembled genomes and 16s rRNA sequencing) in addition to the preference for pathogenic species sequencing relative to commensals. Indeed the common consensus emerging from different phylogenomic studies depicts the bacilli as the ancestral morphology of other shapes (Stackebrandt and Woese 1979, Woese, Blanz et al. 1982, Siefert't and Fox 1998, Veyrier, Biais et al. 2015). An alternative argument suggests that irregular shaped-cell peptidoglycan free (L-forms) bacteria may have preceded the rod shape. This implies that the bacilli shape may have subsequently evolved upon the acquisition of peptidoglycan synthesis and elongation machinery (Errington 2013). Bacterial cell shape determinants have been reviewed in chapter 1, however many components and mechanisms responsible for the bacterial shape still remain to be understood. This is principally because some bacteria are difficult to culture in the laboratory, the lack of adequate genomes particularly from non-pathogenic strains, and the fact that isolation and identification most bacterial species and hence morphologies is incomplete. It is worth to mention that most of the known cell shape determinants are based on studies conducted on model organisms such as *E. coli*, *B. subtilis* and *S. aureus.* Other interesting proteins such as Crescentin were discovered from studying additional models like *Caulobacter crescentus*. It is therefore important to establish other models of varying morphologies, and also increase genome sequencing efforts to include commensal species in order to better delimitate and decipher the complexity of this important subject.

This thesis explored cell shape evolution in multicellular and longitudinally dividing (MuLDi) symbionts in *Neisseriaceae* family using *N. elongata* and *S. muelleri* as bacilli and multicellular shaped models respectively. Mutagenesis work was conducted in *N. elongata* model because it had been used previously in a similar study to establish cell shape evolution from bacilli to cocci (Veyrier, Biais et al. 2015), thus some tools were already available for preliminary mutagenesis and sequence analysis work. Additionally, despite several attempts (including electroporation), it was not possible to perform mutagenesis work in *S. muelleri* because it may not be naturally competent.

The use of complete and closed genome sequences obtained by PacBio and Nanopore technologies, was aimed to increase the precision of the analysis to ensure that all possible genomic factors including epigenetic events that would affect protein function were examined. Through the combined application of genomics, transcriptomics, ultrastructural analysis, PG labelling and mutagenesis studies, this work shades light on the evolution of MuLDi *Neisseriaceae*, with specific attention to fused cellular organization and longitudinal cell division.

6.1 Cell organization and the unconventional mode of cell division-in MuLDi *Neisseriaceae*

Initial works have described cellular organization of filamentous multicellular *Neisseriaceae* based only on electron microscopy imaging (Pankhurst, Auger et al. 1988, Whitehouse, Merrill et al. 1990, Xie and Yokota 2005). Prior to this work, it was not clear how cells in MuLDi *Neisseriaceae* remain fused upon cell division, and how longitudinal cell division occurred. Through electron microscopy imaging and consistent with previous studies, two general morphologies of multicellular *Neisseriaceae* are hereby described; first *Alysiella* genus is characterized by tightly fused pairs of cells that form upright-standing palisade filaments and secondly, *Simonsiella* and *Conchiformibius* genus form long crescent shaped palisade filaments. In MuLDi species, fimbriae are located on the proximal surface that comes in contact with the host epithelial cells of the buccal cavity therefore ensuring attachment and movement through gliding motion. Through immunostaining using anti-fimbriae antibodies the presence of fimbriae on the proximal-convex and proximal-concave poles in *A. filiformis* and *C. steedeae* respectively are described. This observation was consistent with ultrastructural analysis of MuLDi including *S. muelleri* that exhibited similar fimbriae localization as *C. steedae.* Further analysis through Nile red staining of *A. filiformis* and *C. steedae* cells revealed the presence of a membrane between adjoining cells. Also TEM analysis of thin section cuts revealed that (i) cells in the filament share the same outer membrane, (ii) each cell in filament has its own inner membrane (iii) adjoining cells in a filament share a common PG, therefore concluding that cells in MuLDi *Neisseriaceae* are fused through the septum peptidoglycan. Additionally, upon labelling of the PG using triple fluorescent D-amino acids dyes (HADA, TADA, BADA) and epifluorescence imaging, unipolar growth or insertion of nascent PG that begins from the distal pole and proceeds to the proximal end was identified in *A. filiformis*. On the other hand *S. muelleri* and *C. steedae* showed bipolar modes where growth of nascent PG begins simultaneously from both poles and proceeds inwards to the middle distal region. The distal-proximal directional growth of PG in *A. filiformis* is different from what was described in another longitudinally dividing symbiont *Ca. T. hypermnestrae* that have a proximal initiated mode of cell division (Pende, Wang et al. 2018). In MuLDi, septal PG synthesis is more active than at the polar caps as shown in (figure 4 and supplementary figure 7) which may imply that synthesis of new PG is mainly preserved for septal growth. Additionally, the widening of MuLDi *Neisseriaceae* cells seems to occur concomitantly with nascent PG growth as shown through time-lapse imaging (supplementary figure 2). This is consistent with Belma Bejtovic. (2021) who showed that the width of *A. filiformis* increased by 70% during cell division, while the length did not change much.

In regards to DNA localization as shown in (supplementary figure 4b) and also by (Belma Bejtovic. 2021) upon the analysis of DNA localization pattern of 112 *A. filiformis* cells, revealed asymmetrical localization of DNA which is positioned towards the fimbriae rich proximal pole. However, 62.5% of *S. muelleri* cells were shown to be DNA poor in the dorsal regions, while 37.5% had dispersed DNA except at the poles. Currently the chromosomal segregation pattern in MuLDi remains unknown, thus the asymmetrical localization patterns may be associated with the Ori-Ter orientation in MuLDi. It was shown that chromosome segregation occurs diagonally in longitudinally dividing *C. Thiosymbiont Onseti* (Weber, Moessel et al. 2019). It is possible that the Ori-Ter orientation and chromosome segregation in MuLDi may occur in a similar manner as that described in *C. Thiosymbiont Onseti.* If this hypothesis is confirmed, it will imply a critical adaptation towards longitudinal cell division in bacteria.

Is there a link between FtsZ ring assembly, septal PG synthesis and constriction during cell division? According to the Z-ring-centric model, Z-ring progression limits septum closure, in other words, the Z- ring actively pulls the cytoplasmic membrane inwards while septal PG synthesis occurs passively (Erickson 1997, Erickson, Anderson et al. 2010). A different model suggests that septal PG synthesis actively determines the rate of septum closure since the Z-ring acts passively following the developing septum (Nanninga 1998). Alternatively both septal cell wall synthesis and Z-ring constriction may work together (Meier and Goley 2014). However, Coltharp, Buss et al. (2016) show that the rate of septal PG synthesis and closure in *E. coli* is largely influenced by chromosome segregation. While rod shaped bacteria elongate as chromosome segregation and subsequently septation takes place only at the region devoid of chromosome material, MuLDi *Neisseriaceae* must have similarly evolved a mechanism to preserve the chromosome material during septation. It is therefore not a coincidence that chromosome material are located away from poles where septation begins, this may explain why *Alysiella* have unipolar while *Simonsiella* and *Conchiformibius* have bipolar modes of division.
While still in the early stages of understanding MuLDi *Neisseriaceae* morphological and cell division attributes, it is clear that longitudinal cell division, polar localization of fimbriae and fused cells enhances attachment and movement in the mammalian buccal cavity. Some of the interesting questions to be explored in future works should focus on understanding the different patterns of polar directed nascent PG synthesis (dorsal-proximal and proximal-dorsal), and if host attachment factors like fimbriae or even bacterial DNA localization plays a role in the determination of the septation site origin.

6.2 Multiple mutations were responsible for the evolution of MuLDi *Neisseriaceae*

The maximum-likelihood core genome *Neisseriaceae* phylogenetic tree was based on 401 genes from 75 *Neisseriaceae* species. The main inference from the tree reveals that both cocci and MuLDi *Neisseriaceae* evolved from a bacilli shaped ancestor. The evolution of the two cocci clusters were previously described (Veyrier, Biais et al. 2015), where the cocci morphology emerged through stepwise genetic evolution events. The study showed that the bacilli to cocci transition was initiated through the loss of *yacF*, a gene responsible for the coordination of FtsZ (Z-ring) assembly and also elongation. The subsequent evolution step involved the loss of elongation genes *mreB, mreC, mreD, pbpX, rodA* and *rodX*. Cocci cluster C2 (*N. canis, N.*

wadswordthi and *N. sp*-83E034) described in this study lost *yacF* gene but still retained the elongation genes, making them unable to elongate upon exposure to sublethal concentrations of penicillin-G.

Regarding MuLDi *Neisseriaceae* evolution, two separate lineages M1 (*A. filiformis, A. crassa, S. muelleri*) and M2 (*C. steedae, C. kuhniae*) were evident. However, monophyletic *Kingella* species clustered between the two MuLDi species and interestingly shares a common node with M1. This was intriguing as we would expect all MuLDi species to form their own separate cluster, or alternatively *Conchiformibius* and *Simonsiella* species to cluster together since they are morphologically more similar when compared to *Alysiella* species. However, the results support the independent evolution of the two MuLDi lineages. Even though MuLDi *Neisseriaceae* cluster with *Kingella* species, further analysis to determine the most recent common ancestor using PastML was inconclusive. It is therefore possible that the two MuLDi lineages and Kingella evolved independently from a bacilli shaped ancestor. Alternatively, *Kingella* underwent an additional evolutionary step reverting from MuLDi to bacilli shape with transverse cell division. Further work to help understand better the evolution of MuLDi and *Kingella* can be explored further upon the inclusion of more genomes in the analysis. Single gene phylogeny for AmiC1 protein also replicated the core genome phylogeny, however Kingella species seemed to have undergone additional mutations and recombinations. MreB and FtsA phylogenies show the clustering of all MuLDi species, depictive of convergent evolution of these proteins in MuLDi. *C. Kuhniae* MreB seems to have undergone additional mutations relative to the other MuLDi. Finally the independent loss of MraZ and RapZ in MuLDi is shown in the respective phylogenetic trees.

It is important to note that *Neisseriaceae* phylogenies are characterized with series of genetic recombination , thus inference for some clusters may be difficult to resolve. To better understand the impact of genetic recombinations on the clustering pattern of M1 and M2 lineages, recombination analysis of 8 *Neisseriaceae* linages was performed. As shown in figure 6.1 M2 underwent most recombination events, 124 and 130 for *C. steedae* and *C. kuhniae* respectively. *Alysiella* underwent least recombinations of approximately 24 events while *S. muelleri* had 56. In Lineage 1 accounted for most of the recombinations in MuLDi (between 31% and 40%) of total recombinations. Additionally for *Kingella* clustering with M1(figure 6.2) is characterized with between 4 and 15 recombinations in *K. kingae, K.oralis* and *K. bonacrosi, K. negevensis* and *K.*

denitrificans had between 42 and 53 recombinations, with majority of recombinations occurring between L8 *Neisseriaceae*. The frequency of these recombinations may explain the separate existence of M2 clade having undergone most recombinations.

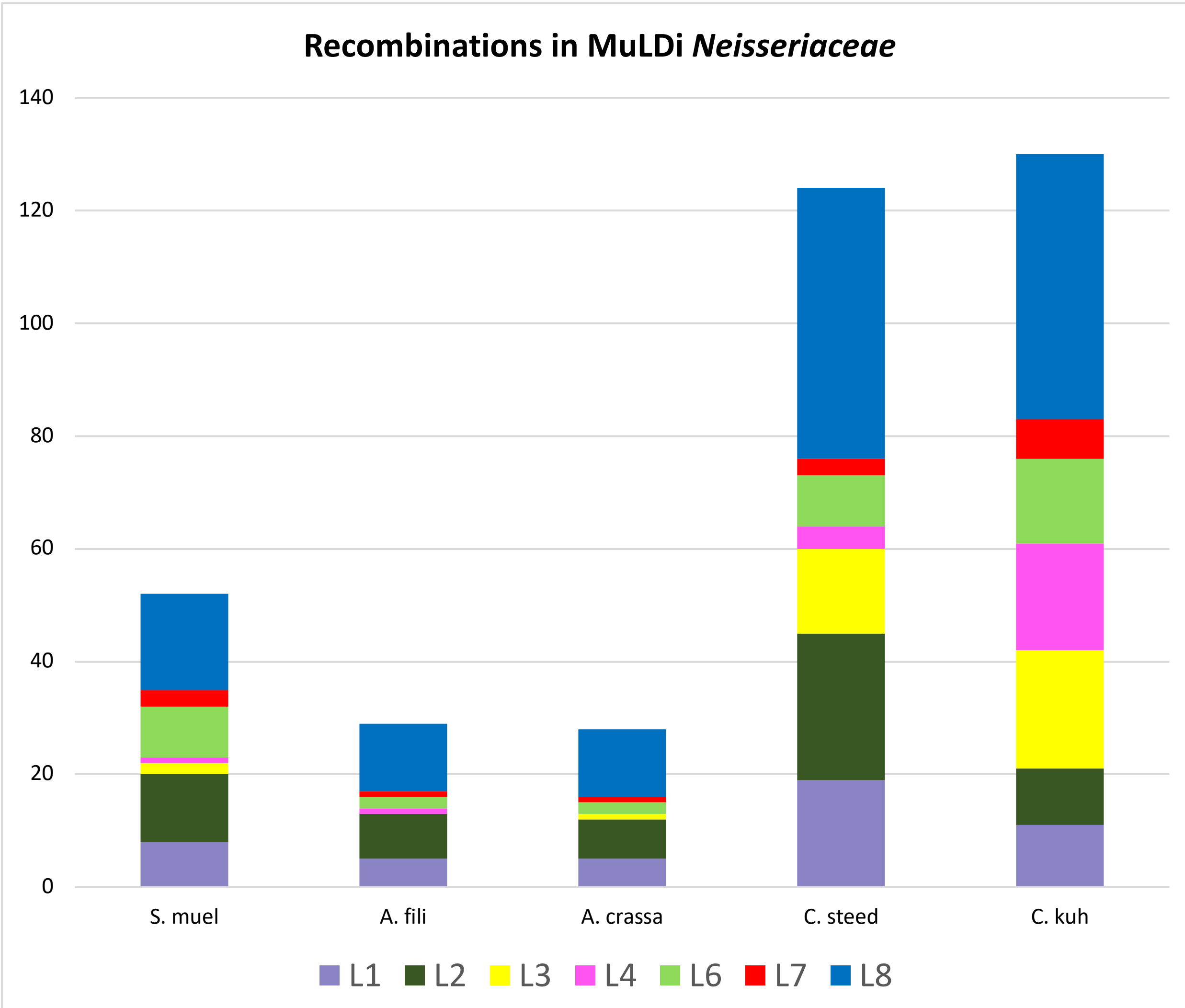

Figure 6.1: showing recombination events in MuLDi. Total recombination event of MuLDi species with different lineages of *Neisseriaceae* were determined. L1: *S. acetivorans, S. alvi* L2: *Vitreoscilla*; L3: *Eikenella*; L4: *Crenobacter*; L5: MuLDi and *Kingella*; L6: *N,sicca, flava, subflava*; L7: *N.gon, N. men, N. lact, N. ciner, N.blantyr*; L8: *U.suis, N. elongata, N. animalis, N. animalaris, N. canis, N. dentiae, N. bacilliformis*

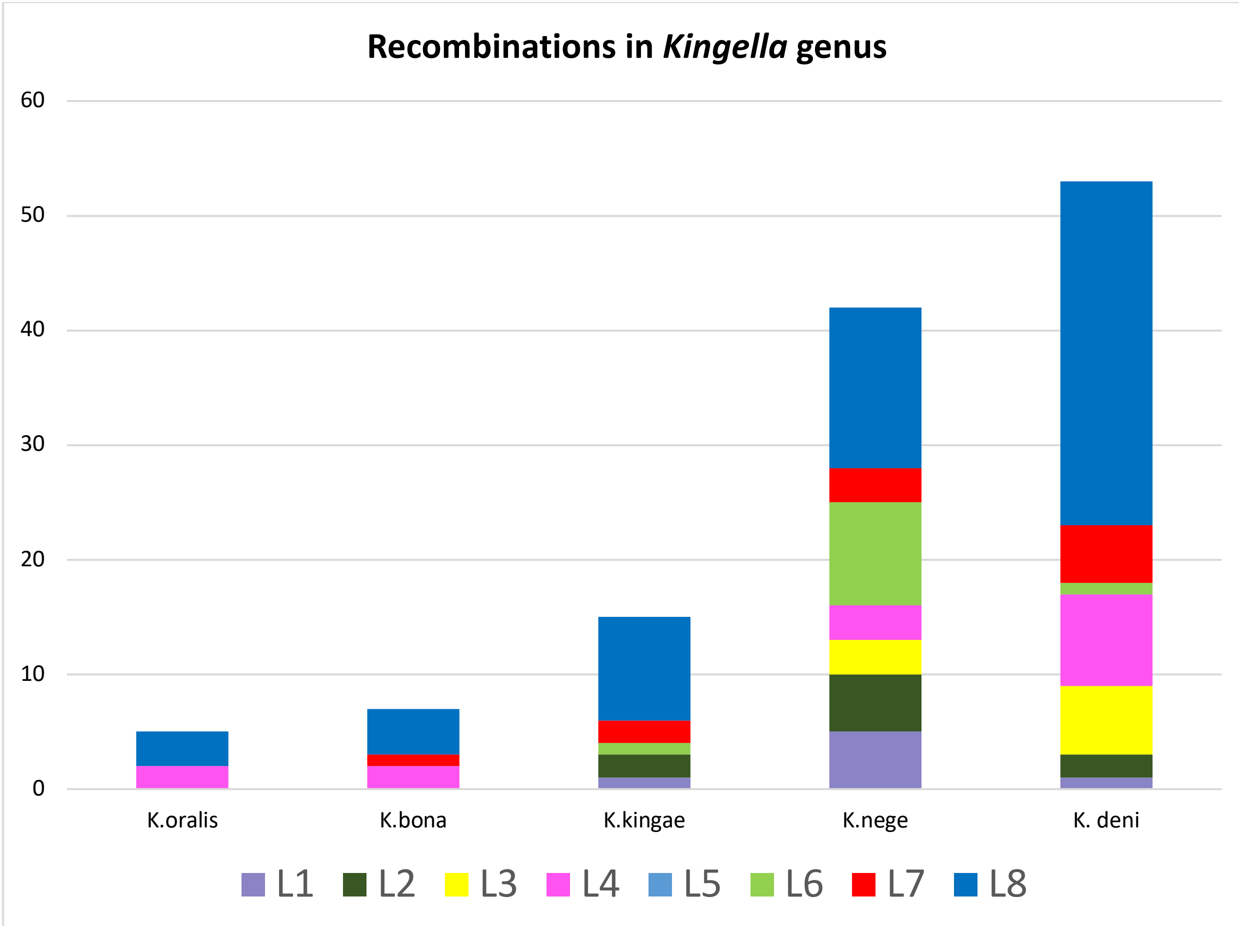

Figure 6.2: showing recombination events in *Kingella* genus. Total recombination event of MuLDi species with different lineages of *Neisseriaceae* were determined. L1: *S. acetivorans, S. alvi* L2: *Vitreoscilla*; L3: *Eikenella*; L4: *Crenobacter*; L5: MuLDi and *Kingella*; L6: *N,sicca, flava, subflava*; L7: *N.gon, N. men, N. lact, N. ciner, N.blantyr*; L8: *U.suis, N. elongata, N. animalis, N. animalaris, N. canis, N. dentiae, N. bacilliformis*

6.3 Regulatory role of MraZ in *Neisseriaceae* and implications of its loss in MuLDi

Comparative genomics analyses between bacilli and MuLDi genomes to determine gene deletions and insertions was performed using MycoHIT software (Veyrier, Pletzer et al. 2009) while amino acid polymorphisms associated with bacilli to MuLDi transition were determined using CapriB software (Guerra Maldonado, Vincent et al. 2020). *N. elongata* and *S. muelleri* were used as the reference genomes for bacilli and MuLDi respectively. Surprisingly a total of 18 proteins underwent various mutations (4 gene deletions, 7 gene insertions and amino acid substitutions in 7 proteins). Some of the genes that encode for proteins involved in PG synthesis, cell division and cell elongation were implicated during MuLDi evolution. By employing the RPLK based method described in article 1, *N. elongata* mutants comprising of 4 gene deletions (△*rapZ,*△ *dgt,* △*gloB,* △*mraZ*), 1 gene insertion of *CdsA-amiC2* from *S. muelleri,* and allelic switching to replace *Neisseria elongata mreB* with that from *Simonsiella muelleri* (containing H185Q and A274T substitutions).

To understand the function of this regulatory gene in *Neisseriaceae* and the implications its loss during the evolution of in MuLDi species, mapping of the *dcw* cluster from 68 *Neisseriaceae* species was done and analyzed in terms of gene content, gene orientation and neighbouring gene conservation patterns (Supplementary figure 9). Most genes are well conserved in majority of the species, displaying a compact *dcw* cluster of about 15 genes orientated in the same direction. Surprisingly, besides the loss of *mraZ* in the MuLDi species, fragmented/split *dcw* clusters with intergenic regions are present in MuLDi, *Kingella* species, *N. shayeganii* and *S. acetivorans.* Some of the intergenic regions are large (>900 Kb) in MuLDi species. Even with a split cluster, some specific sets of genes i.e, *murC -ddI- ftsQ- ftsA- ftsZ, murD-ftsW-murG ftsW-murG* and *mraW- ftsL- ftsI- murE-murF-mraY* remained closely linked suggestive of the need for co-transcription. Prescence of a fragmented or split *dcw* is not associated with morphology due to the commonality of this feature in both MuLDi and some bacilli species. However, it is interesting that in *Kingella* species which also cluster with MuLDi in the phylogenetic analysis (refer to figure 2.8) have a predominantly split *dcw* cluster.

Comparison of bacilli versus MuLDi transcripts obtained from two different sequencing technologies and at different times (initially RNAsequencing of 3 bacilli vs 3 MuLDi was done by Illumina and two years later RNAsequencing of 5 bacilli vs 5 MuLDi was done using Nanopore technology) . Results in both instances showed the differential expression of key cell wall synthesis and cell division genes. In particular, MuLDi species were characterized with the upregulation of cell division genes *minE*, *ftsX* and *ftsY* and downregulation of *murE* and *ftsI* genes required for transpeptidation during septum PG synthesis. The down regulation of the *dcw* cluster gene *ftsI* and MurE in MuLDi was interesting as it was attributed to the loss of *dcw* regulatory gene *mraZ*. Other multicellular species like *Cyanobacteria Dolichospermum flosaquae* NCBI accession number NZ_CP051206.1 also lack *mraZ* which may be responsible for inefficient division in these species.

Finally, to evaluate if the loss of *mraZ* was a sufficient and necessary cause for the transition from bacilli to multicellular phenotype, *mraZ* was deleted and also overexpressed in trans in *N. elongata.* There was however no differences between *N. elongata* WT and *mraZ* null strains (average length measurements of 1.17 µm and 1.23 µm respectively), but shorter cells (average length of 0.74 µm) were obtained in MraZ overexpressing strains. There was no significant difference in the width between wildtype and *mraZ* mutant strains. In order to rule out the hypothesis that the short phenotype resulted in differential growth rates between the mutants and wildtype strains, growth curve analysis was done. As shown in figure 6.3, the wild type, *mraZ* null and overexpressing strains had similar growth rates.

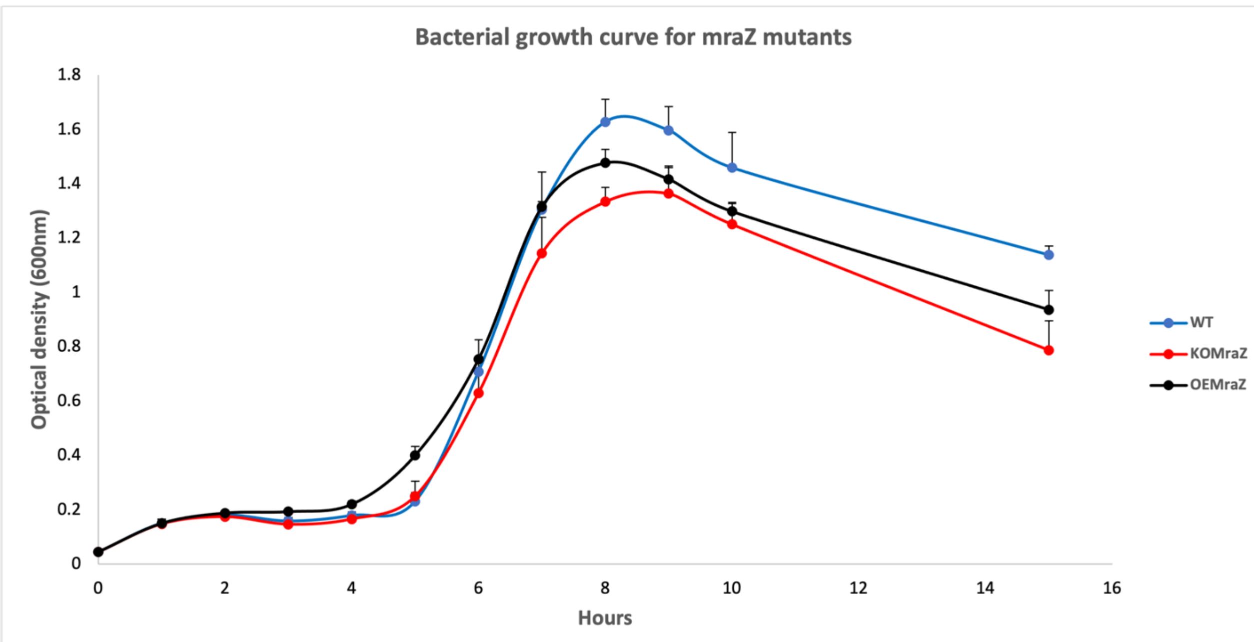

Figure 6.3: growth curve of *N. elongata* wild type and *mraZ* mutant strains

Similar studies to determine the role of MraZ in *E. coli* and *M. gallisepticum* realized the opposite effect with longer cells upon overexpressing *mraZ* (Eraso, Markillie et al. 2014, Fisunov, Evsyutina et al. 2016). Transcriptomic analysis showed that *mraZ* regulated at least 5 genes in the 5' end of the *dcw* cluster where it acts as a repressor of transcription (Eraso, Markillie et al. 2014, Fisunov, Evsyutina et al. 2016, White, Hough-Neidig et al. 2022). Considering the phenotypic effects observed (overexpression of *mraZ* yields shorter cells in *N. elongata* but results in filamentation of *E. coli* and *B. subtilis*). Transcriptomic analysis results show that *mraW, ftsL, ftsI,* *murE* and *murF* genes were down regulated when we compared the wildtype and *mraZ* knockout strains, while the comparison of wildtype with overexpressing strains resulted in the upregulation of *mraW, ftsL, ftsI, murE murF* and *NELON_RS02715*. It is worth to note that the *N. elongata mraZ* knockout strains also contains *S. muelleri* promoter *pdcwSm* located upstream *mraW* may have an effect on the *dcw* cluster transcription of *N. elongata* mutants. However, considering that *fstI* is also downregulated in the MuLDi , the upregulation of the first 7 *dcw* cluster genes upon overexpression of *mraZ* in *N. elongata*, and also the shortening of cells upon overexpression of *mraZ*, implies that *mraZ* is an activator of transcription in *Neisseriaceae*.

The function of MraZ as transcriptional repressor in models like *E. coli* and *B. subtilis* (Eraso, Markillie et al. 2014, White, Hough-Neidig et al. 2022) remains to be established in *Neisseriaceae.* Results obtained in this work suggests that it activates the transcription of some *dcw* cluster genes in *Neisseria elongata*, a similar effect realized in Mollicutes (Fisunov, Evsyutina et al. 2016). It is therefore possible that in some species MraZ acts as an activator of transcription while in others it is an inhibitor, it is also possible that MraZ performs both functions in *N. elongata*. The *mraZ* null mutant was constructed in a manner to replicate the promoter region upstream of *mraW* in *S. muelleri* which contains *pdcwsm* promoter. Therefore *N. elongata mraZ* mutant and the resulting overexpressing strains had *pdcwsm* promoter, while also retaining the native *N. elongata* promoter upstream of *mraZ* as illustrated in figure 6.4.

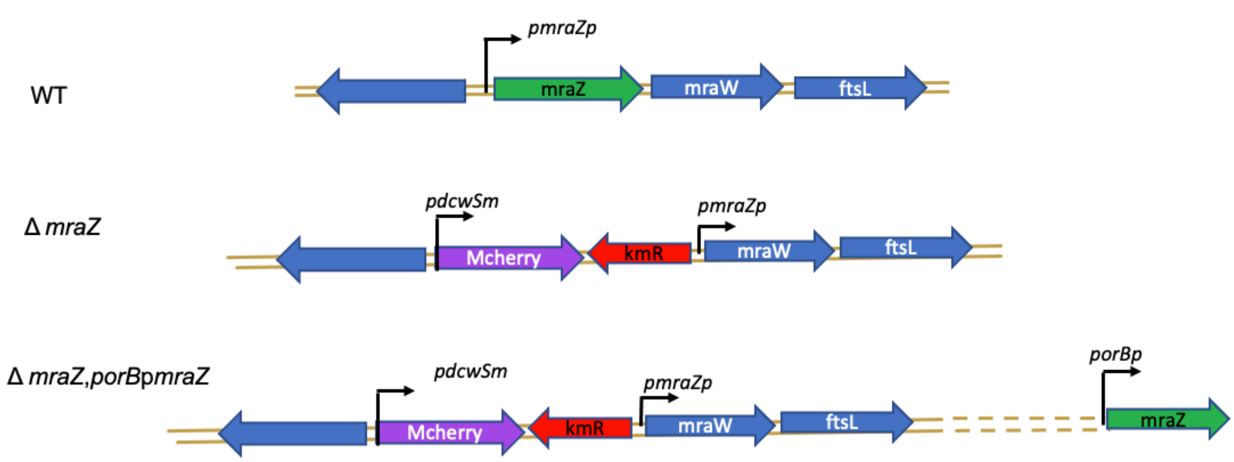

Figure 6.4: **Design of *mraZ* deletion and overexpressing constructs**

The *pdcwsm* promoter used might have had an effect on gene regulation realized. To investigate further the function of MraZ, mutagenesis and transcriptomic analyses were performed *N. meningitidis* in an attempt to better understand the broader function of this protein in *Neisseriaceae* family. In *N. meningitidis* construct *pdcwsm* promoter from *S. muelleri* was not included. Reverse transcription-quantitative real-time PCR (RT-qPCR) determine *mraZ, mraW FtsI* and *FtsL* gene expression relative to DNA gyrase *gyrA* gene as shown in figure 6.5. Even though *mraZ* was deleted it was difficult to overexpress the gene despite using the strong and constitutive *Neisseriaceae* promoter *porBp* in the construct. It is possible that post transcriptional and post translational modifications may have affected the quantity of MraZ binding to the promoter.

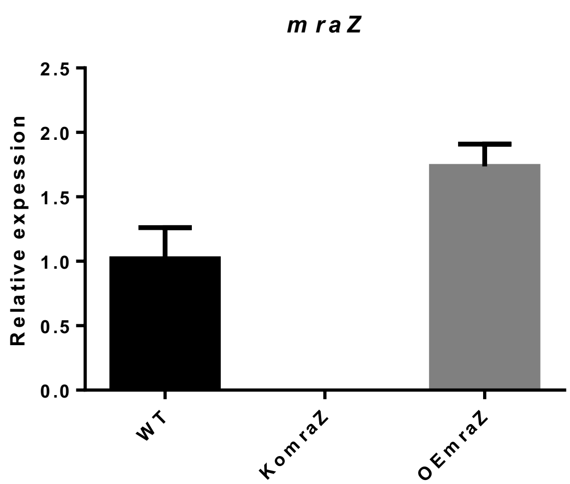

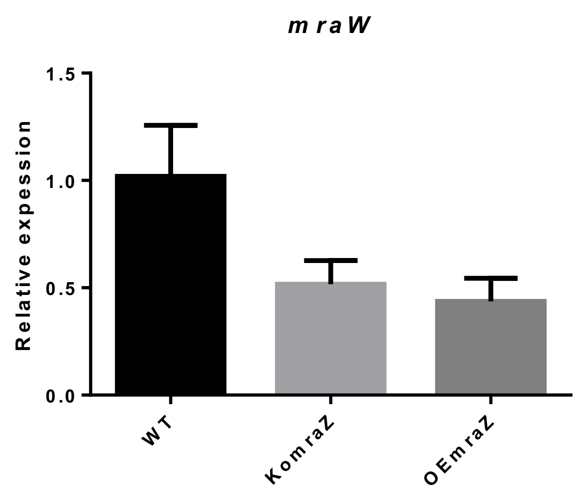

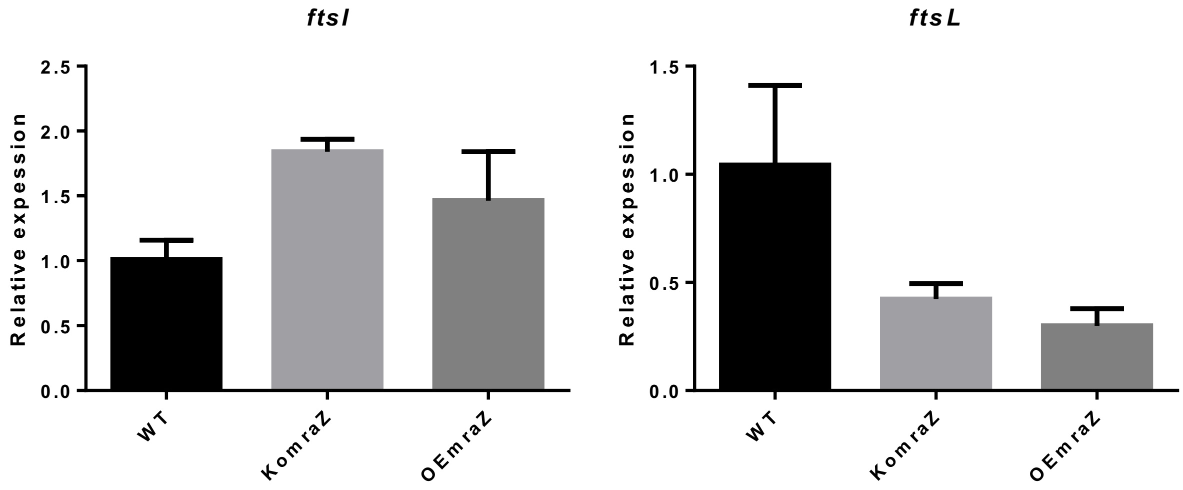

Figure 6.5: Quantitative real-time PCR of *Neisseria meningitidis dcw*: The gene expression pattern was determined relative to *gyrA* gene.

Despite MraZ being able to bind to its own promoter and therefore regulate its own expression, the molecular mechanisms for its regulation are not clear. In particular, the mystery behind different regulatory roles established in this study and others may be explained through the binding activity of MraZ. It was previously shown that in *E. coli* MraZ forms dodecameric structures thus dodecameric binding of MraZ to the promoter (Adams, Udell et al. 2005). Dodecameric transcriptional regulation has been described in bacteria (Snyder, Lary et al. 2004, Gebendorfer, Drazic et al. 2012). Binding of MraZ as a dodecamer would require 6 times more protein than a dimer (Eraso, Markillie et al. 2014). On the other hand, octameric binding of MraZ was shown in *Mycoplasma* species (Fisunov, Evsyutina et al. 2016). It is not clear how MraZ binds to the *pmraZp* promoter in *Neisseriaceae* species, further studies to understand some of these mechanisms will improve our understanding of the regulatory role of this protein.

Similarly the presence of DNA sequences specific for binding a regulatory protein in the vicinity of a promoter is important for the regulatory function. At least three MraZ binding repeat (MBR) sequences located between the promoter *pmraZp* and *mraZ* gene have been characterized in *Mycoplasma* and *E. coli*. They comprise of five nucleotides repeats **GTGGN** (N=T/G) or **GTGTN** (N=G/C) with the former predominantly found in *E. coli* while in *Mycoplasma* has both (Eraso, Markillie et al. 2014, Fisunov, Evsyutina et al. 2016). A reduction of between 80-90 % of

MraZ binding activity was obtained upon introduction of single point mutations in the GTG subsequence of MBR while the removal of AAA subsequence between MBR repeats resulted in 70% reduction of MraZ binding activity in *M. gallisepticum* (Fisunov, Evsyutina et al. 2016). A possible explanation for the regulatory role established in *N. elongata* would be dependent on number and type of MBR. An alignment of the region around *mraZ* promoter and the CDS from 73 *Neisseriaceae* sequences was done in order to characterize the MBR in *Neisseriaceae* as shown in figure 6.3. The alignment revealed four conserved MBR in all but the MuLDi species. MBR I and IV have GTGT subsequence while MBR - II and III have TGGG subsequence. Besides, the MBR are separated by 4-5 spacer nucleotides consistent to what has been described in *E. coli* and *Mycoplasma.* MBR were not identified in the 5' *dcw* region of MuLDi species despite increasing the alignment to 500bp region upstream of *mraW*.

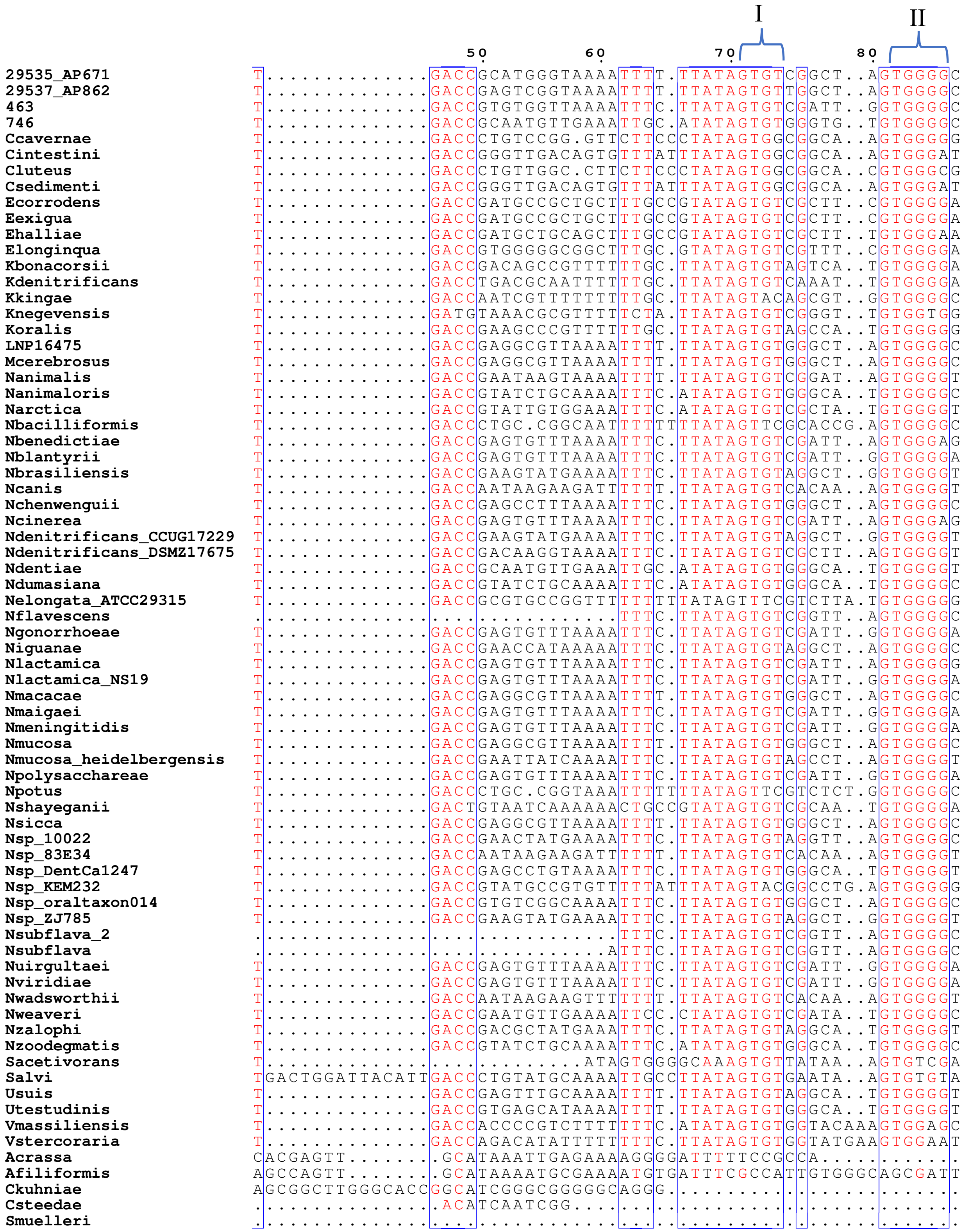

I
II
50
60
70
80
29535_AP671
29537_AP862
463
746
Ccavernae
Cintestini
Cluteus
Csedimenti
Ecorrodens
Eexigua
Ehalliae
Elonginqua
Kbonacorsii
Kdenitrificans
Kkingae
Knegevensis
Koralis
LNP16475
Mcerebrosus
Nanimalis
Nanimaloris
Narctica
Nbacilliformis
Nbenedictiae
Nblantyrii
Nbrasiliensis
Ncanis
Nchenwenguii
Ncinerea
Ndenitrificans_CCUG17229
Ndenitrificans_DSMZ17675
Ndentiae
Ndumasiana
Nelongata_ATCC29315
Nflavescens
Ngonorrhoeae
Niguanae
Nlactamica
Nlactamica_NS19
Nmacacae
Nmaigaei
Nmeningitidis
Nmucosa
Nmucosa_heidelbergensis
Npolysacchareae
Npotus
Nshayeganii
Nsicca
Nsp_10022
Nsp_83E34
Nsp_DentCa1247
Nsp_KEM232
Nsp_oraltaxon014
Nsp_ZJ785
Nsubflava_2
Nsubflava
Nuirgultaei
Nviridiae
Nwadsworthii
Nweaveri
Nzalophi
Nzoodegmatis
Sacetivorans
Salvi
Usuis
Utestudinis
Vmassiliensis
Vstercoraria
Acrassa
Afiliformis
Ckuhniae
Csteedae
Smuelleri

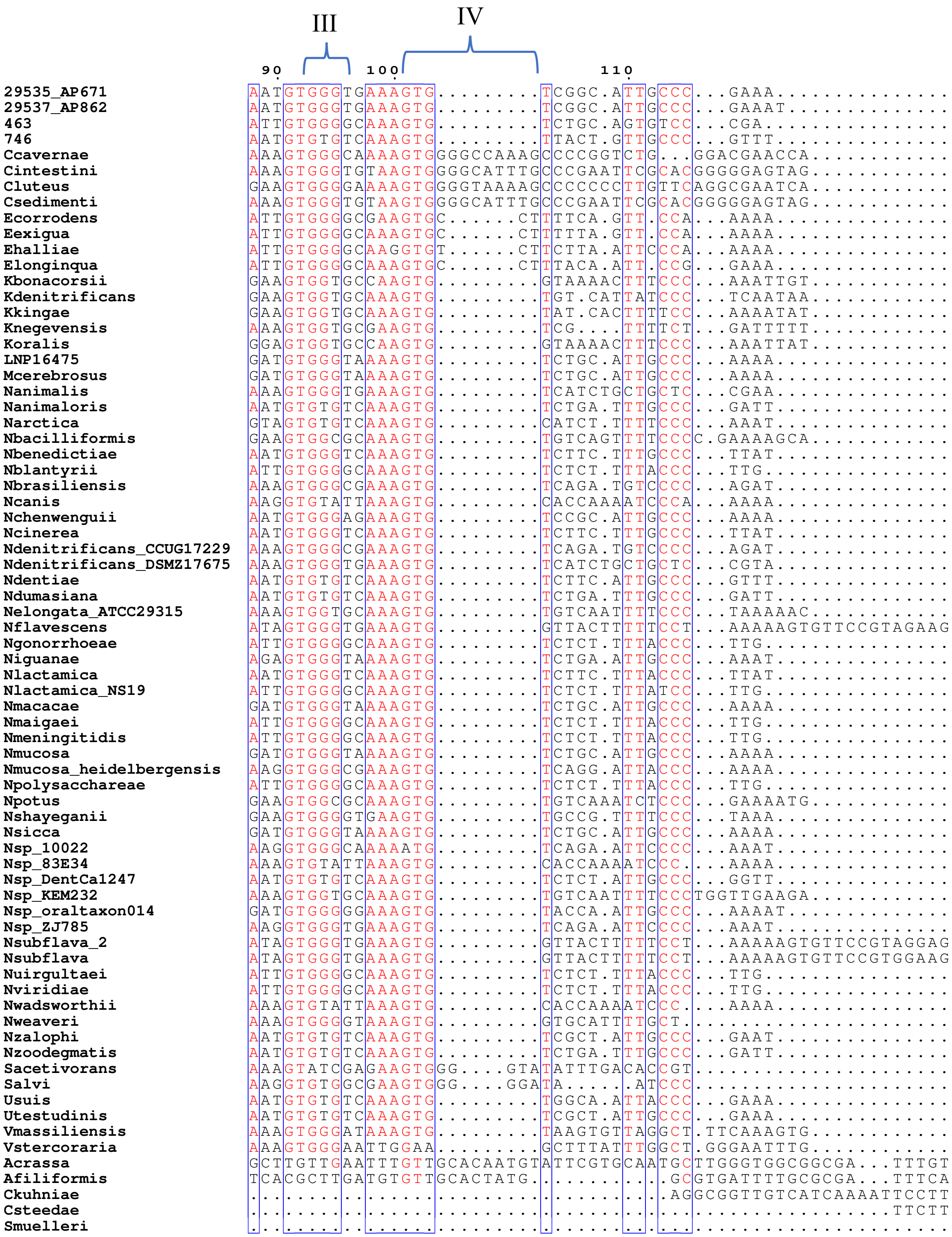

Figure 6.6 Conserved MraZ binding repeats (I,II,III,IV) in *Neisseriaceae*.

6.8 Effect of H185Q and A274T substitutions in MreB of MuLDi *Neisseriaceae*

The protein structure and function is determined by the amino acid sequence, thus non conserved substitutions may affect different properties of a protein, such as folding, DNA binding or even solubility and hence the overall function. Several documented amino acid substitutions in the cell elongation protein MreB affect the structural conformation resulting in size and cell shape changes of the bacterial cell as illustrated in figure 6.8 B. These substitutions include; K27E, A53T, A53K, A53L, A53G, D78V, D83Y, E143A, M272L in *E. coli* and E119G, T167A , D189G, A325P, A325T in *Caulobacter crescentus* (Gitai, Dye et al. 2005, Dye, Pincus et al. 2011, Shi, Bratton et al. 2018). CapriB analysis done in this study identified only two amino acid substitutions in MreB; H185Q and A274T to be associated with transition from bacilli to MuLDi. None of these substitutions has been described earlier as depicted in the alignment of *E. coli*, *N. elongata* and 5 MuLDi *Neisseriaceae.* Interestingly, when compared to *E. coli* MreB protein in longitudinally dividing *Ca. Thiosymbion oneisti* had undergone S185N amino acid substitution (den Blaauwen 2018) since MreB is required for FtsZ localization in *Candidatus Thiosymbion oneisti* and *T. hypermnestrae*. Substitutions from Histidine to Glutamine (H185Q) in MulDi and Serine to Asparagine (S185N) in *Candidatus* might affect the protein function.

The overall effect of these mutations was predicted through structural prediction analysis of *S. muelleri* MreB using RePROF in ProteinPredict (https://predictprotein.org/) that revealed protein conformational changes as shown in figure 6.8 A. Histidine to Glutamine switch may have resulted in the exposure of the solvent accessibility portion while Threonine to Alanine switch may cause the burying of the solvent accessibility portion. The substitution from positively charged polar, Zn^{2+} and Mg^{2+} binding Histidine to polar Glutamine that possesses a neutral charge and the substitution from nonpolar Alanine to polar Threonine (A274T) may potentially impact the protein structure and protein to protein interactions. Direct effect on the protein may occur through MreB filament formation, length and overall MreB dynamics or indirectly by affecting attachment of MreB regulator RodZ (attachment to MreB occurs through the alpha domain with H185Q and A274T) (Colavin, Shi et al. 2018).

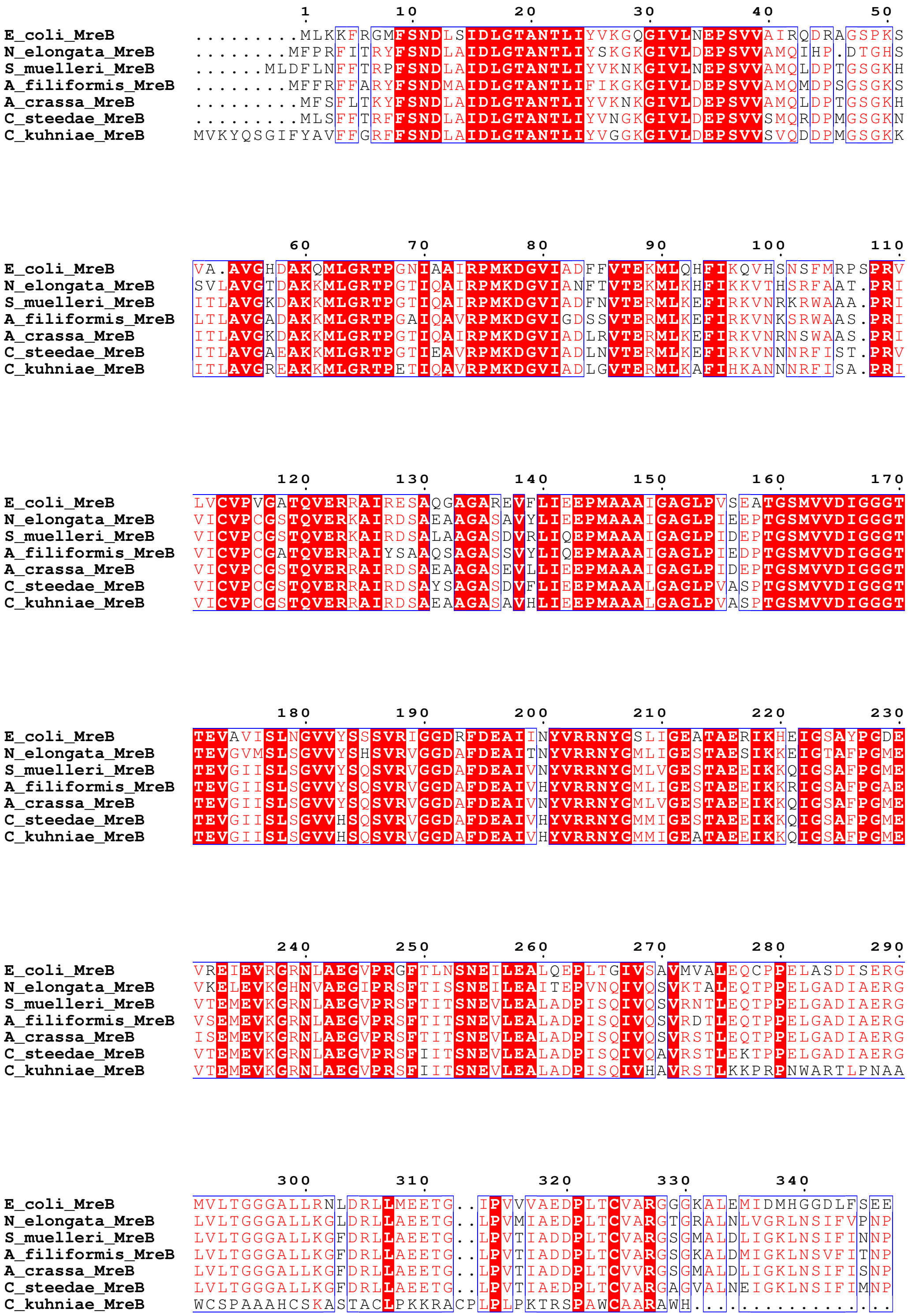

Figure 6.7 Alignment of MreB protein. ESPript (https://espript.ibcp.fr/ESPript/cgi-bin/ESPript.cgi) alignment *of E. coli, N. elongata* and MuLDi *Neisseriaceae* MreB. None of previously described AA substitutions are present.

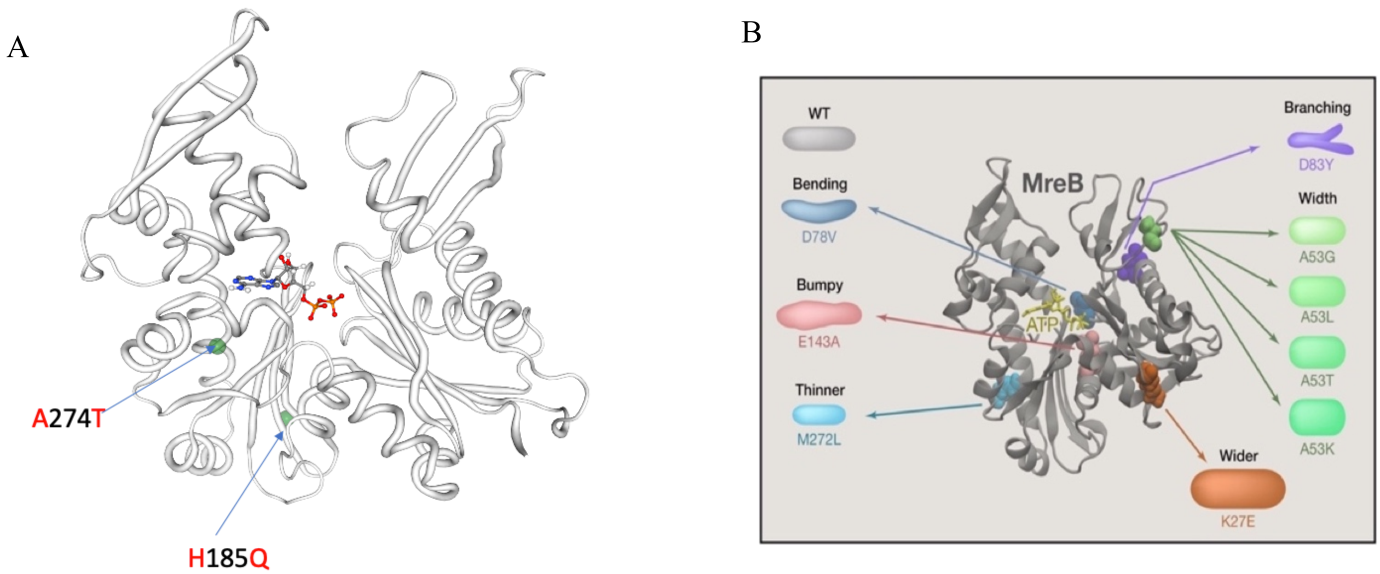

Figure 6.8: MreB mutations associated with morphological changes A) *S. muelleri* MreB predicted using SWISSMODELhttps://swissmodel.expasy.org/interactive/984CQg/models/. B) Morphological changes associated with amino acid substitutions in *E. coli* MreB protein (Shi, Bratton et al. 2018)

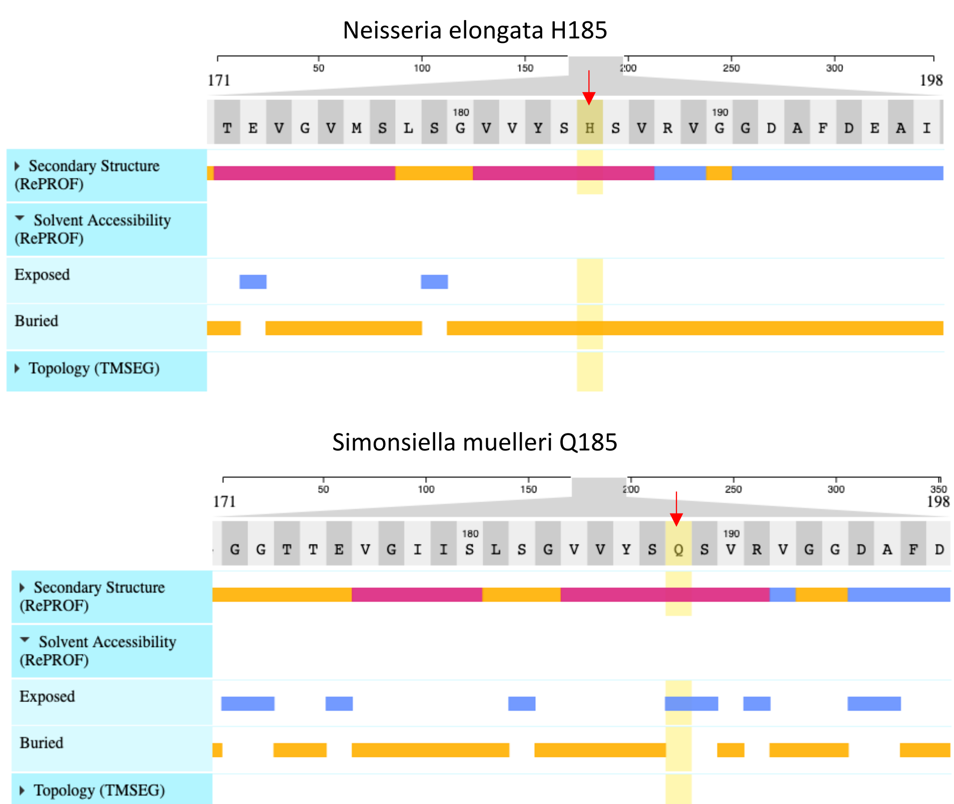

Figure 6.9 ProteinPredict analysis for MreB substitutions in *S. muelleri*. Exposed and buried solvent accessibility motifs are indicated in blue and yellow respectively**.**

7.8 Acquisition of *amiC2* affects septum growth

The implication for acquisition of N-acetylmuramyl-L-alanine amidase encoded by *amiC2* from *Fusobacterum* by MuLDi species through HGT is not clear. It is interesting that *amiC2* gene in MuLDi always exists with phosphatidate cytidyltransferase *cdsA* gene, however the functional implication of the colocalization of these two genes in MuLDi remains to be determined. The role of phospholipids in localization of proteins discussed in chapter one of this thesis may be important in the association of the lipid with AmiC2 and hence septal localization of its amidase function during septation (Renner and Weibel 2012, Kawazura, Matsumoto et al. 2017). Amidases like AmiA and AmiC cleaves the amide bond between the murein backbone and L-ala residue of the peptide chain during daughter cell septation. Amidases have also been shown to enhance multicellular cells cooperation since N-acetylmuramyl-L-alanine amidase promotes cell to cell communication in *Cyanobacteria* (which have 6 or more copies) (Lehner, Zhang et al. 2011, Bornikoel, Carrion et al. 2017). At this point it is not clear if intracellular communication MuLDi cells exists. Therefore the most probable role of AmiC2 in MuLDi is linked to septal fission during division. All *Neisseriaceae* possess AmiC1, but the presence of an additional amidase AmiC2 in MuLDi that have difficulties in complete cell fission after septation may be important in enhancing the process. The size of AmiC1 in *S. muelleri* is 411 amino acids while AmiC2 is 208 amino acids long, whereas AmiC1contains both the PG binding AMIN domain that binds to the peptidoglycan and the catalytic C-terminus domains, AmiC2 has only the catalytic domain as illustrated in the proteins prediction figure 6.10. The lack of AMIN domain in AmiC2 might imply that the septal localization of this amidase is purely dependent on amidase regulatory proteins NlpD and EnvC, These activators have a 44 amino acid LysM domain which binds to the peptidoglycan that is linked to the LytM domain which activates AmiC2 through a long linker. The length of the linkers has been suggested to be key in the spatial regulation of the interaction between the NlpD activator domain and catalytic domain to ensure proper septation occurs (Rocaboy, Herman et al. 2013). The amidase activity of AmiC2 has been determined in N. musculi (Eve Bennet *et al*, unpublished) where deletion of AmiC1 in *N. musculi* resulted in chained cells, while insertion of AmiC2 in this mutant restored normal cell division. These results confirm the importance of acquisition of AmiC2 in the septation of MuLDi cells. It still remains to determine the reason for incomplete cell fission in MuLDi species despite having two amidases and their activators.

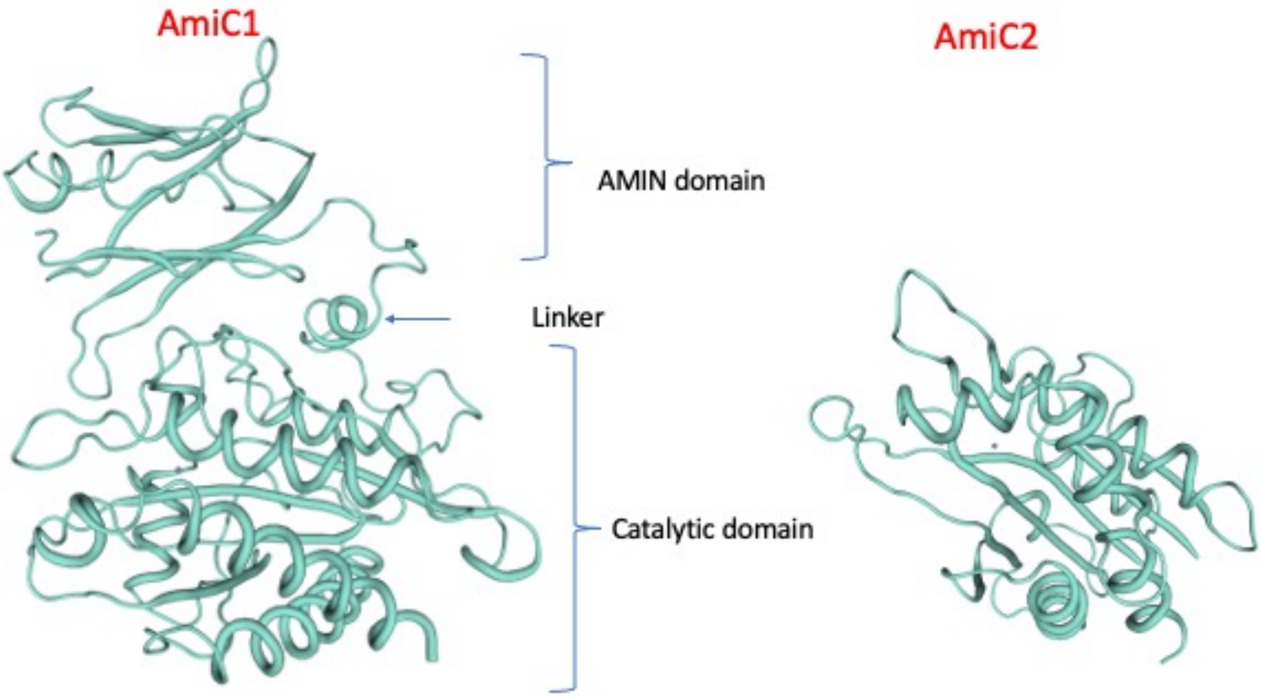

Figure 6.10, Structure of *S. muelleri* AmiC1 and AmiC2 proteins. AmiC1 has both AMIN and catalytic domains while AmiC2 lacks the AMIN domain.

CdsA on the other hand regulates cellular phospholipid composition by catalyzing the synthesis of cytidine diphosphate-diacylglcerol an intermediate for membrane phosphatidylglcerol and cardiolipin synthesis. These anionic phospholipids (aPLs) are involved in the localization of MreB, high concentrations of aPLs repel MreB from polar regions in bacilli species *E.coli* (Billings, Ouzounov et al. 2014, Kawazura, Matsumoto et al. 2017). These studies showed that aPLs have preference to bind disassembled MreB. Cardiolipin also interacts directly with the division site selection amphitropic peripheral protein MinD (Mileykovskaya, Fishov et al. 2003). Even though we did not observe a strong phenotype change by inserting *cdsA-amiC2* alone in *N. elongata*, large cells with enlarged septum were realized in *N. elongata* with *cdsA-amiC2* and *mreB$_{sm}$* while *N. elongata* with *mreB$_{sm}$* resulted in relatively long cells with normal septum. Thus *cdsA -amiC2* genes with MuLDi associated MreB were instrumental in bacilli to MuLDi transition.

8.8 The loss of *rapZ*, *dgt* and *gloB* may have impacted MuLDi evolution

The deletion of *rapZ (yhbJ)* in *E. coli* results in over production of GlmS, an enzyme that is crucial for the synthesis of glucosamine-6-phosphate (GlcN-6-P), an important component for PG biosynthesis. Post transcriptional regulation of GlcN-6-P concentration in *E. coli* is regulated by RapZ through the action of small RNAse *glmY* and *glmZ* (Gonzalez, Durica-Mitic et al. 2017, Khan, Durica-Mitic et al. 2020). The loss of *rapZ* during MuLDi cell shape evolution might have impacted the synthesis of GlmS and therefore GlcN-6-P. However, transcription analysis between wild type *N. elongata*, *rapZ* null and overexpressing strains showed no significant difference in GlmS, GlmU or any other protein implicated in peptidoglycan synthesis pathway. While it is not clear why these proteins were not differentially regulated as was the case in *E. coli*, a different GlcN-6-P regulatory pathway may exist in *N. elongata.* The first step to study this will involve establishing if small RNA's GlmY/GlmZ are present in *Neisseriaceae*.

The *dgt* gene encodes for dGTP triphosphohydrolase that hydrolyzes dGTP to deoxyguanosine and tripolyphosphate (PPP_i) (Wurgler and Richardson 1990, Itsko and Schaaper 2011). In *E. coli dgt* is implicated in the formation of cellular dNTP pool, the binding of single stranded DNA and also in DNA replication. Deletion of *dgt* in *E. coli* resulted in increased cellular dGTP , while its overexpression led significant increase in dGTPase and therefore the decrease in dGTP (Myers, Beauchamp et al. 1987, Quirk, Bhatnagar et al. 1990). DNA binding was also diminished in addition to subtle A.T→G·C base-pair substitutions (Itsko and Schaaper 2011, Singh, Gawel et al. 2015). *gloB* gene on the other hand is part of bacterial glutathione (GSH)-dependent glyoxalase system that enables survival in high methylglyoxal (MG) concentrations that would potentially damage DNA and proteins. A reaction between MG and GSH results in hemithioacetal, that is isomerized to S-lactoylglutathione (SLG) by glyoxalase I (*gloA*). SLG is subsequently hydrolyzed by glyoxalase II (*gloB*) to D-lactate and GSH (O'Young, Sukdeo et al. 2007, Sukdeo and Honek 2008). In *E. coli*, *gloB* mutants had no morphological changes, aside from having reduced tolerance to MG (Ozyamak, Black et al. 2010, Reiger, Lassak et al. 2015).

The loss of *dgt* and *gloB* genes might have contributed to MuLDi morphology in a different manner that we are not able to determine at this point. It is possible that these deletions might have been compensatory resulting in improved fitness of MuLDi species.

6.7 Other genes deletions that could have been implicated in MuLDI evolution.

Due to the lack of sufficient genome sequences from commensal bacteria, the initial comparative genomics analysis for this work was done using fewer bacilli and only 2 MuLDi (*S. muelleri* and *A. filiformis*) species genomes. 11 gene deletions were identified as possible candidates for the morphological transition from bacilli to MuLDi. Approximately 50% of the genes were involved in peptidoglycan synthesis or cell division whereas the rest encoded for hypothetical proteins. The notable genes included *mraZ, rapZ, dacB, mtgA*, *gloB*, and NELON_RS02275. For example, *mtgA* is a monofunctional PG glycosyltransferase that polymerises lipid II molecules to form glycan strands. MtgA also interacts with other proteins involved in PG synthesis and cell division such as FtsW and FtsN (Di Berardino, Dijkstra et al. 1996). Deletion of *mtgA* in *E. coli* was shown to trigger increased cell width (Kadoya, Matsumoto et al. 2015). In the current study, there were no morphological changes associated with *mtgA* deletion in *N. elongata*. The D-alanyl-D-alanine carboxypeptidase/endopeptidase gene *dacB* on the other hand is directly involved in cell wall biosynthesis and modulation in *N. gonorrhoeae* (Stefanova, Tomberg et al. 2003). The deletion of *dacB* had no major phenotypic change in *N. gonorrhoeae* (Peddi, Nicholas et al. 2009). In a different study *dacB* mutant showed altered PG structure associated with increased PG cross-linking (Obergfell, Schaub et al. 2018). In our case the deletion of *dacB* in *N. elongata* had no morphological changes, we did not proceed with PG structure analysis for the mutant. The function of the hypothetical protein NELON_RS02275 in *Neisseria* species has not been described. However, its presence between the bifunctional acetyltransferase/uridyltransferase protein GlmU and the peptidoglycan binding LysM protein motif made us to question its role in peptidoglycan synthesis and the overall bacterial morphology. Again, there was no morphological changes upon the deletion of the gene coding for NELON_RS02275 in *N. elongata.* Surprisingly, even upon accumulating 6 gene deletions (*ΔmraZ, Δ rapZ, Δ dacB*, Δ *mtgA, ΔgloB* , Δ NELON_RS02275) there was no cell shape change as shown in supplementary figure 1. Since 2 of the genes (*mtgA* and NELON_RS02275) identified earlier are not common in all the 5 MuLDi *Neisseriaceae,* and *dacB* gene was also lost in a dozen other bacilli their roles were not investigated further. However, considering that *mtgA* was lost only in multicellular (*S. muelleri, A. filiformis,* A. crassa) M1 clade and in all *Kingella* species but is present in multicellular (*C. steedae* and *C. kuhniae*) M2 clade and other bacilli *Neisseriaceae* may be suggestive of the involvement of *mtgA* in the stepwise evolution of MuLDi species.

6.8 RPLK approach for unmarked and multiple loci modifications in *Neisseriaceae*

The versatility of this 3 gene cassette RPLK has been showcased in this work, where 6 gene deletions in a single *N. elongata* strain were obtained. This to our knowledge is the first study to describe sequential 6 gene deletions plus 2 gene insertions particularly in commensal *Neisseriaceae*. Hence this approach is applicable for generating strains with multiple complex modifications (deletions, insertions and point mutations) to determine protein interactions and gene functions. Additionally, the ability to obtain unmarked mutants in the second recombination step that excises the RPLK cassette is remarkable since the expression of downstream genes is not compromised. We have also showcased the applicability of this method in mutagenesis work across 3 *Neisseriaceae* (*N. elongata, N. meningitidis, N. musculi*), hence this method will facilitate mutagenesis work in multiple *Neisseria* genus. Despite the mutagenesis success obtained using RPLK method, the method cannot be used to modify (delete) essential genes.

7 CONCLUSION AND FUTURE PERSPECTIVES

Neisseriaceae family has been used as a new model to study cell shape evolution from bacilli to multicellular and also cell division from transverse to longitudinal. By employing different imaging techniques together with peptidoglycan labeling using fluorescent D-amino acid dyes peptidoglycan synthesis at the septum and fusion of cells in filaments of MuLDi *Neisseriaceae* were described. More specifically, septum growth is unidirectional (moving from distal to proximal pole) in *Alysiella* and bidirectional (moving from proximal to mid distal region) in *Conchiformibius* and *Simonsiella*.

Through an evolutionary approach and comparative genomics, 18 genes were identified to have undergone either gene deletions, insertions and amino acid permutations that may have resulted in the current multicellular and longitudinal division in *Neisseriaceae.* In particular, the loss of *mraZ* , acquisition of *amiC2* genes in addition to amino acid substitutions H185Q and A274T in MreB protein were implicated in MuLDi phenotype evolution. Mutagenesis work done in bacilli shaped *N. elongata* model resulted morphological modifications upon overexpression of mraZ or insertion of *cdsA-amiC2* and allelic switching of *N. elongata* MreB with that from *S. muelleri*. MraZ was also shown to activate the transcription of *dcw* cluster genes *mraZ, mraW, ftsL, ftsI, murE* and *murF* in *N. elongata.* This regulatory role may partly explain the inefficient mode of cell division in MuLDi as the loss of the gene resulted in the downregulation of *dcw* cluster genes responsible for septation and cell division. With these findings, this work paves way for future studies to better understand the evolution of cell shape and longitudinal division in MuLDi *Neisseriaceae* in addition to the characterization of protein functions. Hence the following recommendations will facilitate the advancement of this work in addition to additional mutagenesis work for identified loci like FtsA and the 4 hypothetical proteins.

We have shown the activatory role of MraZ in *N. elongata*, which is also corroborated by the downregulation of FtsI and MurE in MuLDi *Neisseriaceae*. First, to rule out the effect of *S. muelleri* division and cell wall cluster *pdcwsm* promoter in the expression of dcw genes in *mraZ* overexpressing strain, a control should be included where *mraZ* is overexpressed in wild type *Neisseriaceae*. Secondly, even though we were unsuccessful in overexpressing *mraZ* in *N. meningitidis*, work in other species should be conducted in order to generalize the regulatory role of MraZ in *Neisseriaceae.* Finally, other studies have shown that the protein inhibits the transcription of *dcw* cluster genes while in this work and mycoplasma model we show that it is an activator, this might imply that the protein has dual roles. The crystal structure for *N. elongata* MraZ should be studied and compared to those of *B. subtilis* and *E. coli* that have an inhibitory role.

In regards to MreB (H185Q, A274T) associated with bacilli to cocci transition, it would be informative to perform further experiments to determine the implication of the substitutions singly and in combination through site directed mutagenesis work in *N. elongata* MreB. Additionally the localization pattern and other dynamics of MreB can be studied by tagging it with fluorescent proteins such as GFP and YFP. Moving forward the crystal structure of MuLDi MreB and *N elongata* with (H185Q, A274T) mutations should be studies to better understand the implication of the mutations on MreB filament length and activity. It would also be interesting to study the interaction of MreB with the divisome protein FtsZ. Finally, since these mutations occur close to MreB regulator RodZ binding domain, the impact of these mutations in binding RodZ should be studied.

The role of the amidase AmiC2 and its activators can be determined further in addition to its ability to induce complete cell fission in AmiC1 mutant containing AmiC2 *N. musculi* (Δ AmiC1::AmiC2) as demonstrated in supplementary figure 2 by (Eve Bennet et al. un published). By obtaining purified AmiC2 protein and the activators EnvC and NlpD, peptidoglycan binding experiments can be conducted by incubating the protein with PG extract with and without its activators at room temperature for 3 hours and the binding activity confirmed by running SDS page gel. The PG cleaving activity can be determined by repeating the same experiment at 37 degrees for 16 h and spectrophotometry used to determine cleaving action. Alternatively these results can also be obtained by inactivation the activators in *N. musculi* (Δ AmiC1::AmiC2).

Last but not least it is important to study chromosome segregation pattern in MuLDi and also bacilli *Neisseriaceae* in order to determine the Ori-Ter orientation. It might be a significant factor that may have hindered our ability to obtain a longitudinally dividing mutant in *N. elongata.* In line with this the cellular phospholipid concentrations between MuLDi and bacilli *Neisseriaceae* should also be studied further since they have been shown to interact with important divisome and elongasome proteins therefore impacting the proteins localization patterns that may have an effect on the morphology.

8 BIBLIOGRAPHY

Abboudi, M., S. Matallana Surget, J. F. Rontani, R. Sempere and F. Joux (2008). "Physiological alteration of the marine bacterium Vibrio angustum S14 exposed to simulated sunlight during growth." Curr Microbiol 57(5): 412-417.

Adams, M. A., C. M. Udell, G. P. Pal and Z. Jia (2005). "MraZ from Escherichia coli: cloning, purification, crystallization and preliminary X-ray analysis." Acta Crystallogr Sect F Struct Biol Cryst Commun 61(Pt 4): 378-380.

Ago, R. and D. Shiomi (2019). "RodZ: a key-player in cell elongation and cell division in Escherichia coli." AIMS Microbiol 5(4): 358-367.

Arias, C. A., D. Panesso, D. M. McGrath, X. Qin, M. F. Mojica, C. Miller, L. Diaz, T. T. Tran, S. Rincon, E. M. Barbu, J. Reyes, J. H. Roh, E. Lobos, E. Sodergren, R. Pasqualini, W. Arap, J. P. Quinn, Y. Shamoo, B. E. Murray and G. M. Weinstock (2011). "Genetic basis for in vivo daptomycin resistance in enterococci." N Engl J Med 365(10): 892-900.

Bartlett, T. M., B. P. Bratton, A. Duvshani, A. Miguel, Y. Sheng, N. R. Martin, J. P. Nguyen, A. Persat, S. M. Desmarais, M. S. VanNieuwenhze, K. C. Huang, J. Zhu, J. W. Shaevitz and Z. Gitai (2017). "A Periplasmic Polymer Curves Vibrio cholerae and Promotes Pathogenesis." Cell 168(1-2): 172-185 e115.

Belma Bejtovic. (2021). "Molecular basis of cell growth and division of the oral cavity symbionts Alysiella filiformis and Simonsiella muelleri."

Bendezú, F. O., C. A. Hale, T. G. Bernhardt and P. A. de Boer (2009). "RodZ (YfgA) is required for proper assembly of the MreB actin cytoskeleton and cell shape in E. coli." Embo j 28(3): 193-204.

Bernard, E., T. Rolain, B. David, G. Andre, V. Dupres, Y. F. Dufrene, B. Hallet, M. P. Chapot-Chartier and P. Hols (2012). "Dual role for the O-acetyltransferase OatA in peptidoglycan modification and control of cell septation in Lactobacillus plantarum." PLoS One 7(10): e47893.

Bernhardt, T. G. and P. A. de Boer (2003). "The Escherichia coli amidase AmiC is a periplasmic septal ring component exported via the twin-arginine transport pathway." Mol Microbiol 48(5): 1171-1182.

Bernhardt, T. G. and P. A. de Boer (2005). "SlmA, a nucleoid-associated, FtsZ binding protein required for blocking septal ring assembly over Chromosomes in E. coli." Mol Cell 18(5): 555-564.

Billings, G., N. Ouzounov, T. Ursell, S. M. Desmarais, J. Shaevitz, Z. Gitai and K. C. Huang (2014). "De novo morphogenesis in L-forms via geometric control of cell growth." Mol Microbiol 93(5): 883-896.

Boes, A., S. Olatunji, E. Breukink and M. Terrak (2019). "Regulation of the Peptidoglycan Polymerase Activity of PBP1b by Antagonist Actions of the Core Divisome Proteins FtsBLQ and FtsN." mBio 10(1).

Bonis, M., C. Ecobichon, S. Guadagnini, M. C. Prevost and I. G. Boneca (2010). "A M23B family metallopeptidase of Helicobacter pylori required for cell shape, pole formation and virulence." Mol Microbiol 78(4): 809-819.

Bornikoel, J., A. Carrion, Q. Fan, E. Flores, K. Forchhammer, V. Mariscal, C. W. Mullineaux, R. Perez, N. Silber, C. P. Wolk and I. Maldener (2017). "Role of Two Cell Wall Amidases in Septal Junction and Nanopore Formation in the Multicellular Cyanobacterium Anabaena sp. PCC 7120." Front Cell Infect Microbiol 7: 386.

Boto, L. (2010). "Horizontal gene transfer in evolution: facts and challenges." Proc Biol Sci 277(1683): 819-827.

Brown, J. R. (2003). "Ancient horizontal gene transfer." Nat Rev Genet 4(2): 121-132.

Burmeister, A. R. (2015). "Horizontal Gene Transfer." Evol Med Public Health 2015(1): 193-194.

Cabré, E. J., A. Sánchez-Gorostiaga, P. Carrara, N. Ropero, M. Casanova, P. Palacios, P. Stano, M. Jiménez, G. Rivas and M. Vicente (2013). "Bacterial division proteins FtsZ and ZipA induce vesicle shrinkage and cell membrane invagination." J Biol Chem 288(37): 26625-26634.

Carballido-Lopez, R. (2006). "Orchestrating bacterial cell morphogenesis." Mol Microbiol 60(4): 815-819.

Chaput, C., A. Labigne and I. G. Boneca (2007). "Characterization of Helicobacter pylori lytic transglycosylases Slt and MltD." J Bacteriol 189(2): 422-429.

Chen, S., B. Rudra and R. S. Gupta (2021). "Phylogenomics and molecular signatures support division of the order Neisseriales into emended families Neisseriaceae and Chromobacteriaceae and three new families Aquaspirillaceae fam. nov., Chitinibacteraceae fam. nov., and Leeiaceae fam. nov." Systematic and Applied Microbiology 44(6).

Choi, Y., J. Kim, H. J. Yoon, K. S. Jin, S. Ryu and H. H. Lee (2018). "Structural Insights into the FtsQ/FtsB/FtsL Complex, a Key Component of the Divisome." Sci Rep 8(1): 18061.

Colavin, A., J. Hsin and K. C. Huang (2014). "Effects of polymerization and nucleotide identity on the conformational dynamics of the bacterial actin homolog MreB." Proc Natl Acad Sci U S A 111(9): 3585-3590.

Coltharp, C., J. Buss, T. M. Plumer and J. Xiao (2016). "Defining the rate-limiting processes of bacterial cytokinesis." Proc Natl Acad Sci U S A 113(8): E1044-1053.

Connell, I., W. Agace, P. Klemm, M. Schembri, S. Marild and C. Svanborg (1996). "Type 1 fimbrial expression enhances Escherichia coli virulence for the urinary tract." Proc Natl Acad Sci U S A 93(18): 9827-9832.

Contreras-Martel, C., A. Martins, C. Ecobichon, D. M. Trindade, P. J. Matteï, S. Hicham, P. Hardouin, M. E. Ghachi, I. G. Boneca and A. Dessen (2017). "Molecular architecture of the PBP2-MreC core bacterial cell wall synthesis complex." Nat Commun 8(1): 776.

Costello, E. K., C. L. Lauber, M. Hamady, N. Fierer, J. I. Gordon and R. Knight (2009)."Bacterial community variation in human body habitats across space and time." Science 326(5960): 1694-1697.

Dafar, A., M. Bankvall, H. Çevik-Aras, M. Jontell and F. Sjöberg (2017). "Lingual microbiota profiles of patients with geographic tongue." J Oral Microbiol 9(1): 1355206.

Dajkovic, A. and J. Lutkenhaus (2006). "Z ring as executor of bacterial cell division." J Mol Microbiol Biotechnol 11(3-5): 140-151.

Dandekar, T., B. Snel, M. Huynen and P. Bork (1998). "Conservation of gene order: a fingerprint of proteins that physically interact." Trends in Biochemical Sciences 23(9): 324-328.

Den Blaauwen, T. (2018). "Is Longitudinal Division in Rod-Shaped Bacteria a Matter of Swapping Axis?" Frontiers in Microbiology 9.

Den Blaauwen, T., M. A. de Pedro, M. Nguyen-Distèche and J. A. Ayala (2008)."Morphogenesis of rod-shaped sacculi." FEMS Microbiology Reviews 32(2): 321-344.

Deo, P. N. and R. Deshmukh (2019). "Oral microbiome: Unveiling the fundamentals." J Oral Maxillofac Pathol 23(1): 122-128.

Di Berardino, M., A. Dijkstra, D. Stüber, W. Keck and M. Gubler (1996). "The monofunctional glycosyltransferase of Escherichia coli is a member of a new class of peptidoglycan-synthesising enzymes." FEBS Lett 392(2): 184-188.

Dik, D. A., D. R. Marous, J. F. Fisher and S. Mobashery (2017). "Lytic transglycosylases: concinnity in concision of the bacterial cell wall." Crit Rev Biochem Mol Biol 52(5): 503-542.

Dik, D. A., J. F. Fisher and S. Mobashery (2018). "Cell-Wall Recycling of the Gram-Negative Bacteria and the Nexus to Antibiotic Resistance." Chem Rev 118(12): 5952-5984.

Dillard, J. P. (2011). "Genetic Manipulation of Neisseria gonorrhoeae." Curr Protoc Microbiol Chapter 4: Unit4A 2.

Doolittle, W. F. and E. Bapteste (2007). "Pattern pluralism and the Tree of Life hypothesis." Proc Natl Acad Sci U S A 104(7): 2043-2049.

Du, S. and J. Lutkenhaus (2017). "Assembly and activation of the Escherichia coli divisome." Mol Microbiol 105(2): 177-187.

Dye, N. A., Z. Pincus, I. C. Fisher, L. Shapiro and J. A. Theriot (2011). "Mutations in the nucleotide binding pocket of MreB can alter cell curvature and polar morphology in Caulobacter." Mol Microbiol 81(2): 368-394.

Egan, A. J. F., J. Errington and W. Vollmer (2020). "Regulation of peptidoglycan synthesis and remodelling." Nat Rev Microbiol 18(8): 446-460.

Egan, A. J., R. M. Cleverley, K. Peters, R. J. Lewis and W. Vollmer (2017). "Regulation of bacterial cell wall growth." Febs j 284(6): 851-867.

Eisen, J. A. and C. M. Fraser (2003). "Phylogenomics: intersection of evolution and genomics." Science 300(5626): 1706-1707.

Eraso, J. M., L. M. Markillie, H. D. Mitchell, R. C. Taylor, G. Orr and W. Margolin (2014). "The highly conserved MraZ protein is a transcriptional regulator in Escherichia coli." J Bacteriol 196(11): 2053-2066.

Erickson, H. P. (1997). "FtsZ, a tubulin homologue in prokaryote cell division." Trends Cell Biol 7(9): 362-367.

Erickson, H. P., D. E. Anderson and M. Osawa (2010). "FtsZ in bacterial cytokinesis: cytoskeleton and force generator all in one." Microbiol Mol Biol Rev 74(4): 504-528.

Errington, J. (2013). "L-form bacteria, cell walls and the origins of life." Open Biol 3(1): 120143.

Everts, R. J., D. Speers, S. T. George, B. J. Ansell, H. Karunajeewa and R. D. Ramos (2010). "Neisseria lactamica arthritis and septicemia complicating myeloma." J Clin Microbiol 48(6): 2318.

Fisunov, G. Y., D. V. Evsyutina, T. A. Semashko, A. A. Arzamasov, V. A. Manuvera, A. V. Letarov and V. M. Govorun (2016). "Binding site of MraZ transcription factor in Mollicutes." Biochimie 125: 59-65.

Flores, E. and A. Herrero (2010). "Compartmentalized function through cell differentiation in filamentous cyanobacteria." Nat Rev Microbiol 8(1): 39-50.

Frirdich, E. and E. C. Gaynor (2013). "Peptidoglycan hydrolases, bacterial shape, and pathogenesis." Curr Opin Microbiol 16(6): 767-778.

Frirdich, E., J. Biboy, C. Adams, J. Lee, J. Ellermeier, L. D. Gielda, V. J. Dirita, S. E. Girardin, W. Vollmer and E. C. Gaynor (2012). "Peptidoglycan-modifying enzyme Pgp1 is required for helical cell shape and pathogenicity traits in Campylobacter jejuni." PLoS Pathog 8(3): e1002602.

Frirdich, E., J. Vermeulen, J. Biboy, F. Soares, M. E. Taveirne, J. G. Johnson, V. J. DiRita, S. E. Girardin, W. Vollmer and E. C. Gaynor (2014). "Peptidoglycan LD-carboxypeptidase Pgp2 influences Campylobacter jejuni helical cell shape and pathogenic properties and provides the substrate for the DL-carboxypeptidase Pgp1." J Biol Chem 289(12): 8007-8018.

Frye, S. A., M. Nilsen, T. Tonjum and O. H. Ambur (2013). "Dialects of the DNA uptake sequence in Neisseriaceae." PLoS Genet 9(4): e1003458.

Garcia, S. D., E. M. Descole, A. M. Famiglietti, E. G. Lopez and C. A. Vay (1996). "[Infection of the urinary tract caused by Neisseria cinerea]." Enferm Infecc Microbiol Clin 14(9): 576.

Garner, E. C., R. Bernard, W. Wang, X. Zhuang, D. Z. Rudner and T. Mitchison (2011). "Coupled, circumferential motions of the cell wall synthesis machinery and MreB filaments in B. subtilis." Science 333(6039): 222-225.

Garofalo, C. K., T. M. Hooton, S. M. Martin, W. E. Stamm, J. J. Palermo, J. I. Gordon and S. J. Hultgren (2007). "Escherichia coli from urine of female patients with urinary tract infections is competent for intracellular bacterial community formation." Infect Immun 75(1): 52-60.

Gebendorfer, K. M., A. Drazic, Y. Le, J. Gundlach, A. Bepperling, A. Kastenmuller, K. A. Ganzinger, N. Braun, T. M. Franzmann and J. Winter (2012). "Identification of a hypochlorite-specific transcription factor from Escherichia coli." J Biol Chem 287(9): 6892-6903.

Gitai, Z., N. A. Dye, A. Reisenauer, M. Wachi and L. Shapiro (2005). "MreB actin-mediated segregation of a specific region of a bacterial chromosome." Cell 120(3): 329-341.

Gomase, V. S. and S. Tagore (2009). "Phylogenomics: evolution and genomics intersection." Int J Bioinform Res Appl 5(5): 548-563.

Gonzalez, G. M., S. Durica-Mitic, S. W. Hardwick, M. C. Moncrieffe, M. Resch, P. Neumann, R. Ficner, B. Görke and B. F. Luisi (2017). "Structural insights into RapZ-mediated regulation of bacterial amino-sugar metabolism." Nucleic Acids Res 45(18): 10845-10860.

Goodell, E. W. and U. Schwarz (1985). "Release of cell wall peptides into culture medium by exponentially growing Escherichia coli." J Bacteriol 162(1): 391-397.

Göpel, Y., M. A. Khan and B. Görke (2016). "Domain swapping between homologous bacterial small RNAs dissects processing and Hfq binding determinants and uncovers an aptamer for conditional RNase E cleavage." Nucleic Acids Res 44(2): 824-837.

Gregory, D. A., D. A. Kuhn, K. R. Daly and K. Flygenring (1985). "Statistical association of dietary components with Simonsiella species residing in normal human mouths." Appl Environ Microbiol 50(3): 704-705.

Gueiros-Filho, F. J. and R. Losick (2002). "A widely conserved bacterial cell division protein that promotes assembly of the tubulin-like protein FtsZ." Genes Dev 16(19): 2544-2556.

Guerra Maldonado, J. F., A. T. Vincent, M. Chenal and F. J. Veyrier (2020). "CAPRIB: a user-friendly tool to study amino acid changes and selection for the exploration of intra-genus evolution." BMC Genomics 21(1): 832.

Guiddir, T., A. E. Deghmane, D. Giorgini and M. K. Taha (2014). "Lipocalin 2 in cerebrospinal fluid as a marker of acute bacterial meningitis." BMC Infect Dis 14: 276.

Han, X. Y., T. Hong and E. Falsen (2006). "Neisseria bacilliformis sp. nov. isolated from human infections." J Clin Microbiol 44(2): 474-479.

Hanage, W. P., C. Fraser and B. G. Spratt (2005). "Fuzzy species among recombinogenic bacteria." BMC Biol 3: 6.

Hancock, L. E., B. E. Murray and J. Sillanpaa (2014). Enterococcal Cell Wall Components and Structures. Enterococci: From Commensals to Leading Causes of Drug Resistant Infection. M. S. Gilmore, D. B. Clewell, Y. Ike and N. Shankar. Boston.

Hara, H., S. Yasuda, K. Horiuchi and J. T. Park (1997). "A promoter for the first nine genes of the Escherichia coli mra cluster of cell division and cell envelope biosynthesis genes, including ftsI and ftsW." J Bacteriol 179(18): 5802-5811.

Hedlund, B. P. and J. T. Staley (2002). "Phylogeny of the genus Simonsiella and other members of the Neisseriaceae." Int J Syst Evol Microbiol 52(Pt 4): 1377-1382.

Heidrich, C., M. F. Templin, A. Ursinus, M. Merdanovic, J. Berger, H. Schwarz, M. A. de Pedro and J. V. Holtje (2001). "Involvement of N-acetylmuramyl-L-alanine amidases in cell separation and antibiotic-induced autolysis of Escherichia coli." Mol Microbiol 41(1): 167. 178.

Hoang, T. T., A. J. Kutchma, A. Becher and H. P. Schweizer (2000). "Integration-Proficient Plasmids for Pseudomonas aeruginosa: Site-Specific Integration and Use for Engineering of Reporter and Expression Strains." Plasmid 43(1): 59-72.

Hollard, M. (2022). "Recent Advances in Our Understanding of Bacterial Morphogenesis." Human Genetics & Embryology 13(2): 173.

Holtje, J. V. (1998). "Growth of the stress-bearing and shape-maintaining murein sacculus of Escherichia coli." Microbiol Mol Biol Rev 62(1): 181-203.

Horvath, D. J., Jr., B. Li, T. Casper, S. Partida-Sanchez, D. A. Hunstad, S. J. Hultgren and S. S. Justice (2011). "Morphological plasticity promotes resistance to phagocyte killing of uropathogenic Escherichia coli." Microbes Infect 13(5): 426-437.

Hug, L. A., B. J. Baker, K. Anantharaman, C. T. Brown, A. J. Probst, C. J. Castelle, C. N. Butterfield, A. W. Hernsdorf, Y. Amano, K. Ise, Y. Suzuki, N. Dudek, D. A. Relman, K. M. Finstad, R. Amundson, B. C. Thomas and J. F. Banfield (2016). "A new view of the tree of life." Nat Microbiol 1: 16048.

Humbert, M. V. and M. Christodoulides (2019). "Atypical, Yet Not Infrequent, Infections with Neisseria Species." Pathogens 9(1).

Itsko, M. and R. M. Schaaper (2011). "The dgt gene of Escherichia coli facilitates thymine utilization in thymine-requiring strains." Mol Microbiol 81(5): 1221-1232.

Jahnke, J. P., J. L. Terrell, A. M. Smith, X. Cheng and D. N. Stratis-Cullum (2016). "Influences of Adhesion Variability on the "Living" Dynamics of Filamentous Bacteria in Microfluidic Channels." Molecules 21(8).

Jenkins, C. L., D. A. Kuhn and K. R. Daly (1977). "Fatty acid composition of Simonsiella strains." Arch Microbiol 113(3): 209-213.

Johnson, J. W., J. F. Fisher and S. Mobashery (2013). "Bacterial cell-wall recycling." Ann N Y Acad Sci 1277: 54-75.

Jones, R. A., W. X. Yee, K. Mader, C. M. Tang and A. Cehovin (2022). "Markerless gene editing in Neisseria gonorrhoeae." Microbiology (Reading) 168(6).

Justice, S. S., C. Hung, J. A. Theriot, D. A. Fletcher, G. G. Anderson, M. J. Footer and S. J. Hultgren (2004). "Differentiation and developmental pathways of uropathogenic Escherichia coli in urinary tract pathogenesis." Proc Natl Acad Sci U S A 101(5): 1333-1338.

Justice, S. S., C. Hung, J. A. Theriot, D. A. Fletcher, G. G. Anderson, M. J. Footer and S. J. Hultgren (2004). "Differentiation and developmental pathways of uropathogenic Escherichia coli in urinary tract pathogenesis." Proc Natl Acad Sci U S A 101(5): 1333-1338.

Justice, S. S., D. A. Hunstad, P. C. Seed and S. J. Hultgren (2006). "Filamentation by Escherichia coli subverts innate defenses during urinary tract infection." Proc Natl Acad Sci U S A 103(52): 19884-19889.

Kadoya, R., K. Matsumoto, T. Ooi and S. Taguchi (2015). "MtgA Deletion-Triggered Cell Enlargement of Escherichia coli for Enhanced Intracellular Polyester Accumulation." PLoS One 10(6): e0125163.

Kaiser, D. (2001). "Building a multicellular organism." Annu Rev Genet 35: 103-123.

Kawazura, T., K. Matsumoto, K. Kojima, F. Kato, T. Kanai, H. Niki and D. Shiomi (2017). "Exclusion of assembled MreB by anionic phospholipids at cell poles confers cell polarity for bidirectional growth." Mol Microbiol 104(3): 472-486.

Khan, M. A., S. Durica-Mitic, Y. Göpel, R. Heermann and B. Görke (2020). "Small RNA-binding protein RapZ mediates cell envelope precursor sensing and signaling in Escherichia coli." Embo j 39(6): e103848.

Koonin, E. V., K. S. Makarova and L. Aravind (2001). "Horizontal gene transfer in prokaryotes: quantification and classification." Annu Rev Microbiol 55: 709-742.

Kuhn, B. P. H. a. D. A. (2006). The Genera Simonsiella and Alysiella. SpringerLink. 5: 828 839.

Kuhn, D. A., D. A. Gregory, M. D. Nyby and M. Mandel (1977). "Deoxyribonucleic acid base composition of Simonsiellaceae." Arch Microbiol 113(3): 205-207.

Kysela, D. T., A. M. Randich, P. D. Caccamo and Y. V. Brun (2016). "Diversity Takes Shape: Understanding the Mechanistic and Adaptive Basis of Bacterial Morphology." PLoS Biol 14(10): e1002565.

Laaberki, M. H., J. Pfeffer, A. J. Clarke and J. Dworkin (2011). "O-Acetylation of peptidoglycan is required for proper cell separation and S-layer anchoring in Bacillus anthracis." J Biol Chem 286(7): 5278-5288.

Lederberg, J. (1956). "Bacterial Protoplasts Induced by Penicillin." Proc Natl Acad Sci U S A 42(9): 574-577.

Lehner, J., Y. Zhang, S. Berendt, T. M. Rasse, K. Forchhammer and I. Maldener (2011). "The morphogene AmiC2 is pivotal for multicellular development in the cyanobacterium Nostoc punctiforme." Mol Microbiol 79(6): 1655-1669.

Lewis, K., S. Epstein, A. D'Onofrio and L. L. Ling (2010). "Uncultured microorganisms as a source of secondary metabolites." J Antibiot (Tokyo) 63(8): 468-476.

Li, X. H., Y. L. Zeng, Y. Gao, X. C. Zheng, Q. F. Zhang, S. N. Zhou and Y. J. Lu (2010). "The ClpP protease homologue is required for the transmission traits and cell division of the pathogen Legionella pneumophila." BMC Microbiol 10: 54.

Li, X., Y. Liu, X. Yang, C. Li and Z. Song (2022). "The Oral Microbiota: Community Composition, Influencing Factors, Pathogenesis, and Interventions." Front Microbiol 13: 895537.

Li, Y., H. Xue, S. Q. Sang, C. L. Lin and X. Z. Wang (2017). "Phylogenetic analysis of family Neisseriaceae based on genome sequences and description of Populibacter corticis gen. nov., sp. nov., a member of the family Neisseriaceae, isolated from symptomatic bark of Populus × euramericana canker." PLoS One 12(4): e0174506.

Liu, X., J. Biboy, E. Consoli, W. Vollmer and T. den Blaauwen (2020). "MreC and MreD balance the interaction between the elongasome proteins PBP2 and RodA." PLoS Genet 16(12): e1009276.

Mainardi, J. L., M. Fourgeaud, J. E. Hugonnet, L. Dubost, J. P. Brouard, J. Ouazzani, L. B. Rice, L. Gutmann and M. Arthur (2005). "A novel peptidoglycan cross-linking enzyme for a beta-lactam-resistant transpeptidation pathway." J Biol Chem 280(46): 38146-38152.

Mannik, J., R. Driessen, P. Galajda, J. E. Keymer and C. Dekker (2009). "Bacterial growth and motility in sub-micron constrictions." Proc Natl Acad Sci U S A 106(35): 14861-14866.

Manos, P. S., P. S. Soltis, D. E. Soltis, S. R. Manchester, S. H. Oh, C. D. Bell, D. L. Dilcher and D. E. Stone (2007). "Phylogeny of extant and fossil Juglandaceae inferred from the integration of molecular and morphological data sets." Syst Biol 56(3): 412-430.

Martinez-Torro, C., S. Torres-Puig, M. Marcos-Silva, M. Huguet-Ramon, C. Munoz-Navarro, M. Lluch-Senar, L. Serrano, E. Querol, J. Pinol and O. Q. Pich (2021). "Functional Characterization of the Cell Division Gene Cluster of the Wall-less Bacterium Mycoplasma genitalium." Front Microbiol 12: 695572.

Martinez, L. E., J. M. Hardcastle, J. Wang, Z. Pincus, J. Tsang, T. R. Hoover, R. Bansil and N. R. Salama (2016). "Helicobacter pylori strains vary cell shape and flagellum number to maintain robust motility in viscous environments." Mol Microbiol 99(1): 88-110.

Massidda, O., L. Nováková and W. Vollmer (2013). "From models to pathogens: how much have we learned about Streptococcus pneumoniae cell division?" Environ Microbiol 15(12): 3133-3157.

Mayer, C. (2019). "Peptidoglycan Recycling, a Promising Target for Antibiotic Adjuvants in Antipseudomonal Therapy." J Infect Dis 220(11): 1713-1715.

Mayer, J. A. and K. J. Amann (2009). "Assembly properties of the Bacillus subtilis actin, MreB." Cell Motil Cytoskeleton 66(2): 109-118.

McBride, M. J. (2001). "Bacterial gliding motility: multiple mechanisms for cell movement over surfaces." Annu Rev Microbiol 55: 49-75.

Meier, E. L. and E. D. Goley (2014). "Form and function of the bacterial cytokinetic ring." Curr Opin Cell Biol 26: 19-27.

Meroueh, S. O., K. Z. Bencze, D. Hesek, M. Lee, J. F. Fisher, T. L. Stemmler and S. Mobashery (2006). "Three-dimensional structure of the bacterial cell wall peptidoglycan." Proc Natl Acad Sci U S A 103(12): 4404-4409.

Mileykovskaya, E., I. Fishov, X. Fu, B. D. Corbin, W. Margolin and W. Dowhan (2003). "Effects of phospholipid composition on MinD-membrane interactions in vitro and in vivo." J Biol Chem 278(25): 22193-22198.

Mingorance, J. and J. Tamames (2004). "The bacterial dcw gene cluster: an island in the genome?" SpringeLink(Molecules in Time and Space).

Mishra, N. N., T. T. Tran, R. Seepersaud, C. Garcia-de-la-Maria, K. Faull, A. Yoon, R. Proctor, J. M. Miro, M. J. Rybak, A. S. Bayer, C. A. Arias and P. M. Sullam (2017). "Perturbations of Phosphatidate Cytidylyltransferase (CdsA) Mediate Daptomycin Resistance in Streptococcus mitis/oralis by a Novel Mechanism." Antimicrob Agents Chemother 61(4).

Misra, H. S., G. K. Maurya, R. Chaudhary and C. S. Misra (2018). "Interdependence of bacterial cell division and genome segregation and its potential in drug development." Microbiol Res 208: 12-24.

Muller, A., M. Wenzel, H. Strahl, F. Grein, T. N. V. Saaki, B. Kohl, T. Siersma, J. E. Bandow, H. G. Sahl, T. Schneider and L. W. Hamoen (2016). "Daptomycin inhibits cell envelope synthesis by interfering with fluid membrane microdomains." Proc Natl Acad Sci U S A 113(45): E7077-E7086.

Myers, J. A., B. B. Beauchamp and C. C. Richardson (1987). "Gene 1.2 protein of bacteriophage T7. Effect on deoxyribonucleotide pools." J Biol Chem 262(11): 5288-5292.

Nakamura, Y., T. Itoh, H. Matsuda and T. Gojobori (2004). "Biased biological functions of horizontally transferred genes in prokaryotic genomes." Nat Genet 36(7): 760-766.

Nanninga, N. (1998). "Morphogenesis of Escherichia coli." Microbiol Mol Biol Rev 62(1): 110-129.

Nenninger, A., G. Mastroianni, A. Robson, T. Lenn, Q. Xue, M. C. Leake and C. W. Mullineaux (2014). "Independent mobility of proteins and lipids in the plasma membrane of Escherichia coli." Mol Microbiol 92(5): 1142-1153.

Nguyen, L. T., J. C. Gumbart, M. Beeby and G. J. Jensen (2015). "Coarse-grained simulations of bacterial cell wall growth reveal that local coordination alone can be sufficient to maintain rod shape." Proc Natl Acad Sci U S A 112(28): E3689-3698.

Nielsen, K. M., T. Bohn and J. P. Townsend (2014). "Detecting rare gene transfer events in bacterial populations." Front Microbiol 4: 415.

Nikolaidis, I., S. Favini-Stabile and A. Dessen (2014). "Resistance to antibiotics targeted to the bacterial cell wall." Protein Sci 23(3): 243-259.

Nyby, M. D., D. A. Gregory, D. A. Kuhn and J. Pangborn (1977). "Incidence of Simonsiella in the oral cavity of dogs." J Clin Microbiol 6(1): 87-88.

Nyongesa, S., P. M. Weber, E. Bernet, F. Pulido, C. Nieves, M. Nieckarz, M. Delaby, T. Viehboeck, N. Krause, A. Rivera-Millot, A. Nakamura, N. O. E. Vischer, M. vanNieuwenhze, Y. V. Brun, F. Cava, S. Bulgheresi and F. J. Veyrier (2022). "Evolution of longitudinal division in multicellular bacteria of the Neisseriaceae family." Nat Commun 13(1): 4853.

O'Young, J., N. Sukdeo and J. F. Honek (2007). "Escherichia coli glyoxalase II is a binuclear zinc-dependent metalloenzyme." Arch Biochem Biophys 459(1): 20-26.

Obergfell, K. P., R. E. Schaub, L. L. Priniski, J. P. Dillard and H. S. Seifert (2018). "The low-molecular-mass, penicillin-binding proteins DacB and DacC combine to modify peptidoglycan cross-linking and allow stable Type IV pilus expression in Neisseria gonorrhoeae." Mol Microbiol 109(2): 135-149.

Ozyamak, E., S. S. Black, C. A. Walker, M. J. Maclean, W. Bartlett, S. Miller and I. R. Booth (2010). "The critical role of S-lactoylglutathione formation during methylglyoxal detoxification in Escherichia coli." Mol Microbiol 78(6): 1577-1590.

Pangborn, J., D. A. Kuhn and J. R. Woods (1977). "Dorsal-ventral differentiation in Simonsiella and other aspects of its morphology and ultrastructure." Arch Microbiol 113(3): 197-204.

Pankhurst, C. L., D. Auger and J. Hardie (1988). "Isolation and prevalence of Simonsiella sp. in lesions of erosive lichen planus and on healthy human oral mucosa." Microbial Ecology in Health and Disease 1(1): 17-21.

Park, J. T. and T. Uehara (2008). "How bacteria consume their own exoskeletons (turnover and recycling of cell wall peptidoglycan)." Microbiol Mol Biol Rev 72(2): 211-227, table of contents.

Park, K. T., S. Du and J. Lutkenhaus (2020). "Essential Role for FtsL in Activation of Septal Peptidoglycan Synthesis." mBio 11(6).

Parte, A. C. (2018). "LPSN - List of Prokaryotic names with Standing in Nomenclature (bacterio.net), 20 years on." International Journal of Systematic and Evolutionary Microbiology 68(6): 1825-1829.

Peddi, S., R. A. Nicholas and W. G. Gutheil (2009). "Neisseria gonorrhoeae penicillin-binding protein 3 demonstrates a pronounced preference for N(epsilon)-acylated substrates." Biochemistry 48(24): 5731-5737.

Pedro, M. A. d. (2019). "Peptidoglycan (Murein)." Encyclopedia of Microbiology Fourth Edition: 457-472.

Pende, N., J. Wang, P. M. Weber, J. Verheul, E. Kuru, S. K. R. Rittmann, N. Leisch, M. S. VanNieuwenhze, Y. V. Brun, T. den Blaauwen and S. Bulgheresi (2018). "Host-Polarized Cell Growth in Animal Symbionts." Curr Biol 28(7): 1039-1051 e1035.

Pinho, M. G., M. Kjos and J. W. Veening (2013). "How to get (a)round: mechanisms controlling growth and division of coccoid bacteria." Nat Rev Microbiol 11(9): 601-614.

Pluschke, G. and P. Overath (1981). "Function of phospholipids in Escherichia coli. Influence of changes in polar head group composition on the lipid phase transition and characterization of a mutant containing only saturated phospholipid acyl chains." J Biol Chem 256(7): 3207-3212.

Pogliano, J., N. Pogliano and J. A. Silverman (2012). "Daptomycin-mediated reorganization of membrane architecture causes mislocalization of essential cell division proteins." J Bacteriol 194(17): 4494-4504.

Potluri, L. P., S. Kannan and K. D. Young (2012). "ZipA is required for FtsZ-dependent preseptal peptidoglycan synthesis prior to invagination during cell division." J Bacteriol 194(19): 5334-5342.

Price, M. N., P. S. Dehal and A. P. Arkin (2008). "Horizontal gene transfer and the evolution of transcriptional regulation in Escherichia coli." Genome Biol 9(1): R4.

Priyadarshini, R., M. A. de Pedro and K. D. Young (2007). "Role of peptidoglycan amidases in the development and morphology of the division septum in Escherichia coli." J Bacteriol 189(14): 5334-5347.

Quirk, S., S. K. Bhatnagar and M. J. Bessman (1990). "Primary structure of the deoxyguanosine triphosphate triphosphohydrolase-encoding gene (dgt) of Escherichia coli." Gene 89(1): 13-18.

Raymond, J. B., S. Mahapatra, D. C. Crick and M. S. Pavelka, Jr. (2005). "Identification of the namH gene, encoding the hydroxylase responsible for the N-glycolylation of the mycobacterial peptidoglycan." J Biol Chem 280(1): 326-333.

Reiger, M., J. Lassak and K. Jung (2015). "Deciphering the role of the type II glyoxalase isoenzyme YcbL (GlxII-2) in Escherichia coli." FEMS Microbiol Lett 362(2): 1-7.

Říhová, J., G. Batani, S. M. Rodríguez-Ruano, J. Martinů, F. Vácha, E. Nováková and V. Hypša (2021). "A new symbiotic lineage related to Neisseria and Snodgrassella arises from the dynamic and diverse microbiomes in sucking lice." Mol Ecol 30(9): 2178-2196.

Rohs, P. D. A., J. Buss, S. I. Sim, G. R. Squyres, V. Srisuknimit, M. Smith, H. Cho, M. Sjodt, A. C. Kruse, E. C. Garner, S. Walker, D. E. Kahne and T. G. Bernhardt (2018). "A central role for PBP2 in the activation of peptidoglycan polymerization by the bacterial cell elongation machinery." PLoS Genet 14(10): e1007726.

Rosen, D. A., T. M. Hooton, W. E. Stamm, P. A. Humphrey and S. J. Hultgren (2007). "Detection of intracellular bacterial communities in human urinary tract infection." PLoS Med 4(12): e329.

Rossetti, V., B. E. Schirrmeister, M. V. Bernasconi and H. C. Bagheri (2010). "The evolutionary path to terminal differentiation and division of labor in cyanobacteria." J Theor Biol 262(1): 23-34.

Rossetti, V., M. Filippini, M. Svercel, A. D. Barbour and H. C. Bagheri (2011). "Emergent multicellular life cycles in filamentous bacteria owing to density-dependent population dynamics." J R Soc Interface 8(65): 1772-1784.

Rossetti, V., T. W. Ammann, T. Thurnheer, H. C. Bagheri and G. N. Belibasakis (2013). "Phenotypic diversity of multicellular filamentation in oral Streptococci." PLoS One 8(9): e76221.

Rueda, S., M. Vicente and J. Mingorance (2003). "Concentration and assembly of the division ring proteins FtsZ, FtsA, and ZipA during the Escherichia coli cell cycle." J Bacteriol 185(11): 3344-3351.

Russell, J. J., J. A. Theriot, P. Sood, W. F. Marshall, L. F. Landweber, L. Fritz-Laylin, J. K. Polka, S. Oliferenko, T. Gerbich, A. Gladfelter, J. Umen, M. Bezanilla, M. A. Lancaster, S. He, M. C. Gibson, B. Goldstein, E. M. Tanaka, C. K. Hu and A. Brunet (2017). "Non-model model organisms." BMC Biol 15(1): 55.

Safton, S., G. Cooper, M. Harrison, L. Wright and P. Walsh (1999). "Neisseria canis infection: a case report." Commun Dis Intell 23(8): 221.

Sahare, P. and A. Moon (2014). "Penicillin binding proteins, an insight into novel antibacterial drug target." Int J Eng Sci Res 5: 13-23.

Salje, J., F. van den Ent, P. de Boer and J. Lowe (2011). "Direct membrane binding by bacterial actin MreB." Mol Cell 43(3): 478-487.

Salton, M. R. and R. W. Horne (1951). "Studies of the bacterial cell wall. I. Electron microscopical observations on heated bacteria." Biochim Biophys Acta 7(1): 19-42.

Sauvage, E., F. Kerff, M. Terrak, J. A. Ayala and P. Charlier (2008). "The penicillin-binding proteins: structure and role in peptidoglycan biosynthesis." FEMS Microbiol Rev 32(2): 234-258.

Scheurwater, E., C. W. Reid and A. J. Clarke (2008). "Lytic transglycosylases: bacterial space-making autolysins." Int J Biochem Cell Biol 40(4): 586-591.

Schiffer, G. and J. V. Holtje (1999). "Cloning and characterization of PBP 1C, a third member of the multimodular class A penicillin-binding proteins of Escherichia coli." J Biol Chem 274(45): 32031-32039.

Shaku, M., C. Ealand, O. Matlhabe, R. Lala and B. D. Kana (2020). "Peptidoglycan biosynthesis and remodeling revisited." Adv Appl Microbiol 112: 67-103.

Shi, H., B. P. Bratton, Z. Gitai and K. C. Huang (2018). "How to Build a Bacterial Cell: MreB as the Foreman of E. coli Construction." Cell 172(6): 1294-1305.

Shih, Y. L. and L. Rothfield (2006). "The bacterial cytoskeleton." Microbiol Mol Biol Rev 70(3): 729-754.

Shiomi, D., M. Sakai and H. Niki (2008). "Determination of bacterial rod shape by a novel cytoskeletal membrane protein." Embo j 27(23): 3081-3091.

Siefert't, J. L. and G. E. Fox (1998). "Phylogenetic mapping of bacterial morphology." Microbiology (Reading) 144 (Pt 10): 2803-2808.

Silhavy, T. J., D. Kahne and S. Walker (2010). "The bacterial cell envelope." Cold Spring Harb Perspect Biol 2(5): a000414.

Singh, D., D. Gawel, M. Itsko, A. Hochkoeppler, J. M. Krahn, R. E. London and R. M. Schaaper (2015). "Structure of Escherichia coli dGTP triphosphohydrolase: a hexameric enzyme with DNA effector molecules." J Biol Chem 290(16): 10418-10429.

Snyder, D., J. Lary, Y. Chen, P. Gollnick and J. L. Cole (2004). "Interaction of the trp RNA-binding attenuation protein (TRAP) with anti-TRAP." J Mol Biol 338(4): 669-682.

Snyder, L. A., N. J. Saunders and W. M. Shafer (2001). "A putatively phase variable gene (dca) required for natural competence in Neisseria gonorrhoeae but not Neisseria meningitidis is located within the division cell wall (dcw) gene cluster." J Bacteriol 183(4): 1233-1241.

Spratt, B. G. (1975). "Distinct penicillin binding proteins involved in the division, elongation, and shape of Escherichia coli K12." Proc Natl Acad Sci U S A 72(8): 2999-3003.

Stackebrandt, E. and C. R. Woese (1979). "A phylogenetic dissection of the family Micrococcaceae." Current Microbiology 2(6): 317-322.

Stahl, M., E. Frirdich, J. Vermeulen, Y. Badayeva, X. Li, B. A. Vallance and E. C. Gaynor (2016). "The Helical Shape of Campylobacter jejuni Promotes In Vivo Pathogenesis by Aiding Transit through Intestinal Mucus and Colonization of Crypts." Infect Immun 84(12): 3399-3407.

Stefanova, M. E., J. Tomberg, M. Olesky, J. V. Höltje, W. G. Gutheil and R. A. Nicholas (2003). "Neisseria gonorrhoeae penicillin-binding protein 3 exhibits exceptionally high carboxypeptidase and beta-lactam binding activities." Biochemistry 42(49): 14614-14625.

Steinberger, R. E., A. R. Allen, H. G. Hansa and P. A. Holden (2002). "Elongation correlates with nutrient deprivation in Pseudomonas aeruginosa-unsaturates biofilms." Microb Ecol 43(4): 416-423.

Strahl, H., F. Burmann and L. W. Hamoen (2014). "The actin homologue MreB organizes the bacterial cell membrane." Nat Commun 5: 3442.

Sukdeo, N. and J. F. Honek (2008). "Microbial glyoxalase enzymes: metalloenzymes controlling cellular levels of methylglyoxal." Drug Metabol Drug Interact 23(1-2): 29-50.

Sycuro, L. K., T. J. Wyckoff, J. Biboy, P. Born, Z. Pincus, W. Vollmer and N. R. Salama (2012). "Multiple peptidoglycan modification networks modulate Helicobacter pylori's cell shape, motility, and colonization potential." PLoS Pathog 8(3): e1002603.

Sycuro, L. K., Z. Pincus, K. D. Gutierrez, J. Biboy, C. A. Stern, W. Vollmer and N. R. Salama (2010). "Peptidoglycan crosslinking relaxation promotes Helicobacter pylori's helical shape and stomach colonization." Cell 141(5): 822-833.

Szwedziak, P. and J. Löwe (2013). "Do the divisome and elongasome share a common evolutionary past?" Curr Opin Microbiol 16(6): 745-751.

Trespidi, G., V. C. Scoffone, G. Barbieri, G. Riccardi, E. De Rossi and S. Buroni (2020). "Molecular Characterization of the Burkholderia cenocepacia dcw Operon and FtsZ Interactors as New Targets for Novel Antimicrobial Design." Antibiotics (Basel) 9(12).

Typas, A., M. Banzhaf, C. A. Gross and W. Vollmer (2011). "From the regulation of peptidoglycan synthesis to bacterial growth and morphology." Nat Rev Microbiol 10(2): 123-136.

Typas, A. and V. Sourjik (2015). "Bacterial protein networks: properties and functions." Nat Rev Microbiol 13(9): 559-572.

Uehara, T. and J. T. Park (2008). "Growth of Escherichia coli: significance of peptidoglycan degradation during elongation and septation." J Bacteriol 190(11): 3914-3922.

Uehara, T., T. Dinh and T. G. Bernhardt (2009). "LytM-domain factors are required for daughter cell separation and rapid ampicillin-induced lysis in Escherichia coli." J Bacteriol 191(16): 5094-5107.

Uribe-Convers, S., M. M. Carlsen, L. P. Lagomarsino and N. Muchhala (2017). "Phylogenetic relationships of Burmeistera (Campanulaceae: Lobelioideae): Combining whole plastome with targeted loci data in a recent radiation." Mol Phylogenet Evol 107: 551-563.

van Teeffelen, S. and L. D. Renner (2018). "Recent advances in understanding how rod-like bacteria stably maintain their cell shapes." F1000Res 7: 241.

van Teeseling, M. C. F., M. A. de Pedro and F. Cava (2017). "Determinants of Bacterial Morphology: From Fundamentals to Possibilities for Antimicrobial Targeting." Front Microbiol 8: 1264.

Varma, A. and K. D. Young (2004). "FtsZ collaborates with penicillin binding proteins to generate bacterial cell shape in Escherichia coli." J Bacteriol 186(20): 6768-6774.

Vartoukian, S. R., R. M. Palmer and W. G. Wade (2010). "Strategies for culture of 'unculturable' bacteria." FEMS Microbiol Lett 309(1): 1-7.

Vats, P., J. Yu and L. Rothfield (2009). "The dynamic nature of the bacterial cytoskeleton." Cell Mol Life Sci 66(20): 3353-3362.

Veyrier, F. J., I. G. Boneca, M. F. Cellier and M. K. Taha (2011). "A novel metal transporter mediating manganese export (MntX) regulates the Mn to Fe intracellular ratio and Neisseria meningitidis virulence." PLoS Pathog 7(9): e1002261.

Veyrier, F. J., N. Biais, P. Morales, N. Belkacem, C. Guilhen, S. Ranjeva, O. Sismeiro, G. Pehau-Arnaudet, E. P. Rocha, C. Werts, M. K. Taha and I. G. Boneca (2015). "Common Cell Shape Evolution of Two Nasopharyngeal Pathogens." PLoS Genet 11(7): e1005338.

Veyrier, F., D. Pletzer, C. Turenne and M. A. Behr (2009). "Phylogenetic detection of horizontal gene transfer during the step-wise genesis of Mycobacterium tuberculosis." BMC Evol Biol 9: 196.

Vicente, M., M. J. Gomez and J. A. Ayala (1998). "Regulation of transcription of cell division genes in the Escherichia coli dcw cluster." Cell Mol Life Sci 54(4): 317-324.

Vollmer, W., D. Blanot and M. A. de Pedro (2008). "Peptidoglycan structure and architecture." FEMS Microbiol Rev 32(2): 149-167.

Wang, S., L. Furchtgott, K. C. Huang and J. W. Shaevitz (2012). "Helical insertion of peptidoglycan produces chiral ordering of the bacterial cell wall." Proc Natl Acad Sci U S A 109(10): E595-604.

Weibull, C. (1953). "The isolation of protoplasts from Bacillus megaterium by controlled treatment with lysozyme." J Bacteriol 66(6): 688-695.

Weidel, W. and H. Pelzer (1964). "Bagshaped Macromolecules--a New Outlook on Bacterial Cell Walls." Adv Enzymol Relat Subj Biochem 26: 193-232.

Weidel, W., H. Frank and H. H. Martin (1960). "The rigid layer of the cell wall of Escherichia coli strain B." J Gen Microbiol 22: 158-166.

White, M. L., A. Hough-Neidig, S. J. Khan and P. J. Eswara (2022). "MraZ is a transcriptional inhibitor of cell division in Bacillus subtilis." bioRxiv: 2022.2002.2009.479790.

White, M. L., A. Hough-Neidig, S. J. Khan and P. J. Eswara (2022). "MraZ Transcriptionally Controls the Critical Level of FtsL Required for Focusing Z-Rings and Kickstarting Septation in Bacillus subtilis." J Bacteriol: e0024322.

Whitehouse, R. L., H. Jackson, M. C. Jackson and M. M. Ramji (1987). "Isolation of Simonsiella sp. from a neonate." J Clin Microbiol 25(3): 522-525.

Whitehouse, R. L., H. Merrill, M. C. Jackson and H. Jackson (1990). "A stable variant of Simonsiella muelleri with unusual colonial and cellular morphology." J Bacteriol 172(3): 1673-1675.

Woese, C. R., P. Blanz, R. B. Hespell and C. M. Hahn (1982). "Phylogenetic relationships among various helical bacteria." Current Microbiology 7(2): 119-124.

Wolf, Y. I., I. B. Rogozin, N. V. Grishin and E. V. Koonin (2002). "Genome trees and the tree of life." Trends Genet 18(9): 472-479.

Wurgler, S. M. and C. C. Richardson (1990). "Structure and regulation of the gene for dGTP triphosphohydrolase from Escherichia coli." Proc Natl Acad Sci U S A 87(7): 2740-2744.

Xie, C. H. and A. Yokota (2005). "Phylogenetic analysis of Alysiella and related genera of Neisseriaceae: proposal of Alysiella crassa comb. nov., Conchiformibium steedae gen. nov., comb. nov., Conchiformibium kuhniae sp. nov. and Bergeriella denitrificans gen. nov., comb. nov." J Gen Appl Microbiol 51(1): 1-10.

Yadav, A. K., A. Espaillat and F. Cava (2018). "Bacterial Strategies to Preserve Cell Wall Integrity Against Environmental Threats." Front Microbiol 9: 2064.

Yang, L. C., Y. L. Gan, L. Y. Yang, B. L. Jiang and J. L. Tang (2018). "Peptidoglycan hydrolysis mediated by the amidase AmiC and its LytM activator NlpD is critical for cell separation and virulence in the phytopathogen Xanthomonas campestris." Mol Plant Pathol 19(7): 1705-1718.

Young, K. D. (2006). "The selective value of bacterial shape." Microbiol Mol Biol Rev 70(3): 660-703.

Young, K. D. (2010). "Bacterial shape: two-dimensional questions and possibilities." Annu Rev Microbiol 64: 223-240.

Young, K. T., L. M. Davis and V. J. Dirita (2007). "Campylobacter jejuni: molecular biology and pathogenesis." Nat Rev Microbiol 5(9): 665-679.

Yulo, P. R. J. and H. L. Hendrickson (2019). "The evolution of spherical cell shape; progress and perspective." Biochem Soc Trans 47(6): 1621-1634.

Zarantonelli, M. L., M. Lancellotti, A. E. Deghmane, D. Giorgini, E. Hong, C. Ruckly, J. M. Alonso and M. K. Taha (2008). "Hyperinvasive genotypes of Neisseria meningitidis in France." Clin Microbiol Infect 14(5): 467-472.

Supplementary figures

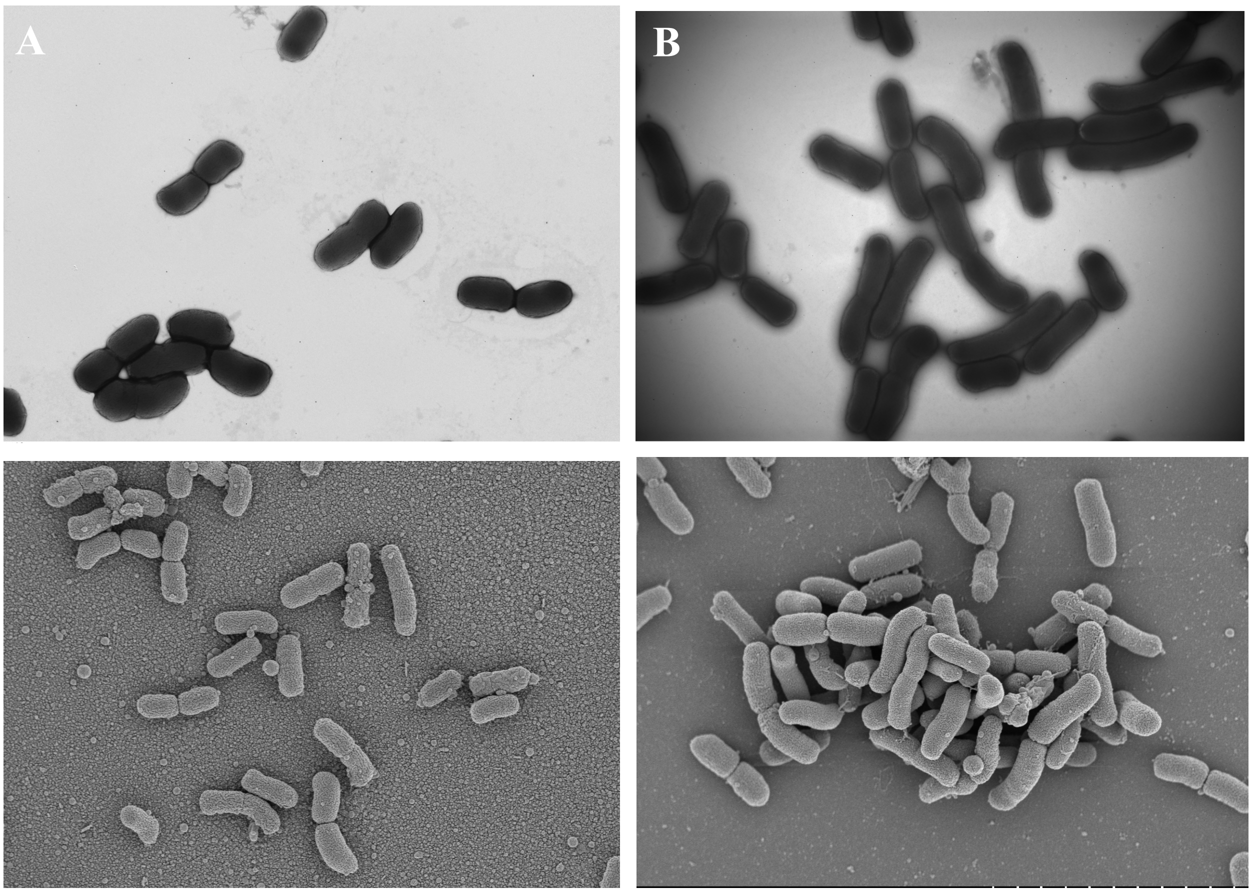

Supplementary figure 1: transmission and scanning electron microscopy of 6 gene deletion strains. A comparing wild type *Neisseria elongata* cells (A and C), (B and D) 6 gene mutant *Neisseria elongata* (*ΔmraZ, ΔrapZ, ΔdacB*, Δ *mtgA, ΔgloB* and Δ NELON_RS02275)

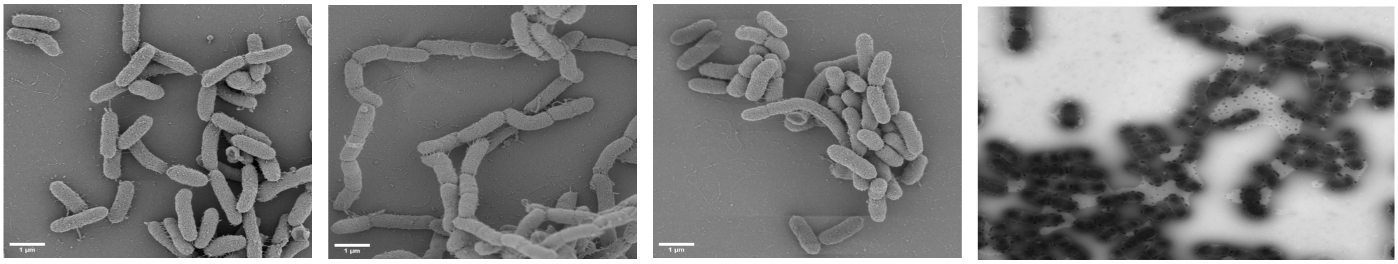

N. musculi (WT) ***ΔamiC1*** ***ΔamiC1:: amiC1*** ***ΔamiC1 :: amiC2***

Supplementary figure 2: Amidase activity of AmiC1 and AmiC2 in *N. musculi* (Eve Bernet unpublished). Scanning and transmission electron microscopy images showing chaining effect of *N. musculi* cells upon the deletion of *amiC1* and reversion of the phenotype through *amiC1* or *amiC2* complementation